

**Numerical Modelling of Hydrodynamic and
Sediment-Bacteria Interaction Processes in Estuarine and
Coastal Waters**

by

Guanghai Gao

Thesis submitted for the degree of Doctor of Philosophy

Cardiff School of Engineering, Cardiff University, UK

September 2008

UMI Number: U585127

All rights reserved

INFORMATION TO ALL USERS

The quality of this reproduction is dependent upon the quality of the copy submitted.

In the unlikely event that the author did not send a complete manuscript and there are missing pages, these will be noted. Also, if material had to be removed, a note will indicate the deletion.



UMI U585127

Published by ProQuest LLC 2013. Copyright in the Dissertation held by the Author.
Microform Edition © ProQuest LLC.

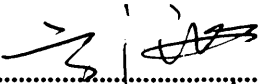
All rights reserved. This work is protected against
unauthorized copying under Title 17, United States Code.



ProQuest LLC
789 East Eisenhower Parkway
P.O. Box 1346
Ann Arbor, MI 48106-1346

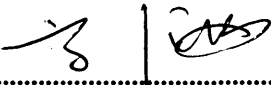
DECLARATION

This work has not previously been accepted in substance for any degree and is not currently submitted in candidature for any degree.

Signed..........(Guanghai Gao)
Date.....18/09/2008.....

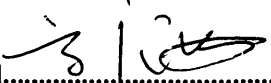
STATEMENT 1

This thesis is being submitted in partial fulfilment of the requirements of the degree of PhD.

Signed..........(Guanghai Gao)
Date.....18/09/2008.....

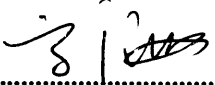
STATEMENT 2

This thesis is the result of my own independent work/investigation, except where otherwise stated. Other sources are acknowledged by explicit references.

Signed..........(Guanghai Gao)
Date.....18/09/2008.....

STATEMENT 3

I hereby give consent for my thesis, if accepted, to be available for photocopying and for inter-library loan, and for the title and summary to be made available to outside organisations.

Signed..........(Guanghai Gao)
Date.....18/09/2008.....

ACKNOWLEDGEMENTS

I would like to express my gratitude and appreciation to my supervisors Professor Roger Falconer and Professor Binliang Lin for their continued helpful advices, support and encouragement through the period of this study.

I would like to thank all my colleagues in Hydro-environmental Research Centre at Cardiff University for their kindness and continuous assistance during this study.

I would like to say that I am indebted to my wife, Yu-Wei, for her continuous love, patience and understanding. I would like to express my appreciation to my little son, Yue-Hang, who lightens up our life with his birth. I am also indebted to my family for their continuous encouragement and support.

Abstract

A study has been undertaken to investigate and improve the representation and modelling of a range of various hydrodynamic, biochemical and sediment transport processes relating to the transport of enteric bacteria organisms in estuarine waters.

In this study a relatively simple turbulence model was first further investigated to predict the complex three-dimensional flow structure in a flume with vegetation. The main purpose of this part of the study was to try and acquire accurate velocity profiles of complex flows without the need for a more advanced two-equation turbulence model, requiring values for a number of unknown coefficients and extra computing cost. The results showed that the simple two layer mixing length model was capable of giving more accurate complex velocity profile predictions, with the advantage of requiring limited coefficient data.

Formulations developed through earlier studies for dynamic decay rates were then refined and included in the numerical model. The model predictions were tested against field data, with good agreement being obtained. Further refinements to the representation of the transport of bacteria through the flow field were included in the model by the novel addition of the interaction of bacteria with the sediments by partitioning the total bacteria into their free-living and attached phases using a dynamic partitioning ratio. This ratio was related to the suspended sediment concentrations. The novel method used in this study was to include the re-suspension and deposition of the absorbed bacteria with the sediments and this approach has been tested against analytical solutions for steady uniform flow conditions, and published field and experimental data. The model was then applied to the Severn Estuary. After calibration against available data sets the model was then run for different scenarios to investigate the effects of different hydro-environmental conditions on the bacteria distributions in the Severn Estuary.

The model was finally used to investigate the impact of the proposed Cardiff-Weston tidal barrage on the hydrodynamic, the sediment transport and bacterial processes within the Severn Estuary. The results showed that the barrage would reduce the currents, as well as significantly reducing the suspended sediment concentrations and bacteria concentration levels in the estuary.

CONTENTS

CHAPTER 1

INTRODUCTION AND OVERVIEW	1
1.1 INTRODUCTION.....	1
1.2 OBJECTIVES OF THESIS	3
1.3 OUTLINE OF THESIS	7

CHAPTER 2

LITERATURE REVIEW	8
2.1 HYDRODYNAMIC MODELLING	8
2.2 SEDIMENT TRANSPORT MODELLING	10
2.2.1 <i>Settling Velocity</i>	10
2.2.2 <i>Deposition and Re-suspension of Cohesive Sediment</i>	12
2.2.3 <i>Deposition and re-suspension of non-cohesive sediment</i>	15
2.3 MODELLING FATE OF FAECAL BACTERIA AND TRANSPORT PROCESSES IN SURFACE WATERS	16
2.3.1 <i>Sources of Faecal Indicator Bacteria</i>	16
2.3.2 <i>Effect of Sediment Transport on Faecal Indicator Bacteria</i>	17
2.3.3 <i>Faecal Bacteria Decay Rate</i>	20
2.3.3.1 <i>Irradiance</i>	20
2.3.3.2 <i>Temperature</i>	25
2.3.3.3 <i>Salinity</i>	25
2.3.3.4 <i>Sediment</i>	25
2.4 SUMMARY.....	27

CHAPTER 3

GOVERNING HYDRODYNAMIC AND SOLUTE TRANSPORT EQUATIONS.....	28
3.2 HYDRODYNAMIC EQUATIONS.....	29
3.2.1 <i>Three-Dimensional Reynolds Averaged Equations</i>	29
3.2.2 <i>Two-Dimensional Depth Integrated Equations</i>	32

3.2.3 <i>Three-Dimensional Layer Integrated Equations</i>	38
3.3 ADVECTIVE-DIFFUSION EQUATION.....	42
3.4 SUMMARY.....	45
 CHAPTER 4	
DEVELOPMENT OF SEDIMENT-BACTERIA INTERACTION CONCEPTUAL MODEL.....	46
4.1 INTRODUCTION.....	46
4.2 SEDIMENT TRANSPORT MODELLING.....	47
4.2.1 <i>Suspended Sediment Transport</i>	47
4.2.2 <i>Bed load Transport</i>	51
4.3 SEDIMENT-BACTERIA INTERACTION MODEL.....	51
4.3.1 <i>Partition of Bacteria between Sediment and Water</i>	51
4.3.2 <i>Exchange of Bacteria in Sediment-water Interface</i>	53
4.3.3 <i>Governing Equations for Faecal Bacteria Transport Processes</i>	55
4.4 FAECAL BACTERIA DECAY RATE.....	60
4.4.1 <i>Decay in Water Column</i>	60
4.4.2 <i>Decay in Bed Sediment</i>	62
4.5 SUMMARY.....	62
 CHAPTER 5	
NUMERICAL SOLUTION OF GOVERNING EQUATIONS.....	64
5.1 INTRODUCTION.....	64
5.2 NUMERICAL SOLUTION OF HYDRODYNAMIC EQUATIONS.....	64
5.2.1 <i>Depth-integrated Equations</i>	64
5.2.2 <i>Layer-integrated Equations</i>	71
5.3 NUMERICAL SOLUTION OF ADVECTIVE-DIFFUSION EQUATION.....	75
5.3.1 <i>Depth-integrated Equations</i>	75
5.3.1.1 <i>Advection Terms</i>	76
5.3.1.2 <i>Diffusion Terms:</i>	80
5.3.1.3 <i>Source Terms:</i>	80
5.3.2 <i>Layer-integrated Equations</i>	82

5.4 BOUNDARY CONDITIONS	84
5.4.1 Closed Boundary Condition	84
5.4.2 Open Boundary Condition	86
5.4.3 Free Surface Boundary	87
5.4.4 Bed Boundary	88
5.5 SUMMARY	88

CHAPTER 6

IDEALISED TEST CASES	90
6.1 INTRODUCTION	90
6.2 HYDRODYNAMIC MODEL TEST	90
6.2.1 Non-vegetated Open Channel Flow	93
6.2.2 Submerged Vegetated Open Channel Flow	94
6.2.3 Emergent Vegetated Open Channel Flow	95
6.3 SEDIMENT TRANSPORT MODEL TEST	96
6.3.1 Test Case 1: Net Entrainment Test	96
6.3.2 Test Case 2: Zero Entrainment at the Bed:	99
6.4 SEDIMENT-BACTERIA INTERACTION MODEL TEST	101
6.4.1 Derivation of Analytical Solutions	101
6.4.2 Validation of Model against Analytical Solutions:	106
6.5 IDEALISED CASE APPLICATION	114
6.5.1 Removal of Bacteria from the Water Column due to Sediment	114
6.5.1.1 Effect of the partition coefficient	115
6.5.1.2 Effect of different sediment sizes giving different settling velocities	117
6.5.2 Re-suspension of Attached Bacteria to Water Column	119
6.5.2.1 Effect of bed bacteria concentration	119
6.5.2.2 Effect of partition coefficient	121
6.6 SUMMARY	123

CHAPTER 7

MODELLING HYDRODYNAMIC, SEDIMENT AND BACTERIAL PROCESSES IN THE

BRISTOL CHANNEL AND SEVERN ESTUARY	124
7.1 INTRODUCTION	124
7.2 MODEL SET UP.....	127
<i>7.2.1 One-dimensional Model Set Up.....</i>	<i>128</i>
<i>7.2.2 Two-dimensional Model Set Up.....</i>	<i>129</i>
7.3. MODEL CALIBRATION AND VALIDATION.....	132
<i>7.3.1 Hydrodynamic Model Calibration and Validation.....</i>	<i>132</i>
<i>7.3.2 Sediment Transport Model Calibration</i>	<i>146</i>
<i>7.3.3 Bacterial Transport Model Calibration</i>	<i>157</i>
7.4 MODEL APPLICATION	161
<i>7.4.1 Sensitivity Test to Bed Bacteria Concentration.....</i>	<i>162</i>
<i>7.4.2 Sensitivity to partition coefficient test.....</i>	<i>170</i>
<i>7.4.3 Significance of Different Sources of Bacteria.....</i>	<i>176</i>
<i>7.4.4 Dry and wet weather conditions.....</i>	<i>182</i>
<i>7.4.5 Effect of tidal energy structures.....</i>	<i>185</i>
7.5 SUMMARY.....	193
 CHAPTER 8	
 CONCLUSIONS AND RECOMMENDATIONS	195
8.1 CONCLUSIONS.....	195
8.2 RECOMMENDATIONS FOR FURTHER STUDY	200
 REFERENCES:	203

LIST OF FIGURES

CHAPTER 2

FIGURE 2.1: SUMMARY OF HOURLY T_{90} VALUES AND SOLAR RADIATION (AFTER BELLAIR 1977)..... 21

FIGURE 2.2 LIGHT ATTENUATION FACTOR PER METER DEPTH AGAINST SUSPENDED MATTER CONCENTRATION (POMMEPUY ET AL 1992)..... 23

FIGURE 2.3 FAECAL COLIFORM DIE-OFF RATES AGAINST LIGHT INTENSITY (AFTER WILKINSON ET AL 1995)..... 24

CHAPTER 3

FIGURE 3.1 CO-ORDINATE SYSTEM FOR TWO-DIMENSIONAL DEPTH INTEGRATED EQUATIONS 32

FIGURE 3.2 CO-ORDINATE SYSTEM FOR LAYER INTEGRATED EQUATIONS 38

CHAPTER 4

FIGURE 4.1 BACTERIA FATE AND TRANSPORT PROCESSES IN ESTUARINE WATERS 47

CHAPTER 5

FIGURE 5.1 DESCRIPTION OF SPACE STAGGERED GRID SYSTEM..... 65

FIGURE 5.2 VERTICAL GRID SYSTEM 71

FIGURE 5.3 CONTROL VOLUME AROUND GRID POINT 76

FIGURE 5.4 NORMALISED VARIABLE DIAGRAM SHOWING THE UNIVERSAL LIMITER BOUNDARIES 79

FIGURE 5.5 CLOSED BOUNDARY..... 85

FIGURE 5.6: FLOW BOUNDARY 86

FIGURE 5.7: WATER ELEVATION BOUNDARY..... 87

CHAPTER 6

FIGURE 6.1 LAYOUT OF CROSS-SECTION AND MEASURING POINTS FOR: (A) NO VEGETATION, (B) SUBMERGED VEGETATION AND (C) EMERGENT VEGETATION (DORCHEH, 2007).....	92
FIGURE 6.2 VELOCITY PROFILE COMPARISONS AT THE 1.4 M AND 4.4 M CROSS-SECTIONS FOR NON-VEGETATED FLOWS.....	94
FIGURE 6.3 VELOCITY PROFILE COMPARISONS AT THE 1.4 M AND 4.4 M CROSS-SECTIONS FOR SUBMERGED VEGETATION FLOW.....	95
FIGURE 6.4 VELOCITY PROFILE COMPARISONS AT THE 1.4 M AND 4.4 M CROSS-SECTIONS FOR EMERGENT VEGETATION FLOW.....	96
FIGURE 6.5 NET ENTRAINMENT EXPERIMENTAL SET UP (VAN RIJN 1986).....	97
FIGURE 6.6 COMPARISON OF PREDICTED AND MEASURED SEDIMENT CONCENTRATIONS FOR NET ENTRAINMENT TEST.....	99
FIGURE 6.7 ZERO ENTRAINMENT EXPERIMENT SET UP (WANG AND RIBBERINK 1986).....	100
FIGURE 6.8 COMPARISON OF SEDIMENT CONCENTRATIONS FOR ZERO ENTRAINMENT TEST.....	101
FIGURE 6.9 ILLUSTRATION OF TEST CASE SET UP.....	102
FIGURE 6.10A COMPARISON OF TOTAL BACTERIA CONCENTRATION FOR DEPOSITION TEST.....	108
FIGURE 6.10B COMPARISON OF SEDIMENT CONCENTRATION FOR DEPOSITION TEST.....	108
FIGURE 6.10C COMPARISON OF FREE-LIVING BACTERIA CONCENTRATION FOR DEPOSITION TEST.....	109
FIGURE 6.10D COMPARISON OF ATTACHED BACTERIA CONCENTRATION FOR DEPOSITION TEST.....	109
FIGURE 6.11A COMPARISON OF TOTAL BACTERIA CONCENTRATION FOR RE-SUSPENSION TEST.....	110

FIGURE 6.11B COMPARISON OF SEDIMENT CONCENTRATION FOR RE-SUSPENSION TEST.....	110
FIGURE 6.11C COMPARISON OF FREE-LIVING BACTERIA CONCENTRATION FOR RE-SUSPENSION TEST	111
FIGURE 6.11D COMPARISON OF ATTACHED BACTERIA CONCENTRATION FOR RE-SUSPENSION TEST	111
FIGURE 6.12A SEDIMENT CONCENTRATION PROFILE.....	112
FIGURE 6.12B TOTAL BACTERIA CONCENTRATION PROFILE	112
FIGURE 6.13 COMPARISON OF MODEL RESULTS AND SITE DATA AT SITE A.....	114
FIGURE 6.14A TOTAL BACTERIA CONCENTRATION FOR DIFFERENT PARTITION COEFFICIENTS	116
FIGURE 6.14B ATTACHED BACTERIA CONCENTRATION FOR DIFFERENT PARTITION COEFFICIENTS	116
FIGURE 6.14C FREE-LIVING BACTERIA CONCENTRATION FOR DIFFERENT PARTITION COEFFICIENTS	117
FIGURE 6.15A TOTAL BACTERIA CONCENTRATION FOR DIFFERENT SETTLING VELOCITIES	118
FIGURE 6.15B ATTACHED BACTERIA CONCENTRATION FOR DIFFERENT SETTLING VELOCITIES	118
FIGURE 6.15C FREE-LIVING BACTERIA CONCENTRATION FOR DIFFERENT SETTLING VELOCITIES	119
FIGURE 6.16A TOTAL BACTERIA CONCENTRATIONS FOR DIFFERENT BED BACTERIA CONCENTRATIONS	120
FIGURE 6.16B ATTACHED BACTERIA CONCENTRATIONS FOR DIFFERENT BED BACTERIA CONCENTRATIONS.....	120
FIGURE 6.16C FREE-LIVING BACTERIA CONCENTRATIONS FOR DIFFERENT BED BACTERIA CONCENTRATIONS.....	121

FIGURE 6.17A TOTAL BACTERIA CONCENTRATIONS FOR DIFFERENT PARTITION COEFFICIENTS	122
FIGURE 6.17B ATTACHED BACTERIA CONCENTRATIONS FOR DIFFERENT PARTITION COEFFICIENTS	122
FIGURE 6.17C FREE-LIVING BACTERIA CONCENTRATIONS FOR DIFFERENT PARTITION COEFFICIENTS	123
CHAPTER 7	
FIGURE 7.1 LOCATION OF THE BRISTOL CHANNEL AND SEVERN ESTUARY	124
FIGURE 7.2: BATHING WATER COMPLIANCE MONITORING SITES, MAIN RIVER CATCHMENTS AND LOCATIONS OF OUTLETS TO THE SEVERN ESTUARY (STAPLETON ET AL 2007)	125
FIGURE 7.3: LOCATION AND TREATMENT TYPE OF WASTE WATER TREATMENT WORKS EFFLUENT INPUTS, WITH POPULATION EQUIVALENTS GREATER THAN 2000 TO THE SEVERN ESTUARY (STAPLETON ET AL 2007)	126
FIGURE 7.4: BATHYMETRY OF THE BRISTOL CHANNEL AND LOWER SEVERN ESTUARY.	130
FIGURE 7.5: LOCATION OF CALIBRATION SITES	132
FIGURE 7.6: WATER ELEVATIONS AT THE SEAWARD BOUNDARY	133
FIGURE 7.7: COMPARISON OF CURRENT SPEEDS AND DIRECTIONS AT SITE F	134
FIGURE 7.8: COMPARISON OF CURRENT SPEEDS AND DIRECTIONS AT SITE M.....	135
FIGURE 7.9: COMPARISON OF CURRENT SPEEDS AND DIRECTIONS AT SITE V.....	135
FIGURE 7.10: COMPARISON OF CURRENT SPEEDS AND DIRECTIONS AT SITE F FOR NEAP TIDE.....	136
FIGURE 7.11: COMPARISON OF CURRENT SPEEDS AND DIRECTIONS AT SITE M FOR NEAP TIDE.....	137
FIGURE 7.12: COMPARISON OF CURRENT SPEEDS AND DIRECTIONS AT SITE V FOR	

NEAP TIDE.....	137
FIGURE 7.13: COMPARISON OF WATER DEPTHS AND CURRENT SPEEDS AND DIRECTIONS AT S WALES FOR 24 TH JULY 2001 SURVEY	138
FIGURE 7.14: COMPARISON OF WATER DEPTHS AND CURRENT SPEEDS AND DIRECTIONS AT S WALES FOR 26 TH JULY 2001 SURVEY	139
FIGURE 7.15: COMPARISON OF WATER DEPTHS AND CURRENT SPEEDS AND DIRECTIONS AT MINEHEAD FOR 30 TH JULY 2001 SURVEY.....	140
FIGURE 7.16: COMPARISON OF WATER DEPTHS AND CURRENT SPEEDS AND DIRECTIONS AT MINEHEAD FOR 1 ST AUGUST 2001 SURVEY.....	141
FIGURE 7.17A: PREDICTED CURRENT SPEEDS AT MEAN EBB FOR SPRING TIDE.....	142
FIGURE 7.17B: PREDICTED CURRENT SPEEDS AT LOW WATER LEVEL FOR SPRING TIDE	142
FIGURE 7.17C: PREDICTED CURRENT SPEEDS AT MEAN FLOOD FOR SPRING TIDE	143
FIGURE 7.17D: PREDICTED CURRENT SPEEDS AT HIGH WATER LEVEL FOR SPRING TIDE	143
FIGURE 7.18A: PREDICTED CURRENT SPEEDS AT MEAN FLOOD FOR NEAP TIDE....	144
FIGURE 7.18B: PREDICTED CURRENT SPEEDS AT HIGH WATER LEVEL FOR NEAP TIDE	144
FIGURE 7.18C: PREDICTED CURRENT SPEEDS AT MEAN EBB FOR NEAP TIDE.....	145
FIGURE 7.18D: PREDICTED CURRENT SPEEDS AT LOW WATER LEVEL FOR NEAP TIDE	145
FIGURE 7.19 SUSPENDED SEDIMENT CONCENTRATIONS AT SOUTHERNDOWN	147
FIGURE 7.20 SUSPENDED SEDIMENT CONCENTRATIONS AT TRECCO BAY	148
FIGURE 7.21A: NON-COHESIVE SEDIMENT CONCENTRATION DISTRIBUTIONS AT MEAN EBB SPRING TIDE	149
FIGURE 7.21B: NON-COHESIVE SEDIMENT CONCENTRATION DISTRIBUTIONS AT	

LOW WATER SPRING TIDE.....	149
FIGURE 7.21C: NON-COHESIVE SEDIMENT CONCENTRATION DISTRIBUTIONS AT MEAN FLOOD SPRING TIDE	150
FIGURE 7.21D: NON-COHESIVE SEDIMENT CONCENTRATION DISTRIBUTIONS AT HIGH WATER SPRING TIDE	150
FIGURE 7.22A: NON-COHESIVE SEDIMENT CONCENTRATION DISTRIBUTIONS AT MEAN FLOOD NEAP TIDE	151
FIGURE 7.22B: NON-COHESIVE SEDIMENT CONCENTRATION DISTRIBUTIONS AT HIGH WATER LEVEL NEAP TIDE	151
FIGURE 7.22C: NON-COHESIVE SEDIMENT CONCENTRATION DISTRIBUTIONS AT MEAN EBB NEAP TIDE.....	152
FIGURE 7.22D: NON-COHESIVE SEDIMENT CONCENTRATION DISTRIBUTIONS AT LOW WATER NEAP TIDE	152
FIGURE 7.23A: COHESIVE SEDIMENT CONCENTRATION DISTRIBUTIONS AT MEAN EBB SPRING TIDE	153
FIGURE 7.23B: COHESIVE SEDIMENT CONCENTRATION DISTRIBUTIONS AT LOW WATER SPRING TIDE	153
FIGURE 7.23C: COHESIVE SEDIMENT CONCENTRATION DISTRIBUTIONS AT MEAN FLOOD SPRING TIDE	154
FIGURE 7.23D: COHESIVE SEDIMENT CONCENTRATION DISTRIBUTIONS AT HIGH WATER SPRING TIDE	154
FIGURE 7.24A: COHESIVE SEDIMENT CONCENTRATION DISTRIBUTIONS AT MEAN FLOOD NEAP TIDE.....	155
FIGURE 7.24B: COHESIVE SEDIMENT CONCENTRATION DISTRIBUTIONS AT HIGH WATER NEAP TIDE	155
FIGURE 7.24C: COHESIVE SEDIMENT CONCENTRATION DISTRIBUTIONS AT MEAN EBB NEAP TIDE.....	156

FIGURE 7.24D: COHESIVE SEDIMENT CONCENTRATION DISTRIBUTIONS AT LOW WATER NEAP TIDE	156
FIGURE 7.25: IRRADIANCE DATA AT SWANSEA.....	159
FIGURE 7.26 ENTEROCOCCI CONCENTRATION COMPARISONS AT TRECCO BAY....	160
FIGURE 7.27: ENTEROCOCCI CONCENTRATION COMPARISONS AT SOUTHERNDOWN	160
FIGURE 7.28: SUSPENDED SEDIMENT CONCENTRATIONS AT THE INVESTIGATION BATHING WATER COMPLIANCE SITES.....	162
FIGURE 7.29: COMPARISON OF ENTEROCOCCI CONCENTRATIONS AT BATHING WATER COMPLIANCE SITES FOR DIFFERENT INITIAL BED CONCENTRATIONS	165
FIGURE 7.30A: COMPARISON OF ENTEROCOCCI CONCENTRATIONS FOR DIFFERENT INITIAL BED CONCENTRATIONS AT MEAN EBB SPRING TIDE	166
FIGURE 7.30B: COMPARISON OF ENTEROCOCCI CONCENTRATIONS FOR DIFFERENT INITIAL BED CONCENTRATIONS AT LOW WATER SPRING TIDE.....	166
FIGURE 7.30C: COMPARISON OF ENTEROCOCCI CONCENTRATIONS FOR DIFFERENT INITIAL BED CONCENTRATIONS AT MEAN FLOOD SPRING TIDE	167
FIGURE 7.30D: COMPARISON OF ENTEROCOCCI CONCENTRATIONS FOR DIFFERENT INITIAL BED CONCENTRATIONS AT HIGH WATER SPRING TIDE	167
FIGURE 7.31A: COMPARISON OF ENTEROCOCCI CONCENTRATIONS FOR DIFFERENT INITIAL BED CONCENTRATIONS AT MEAN FLOOD NEAP TIDE	168
FIGURE 7.31B: COMPARISON OF ENTEROCOCCI CONCENTRATIONS FOR DIFFERENT INITIAL BED CONCENTRATIONS AT HIGH WATER NEAP TIDE.....	168
FIGURE 7.31C: COMPARISON OF ENTEROCOCCI CONCENTRATIONS FOR DIFFERENT INITIAL BED CONCENTRATIONS AT MEAN EBB NEAP TIDE.....	169
FIGURE 7.31D: COMPARISON OF ENTEROCOCCI CONCENTRATIONS FOR DIFFERENT INITIAL BED CONCENTRATIONS AT LOW WATER NEAP TIDE.....	169
FIGURE 7.32: COMPARISON OF ENTEROCOCCI CONCENTRATIONS AT BATHING	

WATER COMPLIANCE SITES FOR DIFFERENT PARTITION COEFFICIENTS.....	172
FIGURE 7.33A: COMPARISON OF ENTEROCOCCI CONCENTRATIONS FOR DIFFERENT PARTITION COEFFICIENTS AT MEAN EBB SPRING TIDE.....	173
FIGURE 7.33B: COMPARISON OF ENTEROCOCCI CONCENTRATIONS FOR DIFFERENT PARTITION COEFFICIENTS AT LOW WATER SPRING TIDE.....	173
FIGURE 7.33C: COMPARISON OF ENTEROCOCCI CONCENTRATIONS FOR DIFFERENT PARTITION COEFFICIENTS AT MEAN FLOOD SPRING TIDE.....	174
FIGURE 7.33D: COMPARISON OF ENTEROCOCCI CONCENTRATIONS FOR DIFFERENT PARTITION COEFFICIENTS AT HIGH WATER SPRING TIDE.....	174
FIGURE 7.34A: COMPARISON OF ENTEROCOCCI CONCENTRATIONS FOR DIFFERENT PARTITION COEFFICIENTS AT MEAN FLOOD NEAP TIDE.....	175
FIGURE 7.34B: COMPARISON OF ENTEROCOCCI CONCENTRATIONS FOR DIFFERENT PARTITION COEFFICIENTS AT HIGH WATER NEAP TIDE	175
FIGURE 7.34C: COMPARISON OF ENTEROCOCCI CONCENTRATIONS FOR DIFFERENT PARTITION COEFFICIENTS AT MEAN EBB NEAP TIDE	176
FIGURE 7.34D: COMPARISON OF ENTEROCOCCI CONCENTRATIONS FOR DIFFERENT PARTITION COEFFICIENTS AT LOW WATER NEAP TIDE	176
FIGURE 7.35: COMPARISON OF ENTEROCOCCI CONCENTRATIONS AT BATHING WATER COMPLIANCE SITES FROM DIFFERENT LOADS DURING DRY WEATHER CONDITIONS	179
FIGURE 7.36: COMPARISON OF ENTEROCOCCI CONCENTRATIONS AT BATHING WATER COMPLIANCE SITES FROM DIFFERENT LOADS DURING WET WEATHER CONDITIONS	181
FIGURE 7.37A: COMPARISON OF ENTEROCOCCI CONCENTRATION DISTRIBUTIONS FOR DRY AND WET WEATHER CONDITIONS FOR MEAN EBB SPRING TIDE.....	182
FIGURE 7.37B: COMPARISON OF ENTEROCOCCI CONCENTRATION DISTRIBUTIONS FOR DRY AND WET WEATHER CONDITIONS FOR LOW WATER SPRING TIDE	182

FIGURE 7.37C: COMPARISON OF ENTEROCOCCI CONCENTRATION DISTRIBUTIONS FOR DRY AND WET WEATHER CONDITIONS AT MEAN FLOOD SPRING TIDE 183

FIGURE 7.37D: COMPARISON OF ENTEROCOCCI CONCENTRATION DISTRIBUTIONS FOR DRY AND WET WEATHER CONDITIONS FOR HIGH WATER SPRING TIDE 183

FIGURE 7.38A: COMPARISON OF ENTEROCOCCI CONCENTRATION DISTRIBUTIONS FOR DRY AND WET WEATHER CONDITIONS AT MEAN FLOOD NEAP TIDE 184

FIGURE 7.38B: COMPARISON OF ENTEROCOCCI CONCENTRATION DISTRIBUTIONS FOR DRY AND WET WEATHER CONDITIONS AT HIGH WATER NEAP TIDE..... 184

FIGURE 7.38C: COMPARISON OF ENTEROCOCCI CONCENTRATION DISTRIBUTIONS FOR DRY AND WET WEATHER CONDITIONS AT MEAN EBB NEAP TIDE..... 185

FIGURE 7.38D: COMPARISON OF ENTEROCOCCI CONCENTRATION DISTRIBUTIONS FOR DRY AND WET WEATHER CONDITIONS AT LOW WATER NEAP TIDE..... 185

FIGURE 7.39 PROPOSED CARDIFF-WESTON BARRAGE SITE (SEVERN TIDAL POWER GROUP) 187

FIGURE 7.40 LAYOUT OF CARDIFF-WESTON BARRAGE (SEVERN TIDAL POWER GROUP) 187

FIGURE 7.41 CURRENTS AT MEAN EBB TIDE, BOTH WITHOUT AND WITH THE BARRAGE 189

FIGURE 7.42 CURRENTS AT MEAN FLOOD TIDE BOTH WITHOUT AND WITH THE BARRAGE 189

FIGURE 7.43 NON-COHESIVE SEDIMENT CONCENTRATIONS AT MEAN EBB TIDE BOTH WITHOUT AND WITH THE BARRAGE 190

FIGURE 7.44 NON-COHESIVE SEDIMENT CONCENTRATIONS AT MEAN FLOOD TIDE BOTH WITHOUT AND WITH THE BARRAGE 190

FIGURE 7.45 COHESIVE SEDIMENT CONCENTRATIONS AT MEAN EBB TIDE BOTH WITHOUT AND WITH THE BARRAGE 191

FIGURE 7.46 COHESIVE SEDIMENT CONCENTRATIONS AT MEAN FLOOD TIDE BOTH

WITHOUT AND WITH THE BARRAGE	191
FIGURE 7.47 ENTEROCOCCI CONCENTRATIONS AT MEAN FLOOD TIDE BOTH WITHOUT AND WITH THE BARRAGE AND WITH AND WITHOUT SEDIMENT-BACTERIA INTERACTIONS	192
FIGURE 7.48 ENTEROCOCCI CONCENTRATIONS AT MEAN EBB TIDE BOTH WITHOUT AND WITH THE BARRAGE AND WITH AND WITHOUT SEDIMENT-BACTERIA INTERACTIONS	193

LIST OF TABLES

TABLE 7.1: RIVER CATCHMENTS INPUT IN ONE-DIMENSIONAL MODEL DOMAIN...	129
TABLE 7.2: WWTW INPUTS IN ONE-DIMENSIONAL MODEL DOMAIN.....	129
TABLE 7.3: RIVER CATCHMENT INPUTS FOR TWO-DIMENSIONAL DOMAIN	130
TABLE 7.4: WWTW INPUTS FOR TWO-DIMENSIONAL DOMAIN.....	131
TABLE 7.5 INVESTIGATION SITE LOCATION	161

ABBREVIATIONS

ADI	Alternating Direction Implicit
DNS	Direct Numerical Simulation
DIVAST	Depth Integrated Velocities And Solute Transport
FIB	Faecal Indicator Bacteria
POL	Proudman Oceanographic Laboratory
RANS	Reynolds averaged Navier-Stokes equations
QUICKEST	Quadratic Upstream Interpolation for Convective Kinematics with Estimated Streaming Terms
SWEs	Shallow Water Equations
TRIVAST	ThRee-dimensional layer Integrated Velocities And Solute Transport
TVD	Total Variation Diminishing
ULTIMATE	Universal Limiter for Transient Interpolation Modelling of the Advective Transport Equation
UV	UltraViolet
WwTWs	Waste water Treatment Works

Chapter 1

Introduction and Overview

1.1 Introduction

In recent years, public and professional concerns of estuarine and coastal water quality have been growing. Pathogens in contaminated waters are often responsible for the spread of waterborne diseases. However, their concentrations are often very difficult to measure. Due to the difficulties of direct measurement of pathogens, classical water quality management and modelling has focused on the levels of indicator organisms (Chapra 1997). Faecal indicator bacteria (FIB) groups such as total coliform, faecal coliform, E coli and enterococci are used world wide to measure the health hazards in bathing and shellfish harvesting waters (Thomann and Mueller 1987 and Sanders et al 2005). This is due principally to the fact that they are easily detected using simple laboratory tests, are generally not present in unpolluted waters, and the number of indicator bacteria tends to be correlated with the extent of contamination (Thomann and Mueller 1987). Therefore, the ability to predict faecal indicator bacteria in estuarine and coastal waters is important for the hydro-environmental management of such water bodies.

Faecal bacteria may enter the water column from different sources, such as waste water treatment works discharges, surface runoff, water creature faeces, inter-tidal beaches and bottom sediment re-suspension. Point sources can be relatively easy quantified and its effect on the water quality of the receiving water body is therefore not too difficult to

investigate. Comparison with point sources, the effect of diffuse or non-outfall sources are difficult to quantify, as it is distributed over large areas and it is difficult to measure directly. Faecal indicator bacteria exist in two forms in estuarine and coastal water, either as free living organisms in the water column or as organisms attached to the sediments. Free-living bacteria may adsorb onto the sediments, transforming to attached bacteria, and the attached bacteria can be desorbed from sediment becoming free-living bacteria. Deposition of the sediments can take faecal bacteria out of the water column and to the bed. The sediments can subsequently be re-suspended to the water column, which can then lead to re-suspension of the faecal bacteria of the attached forms back into the water column. Therefore, the fate and transport of faecal bacteria are highly related to the governing sediment transport processes, particularly where sediment transport processes are significant. The fate and transport processes for bacteria are very complex, and include the processes of advection, dispersion/diffusion, deposition/re-suspension, adsorption/desorption and decay. Each process is affected by different environmental and natural conditions. Advection and dispersion are determined mainly by flow conditions. Deposition and re-suspension are controlled by sediment transport. The bacteria decay rates are influenced by many environmental factors, such as light intensity, temperature, salinity, turbidity levels and pH value etc. Many studies have shown that light intensity is one of the dominant factors determining the rate of the mortality of coliform bacteria (Gameson and Saxon 1967, Gameson and Gould 1975, Bellair et al 1977). In these studies, much higher decay rates were observed under high light intensity conditions in comparison with dark conditions. Suspended sediments contribute to the removal of faecal bacteria from the water column in different ways. Attached faecal bacteria are removed by the sediments settling from the water column under low energy flow conditions, and also

changes in the suspended sediment concentration can affect the light penetration rate in water column, which will further affect the decay rate of faecal bacteria.

Numerical hydro-environmental models have been proven to be effective tools to predict the flow field in 1-D, 2-D and 3-D and the corresponding water quality indicator and sediment transport levels in estuarine and coastal waters. In general, numerical modelling of faecal indicator bacteria is a very complex process, which can be sub-divided into three parts: hydrodynamic modelling, solute transport modelling and biological process modelling. Hydrodynamic modelling is used to study the flow field and provide an accurate level of prediction for velocity and the turbulent diffusion and dispersion mixing processes. Solute transport modelling is used to predict the advection, dispersion /diffusion and the bio-chemical processes for a tracer or solute by using the flow field data from the hydrodynamic modeling. Biological process is used to provide the source/sink terms for indicator bacteria in the solute transport model, with the terms including the kinetic processes of bacteria, which includes both the decay process and physical losses.

In previously studies numerical models for predicting bacterial contamination generally treated bacteria as free-living in present studies, the deposition/re-suspension and adsorption/desorption processes were not included and little attempt has been made to model such processes in terms of predicting the impact of the sediment fluxes on bacteria levels. There is a current lack of sophisticated numerical models which are capable to simulate the sediment effects on bacteria.

1.2 Objectives of Thesis

This research project aims to develop an effective numerical model to simulate fate and transport of faecal bacteria focusing on sediment effects on bacteria using a dynamic partition ratio and a dynamic decay rate modelling. Numerical models have been refined for predicting hydrodynamic, sediment transport and bacterial processes in free surface unsteady flow. The main objectives and achievements of this study are summarised as follows:

(1) Development of a simple turbulence model to investigate vegetation effects on average velocity distribution

The effects of vegetation on the flow structure have been explored in this study. An existing three-dimensional layer integrated numerical model was refined to include the effects of drag force induced by vegetation on the flow structure in a flume. Most similar previous studies have used the $k-\varepsilon$ turbulence model or other two equation type turbulence models. However, extra computing time is needed due to two extra partial differential equations need to be solved, as well as the additional empirical coefficients in these equations included which have not been evaluated for such flow conditions. In this study a simple zero equation mixing length turbulence model was used and tested before inclusion in the numerical model application. The model was applied to model an experiment flume, where experiment data are available. The comparison of experiment and modelling result is encouraging.

(2) Dynamic modelling of faecal bacteria decay rate

Decay rates for faecal indicator bacteria organisms are highly dynamic, with these variations affected by many environmental factors, such as light intensity, temperature, salinity, turbidity levels and pH value etc. In general decay rates have

previously been modelled as a constant in widely used models over the modelling period. In this study the decay rate in a model of the Severn Estuary has been determined from empirical equations, in which the decay rate is related to turbidity level and light intensity.

(3) Numerical modelling of the effects of sediments, including the processes of adsorption and desorption, on the fate and transport of bacteria levels in the surface water

Little attempt has been made previously to model such processes in terms of predicting the impact of the sediment fluxes on the faecal bacteria levels. Details are given of the development of two-dimensional and three-dimensional numerical models of bacterial transport, where the sediment transport processes are included and may be significant.

(4) Development of analytical solution for sediment-bacteria interaction

In this study, analytical solutions for sediment-bacteria interaction have been developed. The advective-diffusion equation was simplified for steady and uniform flow conditions and then solved to obtain analytical solutions for deposition, re-suspension and vertical distributions. All of these solutions have been used to test either the newly developed two-dimensional or three-dimensional sediment-bacteria interaction model. These solutions can be used as primary test by other researchers doing sediment related water quality modelling.

(5) Testing of sediment-bacteria model

Prior to applying any improved process predictions in a numerical model, it must be

tested against known results to ensure that the model is reasonably accurate. These known results can be analytical solutions, experiment results or, ideally, field data. In this study, the tests have been conducted by using both analytical formulations and published experimental results. The analytical solutions, which are self derived, have been mentioned above and will be detailed in Chapter 6.

(6) Numerical model application to idealised cases

After the newly improved model was tested against analytical solutions and published experimental results, the model was then applied to idealised test cases to evaluate the effect of different environmental factors on bacteria fate and transport. Idealised test cases were set up to study the effect of sediment settling of removing bacteria from the water column and the subsequent re-suspension of bacteria from the bed, as well as the vertical bacteria concentration distribution under equilibrium conditions.

(7) Numerical model application to real estuary

The sediment-bacteria interaction model was then applied to predict the fate and transport of bacteria in the Severn Estuary, UK. The Severn Estuary has the second highest tidal range in the world with spring tidal ranges of 14m and also it is well known for its significant suspended sediment levels. For this application the model was firstly calibrated against available data set and then the model was run for different scenarios to investigate the effects of different hydro-environmental conditions on the bacteria distributions in the Severn Estuary.

(8) Refinement of numerical model to investigate influence of a tidal barrage on bacterial levels

Tidal energy provides great potential for renewable energy to satisfy current energy demand and reduce greenhouse gases. Various methods of capturing tidal energy are being exploited for the Severn Estuary including: a tidal barrage, a tidal impoundment and tidal stream turbines. These proposed schemes will all impact on hydrodynamic parameters to varying degrees, which, in turn will affect the sediment transport and water quality indicator levels and distributions. In this study the refined numerical models have been further refined to investigate the impact of the tidal barrage on the hydro-environmental characteristics of the Bristol Channel and the Severn Estuary, with the numerical model refinements being generic and applicable to other sites.

1.3 Outline of Thesis

The detail of this thesis is summarised as follow. Chapter 1 introduces the background to water quality modelling and the objectives of this study. Chapter 2 reviews current developments in hydrodynamic, sediment transport and bacterial modelling. Chapter 3 outlines the hydrodynamic and solute transport governing equations, and discusses the different terms of these equations. Chapter 4 presents the development of both the two-dimensional and three-dimensional conceptual sediment-bacteria interaction models. In Chapter 5 the numerical methods adopted in this study are described and in Chapter 6 the model test cases and the idealised model applications are discussed. In Chapter 7 the models developed have been applied to the Bristol Channel and Severn Estuary, where extensive field data exist. Chapter 8 draws conclusions from the developments and recommends studies for further research.

Chapter 2

Literature Review

2.1 Hydrodynamic Modelling

Prior to modelling the sediment transport processes and the fate of faecal indicator bacteria levels in estuarine and coastal waters, the hydrodynamic features of the flow fields, such as water elevations and velocity components must be predicted. This is undertaken through the hydrodynamic model being used to solve the governing hydrodynamic equations.

The Navier-Stokes equations govern unsteady turbulent flow in coastal and estuarine waters, with the numerical procedures used to solve these equations being called direct numerical simulation (DNS). However, the storage capacity and speed of present day computers is still not sufficient to allow a solution for any practically relevant turbulent flow (Rodi 2000, Tannehill et al 1997). Presently, the Navier-Stokes equations are averaged over time and these time-averaged equations are referred to as Reynolds averaged Navier-Stokes equations (RANS), which were first proposed by Osborne Reynolds. This time-averaging process introduces new terms, known as the Reynolds stress or apparent stress terms into the equations, which require turbulent models to close the system of equations. Details about the various turbulence models and their application in hydraulics can be found in Rodi (2000). According to the number of transport equations used for the turbulence quantities to evaluate the eddy viscosity, a turbulence model can be classified in to three categories: zero-equation

models, which specify both the length and velocity scales using algebraic relation; one-equation models, which use an additional partial differential equation for the velocity scale and specify the length scale algebraically; and two-equation models, which use one partial differential equation for the velocity scale and one for the length scale. Among these models, the zero-equation models (such as the mixing length model) and the two-equation models (such as the $k - \varepsilon$) are most widely used (Sotiropoulos 2005 , Rodi 2000).

In modelling estuarine and coastal waters normally hydrostatic pressure can be assumed, which means the pressure is balanced by the gravity (Blumberg and Mellor 1987). Therefore, the vertical advection must be much smaller than the pressure gradient and gravitational acceleration (Lin and Falconer 1997b). This can considerably simplify the equations and numerical solutions (Vreugdenhil 1994). Applying the kinematic boundary condition on the free surface, the hydrodynamic equations can be further simplified by integrating over the water column. The resulting depth-integrated equations are called the shallow water equations (SWEs), which are broadly used to describe the estuarine and coastal waters (Liang et al 2006). Hydrodynamic models can be divided into: one-dimensional, two-dimensional and three-dimensional models. Normally for river modelling one-dimensional models are used. Depth integrated two-dimensional models are generally used for estuarine and nearshore coastal waters and two-dimensional laterally averaged models are generally used for narrow deep water bodies. For deep and large water bodies where the vertical scales can not be neglected then a three-dimensional model should be used.

In hydrodynamic modelling, the theory is now generally undisputed and the quality of

the numerical solution is the more critical aspect (Falconer et al 2001). Therefore research efforts on numerical schemes and their performances have developed significantly in recent years, such as the TVD-MacCormack scheme developed by Liang et al (2006, 2007) to simulate rapid varying flooding flows.

2.2 Sediment Transport Modelling

Sediment transport in estuarine and coastal water bodies is governed by the sediment particle properties, settling velocity and the hydrodynamic properties of the flow (i.e. velocity or flow field). Suspended sediments in the water column are transported with the flow and will tend to settle out onto the bed due to gravity. The bottom sediments may also be entrained and suspended due to increased levels of turbulence and increased bed shear stresses. In recent years there has been a growing interest in the need to predict sediment transport fluxes in estuarine waters more accurately, there has also been an increased interest directed towards how water pollutants and bacteria interact with solid matter, such as inorganic sediments (Chapra 1997). The high adsorption ability of fine suspended matter in the water column, towards chemical constituents and bacteria, enable fine sediments to act as a means of carrying, or transporting contaminants along the flow field, and with consequential implications for related water quality problems (Mehta et al 1989). Sediment is generally classified as being either cohesive or non-cohesive in nature. In generally, sediment is described as being cohesive if the particle diameter is less than about 0.063mm, with the particles having cohesive properties due to electronic forces compared with gravity forces acting between the particles (van Rijn 1993).

2.2.1 Settling Velocity

The settling velocity of a single sphere sediment particle can be derived by balancing the gravity and drag force (van Rijn 1993, Chien and Wan 1999):

$$\frac{1}{2}C_D\rho w_s^2 \cdot \frac{1}{4}\pi d_s^2 = \frac{1}{6}(\rho_s - \rho)gd_s^3 \quad (2.1)$$

This gives:

$$w_s = \sqrt{\frac{4(s_\rho - 1)gd_s^3}{3C_D}} \quad (2.2)$$

where C_D = drag coefficient, d_s = sphere diameter, ρ = water density, s_ρ = specific gravity.

There are different formulae for evaluating the settling velocity for natural sediments, in which the formula of Van Rijn (1993) is now still widely used, given as follows:

$$w_{s,m} = \begin{cases} \frac{(s_\rho - 1)gD_s^2}{18\nu} & (1 < D_s \leq 100\mu m) \\ \frac{10\nu}{D_s} \left[\left(1 + \frac{0.01(s_\rho - 1)gD_s^3}{\nu^2} \right)^{0.5} - 1 \right] & (100 < D_s \leq 1000\mu m) \\ 1.1[(s_\rho - 1)D_s]^{0.5} & (D_s > 1000\mu m) \end{cases} \quad (2.3)$$

where D_s = characteristic particle size, ν = kinematic viscosity coefficient.

The fall velocity is strongly reduced when the sediment concentrations are larger than 10,000mg/l (Van Rijn 1993), which is called hindered settling. These effects are incorporated in the following relationship for the settling velocity (Van Rijn 1993, Tetra Tech 2002):

$$w_s = w_{s,m} \left(1 - \frac{s}{\rho_s} \right)^n \quad (2.4)$$

where s = suspended sediment concentration, ρ_s = sediment density, n = a coefficient

for normal flow condition is about 4 (Van Rijn 1993).

For cohesive sediment, due to the flocculation processes the individual cohesive particles aggregate to form larger size flocs which increases settling velocity of individual particles (Mehta et al 1989). The settling velocity of individual flocs can be obtained from equation (2.2) by using floc diameter D_f to replace the sphere diameter, based on the balancing of the gravity and drag forces for a single floc (Winterwerp and Van Kesteren 2004).

The settling velocities of cohesive sediment are affected by sediment concentrations (Mehta 1993) and generally fall within the following three ranges:

(i) Free settling ($s < s_1 = 0.1 - 0.3 \text{ g/l}$)

$$w_s = \frac{(s_p - 1)gD_f^2}{18\nu} \quad (2.5)$$

(ii) Flocculation settling ($s_1 < s < s_2 = 0.3 - 10 \text{ g/l}$)

$$w_s = k_1 s^{\frac{4}{3}} \quad (2.6)$$

where k_1 is an empirical coefficient.

(iii) Hindered settling ($s > 10 \text{ g/l}$)

$$w_s = w_{s_0} [1 - k_2 (s - s_2)]^{4.66} \quad (2.7)$$

where w_{s_0} is the settling velocity at the concentration s_2 , and k_2 is the inverse of the concentration at which settling velocity is zero. These formulae have been adopted by Wu and Falconer (1998, 2000).

2.2.2 Deposition and Re-suspension of Cohesive Sediment

Cohesive sediments, also known as mud, in surface waters are typically composed of clay and non-clay minerals in the clay and silt size ranges, organic matters and small quantities of very fine sand (Mehta et al 1989). Cohesive sediment resistance to erosion depends on cohesive bounding forces between particles. Once the bed shear stress is lower than a critical value for deposition, then sediment settlement is dominant. If the bed shear stress is greater than critical erosion shear stress then erosion occurs. Both the critical shear stress for deposition and erosion depend on the bed characteristics. There is no current analytical theory available to determine these values and they are primarily determined from field experiment.

The exchange of cohesive sediment between water column and bed is controlled by the near bed flow conditions and the bed properties. Net deposition to the bed occurs when the flow-induced bed shear stress is less than the critical bed shear stress of deposition. The most widely used expression for the depositional flux is as following (Winterwerp and Van Kesteren 2004) which is originally proposed by Krone (1962):

$$D = \begin{cases} w_s s_b \left[1 - \frac{\tau_b}{\tau_{c,d}} \right] & \tau_b \leq \tau_{c,d} \\ 0 & \tau_b > \tau_{c,d} \end{cases} \quad (2.8)$$

where τ_b is the flow induced bed shear stress, $\tau_{c,d}$ is the critical shear stress for deposition and s_b is the near bed sediment concentration. The critical deposition bed shear stress is generally determined from laboratory or field experiments and the values are ranging from 0.06 to 0.11 N/m^2 (HydroQual 2002) and 0.05 to 0.1 N/m^2 (Winterwerp and Van Kesteren 2004). In the absence of site specific data, it can generally be treated as a calibration parameter (HydroQual 2002, Tetra Tech

2002).

When the bed shear stress is higher than the critical erosion shear stress, sediment will be re-suspended into the water column. The most widely used expression for the re-suspension flux is as following which was originally proposed by Partheniades (1963) and generalised in Winterwerp and Van Kesteren (2004):

$$E = \begin{cases} M \left[\frac{\tau_b - \tau_{c,e}(z,t)}{\tau_{c,e}(z,t)} \right]^{n_0} & \tau_b > \tau_{c,e} \\ 0 & \tau_b \leq \tau_{c,e} \end{cases} \quad (2.9)$$

where τ_b is the flow induced bed shear stress, $\tau_{c,e}$ is the critical shear stress for erosion, typical values are 0.1 to 5 N/m^2 and M is the erosion parameter which should vary with time and depth but in generally take as a constant. Typical values are 0.00001 to 0.0005 $kg/m^2/s$. The exponent n_0 is generally unity.

Equation (2.9) is generally more appropriate for well consolidated, homogeneous beds, in which case $\tau_{c,e}$ and M are more or less constant through the bed. For the bed with strong gradient in strength, an alternative formula was proposed by Mehta and Partheniades (1979) (see Winterwerp and Van Kesteren 2004):

$$E = \begin{cases} E_f \exp \left[n_1 \left(\frac{\tau_b - \tau_{c,e}(z)}{\tau_{c,e}(z)} \right)^{n_2} \right] & \tau_b > \tau_{c,e} \\ 0 & \tau_b \leq \tau_{c,e} \end{cases} \quad (2.10)$$

where E_f is the floc erosion rate (0.000003 to 0.005 $kg/m^2/s$), n_1 (generally 5.0 to 15.0) and n_2 (generally 0.5 to 1.0) are material dependent parameters.

2.2.3 Deposition and re-suspension of non-cohesive sediment

Non-cohesive sediment resistance to erosion depends on the particle size, shape and density. Total load of sediment transport is subdivided into two different modes of transport: bed load and suspended load (Falconer and Chen 1996). The bed load is defined as that part of the total load where the sediment is almost continuously in contact with the bed, being carried by rolling, sliding or hopping, whereas the suspended load is that part of the total load which is maintained in suspension for considerable periods of time by the turbulence of the flow (van Rijn 1993).

The motion of non-cohesive sediment from the bed begins when the bed shear stress τ_b exceeds a critical shear stress referred to as critical Shields' stress τ_{cr} . The widely used Shields' curve can be expressed using a dimensionless mobility parameter

$\theta = \frac{u_*^2}{(s_\rho - 1)gd_s}$ and a dimensionless particle parameter

$D_* = \left[\frac{(s_\rho - 1)g}{v^2} \right]^{\frac{1}{3}} d_s$ as the following form (Bonnefille 1963 , Yalin 1972) (see Van

Rijn 1993):

$$\theta_{cr} = \begin{cases} 0.24(D_*)^{-1} & D_* < 4 \\ 0.14(D_*)^{-0.64} & 4 \leq D_* < 10 \\ 0.04(D_*)^{-0.1} & 10 \leq D_* < 20 \\ 0.013(D_*)^{0.29} & 20 \leq D_* < 150 \\ 0.055 & D_* \geq 150 \end{cases} \quad (2.11)$$

When the bed shear velocity u_* ($u_* = \sqrt{\frac{\tau_b}{\rho}}$) is less than the critical shear velocity

$u_{*,cr} (u_{*,cr} = \sqrt{\frac{\tau_{cr}}{\rho}} = \sqrt{(s_p - 1)gd_s\theta_{cr}})$, no erosion or re-suspension takes place and there

is no bed load. Sediment in suspension in this condition will deposit to the bed. Once the bed shear velocity u_* exceeds the critical shear velocity $u_{*,cr}$ but remains less than the settling velocity w_s , sediment will be eroded from the bed and transported as bed load. Sediment in suspension under this condition will also deposit to the bed. When the bed shear velocity exceeds both the critical shear velocity and settling velocity, sediment will be transported as suspended load (van Rijn 1984a, b, 1993).

Many researchers have proposed mechanisms and formulae to calculate bed load and suspended load, such as Yalin (1972), Engelund and Hansen (1967), Einstein (1942) and van Rijn (1984a, b, 1993). In this study, the van Rijn formulae have been adopted in both two-dimensional and three-dimensional model.

2.3 Modelling Fate of Faecal Bacteria and Transport Processes in Surface Waters

2.3.1 Sources of Faecal Indicator Bacteria

Yang (2005) undertook a detailed literature review of enteric bacteria resources and summarised the potential faecal indicator bacteria sources as follows: waste water treatment works discharges, sewage overflows, surface runoff, upstream river flows, groundwater discharge, water creature faeces, inter-tidal beaches and bottom sediment re-suspension. Outfalls are known as point sources. This type of input can be easily quantified and its effect on the water quality of the receiving water body is relatively easy to investigate. Improvements to existing treatment works, such as employing secondary and tertiary treatments processes and the construction of long sea outfalls can significantly reduce the probability of water quality failing to comply with

standards in force (Wyer et al 1997). The importance of non-outfall sources has been noticed in recent years (Garcia-Armisen and Servais 2007, Yuan et al 2007). In the UK, the implementation of the Urban Wastewater Treatment Directive (91/271/EEC) and the Bathing Water Directive (76/160/EEC) have resulted in the removal of many of the dominant sources of faecal indicator bacteria, which previously masked non-outfall sources (Wyer et al 1997). Wyer et al (1997) showed that after the construction of new outfalls the imperative compliance with the Bathing Water Directive was still not achieved in their studies. Garcia-Armisen and Servais (2007) investigated the input of the point and non-point sources of faecal bacteria to the Seine river and found out that the non-point sources of faecal indicator bacteria would be dominant in a scenario in which activated sludge treatment works were complemented with UV treatment. In comparison with point sources, the effect of diffuse or non-outfall sources are difficult to quantify, as it is distributed over large areas and it is difficult to measure directly. Yuan et al (2007) integrated surface water model with GIS based land use model to investigate the effects of non-point sources on Bohai bay.

2.3.2 Effect of Sediment Transport on Faecal Indicator Bacteria

Faecal bacteria in estuarine and coastal waters can be considered to exist in two forms, either as free-living bacteria or attached to (or adsorbed onto) suspended sediment particles. Some key mechanisms act solely on one or the other of the two forms. For example, settling acts only on the particulate fraction. They can be transported and diffused within the flow in the free-living form, or attached to the sediments and then transported and diffused with sediments. The attached bacteria could settle out when the suspended particles deposit and re-suspend with the particles into the overlying

water column when the sediment is re-suspended. In predicting bacteria concentrations, the input bacteria can enter the water column through various means. They can be input directly in either the attached or free living form or in the form of re-suspension from the bed sediments. After input to the water column the two forms of bacteria transport can exist. They can be transported and diffused with in the flow in the free-living form, or be adsorbed on to the sediments and then be transported with the sediments or be desorbed.

In recent years there have been many studies undertaken about how bacteria exist in sediments and also these studies have frequently revealed higher number of indicator and pathogenic bacteria in sediment than in overlaying waters in both marine and fresh water systems (Hendricks 1971, Stephenson and Rychert 1982, Gary and Adams 1985, Burton et al 1987, Sherer et al 1992) [see in Jamieson et al 2004]. Gannon et al (1983) showed that sedimentation was an important element in the over all faecal bacteria disappearance. Suspended sediments can contribute to the disappearance of faecal bacteria from the water column in different ways. Attached faecal bacteria are adsorbed by the sediments from the water column under low energy flow conditions. Sediment concentrations also affect the light penetration rate in the water column, which further affects the decay rate of faecal bacteria. Allen et al (1987) revealed that water quality testing criteria in use at present do not take into account sediment as a potential reservoir of pathogens. The higher numbers of pathogenic levels occurring in sediments creates a potential health hazard from re-suspension and subsequent ingestion as there is increasing usage of recreational waters; therefore, There is a need to obtain additional information on the survival of indicator and pathogenic bacteria in sediments and the factors which contribute to their survival (Allen et al 1987).

Jamieson et al (2005a) conducted field experiment in Swan Creek, Canada by using tracer bacteria *E. coli* NAR and found appearance of the tracer bacteria in the water column coincided with increases in total suspended solids, which indicated that the *E. coli* NAR that were being re-suspended were sediment related. *E. coli* NAR is a kind of *E. coli* that is resistant to nalidixic acid, is non-pathogenic and rarely found in the natural environment and possesses survival characteristics similar to other *E. coli* (Jamieson et al 2004). Fries et al (2006) investigated the attachment of faecal indicator bacteria to particles in the Neuse river estuary, in eastern North Carolina, United States and found out that an overall average of 38% bacteria associated with particles. Stenstrom (1989) found 56-77% of enterococci attached to inorganic particles. Characklis et al (2005) found an attachment ratio of 45% for enterococci. [see Fries et al 2006].

Gannon et al (1983) and Auer and Niehaus (1993) showed that enteric bacteria are typically associated with fine sediment particles ($0.45-10 \mu m$) in aquatic environments. Grimes (1980) suggested that higher bacteria numbers occur in silty clay sediments rather than sandy sediments as a result of the surface area or particle charge differences; however, their results failed to show particle size effects.

Jamieson et al (2004) revealed that the decline in *E. coli* NAR concentrations in the bed sediment resembled first order kinetics, and the first order inactivation constant (k) was computed for the bed sediment tracer-bacteria at three study locations being from 0.006-0.03 /h. Howell et al (1996) conducted laboratory experiments to determine the first order inactivation constant for *E. coli* in bed sediments and found typical values in the range from 0.002-0.006/h. Jamieson et al (2005a) found that typical shear

stress for values for re-suspension of E. coli NAR Swan Creek ranged from 1.5 to 1.7 N/m², which is comparable with literature values for the critical shear stress for erosion of cohesive sediments.

2.3.3 Faecal Bacteria Decay Rate

In modelling bacteria concentration distributions, the decay term in the governing advection-diffusion equation is generally defined as a first order decay function, as given by Thomann and Mueller (1987):

$$\frac{dC_T}{dt} = -kC_T \quad (2.12)$$

where C_T = bacteria concentration

k = bacteria decay rate (day⁻¹).

The parameter T_{90} is defined as the time for 90% of the initial bacteria to die-off. This parameter can be obtained (in hours) using the analytical solution of the above equation and is related to the decay rate in the following form:

$$T_{90} = \frac{2.303}{k} \times 24 \quad (2.13)$$

This decay rate is influenced by many environmental factors, such as, sunlight intensity, temperature, salinity, sediment concentrations etc.

2.3.3.1 Irradiance

Gameson and Saxon (1967) showed that sunlight is one of the dominant parameters in determining coliform bacteria decay rates. Samples kept in the dark and others exposed to sunlight were immersed at depths down to 4m below the sea surface. The coliform die-off rate was found to be considerably greater for the samples exposed to sunlight. Further experiments were then conducted by Gameson and Gould (1975),

where they reported that the T_{90} value could be as short as 20 minutes in sunshine summer conditions, compared with dark conditions where values were typically 100 times longer. They also investigated the different wavelengths of the radiation responsible for the effects on the faecal bacteria die-off rates. The detailed experimental results can be found in Gameson and Gould (1975). Bellair et al (1977) carried out a series of experiments to investigate the relationship between sunlight intensity and the decay rate for bacteria. The experiments were conducted over a whole day and included recording sunlight intensity and T_{90} values for the bacteria. Under dark conditions the die-off rate was found to be small, but after the sun had risen (about 6am), die-off rates were found to start increasing until noon. The T_{90} values were found to vary from 1.9 hours just before noon to 40 hours during the night, see Figure 2.1.

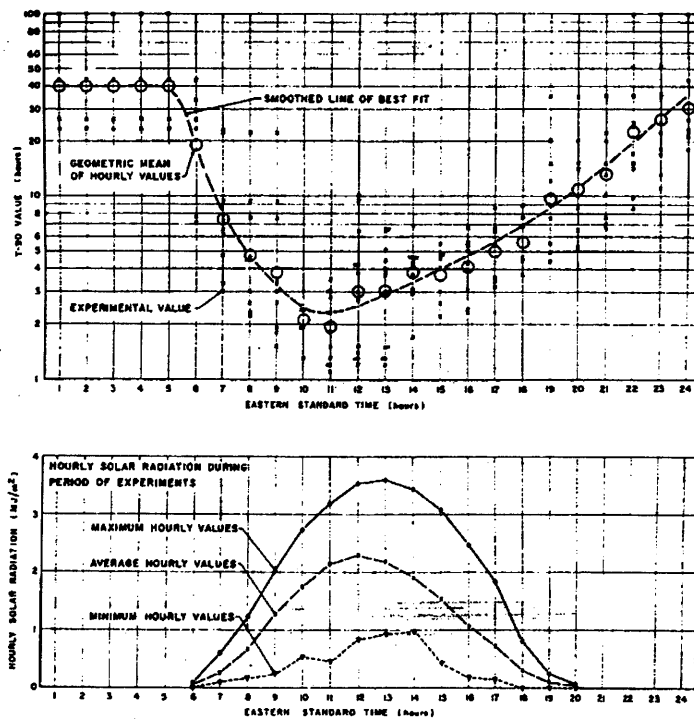


Figure 2.1: Summary of hourly T_{90} values and solar radiation (after Bellair 1977)

Auer and Niehaus (1993) expressed the irradiance mediated decay rate k_i as being proportional to the irradiance I in the form:

$$k_i = \alpha_i I \quad (2.14)$$

where $\alpha_i = 0.00824 \text{ cm}^2 / \text{cal}$

$$I = \text{Irradiance (cal / cm}^2 \text{ / day)}$$

The die-off rate was found to be approximately proportional to the intensity of the irradiance received by the sample at any period during the year (Gameson and Saxon 1967). The relationship between the solar irradiance and the faecal coliform die-off rate was found to be reasonably well expressed by a power law of the form:

$$k_i = \alpha_i I^{\beta_i} \quad (2.15)$$

where k_i = die off or decay rate due to sunlight (day^{-1})

$$I = \text{Irradiance (W/m}^2 \text{)}$$

α_i = Constant of proportionality

β_i = Slope of the \log_{10} plot of die-off against irradiance I .

Bellair et al (1977) conducted experiments to investigate the effect of light attenuation with depth. The light intensity at different depths was measured and it was found that the instantaneous light intensity at 0.5m, 2m and 5m depth was approximately 80, 40 and 10 percent of that at the surface respectively. Thomann and Muller (1987) introduced the extinction coefficient to describe the degree of light penetration, or conversely the extinction of incoming solar radiation. They found a relationship proportional to the water depth which was represented by the Lambert (or Beer-Lambert) law giving:

$$I = I_0 e^{-K_e z} \quad (2.16)$$

where I_0 = irradiance at water surface (W/m^2)

I = Irradiance at depth z (W/m^2)

z = Depth (m)

K_e = Vertical light extinction or attenuation coefficient (m^{-1})

Kirk (1984) estimated the light extinction coefficient, K_e , by using the measured absorption and scattering coefficients, giving an empirical relationship of the form:

$$K_e = \frac{a}{0.847} \left(1 + 0.17 \frac{b}{a}\right)^{\frac{1}{2}} \quad (2.17)$$

where a = absorption coefficient

b = scattering coefficient.

Pommepuy et al (1992) developed a relationship between the suspended matter concentration and light attenuation, with the results being illustrated in Figure 2.2.

(Wilkinson et al 1995).

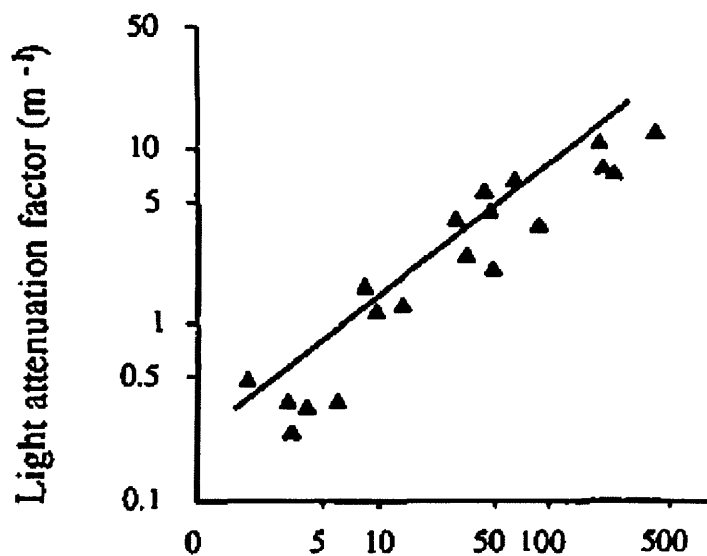


Figure 2.2 Light attenuation factor per meter depth against suspended matter concentration (Pommepuy et al 1992)

Kashefipour et al (2002b) analysed a number of studies in the literature and found that the mortality rate of faecal coliform bacteria was highly sensitive to the strength of

receiving radiance. A time varying formulation was developed to relate the faecal coliform bacteria decay rate to the level of solar radiation giving:

$$k = k_d + aI^b \quad (2.18)$$

k_d = night time decay rate

I = receiving solar radiation

a, b = empirical coefficients (with typical values of 0.236 and 0.629 respectively).

Wilkinson et al (1995) reviewed five studies to investigate the relationship between light intensity and faecal bacteria decay rates in fresh and sea waters under both laboratory and field conditions with light intensity expressed in W / m^2 and the decay rate in day^{-1} the corresponding results are summarized in Figure 2.3. It can also be seen from this graph that the decay rate in the sea water studies (Pommepeuy et al 1992, Bellair et al 1977) were generally higher than the decay rate in fresh water studies (Auer and Niehaus 1993, Sarikaya et al 1987, Evison et al 1987). The effect of salinity on decay rate will be detailed in later section.

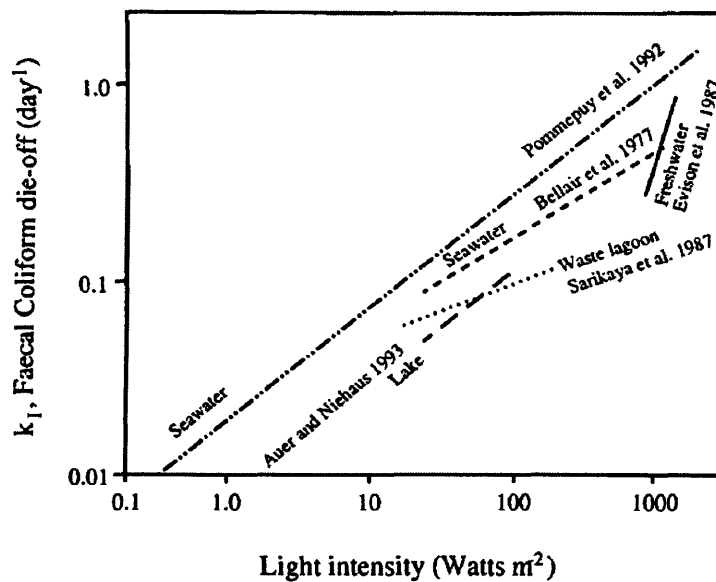


Figure 2.3 Faecal coliform die-off rates against light intensity (after Wilkinson et al 1995)

2.3.3.2 Temperature

Generally the relationship between temperature and decay rate is given as (Thomann and Mueller, 1987):

$$k_t = k_{20}\theta^{(T-20)} \quad (2.19)$$

where k_t = darkness condition decay rate at temperature T

k_{20} = the decay rate at T=20° C

θ = a dimensionless constant, which describes the relationship between the decay rate and temperature; typical values for θ for bacteria are about 1.07 (Thomann and Mueller, 1987)

T= water temperature (° C)

2.3.3.3 Salinity

Many researchers found that the decay rate for seawater is significantly greater than in freshwater (Anderson 1979, Solic and Krstulovic 1992 and Mancini 1978). Mancini (1978) conducted laboratory and field data studies and found that bacteria decay rates were typically 0.8/day and 1.4/day at 20 °C for fresh and sea water respectively.

Mancini (1978) analyzed the reported data of mortality rates for various percentages of sea water at 20° C, with the resulting correlation for sea water and coliform mortality rates being given as:

$$k_{salt} = 0.8 + 0.006(\%seawater) \quad (2.20)$$

2.3.3.4 Sediment

Chamberlin and Mitchell (1978) found that sedimentation could be a key factor

responsible for the reduction in faecal bacteria levels from the water column. Plummer et al (1987) confirmed that there are three types of bacteria occurring in natural water bodies including: (i) free living bacteria whose abundance is independent of turbidity, (ii) bacteria attached to suspended particles in the water column, and (iii) bacteria which have settled on the bed. The free-living bacteria move with the flow, while the attached bacteria move with the suspended particles, which can be deposited on the bed with the sediments, and also the turbulent flow can cause the particles with the attached bacteria to re-suspend into the overlying water body (Stapleton et al 2007).

The effects of sedimentation and irradiance and temperature on decay rate were summarized by Auer and Niehaus (1993) in the form given below:

$$k = k_d + k_i + k_{ss} \quad (2.21)$$

k_d = decay rate in darkness condition, includes effect of temperature, salinity, predation, etc (d^{-1})

k_i = decay rate as mediated by irradiance (day^{-1})

k_{ss} = decay rate mediated by sedimentation loss (day^{-1})

Decay rate mediated by sedimentation loss, k_{ss}

Auer and Niehaus (1993) stated that the sedimentation loss rate, k_s , may be calculated by dividing the sedimentation velocity by the distance across which the particles must settle before they are lost to the bottom:

$$k_{ss} = w_s / z_e$$

Where w_s is the sedimentation velocity and z_e is the depth in m, giving:

$$w_s = M_s / AtC_{ss}$$

where M_s = mass of sediment collected, (g)

A = area of the sediment trap opening, (m^2)

t = time of incubation,(d)

C_{ss} = water column sediment concentration (g/m^3)

2.4 Summary

In this chapter previous studies relating to the modelling of hydrodynamics, sediment transport and faecal bacteria fluxes have been reviewed. The faecal bacteria were found to be highly sediment-related and were also found to be effected by many environmental and natural factors, such as: irradiance, temperature, salinity and sediment concentration etc. There is a current lack of sophisticated numerical models to simulate sediment bacteria interaction processes and the dynamic decay rate of bacteria.

Chapter 3

Governing Hydrodynamic and Solute Transport Equations

3.1 Introduction

Coastal, estuarine and river waters provide a rich and diverse ecosystem and can be considered from the physical, chemical and biological perspective, such as the geometry and bathymetry, bed slope and roughness, hydrodynamic characteristics, mixing characteristics, water quality indicator concentrations and suspended solids levels. In the context of the increasing use of hydroinformatics tools, made by water engineers and environmental managers, it is important to be able to predict numerically the hydrodynamic, solute and suspended sediment transport processes in water system coastal and river basin systems (Thomann and Muller 1987 and Falconer et al 2005).

This chapter covers an overview of the governing model equations, which are based on the conservation law of mass, both fluid and solute, and Newton's second law of motion. The parameters describing the hydrodynamic and solute transport processes occurring specifically in coastal and river basin systems are also discussed. Details are given of the 3-D and 2-D equations used to undertake numerical model studies, together with the coefficients and empirical formulae used in such equations to obtain numerical simulations for planning and environmental water management impact assessment studies.

3.2 Hydrodynamic Equations

3.2.1 Three-Dimensional Reynolds Averaged Equations

The numerical models generally used to predict hydrodynamic, water quality and sediment transport processes in coastal, estuarine and river waters are based on first solving the governing hydrodynamic equations of motion. In a Cartesian co-ordinate system, the corresponding 3-D Reynolds averaged equations for mass and momentum conservation in the x-direction can be respectively written in a general form as (Falconer, 1993):

$$\frac{\partial u}{\partial x} + \frac{\partial v}{\partial y} + \frac{\partial w}{\partial z} = 0 \quad (3.1)$$

$$\underbrace{\frac{\partial u}{\partial t}}_1 + \underbrace{\frac{\partial u^2}{\partial x} + \frac{\partial uv}{\partial y} + \frac{\partial uw}{\partial z}}_2 = \underbrace{X}_3 - \underbrace{\frac{1}{\rho} \frac{\partial P_w}{\partial x}}_4 + \quad (3.2)$$

$$\underbrace{\frac{1}{\rho} \left\{ \frac{\partial}{\partial x} \left[\mu \frac{\partial u}{\partial x} - \overline{\rho u' u'} \right] + \frac{\partial}{\partial y} \left[\mu \frac{\partial u}{\partial y} - \overline{\rho u' v'} \right] + \frac{\partial}{\partial z} \left[\mu \frac{\partial u}{\partial z} - \overline{\rho u' w'} \right] \right\}}_5$$

where u, v and w are the time averaged velocity components in the x, y and z directions respectively, t is time, X is the body force in the x -directions, P_w is the pressure, ρ is the water density, μ is the viscosity and u', v' and w' are the fluctuating velocity components in the x, y and z directions respectively. The expressions $\overline{u'u'}$, $\overline{u'v'}$ and $\overline{u'w'}$ are known as the Reynolds or apparent stresses in the x -direction, and on the x, y and z planes respectively, These terms exist due to the turbulence of the flow and for laminar flow they are zero. For the numbered terms in equation (3.2), these terms refer to: the local acceleration (term 1), the advective (or

convective) acceleration (2), the body force (3), the pressure gradient (4) and the laminar and turbulent shear stresses (5), see Falconer (1993).

For the Reynolds stresses, Boussinesq (see Falconer 1993 and Goldstein 1938) proposed that they could be represented in diffusive manner as follows:

$$\begin{aligned}
 -\rho \overline{u'u'} &= \eta \left(\frac{\partial u}{\partial x} + \frac{\partial u}{\partial x} \right) \\
 -\rho \overline{u'v'} &= \eta \left(\frac{\partial u}{\partial y} + \frac{\partial v}{\partial x} \right) \\
 -\rho \overline{u'w'} &= \eta \left(\frac{\partial u}{\partial z} + \frac{\partial w}{\partial x} \right)
 \end{aligned} \tag{3.3}$$

where η = absolute eddy viscosity, ε = kinematic eddy viscosity = η / ρ . In general $\eta \gg \mu$, or $\varepsilon \gg \nu$.

In the y and z directions similar equations can be obtained for the conservation of momentum giving respectively:-

$$\frac{\partial v}{\partial t} + \frac{\partial vu}{\partial x} + \frac{\partial v^2}{\partial y} + \frac{\partial vw}{\partial z} = Y - \frac{1}{\rho} \frac{\partial P_w}{\partial y} + \tag{3.4}$$

$$\frac{1}{\rho} \left\{ \frac{\partial}{\partial x} \left[\mu \frac{\partial v}{\partial x} - \rho \overline{v'u'} \right] + \frac{\partial}{\partial y} \left[\mu \frac{\partial v}{\partial y} - \rho \overline{v'v'} \right] + \frac{\partial}{\partial z} \left[\mu \frac{\partial v}{\partial z} - \rho \overline{v'w'} \right] \right\}$$

$$\frac{\partial w}{\partial t} + \frac{\partial wu}{\partial x} + \frac{\partial wv}{\partial y} + \frac{\partial w^2}{\partial z} = Z - \frac{1}{\rho} \frac{\partial P_w}{\partial z} + \tag{3.5}$$

$$\frac{1}{\rho} \left\{ \frac{\partial}{\partial x} \left[\mu \frac{\partial w}{\partial x} - \rho \overline{w'u'} \right] + \frac{\partial}{\partial y} \left[\mu \frac{\partial w}{\partial y} - \rho \overline{w'v'} \right] + \frac{\partial}{\partial z} \left[\mu \frac{\partial w}{\partial z} - \rho \overline{w'w'} \right] \right\}$$

In considering the rotation of the earth, the body force term can be expressed in the

following term:

$$\begin{aligned} X &= fv \\ Y &= -fu \\ Z &= -g \end{aligned} \tag{3.6}$$

where: Coriolis coefficient $f = 2\omega \sin\theta_L$, $\omega =$ angular speed of earth's rotation $\approx 7.3 \times 10^{-5}$ rads/s i.e. $2\pi/(24 \times 3600)$ and $\theta_L =$ latitude of site and g is the gravity acceleration $g \approx 9.807 m/s^2$.

For flows in estuarine and coastal waters normally a hydrostatic pressure distribution can be assumed, since the vertical acceleration of the fluid is small compared to that of gravity acceleration, and the Navier-Stokes equation in the vertical z-direction can be reduced to give:

$$\frac{\partial P_w}{\partial z} + \rho g = 0 \tag{3.7}$$

At free surface the continuity of stress is assumed, i.e. the stresses in the water just below the surface are assumed to be the same as those in the air just above, giving for the pressure

$$P_w = P_a \tag{3.8}$$

where P_a is the atmospheric pressure.

Integrating from the surface, using boundary condition(3.8), and assuming a constant density gives

$$P_w(z) = \rho g(\xi - z) + P_a \tag{3.9}$$

From equation(3.9), the pressure gradients can be determined giving:

$$\frac{\partial P_w}{\partial x} \approx \rho g \frac{\partial \xi}{\partial x} \quad (3.10)$$

$$\frac{\partial P_w}{\partial y} \approx \rho g \frac{\partial \xi}{\partial y}$$

3.2.2 Two-Dimensional Depth Integrated Equations

For estuarine and coastal waters the vertical velocity component w is normally small in comparison to the horizontal velocity components u and v , and the continuity and momentum equations can be integrated over the depth $(h + \xi)$, using the notation given in Figure 3.1, and solved numerically to give the depth averaged velocity (or flow) field.

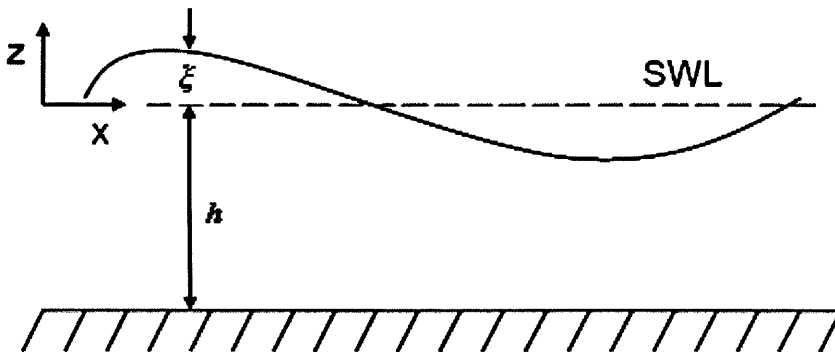


Figure 3.1 Co-ordinate system for two-dimensional depth integrated equations

Integrating equation (3.1) and expanding using Leibniz's rule, gives the depth integrated continuity equation, as detailed in Falconer (1993):

$$\frac{\partial \xi}{\partial t} + \frac{\partial p}{\partial x} + \frac{\partial q}{\partial y} = q_m \quad (3.11)$$

where $p = UH$, $q = VH$; U, V are the depth averaged velocity components in the x and y directions respectively; $q_m =$ external source or sink discharge per unit area.

Similarly, the momentum equations for an incompressible turbulent flow in a Cartesian co-ordinate system can be integrated over the depth to give the depth integrated momentum equations, with the derivation being detailed in Falconer (1993):

$$\frac{\partial UH}{\partial t} + \beta \left\{ \frac{\partial U^2 H}{\partial x} + \frac{\partial UVH}{\partial y} \right\} = fVH + gH \frac{\partial \xi}{\partial x} + \frac{\tau_{xw}}{\rho} - \frac{\tau_{xb}}{\rho} + \bar{\varepsilon} H \left(\frac{\partial^2 U}{\partial x^2} + \frac{\partial^2 U}{\partial y^2} \right) \quad (3.12)$$

$$\frac{\partial VH}{\partial t} + \beta \left\{ \frac{\partial UVH}{\partial x} + \frac{\partial V^2 H}{\partial y} \right\} = -fUH + gH \frac{\partial \xi}{\partial y} + \frac{\tau_{yw}}{\rho} - \frac{\tau_{yb}}{\rho} + \bar{\varepsilon} H \left(\frac{\partial^2 V}{\partial x^2} + \frac{\partial^2 V}{\partial y^2} \right) \quad (3.13)$$

where U, V = Depth average velocities in the x and y directions, H = Total depth of flow ($h + \xi$), β = Momentum correction factor for non-uniform vertical velocity profile, $\bar{\varepsilon}$ = Depth average eddy viscosity, τ_w = Wind stress and τ_b = Bed shear stress.

Momentum correction factor

The momentum correction factor β is defined as:

$$\beta = \frac{1}{U^2 H} \int_0^H u^2 dz \quad (3.14)$$

where U = depth average velocity, u = local velocity, H = total water depth and z = vertical co-ordinate

In practical model studies, and in the absence of extensive field data, β is generally either set to unity or a vertical velocity profile is assumed (see Falconer 1993).

For a Seventh Power law velocity profile assumption, i.e.

$$u = U_{max} \left(\frac{z}{H} \right)^{\frac{1}{7}} \quad (3.15)$$

Equation (3.14) gives a value of $\beta = 1.016$.

For a logarithmic vertical velocity profile assumption of the form:

$$u = \frac{u_*}{\kappa_{von}} \log_e(z) + u_* C_1 \quad (3.16)$$

where u_* = shear velocity = $\sqrt{\frac{\tau_0}{\rho}}$ (where τ_0 = boundary shear stress), κ_{von} = von

Karman's constant (=0.4) and C_1 = constant of integration, giving for the momentum correction coefficient:

$$\beta = 1 + \frac{g}{C^2 \kappa_{von}^2} \quad (3.17)$$

where C is the de Chezy bed roughness coefficient.

According to Koutitas and Gousidou-Koutita (1986) and Falconer and Chen (1991) the wind generated velocity profiles in semi-enclosed coastal domains can give a value for β of 1.2, based on a parabolic velocity distribution assumption for wind generated flow field.

Wind surface shear stress

The shear stress due to wind action on the water surface is usually expressed as a quadratic function, as by Dronkers (1964), and of the form:

$$\begin{aligned}\tau_{yw} &= \gamma_w \rho_a W_y \sqrt{W_x^2 + W_y^2} \\ \tau_{xw} &= \gamma_w \rho_a W_x \sqrt{W_x^2 + W_y^2}\end{aligned}\tag{3.18}$$

where γ_w = Air-water resistance coefficient, generally ≈ 0.0026 .

Wu (1969) has proposed a set of constants and expressions for the air-water resistance coefficient. They are the most widely used expressions for the air-water resistance coefficient. The expressions are given in a piecewise formulation of the following form:

$$\begin{aligned}\gamma_w &= 1.25 \times 10^{-3} W_s^{-0.2} & (W_s \leq 1m/s) \\ \gamma_w &= 0.5 \times 10^{-3} W_s^{-0.5} & (1m/s < W_s \leq 15m/s) \\ \gamma_w &= 2.6 \times 10^{-3} & (W_s > 15m/s)\end{aligned}$$

where ρ_a = air density, $= 1.29\text{kg/m}^3$, and W_x, W_y = wind velocity components in the in x, y directions, $W_s = \sqrt{W_x^2 + W_y^2}$ with the wind being measured at 10 m above water surface.

Bed shear stress

For a two-dimensional flow the bed shear stress can be represented in the form of a quadratic friction law, as given by Henderson (1966), as follows:

$$\begin{aligned}\tau_{xb} &= \rho g U \sqrt{U^2 + V^2} / C^2 \\ \tau_{yb} &= \rho g V \sqrt{U^2 + V^2} / C^2\end{aligned}\tag{3.19}$$

C = Chezy roughness coefficient.

where typically, $30m^{1/2} / s < C < 100m^{1/2} / s$

Alternatively, C can be evaluated from the Manning equation of the form:

$$C = \frac{H^{1/6}}{n} \quad (3.20)$$

where n = Manning roughness coefficient and typically 0.012 for smooth lined rivers to 0.04 for irregular and vegetated rivers. Although the Manning's coefficient is primarily used for one-dimensional rivers, this parameter has been widely used in two-dimensional flow fields with high level of accuracy often being obtained for complex flow fields (Falconer et al 2005).

Finally, the Colebrook-White equation can be used to give:-

$$C = \sqrt{\frac{8g}{f}} = -18 \log_{10} \left[\frac{k_s}{12H} + \frac{2.5C}{R_e \sqrt{8g}} \right] \quad (3.21)$$

where: f = Darcy-Weisbach bed resistance coefficient, k_s = equivalent sand grain roughness, and R_e = Reynolds number for open channel flow ($= \frac{4U_s H}{\nu}$), where U_s = fluid speed).

For fully rough flow this can be simplified to

$$C = \sqrt{\frac{8g}{f}} = -18 \log_{10} \left[\frac{k_s}{12H} \right]$$

The Colebrook-White equation is better for representing the bed roughness on shallow flood plains, such as wetland systems etc, since it includes Reynolds number flow effects at low Reynolds numbers and incorporates turbulent transitional flow as well as

turbulent rough flow (Falconer 1993 and Falconer and Owens 1987). In contrast, the equations that use the Chezy C and Manning n coefficients assume turbulent rough flow only.

Depth averaged eddy viscosity

The value of the depth averaged eddy viscosity $\bar{\varepsilon}$ can be determined either from field data or by assuming that bed generated turbulence dominates over free shear layer turbulence. Elder (1959) used the logarithmic velocity profile assumption and derived a minimum value for the coefficient for open channel flow to give:

$$\bar{\varepsilon} = \frac{k}{6} u_* H = 0.0667 u_* H \quad (3.22)$$

In order to know more about the depth averaged eddy viscosity and use an appropriate value a literature review has been undertaken, leading to the following main finding:

Fischer (1973) found the value of $\bar{\varepsilon}$ is generally greater than that given by Elder (1959) and by using laboratory floating particle experiments he found the value was more typically:

$$\bar{\varepsilon} = 0.15 u_* H \quad (3.23)$$

Fischer (1973) cited the measured variation of $\bar{\varepsilon}$ with depth in a number of experiments and his results match this value. Fischer et al (1979) found for most practical estuary studies that even this value was lower compared to measured data recorded in well-mixed estuaries where the value for $\bar{\varepsilon}$ varied from $0.42 u_* H$ to $1.61 u_* H$. Chang (1971) obtained results for $\bar{\varepsilon}$ varying from $0.62 u_* H$ to $1.2 u_* H$, as cited by Fischer (1973).

3.2.3 Three-Dimensional Layer Integrated Equations

For the three-dimensional layer integrated model, the water column was divided in to several layers as illustrated in Figure 3.2.

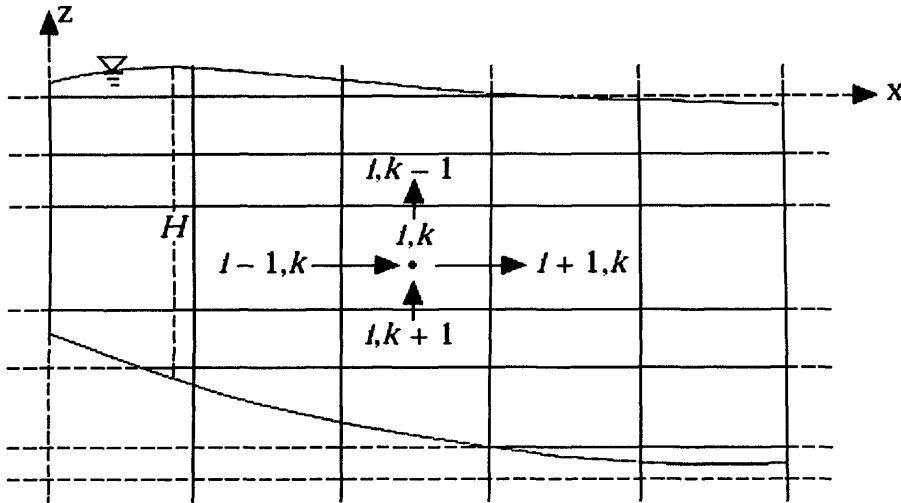


Figure 3.2 Co-ordinate system for layer integrated equations

For three-dimensional layer integrated model, each layer has a different velocity from that in the adjacent layers, with the governing equations for mass and momentum conservation being integrated over the layer thickness. As illustrated in Figure 3.2, there are three types of layer, including: a top layer ($k = 1$), a bottom layer ($k = k_{\max}$) and a middle layer. The top and bottom layer thicknesses are not uniform and define both the free surface and bed topography respectively. In contrast the middle layers have a uniform thickness (Lin and Falconer 1997b).

Continuity equation:

Integrating the continuity equation over the k_{th} layer gives:

$$\int_{k+\frac{1}{2}}^{k-\frac{1}{2}} \left(\frac{\partial u}{\partial x} + \frac{\partial v}{\partial y} + \frac{\partial w}{\partial z} \right) dz = 0 \quad (3.24)$$

which leads to :

$$\int_{k+\frac{1}{2}}^{k-\frac{1}{2}} \left(\frac{\partial u}{\partial x} + \frac{\partial v}{\partial y} \right) dz + w_{k-\frac{1}{2}} - w_{k+\frac{1}{2}} = 0 \quad (3.25)$$

where $k \pm 1/2$ refers to the vertical elevations of the interface between the $k+1, k$ and $k-1$ layers. Expanding equation (3.25), using Leibnitz rule (Hall 1987, and Lin and Falconer 1997b) and simplifying the resulting equation, then the layer integrated continuity equation gives the vertical velocity component w at the interface $k-1/2$:

$$w_{k-\frac{1}{2}} + \sum_{k=k}^{k_{\max}} \left[\frac{\partial(h_k u_k)}{\partial x} + \frac{\partial(h_k v_k)}{\partial y} \right] = 0 \quad (3.26)$$

At the water surface, the continuity equation reduces to:

$$\frac{\partial \zeta}{\partial t} + \sum_{k=1}^{k_{\max}} \left[\frac{\partial(h_k u_k)}{\partial x} + \frac{\partial(h_k v_k)}{\partial y} \right] = 0 \quad (3.27)$$

Momentum equations:

Integrating the momentum equation over the k_{th} layer gives:

$$\begin{aligned} & \int_{k+\frac{1}{2}}^{k-\frac{1}{2}} \left(\frac{\partial u}{\partial t} + \frac{\partial uu}{\partial x} + \frac{\partial uv}{\partial y} \right) dz + \left(u_{k-\frac{1}{2}} w_{k-\frac{1}{2}} \right) - \left(u_{k+\frac{1}{2}} w_{k+\frac{1}{2}} \right) \\ & = \int_{k+\frac{1}{2}}^{k-\frac{1}{2}} f_v dz - \int_{k+\frac{1}{2}}^{k-\frac{1}{2}} \frac{1}{\rho} \frac{\partial P_w}{\partial x} dz + \int_{k+\frac{1}{2}}^{k-\frac{1}{2}} \frac{1}{\rho} \left(\frac{\partial \tau_{xx}}{\partial x} + \frac{\partial \tau_{xy}}{\partial y} \right) dz \\ & + \frac{1}{\rho} \left(\tau_{xz} \Big|_{k-\frac{1}{2}} - \tau_{xz} \Big|_{k+\frac{1}{2}} \right) \end{aligned} \quad (3.28)$$

$$\begin{aligned}
& \int_{k+\frac{1}{2}}^{k-\frac{1}{2}} \left(\frac{\partial v}{\partial t} + \frac{\partial uv}{\partial x} + \frac{\partial v^2}{\partial y} \right) dz + \left(v_{k-\frac{1}{2}} w_{k-\frac{1}{2}} \right) - \left(v_{k+\frac{1}{2}} w_{k+\frac{1}{2}} \right) \\
&= - \int_{k+\frac{1}{2}}^{k-\frac{1}{2}} f u dz - \int_{k+\frac{1}{2}}^{k-\frac{1}{2}} \frac{1}{\rho} \frac{\partial P_w}{\partial y} dz + \int_{k+\frac{1}{2}}^{k-\frac{1}{2}} \frac{1}{\rho} \left(\frac{\partial \tau_{yx}}{\partial x} + \frac{\partial \tau_{yy}}{\partial y} \right) dz \\
&+ \frac{1}{\rho} \left(\tau_{yz} \Big|_{k-\frac{1}{2}} - \tau_{yz} \Big|_{k+\frac{1}{2}} \right)
\end{aligned} \tag{3.29}$$

From a hydrostatic pressure distribution assumption, the pressure gradient component can be expressed as given in equation(3.10), and applying the Boussinesq approximation of equation (3.3) for shear stress term, then the layer integrated momentum equations become:

$$\begin{aligned}
& \frac{\partial(u_k h_k)}{\partial t} + \beta_k \left(\frac{\partial(u_k^2 h_k)}{\partial x} + \frac{\partial(u_k v_k h_k)}{\partial y} \right) = f v_k h_k - g h_k \frac{\partial \zeta}{\partial x} \Big|_k \\
&+ \left[\frac{\partial}{\partial x} \varepsilon_h h_k \left(\frac{\partial u_k}{\partial x} + \frac{\partial u_k}{\partial x} \right) + \frac{\partial}{\partial y} \varepsilon_h h_k \left(\frac{\partial u_k}{\partial y} + \frac{\partial v_k}{\partial x} \right) \right]
\end{aligned} \tag{3.30}$$

$$\begin{aligned}
&+ (w_{k+\frac{1}{2}} u_{k+\frac{1}{2}}) - (w_{k-\frac{1}{2}} u_{k-\frac{1}{2}}) + \frac{1}{\rho} \left(\tau_{xz} \Big|_{k-\frac{1}{2}} - \tau_{xz} \Big|_{k+\frac{1}{2}} \right) \\
& \frac{\partial(v_k h_k)}{\partial t} + \beta_k \left(\frac{\partial(u_k v_k h_k)}{\partial x} + \frac{\partial(v_k^2 h_k)}{\partial y} \right) = -f u_k h_k - g h_k \frac{\partial \zeta}{\partial y} \Big|_k \\
&+ \left[\frac{\partial}{\partial x} \varepsilon_h h_k \left(\frac{\partial v_k}{\partial x} + \frac{\partial v_k}{\partial y} \right) + \frac{\partial}{\partial y} \varepsilon_h h_k \left(\frac{\partial v_k}{\partial y} + \frac{\partial v_k}{\partial y} \right) \right]
\end{aligned} \tag{3.31}$$

where u_k, v_k and w_k are the velocity components for the layer k in the x, y and z directions respectively, h_k is the thickness of layer k, ε_h is the horizontal eddy viscosity in the layer k and β_k is the momentum correction factor for the layer k.

For the surface layer (i.e. $k = 1$), then $(w_{k-\frac{1}{2}} u_{k-\frac{1}{2}})$ and $(w_{k-\frac{1}{2}} v_{k-\frac{1}{2}})$ can be eliminated by applying the kinematic free surface boundary condition. At the bed boundary $(w_{k+\frac{1}{2}} u_{k+\frac{1}{2}})$ and $(w_{k+\frac{1}{2}} v_{k+\frac{1}{2}})$ are zero due to the no-slip boundary condition.

Vertical and horizontal viscosity:

In modeling estuarine and coastal waters, the ratio of the vertical length scale to the horizontal length scale is generally very small. The eddy viscosity terms in vertical direction are generally more important than the corresponding horizontal viscosity terms in horizontal direction. In the current study, the horizontal eddy viscosity ϵ_h was assumed to be constant in the vertical, and its value was assumed to be equal to the depth-averaged eddy viscosity $\bar{\epsilon}$. Lin and Falconer (1997b) represented the vertical eddy viscosity ϵ_v by using a two-layer mixing length model suggested by (Rodi, 1984, 2000) of the form:

$$\epsilon_v = l^2 \left[\left(\frac{\partial u}{\partial z} \right)^2 + \left(\frac{\partial v}{\partial z} \right)^2 \right]^{\frac{1}{2}} \quad (3.32)$$

where l is mixing length, defined as :

$$l = k_{von} z \quad \text{for} \quad k_{von} z \leq 0.1H$$

$$l = 0.1H \quad \text{for} \quad k_{von} z > 0.1H$$

and k_{von} is von Karman's constant.

Surface wind shear stress:

At the water surface, the shear stress was equated directly to the wind shear stress giving:

$$\tau_{xz} = \gamma_w \rho_a W_y \sqrt{W_x^2 + W_y^2} \quad (3.33)$$

$$\tau_{yz} = \gamma_w \rho_a W_x \sqrt{W_x^2 + W_y^2}$$

with the parameters being as defined previously.

Bed shear stress:

By assuming a logarithmic velocity profile within the bottom layer, Lin and Falconer (1997b) and Hakimzadeh and Falconer (2007) represented bed shear stress in the following form, as proposed by French (1986):

$$\frac{\tau_b}{\rho} = u \sqrt{u^2 + v^2} \left[2.5 \ln \left(\frac{30d}{2.72k_s} \right) \right]^{-2} \quad (3.34)$$

where d is the thickness of the bottom layer, and k_s is roughness length.

3.3 Advective-Diffusion Equation

In modelling the flux of water quality indicators and suspended sediment concentrations within estuaries and coastal waters, the mass conservation equation can be written in general terms for any substance introduced into the water column, as given by Harleman (1966) and Falconer et al (2005):

$$\underbrace{\frac{\partial \varphi}{\partial t}}_1 + \underbrace{\frac{\partial u\varphi}{\partial x} + \frac{\partial v\varphi}{\partial y} + \frac{\partial w\varphi}{\partial z}}_2 + \underbrace{\frac{\partial}{\partial x} \overline{u'\varphi'} + \frac{\partial}{\partial y} \overline{v'\varphi'} + \frac{\partial}{\partial z} \overline{w'\varphi'}}_3 = \underbrace{\varphi_s + \varphi_d + \varphi_k}_4 \quad (3.35)$$

where u, v and w = time averaged velocity component in x, y and z direction respectively, φ = time averaged solute concentration, φ_s = source or sink solute input (e.g. an outfall), φ_d = solute decay or growth term, and φ_k = total kinetic transformation rate for solute. Equation (3.35) is referred to as the advective-diffusion equation. Variable φ can be referred as salinity, sediment

concentration, or other water quality indicators. Here in this chapter only the general form of the advective-diffusion equation is discussed. The specific formats of this advective-diffusion equation for sediment and bacteria transport for this study will be detailed in Chapter 4. The numbered terms refer to: (1) local effects; (2) transport by advection; (3) turbulence effects; and (4) source (or sink) terms, including decay (or growth); and kinetic transformation effects.

The cross product terms $\overline{u'\varphi'}$, $\overline{v'\varphi'}$ and $\overline{w'\varphi'}$ represent the flux due to the turbulent fluctuations. By analogy with Fick's law of diffusion, which assumes that the mass flux is proportional to the gradient of the mean concentration and the flux is in the direction of decreasing concentration (Harleman 1966), the turbulence diffusion effect can be expressed in following:

$$\left. \begin{aligned} \overline{u'\varphi'} &= -D_{tx} \frac{\partial \varphi}{\partial x} \\ \overline{v'\varphi'} &= -D_{ty} \frac{\partial \varphi}{\partial y} \\ \overline{w'\varphi'} &= -D_{tz} \frac{\partial \varphi}{\partial z} \end{aligned} \right\} \quad (3.36)$$

where D_{tx}, D_{ty}, D_{tz} = turbulent diffusion coefficients in x, y, z directions. For well-mixed estuarine and river flows it is common to assume isotropic turbulence and to approximate the horizontal diffusion terms to the depth mean coefficients as given by Fischer (1973):

$$D_{tx} = D_{ty} = 0.15u_*H \quad (3.37)$$

For the vertical diffusion coefficient, it is common to assume a linear shear stress distribution and a logarithmic velocity profile which gives (Falconer et al 2005) and (Vieira, 1993):

$$D_{tz} = u_* \kappa_{\text{von}} z \left(1 - \frac{z}{H} \right) \quad (3.38)$$

The turbulent diffusion coefficients are often related to the turbulent eddy viscosity by Schmidt numbers through the following equation:

$$D_{tx} = \varepsilon_x / \sigma_x, \quad D_{ty} = \varepsilon_y / \sigma_y, \quad D_{tz} = \varepsilon_z / \sigma_z \quad (3.39)$$

where $\sigma_x, \sigma_y, \sigma_z$ = turbulent Schmidt number in x, y and z direction respectively, $\varepsilon_x, \varepsilon_y, \varepsilon_z$ = eddy viscosity in x, y and z direction respectively. Experiments have shown that the Schmidt number varies only little across any flow field and also little from flow to flow (Rodi 2000). Therefore many models make use of the Schmidt number as a constant, such as Lin and Falconer (1996) with values ranging from 0.5 to 1.0.

In solving for the depth integrated solute distribution, equation (3.36) can be substituted into equation (3.35) and then integrated over the depth by using the bed and kinematic free surface conditions, giving the general two-dimensional depth-integrated governing solute transport equation (Falconer and Chen 1996):

$$\frac{\partial \phi H}{\partial t} + \frac{\partial \phi UH}{\partial x} + \frac{\partial \phi VH}{\partial y} - \frac{\partial}{\partial x} \left[HD_{xx} \frac{\partial \phi}{\partial x} \right] - \frac{\partial}{\partial y} \left[HD_{yy} \frac{\partial \phi}{\partial y} \right] = H [\phi_s + \phi_d + \phi_k] \quad (3.40)$$

where ϕ = depth averaged solute concentration, and ϕ_s, ϕ_d, ϕ_k = Corresponding depth averaged value for $\varphi_s, \varphi_d, \varphi_k$ respectively, and D_{xx}, D_{yy} = Depth averaged horizontal dispersion and turbulent diffusion coefficients in the x, y direction respectively. The dispersion terms are due to the vertical non-uniformities of mean flow velocity.

Depth averaged horizontal dispersion and turbulent diffusion coefficient:

Falconer and Chen (1996) cited the following representation from Preston (1985):

$$D_{xx} = \frac{(D_l U^2 + D_t V^2) H g^{0.5}}{V_s C} + D_w$$

$$D_{yy} = \frac{(D_l V^2 + D_t U^2) H g^{0.5}}{V_s C} + D_w$$
(3.41)

where D_l = Depth average horizontal dispersion constant, D_t = Depth average turbulent diffusion constant, D_w = wind induced dispersion coefficient, $V_s = \sqrt{U^2 + V^2}$. Elder (1959) gave the minimum value of $D_l = 5.93$ and Fischer (1973) gave $D_l = 0.15$ based on analysing field data. However, in practice studies these values tend to be rather low compared with the measured value D_l and D_t ranging from 8.6 to 7500 and 0.42 to 1.61 respectively (Falconer and Chen 1996). In absence of field data Falconer et al (2005) have suggested that values of D_l and D_t 13.0 and 1.2.

3.4 Summary

The governing hydrodynamic and solute transport equations have been reviewed in this chapter. The two-dimensional and three-dimensional hydrodynamic and solute transport equations have been presented for the two- and three-dimensional numerical modelling studies. Different terms and parameters of the mass and momentum equations have been discussed and formalised.

Chapter 4

Development of Sediment-bacteria Interaction Conceptual Model

4.1 Introduction

Faecal bacteria in estuarine and coastal waters can be considered to exist in two forms, either as free-living bacteria within the water column, or attached to suspended particles. The bacteria can be transported and diffused within the water column in their free-living form, or they can be adsorbed onto the sediments and then transported and diffused with the sediments. The adsorbed bacteria can settle out when the suspended particles deposit on the bed and be re-suspended with the particles into the overlying water column when the sediment particles are re-suspended. These processes are illustrated in Figure 4.1. With the bacteria being transported by the water column, the bacteria can also decay and with this process being dynamic and dependent upon many environmental factors, such as light intensity, temperature, salinity and turbidity levels etc. However, there is a current lack of understanding of the whole processes of bacteria fluxes and diffusion in estuarine and coastal waters. Therefore, developing a methodology for describing these quantitative relationships is essential. In this chapter a new approach for modelling the fate and transport of bacteria concentrations is presented. Before describing further this approach it is first necessary to consider the formulation for the transport of both non-cohesive and cohesive sediment particles.

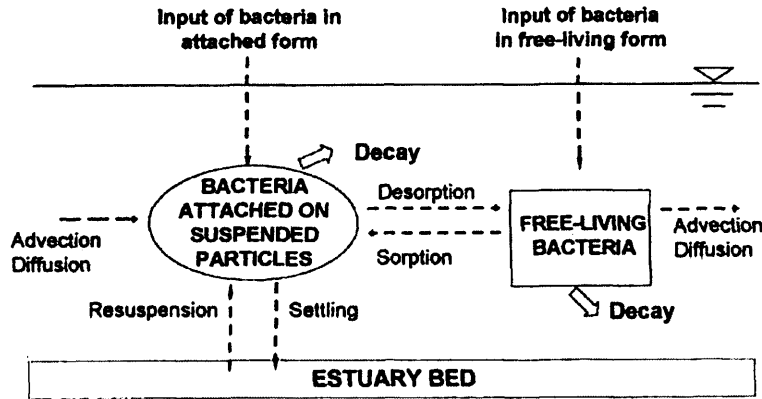


Figure 4.1 Bacteria fate and transport processes in estuarine waters

4.2 Sediment Transport Modelling

4.2.1 Suspended Sediment Transport

Sediment transport formulations for predicting suspended sediment fluxes in a three-dimensional numerical model are generally based on solving three-dimensional advective-diffusion equation. The three-dimensional advective-diffusion equation for sediment transport processes can be written in a similar manner to equation (3.35) giving:

$$\frac{\partial s}{\partial t} + \frac{\partial us}{\partial x} + \frac{\partial vs}{\partial y} + \frac{\partial (w - w_s)s}{\partial z} - \frac{\partial}{\partial x} \left(D_{tx} \frac{\partial s}{\partial x} \right) - \frac{\partial}{\partial y} \left(D_{ty} \frac{\partial s}{\partial y} \right) - \frac{\partial}{\partial z} \left(D_{tz} \frac{\partial s}{\partial z} \right) = 0 \quad (4.1)$$

where s = sediment concentration, w_s = sediment settling velocity.

In solving the three-dimensional sediment transport equation (4.1), an operator splitting algorithm is used to split the three-dimensional advective-diffusion equation into a vertical one-dimensional equation and a horizontal two-dimensional formulation, as proposed by Lin and Falconer (1996) and Wu and Falconer (2000). This will be detailed in Chapter 5.

The two-dimensional horizontal advective-diffusion equation for sediment transport

can be written as:

$$\frac{\partial s}{\partial t} + \frac{\partial us}{\partial x} + \frac{\partial vs}{\partial y} - \frac{\partial}{\partial x} \left(D_{tx} \frac{\partial s}{\partial x} \right) - \frac{\partial}{\partial y} \left(D_{ty} \frac{\partial s}{\partial y} \right) = 0 \quad (4.2)$$

The one-dimensional vertical advective-diffusion equation for sediment transport can be written as:

$$\frac{\partial s}{\partial t} + \frac{\partial (w - w_s s)}{\partial z} - \frac{\partial}{\partial z} \left(D_{tz} \frac{\partial s}{\partial z} \right) = 0 \quad (4.3)$$

With the vertical boundary conditions as following:

At the free surface the vertical sediment flux is zero

$$-w_s s - D_{tz} \frac{\partial s}{\partial z} = 0 \quad (4.4)$$

At the bed

$$-w_s s - D_{tz} \frac{\partial s}{\partial z} = E - D \quad (4.5)$$

where E is the erosion flux rate, D is the deposition flux rate, and $E - D =$ net sediment flux rate, which describe the exchange of sediments particles between water and sediment bed.

The net sediment flux rate for non-cohesive sediment can be expressed in the form (Van Rijn 1993):

$$E - D = w_s (s_{a,e} - s_a) \quad (4.6)$$

where $s_a =$ sediment concentration at a reference level (i.e. the concentration at an elevation 'a' above bed); and $s_{a,e} =$ equilibrium sediment concentration at reference level a. The equilibrium concentration is that value which occurs when the sediment flux vertically upwards from the bed due to turbulence is in equilibrium with the net sediment flux downwards due to the fall velocity (or gravity).

The equilibrium reference concentration used in this study was proposed by van Rijn

(1993), given as:

$$s_{a,e} = 0.015 \frac{D_{50} T^{1.5}}{a D_*^{0.3}} \quad (4.7)$$

D_{50} = sediment diameter of which 50% of the bed material is finer, T = transport stage parameter; D_* = particle parameter.

For cohesive sediment transport, the deposition sediment flux rate can be expressed in the form of equation (2.8) as follows:

$$D = \begin{cases} w_s s_a \left[1 - \frac{\tau_b}{\tau_{c,d}} \right] & \tau_b \leq \tau_{c,d} \\ 0 & \tau_b > \tau_{c,d} \end{cases}$$

The erosion flux rate can be calculated by using equation (2.9) as follows:

$$E = \begin{cases} M \left[\frac{\tau_b - \tau_{c,e}(z,t)}{\tau_{c,e}(z,t)} \right]^{n_0} & \tau_b > \tau_{c,e} \\ 0 & \tau_b \leq \tau_{c,e} \end{cases}$$

Sediment transport formulations for predicting suspended sediment fluxes in depth integrated two-dimensional numerical models are based on solving the depth integrated form of equation (4.1), which can be shown to be of the form:

$$\frac{\partial SH}{\partial t} + \frac{\partial SUH}{\partial x} + \frac{\partial SVH}{\partial y} - \frac{\partial}{\partial x} \left(HD_{xx} \frac{\partial S}{\partial x} \right) - \frac{\partial}{\partial y} \left(HD_{yy} \frac{\partial S}{\partial y} \right) = E - D \quad (4.8)$$

where S = depth-averaged suspended sediment concentration.

The depth-averaged net sediment flux rate for non-cohesive sediment can be expressed in the form (Yuan 2007):

$$E - D = \gamma w_s (S_e - \alpha S) \quad (4.9)$$

where w_s = particle settling velocity, γ = a profile factor given by the ratio of the

equilibrium bed concentration $s_{a,e}$, to the depth averaged equilibrium sediment concentration S_e . The depth averaged equilibrium sediment concentration evaluated using van Rijn (1984b) and the procedures were also detailed in Falconer and Chen (1996).

For modelling cohesive sediment transport the governing depth-integrated advective-diffusion equation (4.8) is used, but with the net sediment flux rate, being rewritten in the following form (Falconer and Chen 1996), which is simplified format of equation (2.8) and (2.9):

$$D = \begin{cases} w_s S \left[1 - \frac{\tau_b}{\tau_{c,d}} \right] & \tau_b \leq \tau_{c,d} \\ 0 & \tau_b > \tau_{c,d} \end{cases} \quad (4.10)$$

$$E = \begin{cases} M \left[\frac{\tau_b - \tau_{c,e}}{\tau_{c,e}} \right] & \tau_b > \tau_{c,e} \\ 0 & \tau_b \leq \tau_{c,e} \end{cases} \quad (4.11)$$

where τ_b = bed shear stress, $\tau_{c,d}$ = critical shear stress for deposition, $\tau_{c,e}$ = critical shear stress for erosion and M = empirical erosion constant.

Most of the parameters included in the above formulations are sensitive to the sediment characteristics locally. During numerical modelling studies of estuarine flows the value used must be chosen with extreme care. Typically values of the critical stress for erosion and deposition are given in van Rijn (1993) for a range of different mud types. For the empirical erosion coefficient M, reported values are

typically in the range of 0.00001 to 0.0005 for soft natural mud (Falconer and Chen 1996).

4.2.2 Bed load Transport

The bed load sediment flux is calculated using the following equation (van Rijn 1984a, b):

$$q_b = s_b u_b \delta_b = s_a u_a a \quad (4.12)$$

where s_b = bed load concentration, u_b = velocity of bed load particles, δ_b = saltation height, and u_a = effective particle velocity, given as:

$$u_a = \alpha u_b$$

where $u_b = [(1-s)gD_{50}]^{0.5} \times 1.5T^{0.6}$ and $\alpha = 2.3$.

4.3 Sediment-Bacteria Interaction Model

4.3.1 Partition of Bacteria between Sediment and Water

As shown in Figure 4.1, bacteria can exist in two phases, namely the adsorbed (or attached) and the free-living phases. The concentration of the free-living bacteria is defined as follows:

$$C_d' = \frac{CFU_d}{V_w} \quad (4.13)$$

where V_w is the volume of water and CFU_d (Colony Forming Units) is the amount of free-living bacteria indicator in the volume V_w .

The concentration of attached bacteria C_p is defined as:

$$C_p = \frac{CFU_p}{V_{w+s}} \quad (4.14)$$

where V_{w+s} is the volume of water and solids, which is referred to as the bulk volume,

and CFU_p is the amount of attached bacteria. Hence C_p represents the concentration of attached bacteria relative to the total volume of water and solids.

The porosity n_e is defined as the ratio of the volume of water to the bulk volume, as given by:

$$n_e = \frac{V_w}{V_{w+s}} \quad (4.15)$$

and C_d is the free-living bacteria concentration relative to bulk volume, as given by ;

$$C_d = \frac{CFU_d}{V_{w+s}} = n_e C'_d \quad (4.16)$$

The total bacteria concentration in the water column C_T is therefore given by:

$$C_T = C_d + C_p \quad (4.17)$$

For a given concentration of suspended solids, the quantity of bacteria on particles is often expressed as a mass specific concentration P (cfu/unit weight of suspended solids), so the volume specific concentration on particles C_p can be expressed as:

$$C_p = S \cdot P \quad (4.18)$$

where S is the suspended solid concentration, and P is the mass specific bacteria concentration, which can be defined as follows:

$$S = \frac{M_s}{V_{w+s}} \quad (4.19)$$

$$P = \frac{CFU_p}{M_s} \quad (4.20)$$

where M_s is the mass of suspended sediment.

Chapra (1997) expressed the tendency of bacteria to attach to particles by using a partition coefficient of the form:

$$K_D = \frac{P}{C_d} \quad (4.21)$$

Assuming that the rate at which bacteria adsorb and desorb from the particulate matter is fast, then a local equilibrium can be assumed to give:

$$C_T = C_d + K_D \cdot S \cdot C_d \quad (4.22)$$

which can be solved to give:

$$C_d = f_d C_T \quad (4.23)$$

where

$$f_d = \frac{1}{1 + K_D S} \quad (4.24)$$

and f_d is the fraction of bacteria that is free-living in the water column.

For the attached bacteria, we have:

$$C_p = f_p C_T \quad (4.25)$$

where

$$f_p = \frac{K_D S}{1 + K_D S} \quad (4.26)$$

and:

$$f_p + f_d = 1 \quad (4.27)$$

4.3.2 Exchange of Bacteria in Sediment-water Interface

Bacteria settlement

One of the effects of sediment transport on the adsorbed bacteria is the settling of sediment which takes the adsorbed bacteria out of the water column to the bed sediments. The settlement flux of bacteria from the water column to the bed sediments F_{dep} , can be expressed as:

$$F_{dep} = q_{dep}P \quad (4.28)$$

where q_{dep} = sediment deposition flux ($kg / m^2 / s$), $P = \frac{c_p}{s}$ = attached bacteria concentration on suspended sediment ($cfu / 0.1g$)

Bacteria re-suspension

The re-suspension of bacteria from the bed sediments to the water column F_{ero} , can be expressed as:

$$F_{ero} = q_{ero}P_b \quad (4.29)$$

where: P_b = bacteria concentration on bed sediments ($cfu / 0.1g$), q_{ero} = sediment re-suspension flux rate ($kg / m^2 / s$).

To summarise, the net bacteria flux F_{net} , due to settling and re-suspension of the sediments can be expressed as:

$$F_{net} = \max(q_{ero}, 0)P_b + \min(-q_{dep}, 0)P \quad (4.30)$$

Bacteria concentrations in the bed sediment

The concentration of bacteria on the bed sediment P_b , varies depending on the exchange of bacteria between the water column and the bed sediments. Another reduction in the bed sediment concentration arises as a result of the decay of the bacteria in the bed sediments. Assuming that the deposited sediments and the bed sediments are well mixed immediately after deposition, then the exchange rate of bed bacteria concentration can be expressed in the following form:

$$\frac{dP_b}{dt} = \frac{q_{dep}}{M_b}(P - P_b) - k_b P_b \quad (4.31)$$

where M_b = mass of the bed sediment per unit area, k_b = bacteria decay rate in bed sediment.

Likewise, in equation(4.31), the mass of bed sediments per unit area M_b also varies temporarily as given by:

$$\frac{dM_b}{dt} = q_{dep} - q_{ero} \quad (4.32)$$

4.3.3 Governing Equations for Faecal Bacteria Transport Processes

Free-living bacteria transport

The fate and transport of free-living bacteria can be described by the following three-dimensional advection-diffusion equation:

$$\begin{aligned} & \frac{\partial c_d}{\partial t} + \frac{\partial uc_d}{\partial x} + \frac{\partial vc_d}{\partial y} + \frac{\partial wc_d}{\partial z} \\ & - \frac{\partial}{\partial x} \left(D_{tx} \frac{\partial c_d}{\partial x} \right) - \frac{\partial}{\partial y} \left(D_{ty} \frac{\partial c_d}{\partial y} \right) - \frac{\partial}{\partial z} \left(D_{tz} \frac{\partial c_d}{\partial z} \right) \\ & = c_o^d + c_t^d - kc_d \end{aligned} \quad (4.33)$$

where c_d = free-living faecal bacteria concentration, c_o^d = source or sink of free-living bacteria; and c_t^d = transformation term defining the desorption of attached bacteria to the free-living form and vice versa; and k = the decay rate of bacteria in water column.

For a two-dimensional modelling study, the fate and transport of free-living bacteria can be described by the following two-dimensional depth integrated advection-diffusion equation:

$$\begin{aligned}
& \frac{\partial C_d H}{\partial t} + \frac{\partial C_d U H}{\partial x} + \frac{\partial C_d V H}{\partial y} \\
& - \frac{\partial}{\partial x} \left(H D_{xx} \frac{\partial C_d}{\partial x} \right) - \frac{\partial}{\partial y} \left(H D_{yy} \frac{\partial C_d}{\partial y} \right) \\
& = C_o^d + C_t^d - k C_d H
\end{aligned} \tag{4.34}$$

where C_d = depth averaged free-living faecal bacteria concentration, C_o^d = source or sink of free-living bacteria; and C_t^d = transformation term defining the desorption of attached bacteria from sediments to the free-living form and vice versa; and k = the decay rate of bacteria in water column.

Equations (4.33) and (4.34) have been solved to predict bacteria concentration levels in most studies of bacteria transport modelling, with this representation having been proven to work properly for the case where sediment transport is not significant. However, for studies where sediment transport processes are significant, then solving these equations alone will not give accurate results, since the transport of bacteria through the process of sediment transport, via erosion and deposition, has not been included in the transport model.

Attached bacteria transport

In studying the transport of attached bacteria, this part of bacteria may be transported and diffused with the suspended sediments, as described by the following three-dimensional equation:

$$\begin{aligned}
& \frac{\partial c_p}{\partial t} + \frac{\partial u c_p}{\partial x} + \frac{\partial v c_p}{\partial y} + \frac{\partial (w - w_s) c_p}{\partial z} \\
& - \frac{\partial}{\partial x} \left(D_{ix} \frac{\partial c_p}{\partial x} \right) - \frac{\partial}{\partial y} \left(D_{iy} \frac{\partial c_p}{\partial y} \right) - \frac{\partial}{\partial z} \left(D_{iz} \frac{\partial c_p}{\partial z} \right) \\
& = c_o^p + c_t^p + c_b^p - k c_p
\end{aligned} \tag{4.35}$$

where c_p = attached bacteria concentration, c_o^p = source or sink of bacteria in attached form; and c_i^p = transformation term defining the adsorption of free-living bacteria to attached bacteria and vice versa; and c_b^p = source term defining attached bacteria from or to the bed sediment, for sediment erosion or deposition, respectively; k = the decay rate for bacteria in attached form in water column.

For two-dimensional modelling, the fate and transport of attached bacteria can be described by the following two-dimensional depth integrated advection-diffusion equation:

$$\begin{aligned} & \frac{\partial HC_p}{\partial t} + \frac{\partial UHC_p}{\partial x} + \frac{\partial VHC_p}{\partial y} \\ & - \frac{\partial}{\partial x} \left(HD_{xx} \frac{\partial C_p}{\partial x} \right) - \frac{\partial}{\partial y} \left(HD_{yy} \frac{\partial C_p}{\partial y} \right) \\ & = C_o^p + C_i^p + C_b^p - kC_p H \end{aligned} \quad (4.36)$$

where C_p = depth averaged attached bacteria concentration in water column, C_o^p = source or sink of bacteria in attached form; and C_i^p = transformation term defining the adsorption of free-living bacteria to attached bacteria form and vice versa; and C_b^p = source term defining attached bacteria from or to the bed sediments, for sediment erosion or deposition, respectively; k = the decay rate for bacteria in attached form.

Total bacteria transport

In order to predict bacteria concentrations correctly, both for free-living and attached bacteria, then the transport equation must be solved simultaneously for both bacterial components in the numerical model. However, there are difficulties in solving these

equations accurately since the transformation terms are difficult to quantify. The transform processes between the free-living and adsorbed bacteria are very complex, so it is almost impossible to quantify these terms. Wu et al (2001, 2005) pointed out that in modelling heavy metals there was a problem of using separate equations to model dissolved and particulate metals due to the complex nature of the transformation between the particulate and dissolved phase. Similar modifications can be made in the advection-diffusion equation for bacteria, by using $c_i^d = -c_i^p$ and $C_i^d = -C_i^p$ which can avoid calculating the transformation term.

Equations (4.33) and (4.35) can be added and setting $c_i^d = -c_i^p$ gives

$$\begin{aligned} & \frac{\partial c_r}{\partial t} + \frac{\partial uc_r}{\partial x} + \frac{\partial vc_r}{\partial y} + \frac{\partial wc_r}{\partial z} - \frac{\partial(w_s sP)}{\partial z} \\ & - \frac{\partial}{\partial x} \left(D_{tx} \frac{\partial c_r}{\partial x} \right) - \frac{\partial}{\partial y} \left(D_{ty} \frac{\partial c_r}{\partial y} \right) - \frac{\partial}{\partial z} \left(D_{tz} \frac{\partial c_r}{\partial z} \right) \\ & = c_o^d + c_o^p + c_b^p - kc_r \end{aligned} \quad (4.37)$$

where c_r = concentration of total bacteria.

In solving the three-dimensional equation (4.37), an operator splitting algorithm, which is similar to that used to solve three-dimensional sediment transport equation, is used to split the three-dimensional advection-diffusion equation into a vertical one-dimensional and a horizontal two-dimensional set of equations.

The two-dimensional horizontal advective-diffusion equation for total bacteria transport can be written as:

$$\frac{\partial c_r}{\partial t} + \frac{\partial uc_r}{\partial x} + \frac{\partial vc_r}{\partial y} - \frac{\partial}{\partial x} \left(D_{tx} \frac{\partial c_r}{\partial x} \right) - \frac{\partial}{\partial y} \left(D_{ty} \frac{\partial c_r}{\partial y} \right) = c_o^d + c_o^p - kc_r \quad (4.38)$$

The one-dimensional vertical advective-diffusion equation for total bacteria transport can be written as:

$$\frac{\partial c_T}{\partial t} + \frac{\partial wc_T}{\partial z} - \frac{\partial (w_s s P)}{\partial z} - \frac{\partial}{\partial z} \left(D_{tz} \frac{\partial c_T}{\partial z} \right) = 0 \quad (4.39)$$

With the vertical boundary conditions as following:

At the free surface

$$-w_s s P - D_{tz} \frac{\partial c_T}{\partial z} = 0 \quad (4.40)$$

At the bed

$$-w_s s P - D_{tz} \frac{\partial c_T}{\partial z} = F_{net} \quad (4.41)$$

where F_{net} is the net bacteria flux rate, or net erosion or deposition rate, which describe the exchange of bacteria between bed sediment and overlay water.

The net bacteria flux rate can be expressed in the following form:

$$F_{net} = \max(q_{ero}, 0)P_b + \min(-q_{dep}, 0)P \quad (4.42)$$

Likewise, for a 2-D depth averaged model, adding equations (4.34) and (4.36) and using $C_i^d = -C_i^p$ gives

$$\begin{aligned} & \frac{\partial HC_T}{\partial t} + \frac{\partial UHC_T}{\partial x} + \frac{\partial VHC_T}{\partial y} \\ & - \frac{\partial}{\partial x} \left(HD_{xx} \frac{\partial C_T}{\partial x} \right) - \frac{\partial}{\partial y} \left(HD_{yy} \frac{\partial C_T}{\partial y} \right) \\ & = C_o^d + C_o^p + C_b^p - kC_T H \end{aligned} \quad (4.43)$$

where C_T = depth averaged total bacteria concentration. $C_b^p = F_{net}$, which is source term defining bacteria from or to the bed sediments, and F_{net} can be calculated by using equation (4.42).

By solving total bacteria transport equations, the total bacterial concentration level is

determined, wherein equations (4.23) and (4.25) can then be used to determine the free-living and attached bacteria levels.

4.4 Faecal Bacteria Decay Rate

4.4.1 Decay in Water Column

The decay rate of bacteria is highly dynamic and is affected by many environmental factors, such as light intensity, temperature, salinity, turbidity levels and pH values etc. In general the decay rate has historically been modelled as a constant over the simulation period in many model studies. In improving on this simplified representation of a complex process, Kashefipour et al (2002a) represented the variation in the light intensity effects on coliform decay by using different decay rates for day and night conditions. In a subsequent study, Kashefipour et al (2002b) developed an equation dynamically relating the decay rate to the light intensity and through the use of a neural network. This procedure improved on the accuracy of the model.

Following on from the literature review in Chapter 2, many researchers have found that the light intensity, temperature and salinity are major factors that affect bacterial decay rate. In this study, the decay rate is related to different environmental factors as detailed in this section.

Light Intensity

Solar irradiance is a dominant factor that causes the decay of bacteria in surface waters. Auer and Niehaus (1993) expressed the irradiance mediated death rate k_i as being proportional to the irradiance I in the following form:

$$k_i = \alpha_i I$$

In this study, this relationship has been used as an option to calculate the decay rate caused by light intensity. The light intensity attenuates over the water depth and is proportional to the water depth and may be represented by the Lambert (or Beer-Lambert) law (Thomann and Muller 1987):

$$I = I_0 e^{-K_e z}$$

where I_0 = irradiance at water surface (W/m^2), I = Irradiance at depth z (W/m^2), z = Depth (m), and K_e = Vertical light extinction or attenuation coefficient (m^{-1})

The extinction coefficient is generally calculated using the equation suggest by Xu et al (2002) in the following form:

$$K_e = 0.69 \times s + 24.09 \quad (4.44)$$

where s = suspended solids concentration in (mg/l)

Temperature

Generally the relationship between temperature and the decay rate is given as following:

$$k_t = k_{20} \theta^{(T-20)}$$

where k_t = Darkness condition decay rate at temperature T , k_{20} = the decay rate at $T=20^\circ\text{C}$, θ = a dimensionless constant which describe the relationship between the decay rate and temperature, typically the value of θ for bacteria is 1.07. (Thomann and Mueller, 1987), T = water temperature. ($^\circ\text{C}$)

Salinity

Mancini (1978) analyzed the reported data of mortality rates for various percentages of salinity in sea water at 20°C and the result of the correlation for sea water and

coliform mortality rates are given by:

$$k_{salt} = 0.8 + 0.006(\%seawater)$$

Chapra (1997) modified this equation to change the salinity unit from percent to ppt in the following form (see Bai 2004):

$$k_{salt} = 0.8 + 0.02S_{salt} \quad (4.45)$$

where S_{salt} = salinity in ppt.

4.4.2 Decay in Bed Sediment

In general, the decline in tracer bacteria concentrations in bed sediment resembles first order kinetics (Jamieson et al 2004 and Jamieson et al 2005a). Howell et al (1996) showed that the first order inactivation constant for E coli in bed sediments in the range from 0.002-0.006/h by conducting laboratory experiment. Jamieson et al (2004) computed the first order inactivation constant (k) for tracer-bacteria in bed sediments at three study locations, with the value ranging form 0.006-0.03 /h. Jamieson et al (2005a) illustrated that enteric bacteria can survive in bed sediment for up to 6 weeks and that inactivation of the tracer bacteria resembled a typical first-order decay. Some researchers even found the growth of faecal bacteria in bed sediment. In this study, the decay rate of faecal bacteria in the bed sediments was assumed to be constant.

4.5 Summary

Details are given of the development of a three- and two-dimensional sediment-bacteria interaction model, where the deposition and re-suspension of bacteria with sediments are included. Total bacteria concentrations were partitioned

by using a dynamic fraction ratio. The details of a dynamic decay rate model are also discussed. In next chapter the numerical methods and numerical treatment of the various terms and the corresponding boundary conditions will be outlined in more detail.

Chapter 5

Numerical Solution of Governing Equations

5.1 Introduction

Flow and solute transport processes can be described by sets of governing equations, as detailed in Chapter 3. These equations are based on the principles of conservation of mass and momentum and only have analytical solutions for idealised cases. Numerical methods provide a valuable tool to approximate the solution of these governing partial differential equations and such tools are increasingly important in environmental water management. In this chapter details are given of the numerical methods and procedures used to solve these equations.

5.2 Numerical Solution of Hydrodynamic Equations

5.2.1 Depth-integrated Equations

In the two-dimensional depth integrated model a regular mesh is used. The discrete variables are represented in a space staggered grid system, as shown in Figure 5.1, where water elevations are defined at the centre of grid squares, and velocity and bed levels below datum are described at centre of sides of the grid squares.

The Alternating Direction Implicit method is used to solve the governing equations. Each time step is divided into two half time steps. For the first half time step, from time level n to $n+1/2$, values of water elevation and velocity in the x direction are solved implicitly, while velocity components in the y direction are expressed

explicitly. For the second half time step, from time level $n+1/2$ to $n+1$, values of water elevation and velocity in the y direction are solved implicitly, while velocity components in the x direction are now expressed explicitly.

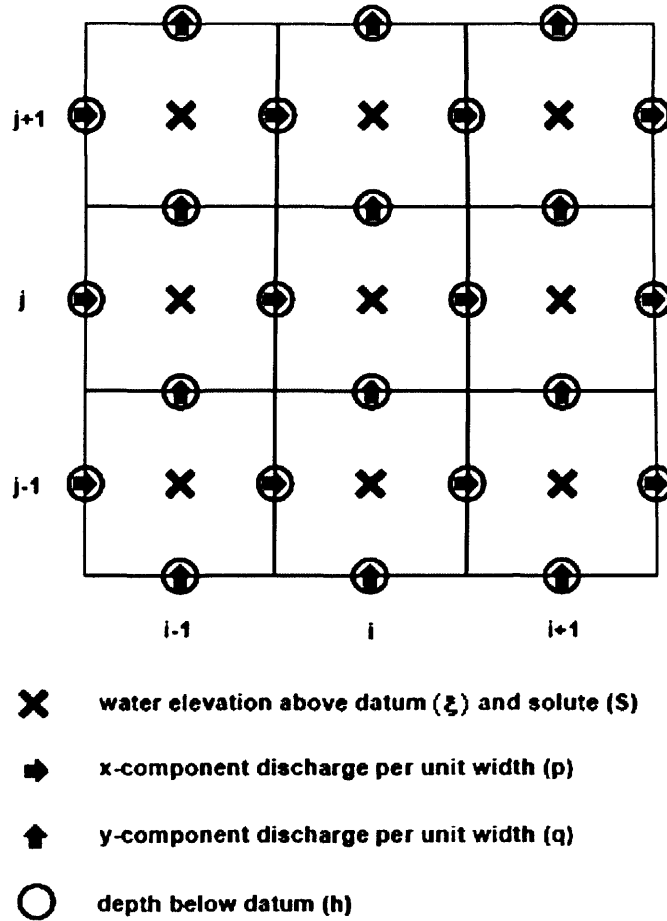


Figure 5.1 Description of space staggered grid system

The continuity equation (3.11) can be expressed in its finite difference form for the first and second half time steps respectively as follows:

$$\frac{2}{\Delta t} \left(\xi_{i,j}^{n+1/2} - \xi_{i,j}^n \right) + \frac{1}{\Delta x} \left(p_{i+1/2,j}^{n+1/2} - p_{i-1/2,j}^{n+1/2} \right) + \frac{1}{\Delta y} \left(q_{i,j+1/2}^n - q_{i,j-1/2}^n \right) = q_m \quad (4.46)$$

$$\frac{2}{\Delta t} \left(\xi_{i,j}^{n+1} - \xi_{i,j}^{n+1/2} \right) + \frac{1}{\Delta x} \left(p_{i+1/2,j}^{n+1/2} - p_{i-1/2,j}^{n+1/2} \right) + \frac{1}{\Delta y} \left(q_{i,j+1/2}^{n+1} - q_{i,j-1/2}^{n+1} \right) = q_m \quad (4.47)$$

where $i, j =$ grid point location in x and y directions respectively and superscripts n , $n + \frac{1}{2}$ and $n + 1$ represent time levels at time $t = n\Delta t$, $t = (n + \frac{1}{2})\Delta t$ and $t = (n + 1)\Delta t$ respectively, and Δt represents the time step for computations. It can be seen by summing the above two equations that the scheme is fully centred in both time and space over the whole time step, giving second order accuracy.

The x -direction momentum equation can be written in the following manner for the first half time step:

$$\begin{aligned}
& \frac{p_{i+\frac{1}{2},j}^{n+\frac{1}{2}} - p_{i+\frac{1}{2},j}^{n-\frac{1}{2}}}{\Delta t} + \beta \left[\frac{\left(\hat{U} \hat{p} \right)_{i+\frac{3}{2},j}^n - \left(\hat{U} \hat{p} \right)_{i-\frac{1}{2},j}^n}{2\Delta x} + \frac{\left(\bar{V} \hat{p} \right)_{i+\frac{1}{2},j+\frac{1}{2}}^n - \left(\bar{V} \hat{p} \right)_{i+\frac{1}{2},j-\frac{1}{2}}^n}{\Delta y} \right] \\
& = f q_{i+\frac{1}{2},j}^n - \frac{g H_{i+\frac{1}{2},j}^n}{2\Delta x} \left(\xi_{i+1,j}^{n+\frac{1}{2}} + \xi_{i+1,j}^{n-\frac{1}{2}} - \xi_{i,j}^{n+\frac{1}{2}} - \xi_{i,j}^{n-\frac{1}{2}} \right) + \frac{\rho_a}{\rho} \gamma W_x W_s \\
& \quad - \frac{g \left(p_{i+\frac{1}{2},j}^{n+\frac{1}{2}} + p_{i+\frac{1}{2},j}^{n-\frac{1}{2}} \right) \sqrt{\left(\hat{p}_{i+\frac{1}{2},j}^n \right)^2 + \left(\bar{q}_{i+\frac{1}{2},j}^n \right)^2}}{2 \left(H_{i+\frac{1}{2},j}^n C_{i+\frac{1}{2},j}^n \right)^2} \\
& \quad + \varepsilon H \left[\frac{\hat{U}_{i+\frac{3}{2},j}^n - 2 \cdot \hat{U}_{i+\frac{1}{2},j}^n + \hat{U}_{i-\frac{1}{2},j}^n}{\Delta x^2} + \frac{\hat{U}_{i+\frac{1}{2},j+1}^n - 2 \cdot \hat{U}_{i+\frac{1}{2},j}^n + \hat{U}_{i+\frac{1}{2},j-1}^n}{\Delta y^2} \right] \tag{4.48}
\end{aligned}$$

where \hat{U} denotes a value corrected by iteration, by setting

$$\hat{U}^n = \begin{cases} U^{n-\frac{1}{2}} \\ \frac{1}{2} \left(U^{n-\frac{1}{2}} + U^{n+\frac{1}{2}} \right) \end{cases} \tag{4.49}$$

\bar{V} represents a value obtained by averaging the corresponding values for the

surrounding grid points:

$$\bar{V}_{i+\frac{1}{2},j+\frac{1}{2}}^n = \frac{1}{2} \left(V_{i,j+\frac{1}{2}}^n + V_{i+1,j+\frac{1}{2}}^n \right) \quad (4.50)$$

and \bar{p} denotes a value obtained from the upwind algorithm where

$$\bar{p}_{i+\frac{1}{2},j}^n = \begin{cases} p_{i+\frac{1}{2},j-1}^n & \text{if } V_{i+\frac{1}{2},j}^n > 0 \\ p_{i+\frac{1}{2},j+1}^n & \text{if } V_{i+\frac{1}{2},j}^n < 0 \end{cases} \quad (4.51)$$

Similarly, the y direction momentum equation can be written for the second half time step as:

$$\begin{aligned} & \frac{q_{i,j+\frac{1}{2}}^{n+1} - q_{i,j+\frac{1}{2}}^n}{\Delta t} + \beta \left[\frac{\left(\hat{V} \hat{q} \right)_{i,j+\frac{3}{2}}^{n+\frac{1}{2}} - \left(\hat{V} \hat{q} \right)_{i,j-\frac{1}{2}}^{n+\frac{1}{2}}}{2\Delta y} + \frac{\left(\bar{U} \hat{q} \right)_{i+\frac{1}{2},j+\frac{1}{2}}^{n+\frac{1}{2}} - \left(\bar{U} \hat{q} \right)_{i-\frac{1}{2},j+\frac{1}{2}}^{n+\frac{1}{2}}}{\Delta x} \right] \\ & = -f \cdot p_{i,j+\frac{1}{2}}^{n+\frac{1}{2}} - \frac{gH_{i+\frac{1}{2},j}^{n+\frac{1}{2}}}{2\Delta y} \left(\xi_{i,j+1}^{n+1} + \xi_{i,j+1}^n - \xi_{i,j}^{n+1} - \xi_{i,j}^n \right) + \frac{\rho_a}{\rho} \gamma W_y W_s \\ & \frac{g \left(q_{i,j+\frac{1}{2}}^{n+1} + q_{i,j+\frac{1}{2}}^n \right) \sqrt{\left(q_{i,j+\frac{1}{2}}^{n+\frac{1}{2}} \right)^2 + \left(\bar{p}_{i,j+\frac{1}{2}}^{n+\frac{1}{2}} \right)^2}}{2 \left(H_{i,j+\frac{1}{2}}^{n+\frac{1}{2}} C_{i,j+\frac{1}{2}}^{n+\frac{1}{2}} \right)^2} \\ & + \bar{\varepsilon} H \left[\frac{\hat{V}_{i+1,j+\frac{1}{2}}^n - 2 \cdot \hat{V}_{i,j+\frac{1}{2}}^n + \hat{V}_{i-1,j+\frac{1}{2}}^n}{\Delta x^2} + \frac{\hat{V}_{i,j+\frac{3}{2}}^n - 2 \cdot \hat{V}_{i,j+\frac{1}{2}}^n + \hat{V}_{i,j-\frac{1}{2}}^n}{\Delta y^2} \right] \quad (4.52) \end{aligned}$$

Re-arranging equation (4.46) gives:

$$a_{2i-1} p_{i-\frac{1}{2},j}^{n+\frac{1}{2}} + b_{2i-1} \xi_{i,j}^{n+\frac{1}{2}} + c_{2i-1} p_{i+\frac{1}{2},j}^{n+\frac{1}{2}} = d_{2i-1} \quad (4.53)$$

where

$$a_{2i-1} = -\frac{\Delta t}{\Delta x}$$

$$b_{2i-1} = 2$$

$$c_{2i-1} = \frac{\Delta t}{\Delta x}$$

$$d_{2i-1} = 2\xi_{i,j}^n - \frac{\Delta t}{\Delta y} \left(q_{i,j+\frac{1}{2}}^n - q_{i,j-\frac{1}{2}}^n \right) + \Delta t q_m$$

Re-arranging equation (4.48) gives:

$$a_{2i} \xi_{i,j}^{n+\frac{1}{2}} + b_{2i} p_{i+\frac{1}{2},j}^{n+\frac{1}{2}} + c_{2i} \xi_{i+1,j}^{n+\frac{1}{2}} = d_{2i} \quad (4.54)$$

where

$$a_{2i} = -gH \frac{\Delta t}{\Delta x}$$

$$b_{2i} = 2 + \Delta t \frac{g \sqrt{\left(\hat{p}_{i+\frac{1}{2},j}^n \right)^2 + \left(\overline{q}_{i+\frac{1}{2},j}^n \right)^2}}{\left[(HC)_{i+\frac{1}{2},j}^n \right]^2}$$

$$c_{2i} = gH \frac{\Delta t}{\Delta x}$$

$$\begin{aligned}
d_{2i} = & \left(2 - \Delta t \frac{g \sqrt{\left(\hat{p}_{i+\frac{1}{2},j}^n \right)^2 + \left(\hat{q}_{i+\frac{1}{2},j}^n \right)^2}}{\left[(HC)_{i+\frac{1}{2},j}^n \right]^2} \right) p_{i+\frac{1}{2}}^{n-\frac{1}{2}} \\
& - gH \frac{\Delta t}{\Delta x} \left(\xi_{i+1,j}^{n-\frac{1}{2}} - \xi_{i,j}^{n-\frac{1}{2}} \right) \\
& - \beta \left[\frac{\Delta t}{\Delta x} \left((\hat{p}\hat{U})_{i+\frac{3}{2},j}^n - (\hat{p}\hat{U})_{i-\frac{1}{2},j}^n \right) + \frac{2\Delta t}{\Delta y} \left((\hat{p}\bar{V})_{i+\frac{1}{2},j+\frac{1}{2}}^n - (\hat{p}\bar{V})_{i+\frac{1}{2},j-\frac{1}{2}}^n \right) \right] \\
& + 2\bar{\varepsilon} H \left[\frac{\Delta t}{\Delta x^2} \left(\hat{U}_{i+\frac{3}{2},j}^n - 2\hat{U}_{i+\frac{1}{2},j}^n + \hat{U}_{i-\frac{1}{2},j}^n \right) + \frac{\Delta t}{\Delta y^2} \left(\hat{U}_{i+\frac{1}{2},j+1}^n - 2\hat{U}_{i+\frac{1}{2},j}^n + \hat{U}_{i+\frac{1}{2},j-1}^n \right) \right] \\
& + 2\Delta t \frac{\rho_a}{\rho} \gamma W_x W_s + 2\Delta t \cdot f \cdot q_{i+\frac{1}{2},j}^n
\end{aligned}$$

Similar re-arranging can be made to equation (4.47) and (4.52) gives:

$$a_{2j-1} q_{i,j-\frac{1}{2}}^{n+1} + b_{2j-1} \xi_{i,j}^{n+1} + c_{2j-1} q_{i,j+\frac{1}{2}}^{n+1} = d_{2j-1} \quad (4.55)$$

where

$$a_{2j-1} = -\frac{\Delta t}{\Delta y}$$

$$b_{2j-1} = 2$$

$$c_{2j-1} = \frac{\Delta t}{\Delta y}$$

$$d_{2j-1} = 2\xi_{i,j}^{n+\frac{1}{2}} - \frac{\Delta t}{\Delta x} \left(p_{i+\frac{1}{2},j}^{n+\frac{1}{2}} - p_{i-\frac{1}{2},j}^{n+\frac{1}{2}} \right) + \Delta t q_m$$

and

$$a_{2j} \xi_{i,j}^{n+1} + b_{2j} q_{i,j+\frac{1}{2}}^{n+1} + c_{2j} \xi_{i,j+1}^{n+1} = d_{2j} \quad (4.56)$$

where

$$a_{2j} = -gH \frac{\Delta t}{\Delta y}$$

$$b_{2j} = 2 + \Delta t \frac{g \sqrt{\left(\bar{p}_{i,j+\frac{1}{2}}^{n+\frac{1}{2}} \right)^2 + \left(\hat{q}_{i,j+\frac{1}{2}}^{n+\frac{1}{2}} \right)^2}}{\left[(HC)_{i,j+\frac{1}{2}}^{n+\frac{1}{2}} \right]^2}$$

$$c_{2j} = gH \frac{\Delta t}{\Delta y}$$

$$d_{2j} = \left(2 - \Delta t \frac{g \sqrt{\left(\bar{p}_{i,j+\frac{1}{2}}^{n+\frac{1}{2}} \right)^2 + \left(\hat{q}_{i,j+\frac{1}{2}}^{n+\frac{1}{2}} \right)^2}}{\left[(HC)_{i,j+\frac{1}{2}}^{n+\frac{1}{2}} \right]^2} \right) q_{i,j+\frac{1}{2}}^n$$

$$- gH \frac{\Delta t}{\Delta y} (\xi_{i,j+1}^n - \xi_{i,j}^n)$$

$$- \beta \left[\frac{2\Delta t}{\Delta x} \left((\bar{p}\bar{U})_{i+\frac{1}{2},j+\frac{1}{2}}^{n+\frac{1}{2}} - (\bar{p}\bar{U})_{i-\frac{1}{2},j+\frac{1}{2}}^{n+\frac{1}{2}} \right) + \frac{\Delta t}{\Delta y} \left((\hat{q}\hat{V})_{i,j+\frac{3}{2}}^{n+\frac{1}{2}} - (\hat{q}\hat{V})_{i,j-\frac{1}{2}}^{n+\frac{1}{2}} \right) \right]$$

$$+ 2\bar{\varepsilon} H \left[\frac{\Delta t}{\Delta x^2} \left(\hat{V}_{i+1,j+\frac{1}{2}}^{n+\frac{1}{2}} - 2\hat{V}_{i,j+\frac{1}{2}}^{n+\frac{1}{2}} + \hat{V}_{i-1,j+\frac{1}{2}}^{n+\frac{1}{2}} \right) + \frac{\Delta t}{\Delta y^2} \left(\hat{V}_{i,j+\frac{3}{2}}^{n+\frac{1}{2}} - 2\hat{V}_{i,j+\frac{1}{2}}^{n+\frac{1}{2}} + \hat{V}_{i,j-\frac{1}{2}}^{n+\frac{1}{2}} \right) \right]$$

$$+ 2\Delta t \frac{\rho_a}{\rho} \gamma W_y W_s - 2\Delta t \cdot f \cdot p_{i,j+\frac{1}{2}}^{n+\frac{1}{2}}$$

These equations can be expressed in a matrix form as follows:

locations as for the two-dimensional depth integrated model (see Figure 5.1).

The layer integrated governing equations are solved using a combined explicit and implicit scheme. The vertical diffusion terms were treated implicitly, whilst the remaining terms were treated explicitly (Lin and Falconer 1997b).

For the first half time step the depth integrated equations are first solved to obtain the water elevation field across the domain, as discussed in section 5.2.1. The layer integrated equations in the x direction are solved using the water elevation obtained from solving the depth integrated equations. Lin and Falconer (1997b) expressed the momentum equation in the x direction for the three-dimensional model as follows:

$$\frac{\partial(u_k h_k)}{\partial t} - \left[\left(\varepsilon_v \frac{\partial u}{\partial z} \right)_{k-\frac{1}{2}} - \left(\varepsilon_v \frac{\partial u}{\partial z} \right)_{k+\frac{1}{2}} \right] = S_{x0} \quad (4.58)$$

where S_{x0} represents the terms treated explicitly. The following is the finite difference representation for equation(4.58):

$$\begin{aligned} & \left((uh)_k^{n+\frac{1}{2}} - (uh)_k^{n-\frac{1}{2}} \right) \\ & - \Delta t \left(\frac{\varepsilon_v}{h} \right)_{k-\frac{1}{2}} \left[\left(u_{k-1}^{n+\frac{1}{2}} - u_k^{n+\frac{1}{2}} \right) + \left(u_{k-1}^{n-\frac{1}{2}} - u_k^{n-\frac{1}{2}} \right) \right] / 2 \\ & + \Delta t \left(\frac{\varepsilon_v}{h} \right)_{k+\frac{1}{2}} \left[\left(u_k^{n+\frac{1}{2}} - u_{k+1}^{n+\frac{1}{2}} \right) + \left(u_k^{n-\frac{1}{2}} - u_{k+1}^{n-\frac{1}{2}} \right) \right] / 2 = S_x \end{aligned} \quad (4.59)$$

where

$$S_x = ADV + COR + PRE + DIF + VTC$$

where:

$$ADV = -\frac{\Delta t}{\Delta x} \left[u' q_x \Big|_{i+1,j,k}^n - u' q_x \Big|_{i,j,k}^n + q_y \Big|_{i+\frac{1}{2},j+\frac{1}{2},k}^n u' \Big|_{i+\frac{1}{2},j+\frac{1}{2},k}^n - q_y \Big|_{i+\frac{1}{2},j-\frac{1}{2},k}^n u' \Big|_{i+\frac{1}{2},j-\frac{1}{2},k}^n \right]$$

$$COR = \Delta t \cdot f \cdot q_y \Big|_{i+\frac{1}{2},j,k}^n$$

$$PRE = -\frac{g\Delta t}{2\Delta x} h^n \Big|_{i+\frac{1}{2},j,k} \left[\xi_{i+1,j}^{n+\frac{1}{2}} + \xi_{i+1,j}^{n-\frac{1}{2}} - \xi_{i,j}^{n+\frac{1}{2}} - \xi_{i,j}^{n-\frac{1}{2}} \right]$$

$$DIF = \frac{\Delta t}{(\Delta x)^2} \left\{ \begin{aligned} & 2 \left[\varepsilon_h h^n \Big|_{i+1,j,k} \left(u'_{i+\frac{3}{2},j,k} - u'_{i+\frac{1}{2},j,k} \right) - \varepsilon_h h^n \Big|_{i,j,k} \left(u'_{i+\frac{1}{2},j,k} - u'_{i-\frac{1}{2},j,k} \right) \right] \\ & + \left[\varepsilon_h h^n \Big|_{i+\frac{1}{2},j+\frac{1}{2},k} \left(u'_{i+\frac{1}{2},j+1,k} - u'_{i+\frac{1}{2},j,k} \right) - \varepsilon_h h^n \Big|_{i+\frac{1}{2},j-\frac{1}{2},k} \left(u'_{i+\frac{1}{2},j,k} - u'_{i+\frac{1}{2},j-1,k} \right) \right] \\ & + \left[\varepsilon_h h^n \Big|_{i+1,j,k} \left(v_{i+\frac{3}{2},j,k} - v_{i+\frac{1}{2},j,k} \right) - \varepsilon_h h^n \Big|_{i,j,k} \left(v_{i+\frac{1}{2},j,k} - v_{i-\frac{1}{2},j,k} \right) \right] \end{aligned} \right\}$$

$$VTC = \Delta t \left[(wu')_{i+\frac{1}{2},j,k+\frac{1}{2}} - (wu')_{i+\frac{1}{2},j,k-\frac{1}{2}} \right]$$

Re-arranging gives:

$$p_k u_{k-1}^{n+\frac{1}{2}} + q_k u_k^{n+\frac{1}{2}} + r_k u_{k+1}^{n+\frac{1}{2}} = s_k + S_x \quad (4.60)$$

where:

obtain w can be shown to be as follows:

$$w_{i,j,k-\frac{1}{2}}^{n+\frac{1}{2}} = w_{i,j,k+\frac{1}{2}}^{n+\frac{1}{2}} - \frac{h_{i,j,k+\frac{1}{2}}^{n+\frac{1}{2}} + h_{i,j,k-\frac{1}{2}}^{n+\frac{1}{2}}}{2\Delta x} \left[(uh)_{i+\frac{1}{2},j,k}^{n+\frac{1}{2}} - (uh)_{i-\frac{1}{2},j,k}^{n+\frac{1}{2}} \right] - \frac{h_{i,j,k+\frac{1}{2}}^n + h_{i,j,k-\frac{1}{2}}^n}{2\Delta y} \left[(vh)_{i+\frac{1}{2},j,k}^n - (vh)_{i-\frac{1}{2},j,k}^n \right] \quad (4.62)$$

For the bottom layer, where $k = k_{max}$, the vertical velocity is zero:

$$w_{i,j,k+\frac{1}{2}}^{n+\frac{1}{2}} = 0 \quad (4.63)$$

For the second half-time step, the same procedure is followed to calculate the velocity components in y direction and z directions.

5.3 Numerical Solution of Advective-Diffusion Equation

5.3.1 Depth-integrated Equations

The two-dimensional depth integrated advective-diffusion equation (3.39), which has been discussed in Chapter 3, is given here for completeness:

$$\frac{\partial \phi H}{\partial t} + \frac{\partial \phi UH}{\partial x} + \frac{\partial \phi VH}{\partial y} - \frac{\partial}{\partial x} \left[HD_{xx} \frac{\partial \phi}{\partial x} \right] - \frac{\partial}{\partial y} \left[HD_{yy} \frac{\partial \phi}{\partial y} \right] = \Phi_s \quad (4.64)$$

This equation includes the following terms: advection, dispersion-diffusion and a source or sink term. In the solute transport model a space staggered grid mesh is used to solve the advective-diffusion equation. Solute concentrations have been introduced at the centre of each grid square. For solving this equation, an explicit scheme has been adopted. The finite difference formulation of depth integrated equation is written in the following form (Lin and Falconer 1997a):

$$\phi_{i,j}^{n+\frac{1}{2}} = \phi_{i,j}^n + \text{advection} + \text{dispersion} + \text{source} \quad (4.65)$$

The advection term components in equation (4.65) were predicted using the

ULTIMATE QUICKEST scheme, with the dispersion terms being represented using an explicit second order central scheme and the source terms being calculated using the Euler method. Details of the representation of these methods for different terms are shown below. Figure 5.3 shows a control volume around the grid square i,j .

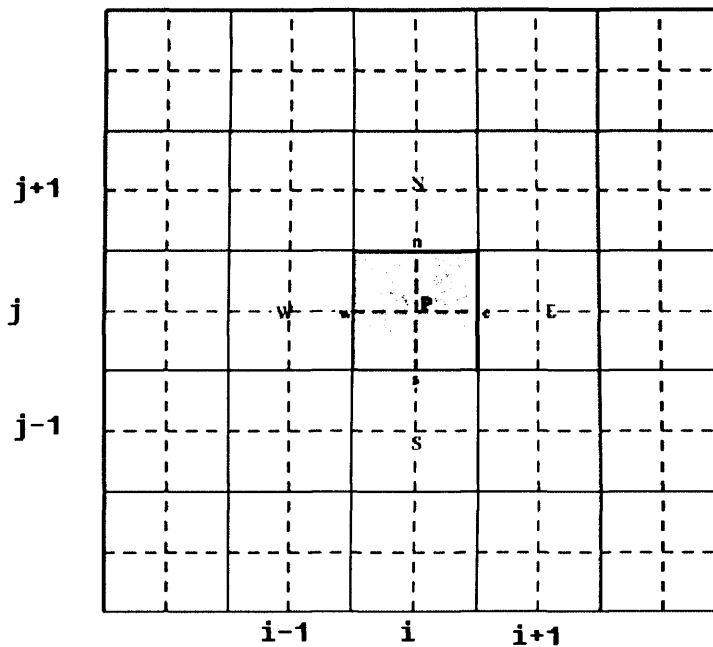


Figure 5.3 Control volume around grid point

5.3.1.1 Advection Terms

The advection term can be expressed as the sum of the four face values which gives:

$$advection = [(C_r)_e \phi_e - (C_r)_w \phi_w] + [(C_r)_n \phi_n - (C_r)_s \phi_s] \quad (4.66)$$

where the subscripts w, e, s and n denote west, east, south and north grid face values respectively, C_r = courant number at the grid face and can be shown for different faces to be as follows:

$$\begin{aligned}
(C_r)_w &= \frac{\Delta t}{\Delta x} U_{i-\frac{1}{2},j}^{n+\frac{1}{2}} \\
(C_r)_e &= \frac{\Delta t}{\Delta x} U_{i+\frac{1}{2},j}^{n+\frac{1}{2}} \\
(C_r)_s &= \frac{\Delta t}{\Delta y} V_{i,j-\frac{1}{2}}^{n+\frac{1}{2}} \\
(C_r)_n &= \frac{\Delta t}{\Delta y} V_{i,j+\frac{1}{2}}^{n+\frac{1}{2}}
\end{aligned} \tag{4.67}$$

The face values were calculated using the two-dimensional third order QUICKEST scheme, which is similar to the method introduced by Leonard and Niknafs (1990).

The west face value is showed as an example, giving:

$$\begin{aligned}
\phi_w &= \phi_{i-1,j} - \frac{(C_r)_{wx}}{2} GRADN \\
&\quad - \frac{(1-(C_r)_{wx}^2)}{6} CURVN - \frac{(C_r)_{wy}}{2} GRADT \\
&\quad + \left(\frac{(C_r)_{wy}^2}{6} - \frac{1}{24} \right) CURVT + \frac{(C_r)_{wx} (C_r)_{wy}}{3} TWIST
\end{aligned} \tag{4.68}$$

where

$$(C_r)_{wx} = \text{Courant number at west face in x direction} = \frac{\Delta t}{\Delta x} U_{i-\frac{1}{2},j}$$

$$(C_r)_{wy} = \text{Courant number at west face in y direction} = \frac{\Delta t}{\Delta y} V_{i-\frac{1}{2},j}$$

$$GRADN = \phi_{i,j} - \phi_{i-1,j}$$

$$CURVN = \begin{cases} \phi_{i,j} - 2\phi_{i-1,j} + \phi_{i-2,j} & \text{if } U_{i-\frac{1}{2},j} > 0 \\ \phi_{i,j+1} - 2\phi_{i,j} + \phi_{i-1,j} & \text{if } U_{i-\frac{1}{2},j} < 0 \end{cases}$$

$$GRADT = \begin{cases} \phi_{i-1,j} - \phi_{i-1,j-1} & \text{if } U_{i-\frac{1}{2},j} > 0, V_{i-\frac{1}{2},j} > 0 \\ \phi_{i-1,j+1} - \phi_{i-1,j} & \text{if } U_{i-\frac{1}{2},j} > 0, V_{i-\frac{1}{2},j} < 0 \\ \phi_{i,j} - \phi_{i,j-1} & \text{if } U_{i-\frac{1}{2},j} < 0, V_{i-\frac{1}{2},j} > 0 \\ \phi_{i,j+1} - \phi_{i,j} & \text{if } U_{i-\frac{1}{2},j} < 0, V_{i-\frac{1}{2},j} < 0 \end{cases}$$

$$CURVT = \begin{cases} \phi_{i-1,j+1} - 2\phi_{i-1,j} + \phi_{i-1,j-1} & \text{if } U_{i-\frac{1}{2},j} > 0 \\ \phi_{i,j+1} - 2\phi_{i,j} + \phi_{i,j-1} & \text{if } U_{i-\frac{1}{2},j} < 0 \end{cases}$$

$$TWIST = \begin{cases} (\phi_{i,j} - \phi_{i,j-1}) - (\phi_{i-1,j} - \phi_{i-1,j-1}) & \text{if } V_{i-\frac{1}{2},j} > 0 \\ (\phi_{i,j+1} - \phi_{i,j}) - (\phi_{i-1,j+1} - \phi_{i-1,j}) & \text{if } V_{i-\frac{1}{2},j} < 0 \end{cases}$$

Use of the third order QUICKEST scheme may still generate non-physical oscillations if sharp gradients occur in the concentration distribution (Lin and Falconer 1997a and Kolahdoozan 1999). By using the universal limiting procedure, which has been developed by Leonard (1991), then any non-physical oscillations can be eliminated. Lin and Falconer (1997a) modified this one-dimensional ULTIMATE algorithm for two-dimensional problems and it is believed this method can be applied arbitrarily to higher order transient interpolation models of the advective transport equation (Lin and Falconer 1997a). In order to eliminate non-physical oscillations, two normalised variables need to be introduced for each cell face. For the east cell face, if $(C_r)_{ex} > 0$,

the normalised variables $\bar{\phi}_p^n$ and $\bar{\phi}_e^n$ are expressed in the following:

$$\bar{\phi}_p^n = \frac{\phi_{i,j}^n - \phi_{i-1,j}^n}{\phi_{i+1,j}^n - \phi_{i-1,j}^n} \quad (4.69)$$

$$\bar{\phi}_e^n = \frac{\phi_{i+\frac{1}{2},j}^n - \phi_{i-1,j}^n}{\phi_{i+1,j}^n - \phi_{i-1,j}^n} \quad (4.70)$$

If these two normalised variables satisfy the following conditions

$$\bar{\phi}_e^n \leq \frac{\bar{\phi}_p^n}{(C_r)_{ex}} \quad \text{for} \quad 0 < \bar{\phi}_p^n \leq 1 \quad (4.71)$$

$$\bar{\phi}_p^n \leq \bar{\phi}_e^n \leq 1 \quad \text{for} \quad 0 \leq \bar{\phi}_p^n \leq 1 \quad (4.72)$$

$$\bar{\phi}_e^n = \bar{\phi}_p^n \quad \text{for} \quad \bar{\phi}_p^n < 0 \quad \text{or} \quad \bar{\phi}_p^n > 1 \quad (4.73)$$

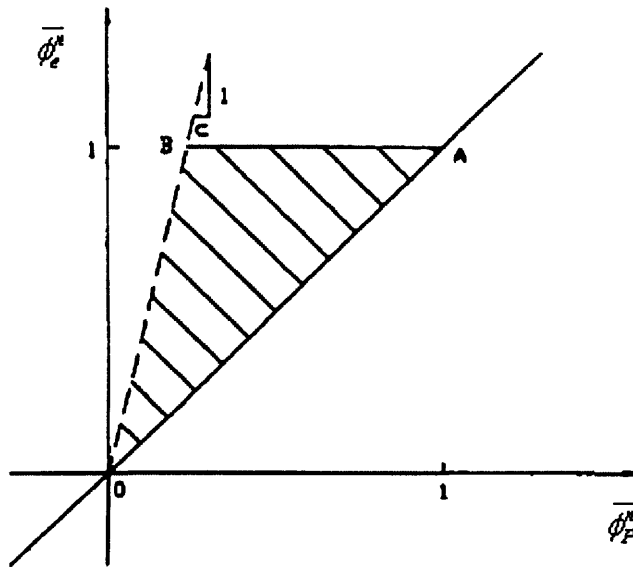


Figure 5.4 Normalised variable diagram showing the universal limiter boundaries

then an oscillation free solution can be obtained. This is shown in Figure 5.4, which

was originally presented by Leonard (1991). If the point $\left(\bar{\phi}_p^n, \bar{\phi}_e^n\right)$ lies within the shaded area in Figure 5.4, then the unadjusted face value ϕ_e is used to solve equation(4.66). If the point is outside the area, then the normalised face value $\bar{\phi}_e^n$ will be replaced with the nearest allowable $\bar{\phi}_e^n$ value, and the face value ϕ_e is given as:

$$\phi_e = \phi_{i-1,j} + \bar{\phi}_e^n(\phi_{i+1,j} - \phi_{i-1,j}) \quad (4.74)$$

A similar procedure is adopted to get the other cell face values.

5.3.1.2 Diffusion Terms:

The diffusion terms are represented using an explicit second order central difference scheme and can be represented as:

$$\text{dispersion} = \frac{\Delta t}{\frac{1}{2}\left(H_{i,j}^{n+\frac{1}{2}} + H_{i,j}^{n-\frac{1}{2}}\right)} \left[\frac{1}{\Delta x} (H_e D_{xx}{}_{i+\frac{1}{2},j} (\phi_{i+1,j}^n - \phi_{i,j}^n) - H_w D_{xx}{}_{i-\frac{1}{2},j} (\phi_{i,j}^n - \phi_{i-1,j}^n)) + \frac{1}{\Delta y} (H_n D_{yy}{}_{i,j+\frac{1}{2}} (\phi_{i,j+1}^n - \phi_{i,j}^n) - H_s D_{yy}{}_{i,j-\frac{1}{2}} (\phi_{i,j}^n - \phi_{i,j-1}^n)) \right] \quad (4.75)$$

where D_{xx} and D_{yy} are dispersion diffusion coefficient in x and y directions respectively and H_e, H_w, H_n and H_s are the water depth at control volume faces

5.3.1.3 Source Terms:

For sediment and faecal bacteria, the source and sink terms in the advective-diffusion equation are in a different format, therefore the numerical treatment will also be

different. In this section the treatment of the source and sink terms for sediment, faecal bacteria and the sediment-bacteria interaction model are discussed.

Source and sink terms for sediment transport model:

For the sediment transport equation the source term is the net re-suspension and deposition rate. Therefore the source term for sediment transport can be represented as:

$$\Phi_s = q_{ero} - q_{dep} \quad (4.76)$$

where q_{ero} = sediment re-suspension rate ($kg / m^2 / s$), q_{dep} = sediment deposition rate ($kg / m^2 / s$), so

$$source = \frac{(q_{ero} - q_{dep}) \cdot \Delta t}{H} \quad (4.77)$$

The method used to calculate the net re-suspension and deposition rate for both the cohesive and non-cohesive sediments have been detailed in Chapter 4.

Source and sink terms for bacteria transport model:

For the conventional bacteria transport equation, the source term includes both the different types of input of bacteria and the decay term. Therefore the source term for bacteria transport can be represented as:

$$\Phi_s = H \left(\phi_0 - k \phi \right) \quad (4.78)$$

giving

$$source = \Delta t \cdot \phi_0 - \Delta t \cdot k \phi_{i,j}^n \quad (4.79)$$

where ϕ_0 = external input of bacteria

$\phi_{i,j}^n =$ bacteria concentration at time $n \cdot \Delta t$

$k =$ decay rate

Source and sink terms for sediment-bacteria transport model:

For the sediment-bacteria transport model, the source term includes both the different types of input of bacteria which includes the bacteria input from bed sediment and the decay term. Therefore the source term can be represented as:

$$\Phi_s = H(\phi_0 - k\phi) + \phi_b \quad (4.80)$$

where $\phi_0 =$ external input of bacteria such as outfall, $\phi_b =$ bacteria input from bed sediment, $k =$ decay rate and

$$\phi_b = F_{net} = \max(q_{ero}, 0)P_b + \min(-q_{dep}, 0)P \quad (4.81)$$

where $P =$ bacteria concentration on suspended sediment, $P_b =$ bacteria concentration on bed sediment giving

$$source = \Delta t \phi_0 - \Delta t k \phi + \Delta t \phi_b / H \quad (4.82)$$

5.3.2 Layer-integrated Equations

The three-dimensional advective-diffusion equation (3.35) is repeated here for completeness giving:

$$\begin{aligned} & \frac{\partial \phi}{\partial t} + \frac{\partial u\phi}{\partial x} + \frac{\partial v\phi}{\partial y} + \frac{\partial (w - w_s)\phi}{\partial z} \\ & - \frac{\partial}{\partial x} \left(D_x \frac{\partial \phi}{\partial x} \right) - \frac{\partial}{\partial y} \left(D_y \frac{\partial \phi}{\partial y} \right) - \frac{\partial}{\partial z} \left(D_z \frac{\partial \phi}{\partial z} \right) = \phi_o \end{aligned} \quad (4.83)$$

This equation includes the following terms: advection, dispersion-diffusion and a

source or sink term. In solving this three-dimensional equation, an operator splitting algorithm, as proposed in Lin and Falconer (1996) and Wu and Falconer (2000), has been used to split the three-dimensional advective-diffusion terms into a vertical one-dimensional and a horizontal two-dimensional set of equations. The three-dimensional equation is split in to the following equations:

$$\frac{\partial \varphi}{\partial t} + \frac{\partial(w - w_s \varphi)}{\partial z} - \frac{\partial}{\partial z} \left(D_{tz} \frac{\partial \varphi}{\partial z} \right) = 0 \quad (4.84)$$

and

$$\frac{\partial \varphi \Delta z}{\partial t} + \frac{\partial u \Delta z}{\partial x} + \frac{\partial v \Delta z}{\partial y} - \frac{\partial}{\partial x} \left(\Delta z D_{tx} \frac{\partial \varphi}{\partial x} \right) - \frac{\partial}{\partial y} \left(\Delta z D_{ty} \frac{\partial \varphi}{\partial y} \right) = \Delta z \varphi_o \quad (4.85)$$

The layer-integrated two-dimensional advective-diffusion equation (4.85) was first solved horizontally, and then the one-dimensional vertical advective-diffusion equation (4.84) was solved for in the z direction.

For the layer-integrated equation, this equation was solved using a similar method to that discussed in the previous section for the two-dimensional depth integrated equation. Hence, the ULTIMATE QUICKEST scheme was used for advection term, the central difference scheme for the diffusion terms and Euler method for the source and sink terms.

For the vertical one-dimensional advective-diffusion equation, this equation could be solved using a non-uniform grid in the vertical direction. Since the diffusion process is the key term in this equation, and also some of the grid sizes were very small near the sea bed and water surface, then this equation was solved using an centred implicit method to avoid the use of a very small time step. The discretised equation was then expressed in the following form:

$$-a_{T,k} \varphi_{k-1}^{n+1} + a_{p,k} \varphi_k^{n+1} - a_{B,k} \varphi_{k+1}^{n+1} = b_k \quad (4.86)$$

where

$$a_{T,k} = D_{tz}^T A(|P_e^T|) + [F^T, 0],$$

$$a_{B,k} = D_{tz}^B A(|P_e^B|) + [-F^B, 0],$$

$$a_{p,k} = a_T + a_B + \frac{\Delta z}{\Delta t},$$

$$b_k = \frac{\Delta z}{\Delta t} \phi_k^n$$

and

$$A(|P_e|) = [0, (1 - 0.1|P_e|)^5]$$

$$P_e = \frac{w - w_s}{D_{tz}} \Delta z$$

where the symbol [a,b] is used to denote the greater of a and b, T and B denote the top and bottom control volume faces, P_e is the grid Peclet number and F is the mass flow rate.

These finite difference equations were arranged in a matrix form, giving a tri-diagonal matrix, which was also solved using the Thomas algorithm.

5.4 Boundary Conditions

Generally, two types of boundary conditions exist; the first type being a closed boundary (also known as a wall boundary condition) and the second type being an open boundary. For the three-dimensional modelling study, specific surface and bed boundary conditions also needed to be specified.

5.4.1 Closed Boundary Condition

For a closed boundary condition, as shown in Figure 5.5, no flow is

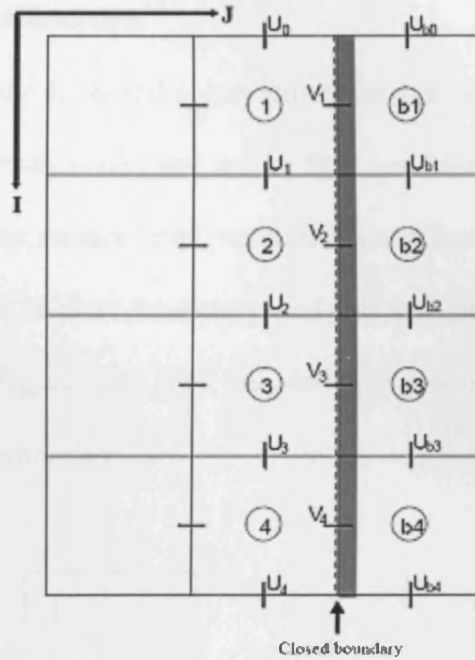


Figure 5.5 Closed Boundary.

allowed across the boundary, so for the closed boundary condition

$$V_i = 0 \quad (i = 1, 2, 3, 4) \quad (4.87)$$

For the velocity component parallel to the closed boundary, this term can be expressed as follows;

$$U_{bi} = \lambda U_i \quad (i = 0, 1, 2, 3, 4) \quad (4.88)$$

where $\lambda = -1$ for a no-slip boundary, $\lambda = 1$ for a free-slip boundary, and $0 < \lambda < 1$ for a partial slip boundary

The closed boundary condition for the solute transport is:

$$\left. \frac{\partial \phi}{\partial n} \right|_w = 0 \quad \text{and} \quad \left. \frac{\partial \phi^2}{\partial n^2} \right|_w = 0$$

which means that there is no solute flux across a wall boundary. The subscript w indicates that the value was taken from the wall boundary and n indicates that the direction is perpendicular to the wall.

5.4.2 Open Boundary Condition

For an open boundary the flow and solute flux were permitted across the boundaries. Therefore suitable hydrodynamic and solute flux conditions needed to be satisfied, such as a measured water surface level, velocities and solute concentration values. If the open boundary was a flow boundary and the velocities at the boundary were defined as shown in Figure 5.6, then the following boundary condition could be obtained for the hydrodynamics:

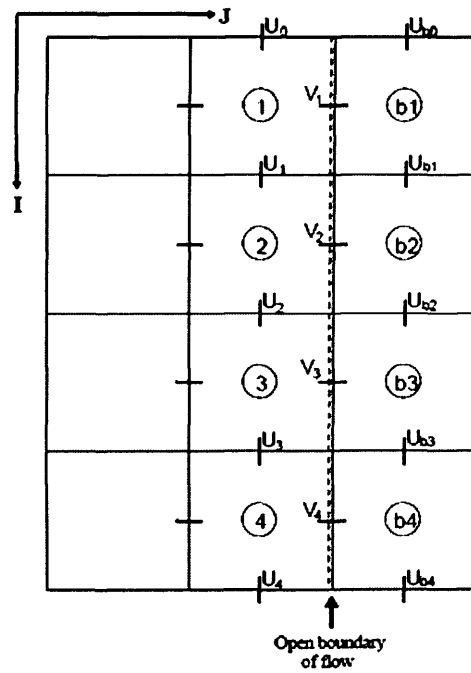


Figure 5.6: Flow Boundary

$$\begin{cases} U_i = U_{bi} & (i=0, 1, 2, 3, 4) \\ V_i = V_{bi} & (i=1, 2, 3, 4) \end{cases} \quad (4.89)$$

If the open boundary condition was of a water elevation type, as shown in Figure 5.7, then the following condition could be obtained for the hydrodynamics conditions:

$$\begin{cases} V_i = V_{ai} & (i=1,2,3,4) \\ U_i = U_{ai} & (i=0,1,2,3,4) \\ \zeta_i = \zeta_{bi} & (i=1,2,3,4) \end{cases} \quad (4.90)$$

where ζ_{bi} is the known water level at the open boundary.

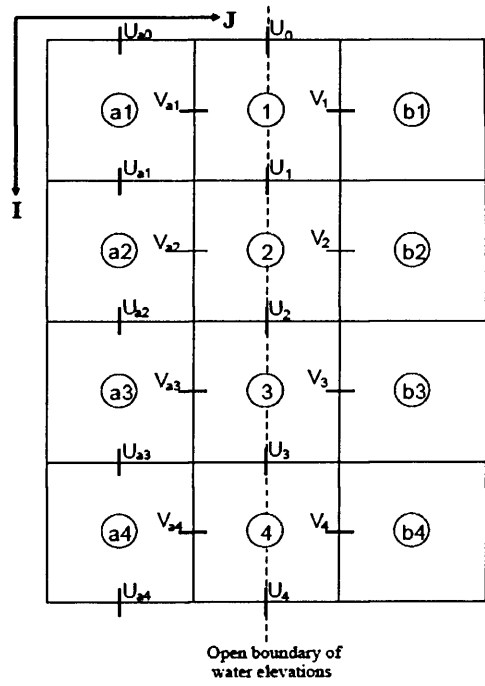


Figure 5.7: Water Elevation Boundary.

The solute concentration values at the open boundary were described from known boundary value, φ_{bi}

$$\varphi_i = \varphi_{bi} \quad (i=1,2,3,4) \quad (4.91)$$

5.4.3 Free Surface Boundary

For the three-dimensional model, at the free surface boundary the shear stress was set to the wind shear stress, as given by:

$$\begin{aligned}\tau_{xz}|_{\zeta} &= \rho_a \gamma_w W_x \sqrt{W_x^2 + W_y^2} \\ \tau_{yz}|_{\zeta} &= \rho_a \gamma_w W_y \sqrt{W_x^2 + W_y^2}\end{aligned}\quad (4.92)$$

The surface boundary condition for the advective-diffusion terms was to set the solute flux across the free surface to zero, giving:

$$(w - w_s)\phi - D_{iz} \frac{\partial \phi}{\partial z} = 0 \quad (4.93)$$

5.4.4 Bed Boundary

For the bed boundary condition, a no-slip boundary was applied, with the corresponding velocity components at the bed being set to zero, giving:

$$\begin{cases} \overline{u}_{i,j,k_{max}+\frac{1}{2}} = 0 \\ \overline{v}_{i,j,k_{max}+\frac{1}{2}} = 0 \\ \overline{w}_{i,j,k_{max}+\frac{1}{2}} = 0 \end{cases} \quad (4.94)$$

For the bed shear stress a logarithmic velocity profile was assumed within the bottom layer, with Lin and Falconer (1997b) representing the bed shear stress in the following form, and as suggested in French (1986):

$$\frac{\tau_b}{\rho} = \left| \frac{u_{k_{max}}^{n+1/2} + u_{k_{max}}^{n-1/2}}{2} \right| \left| \frac{u_{k_{max}}^{n+1/2} + u_{k_{max}}^{n-1/2}}{2} \right| \left[2.5 \ln \left(\frac{30d}{2.72k_s} \right) \right]^{-2}$$

where d is the thickness of the bottom layer, and k_s is roughness height.

5.5 Summary

Details have been given herein of the numerical solution procedures for the two-dimensional and layer integrated three-dimensional flow and solute transport models. The two-dimensional depth integrated hydrodynamic equations have been solved using an Alternating Direction Implicit (ADI) scheme and the ULTIMATE QUICKEST scheme has been used to solve the solute transport equations and, in this study, to predict both the sediment and bacteria transport processes.

The three-dimensional layer integrated hydrodynamic equations were solved using a combined explicit and implicit finite difference method. The advective-diffusive equation was solved using an operator splitting scheme, where the equation was split into a set of horizontal and vertical equations. The horizontal equations were solved using the ULTIMATE QUICKEST scheme and an implicit scheme was used to treat the vertical diffusive term, to avoid the use of a very small time step.

Chapter 6

Idealised Test Cases

6.1 Introduction

Prior to applying any refined or new numerical model, it is desirable to test the model against known analytical results or experimental data to ensure that the model works properly. In this chapter, tests have been conducted by using both analytical and published experimental results. Derivations of sediment-bacteria interaction analytical solutions are detailed in this chapter. Idealised cases are also set up to investigate the effects of different environmental factors and parameters. The two-dimensional sediment-bacteria interaction model developed is based on the original DIVAST model framework. The DIVAST model has been used by many researchers in the past, so only the new sediment-bacteria interaction model has been tested against the analytical solutions for re-suspension and deposition of sediment and bacteria. The three-dimensional sediment-bacteria interaction has been developed around the TRIVAST model framework. The three-dimensional hydrodynamic model has been tested against experimental flume data, the sediment transport model against published experiment data, and the sediment-interaction model against an analytical solution for steady flow conditions.

6.2 Hydrodynamic Model Test

For the 3-D hydrodynamic model tests the model has been tested against flume experiment data. These experiments were conducted by Dorcheh (2007) in the

Hyder Hydraulics Laboratory at Cardiff University. Three sets of experimental data, namely non-vegetated open channel flow, submerged vegetated open channel flow and emergent vegetated open channel flow were chosen from data collected in a wide rectangular experimental flume. In Dorcheh's (2007) wide channel experiments the flume had a width of 1200 mm and a maximum depth of 300 mm. The experiments were conducted for non-vegetated and vegetated flow conditions. For the vegetated flow conditions, both emergent and submerged vegetated flows were considered for three vegetation density conditions, namely: low density, medium density and high density. In this study only the low density vegetation data were used to test the numerical model.

In these experiments rigid wood rods were used to represent the vegetation. The rods used in Dorcheh (2007) were 24 mm in diameter and 180 mm in length for the submerged conditions and 300 mm for the emergent conditions. The flow rate was kept a constant of 15 l/s for all of these experiments and velocity measurements were taken at two cross-sections. The cross-sections were located at the mid-length along the flume, i.e. at 4.4 m, and near the end of the channel, i.e. at 1.4 m. In the vertical direction measurements were taken at 50 mm from the channel bed and at 50mm intervals towards the water surface, i.e. at 50, 100, 150, 200, 250 and 275 mm. Figure 6.1 shows the layout of the cross-sections and the measuring points for different experiment conditions. The distance between the rods in the flow direction was uniform at 0.208 m.

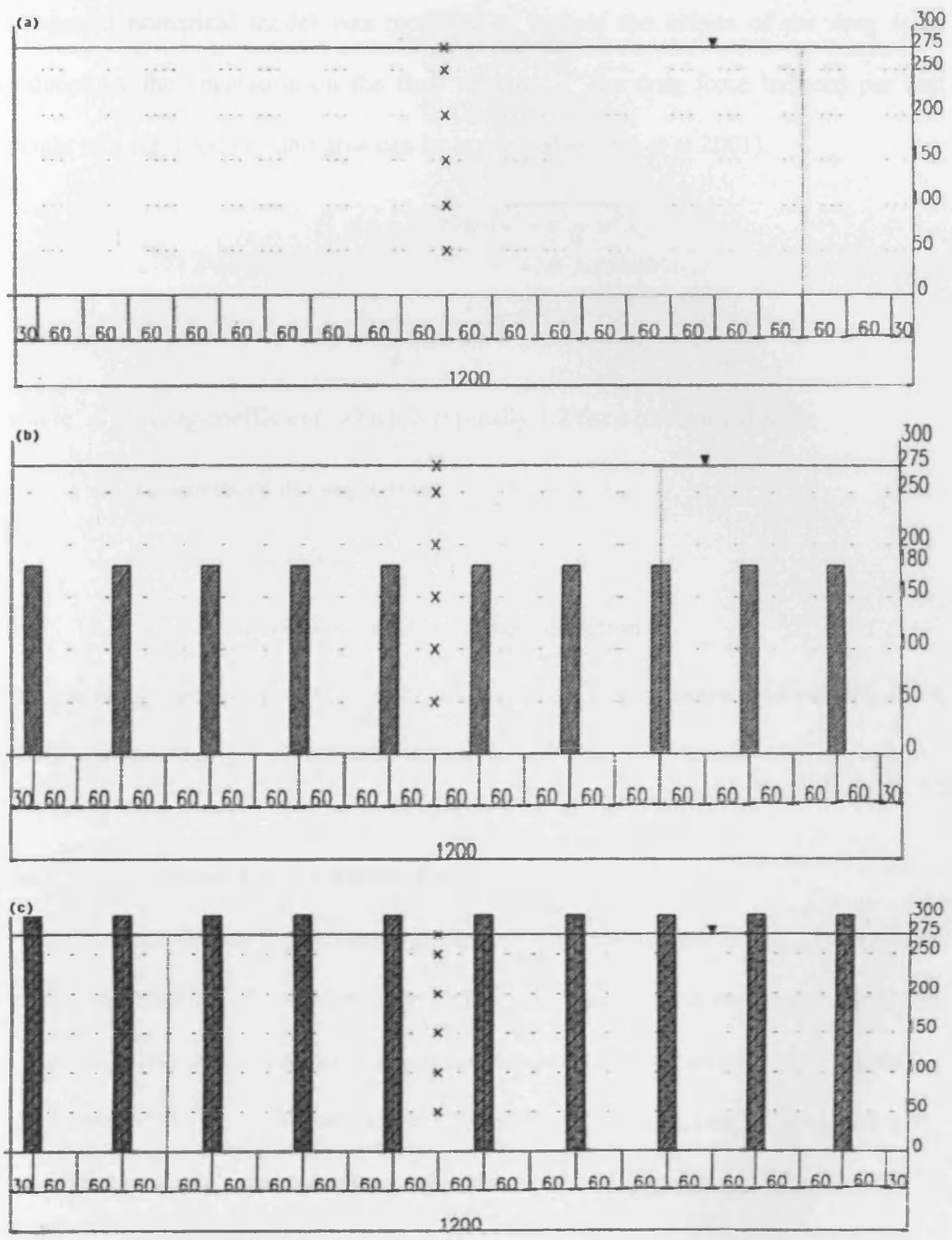


Figure 6.1 Layout of cross-section and measuring points for: (a) no vegetation, (b) submerged vegetation and (c) emergent vegetation (Dorcheh, 2007)

In order to model the configurations with the rods, the three-dimensional layer

integrated numerical model was modified to include the effects of the drag force induced by the vegetation on the flow structure. The drag force induced per unit height of a rigid rod per unit area can be expressed as (Wu et al 2001):

$$F_x = -\frac{1}{2} C_D D_v u \sqrt{u^2 + v^2 + w^2} \lambda_v \quad (6.1)$$

$$F_y = -\frac{1}{2} C_D D_v v \sqrt{u^2 + v^2 + w^2} \lambda_v$$

where C_D = drag coefficient, which is typically 1.2 for a circular cylinder;

D_v = diameter of the vegetation;

λ_v = vegetation density;

u, v, w = velocity component in x, y and z direction .

For turbulence modelling, a two-layer mixing length model suggested by (Rodi, 1984, 2000) was included, which has been detailed in Chapter 3.

6.2.1 Non-vegetated Open Channel Flow

Numerical simulations for the case without rods were carried out first. The predicted vertical distribution of longitudinal velocity were compared to measured data at the 1.4 m and 4.4m cross-sections. The measurement locations are shown in Figure 6.1 and comparisons in the results are shown in Figure. 6.2. It can be seen that good agreement has been obtained between the measured and calculated results.

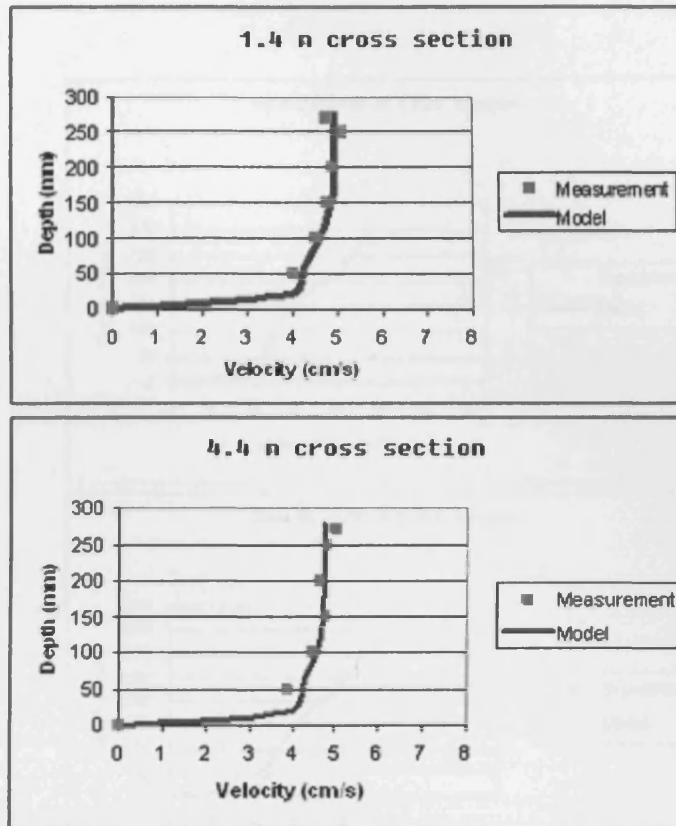


Figure 6.2 Velocity profile comparisons at the 1.4 m and 4.4 m cross-sections for non-vegetated flows

6.2.2 Submerged Vegetated Open Channel Flow

The numerical model was then set up to study the submerged vegetation case. Calculated vertical distributions of longitudinal velocity were compared to the measured data at the 1.4 m and 4.4 m cross-section respectively and along the middle of the flume. The comparisons are shown in Figure. 6.3. Again good agreement has been obtained between the measured and calculated results. It can be seen from Figure 6.3 that the existence of vegetation decelerates the velocities (or total flow component) in the vegetation layer, whereas the flow velocity or flow is accelerated in the non-vegetated layer.

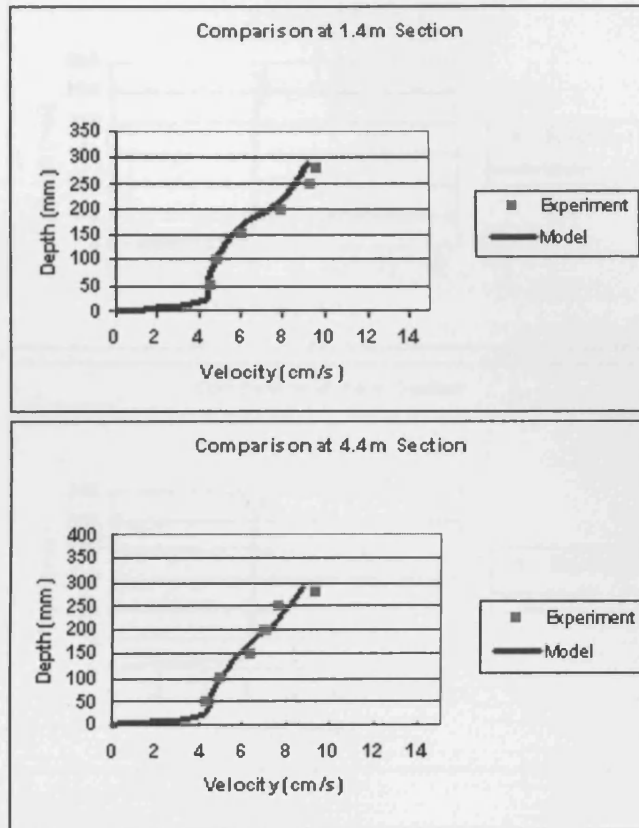


Figure 6.3 Velocity profile comparisons at the 1.4 m and 4.4 m cross-sections for submerged vegetation flow

6.2.3 Emergent Vegetated Open Channel Flow

Figure 6.4 shows comparisons of the simulated vertical velocity distribution against experiment data for flow through emergent vegetation. Again it can be seen that the comparisons are encouraging. From the predicted results it can be seen that the velocity distribution over an emergent vegetation layer is nearly uniform, apart from very close to the bed.



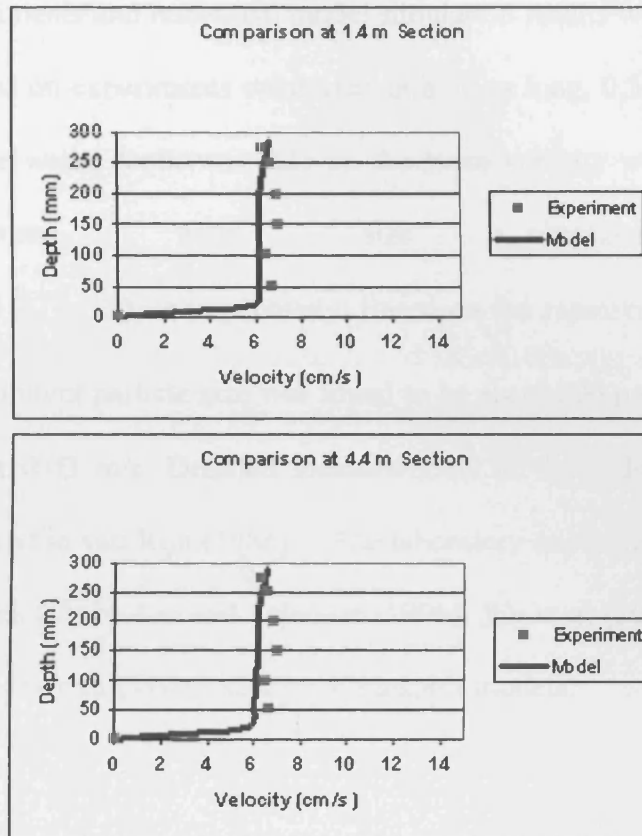


Figure 6.4 Velocity profile comparisons at the 1.4 m and 4.4 m cross-sections for emergent vegetation flow.

It can be seen from above results, the hydrodynamic model has produced good agreements for all three test cases, by using a simple two layer mixing length turbulence model.

6.3 Sediment Transport Model Test

The sediment transport part of the model used for this study was validated against two published test cases. One was for net entrainment, based on a test conducted by van Rijn (1986), and the other being a zero entrainment case, based on tests conducted by Wang and Ribberink (1986).

6.3.1 Test Case 1: Net Entrainment Test

Laboratory experiments and numerical model simulation results were reported by van Rijn (1986), based on experiments conducted in a 30 m long, 0.5 m wide and 0.7 m deep flume. The water depth was 0.25 m, the mean velocity was 0.67m/s and the bed sediment grain size characteristics were $D_{50} = 230\mu\text{m}$ and $D_{90} = 320\mu\text{m}$ respectively. Based on the representative particle size the suspended sediment particle size was found to be about 200 μm , resulting in a fall velocity of about 0.03 m/s. Detailed measurements of the sediment concentration profile can be found in van Rijn (1986). The laboratory experimental data were also reproduced numerically by Lin and Falconer (1996), Wu et al (2000) and Liang et al (2005) to validate their suspended sediment transport models.

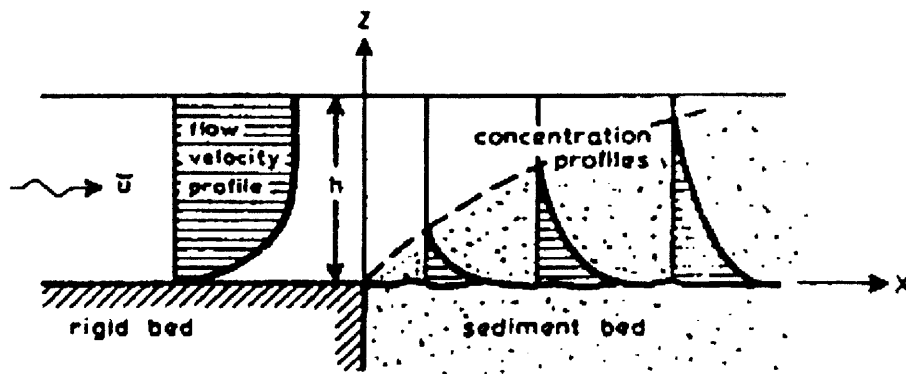
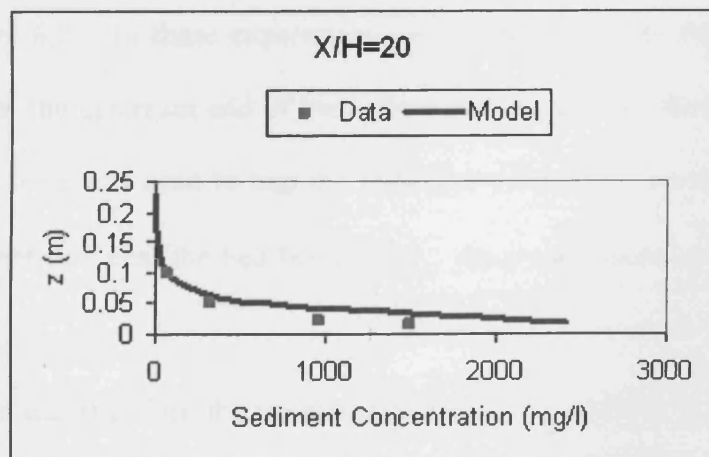
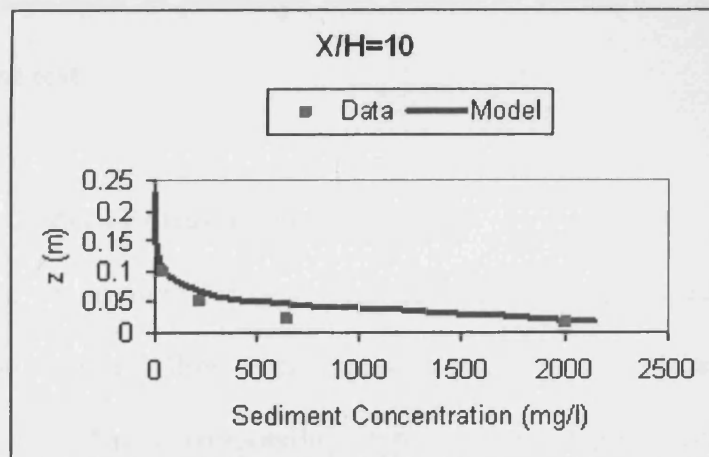
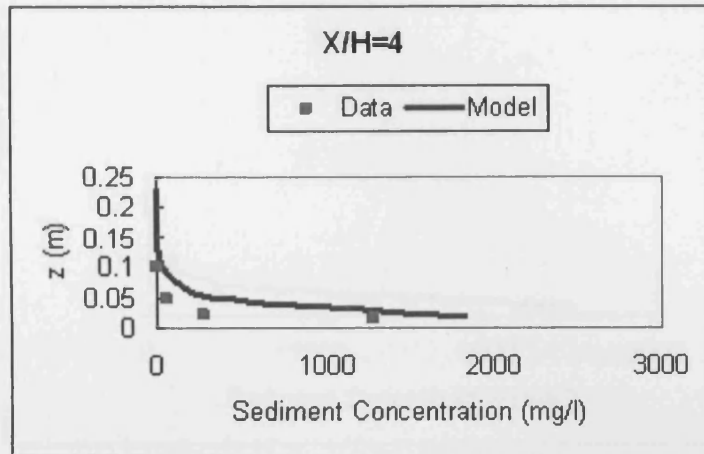


Figure 6.5 Net entrainment experimental set up (van Rijn 1986)

The three-dimensional layer integrated model's predicted and measured sediment concentrations were compared at four sections, which are shown in Figure 6.6. It can be seen that the level of agreement between the numerical model and the experiment results are very encouraging, which demonstrates that the entrainment mechanisms as represented by this sediment transport formulation are encouragingly accurate.



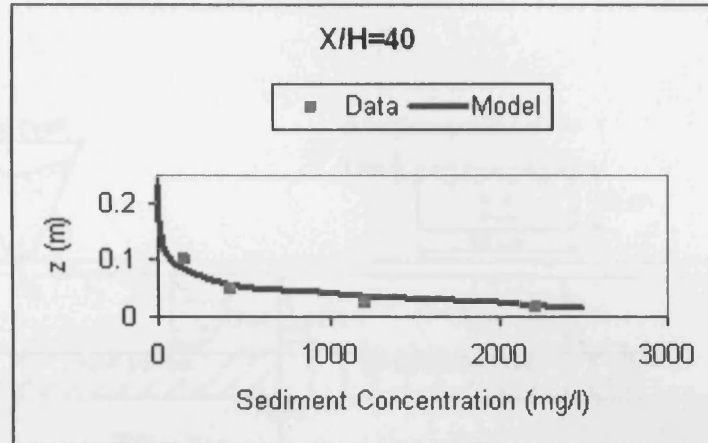


Figure 6.6 Comparison of predicted and measured sediment concentrations for net entrainment test

6.3.2 Test Case 2: Zero Entrainment at the Bed:

An experimental programme for measuring the sediment concentration profile in a steady horizontal uniform flow over a porous bed was undertaken by Wang and Ribberink (1986). The corresponding experimental results have been used to validate the numerical model refined for this study. The experimental layout is shown in Figure 6.7. In these experimental tests sediment was supplied above the water surface, at the upstream end of the inflow section, and as shown in Figure 6.7. A perforated bottom was used to trap the sediment particles in contact with the bed, with the sediment flux near the bed being $-w_s s_a$, since re-suspension hardly occurred for these tests.

The water depth was 0.215 m, the upstream discharge was $0.06 \text{ m}^3/\text{s}$, the fall velocity $w_s = 0.007 \text{ m/s}$ and $k = 0.4$. In the numerical model 7 layers were used in the vertical direction and 92 grids cells in the x-direction, with a regular grid size of 0.25 m.

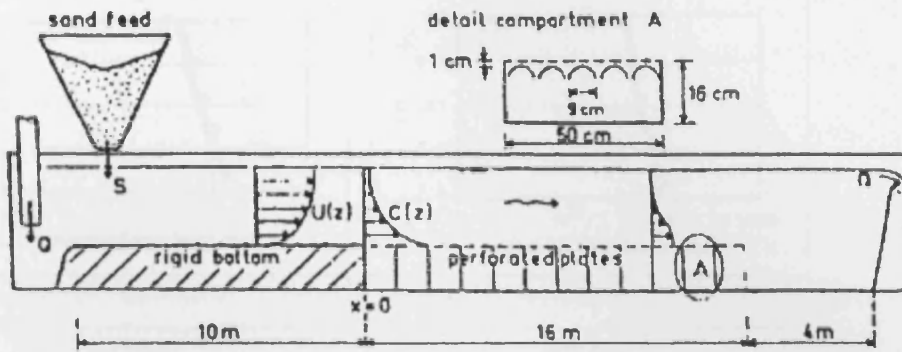
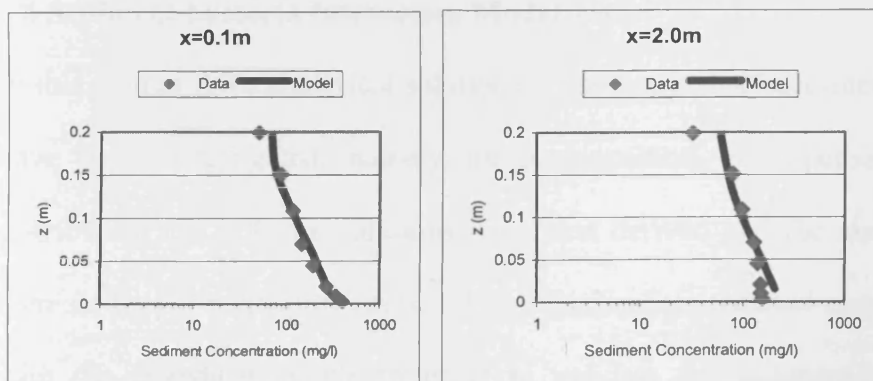


Figure 6.7 Zero entrainment experiment set up (Wang and Ribberink 1986)

The model predicted and measured sediment concentrations were compared at six sections, as shown in Figure 6.8. It can be seen from these comparisons that the agreement between the numerically predicted and the experimentally measured results are again encouraging, which demonstrates that the transport mechanism for this sediment transport model is performing fairly accurately.



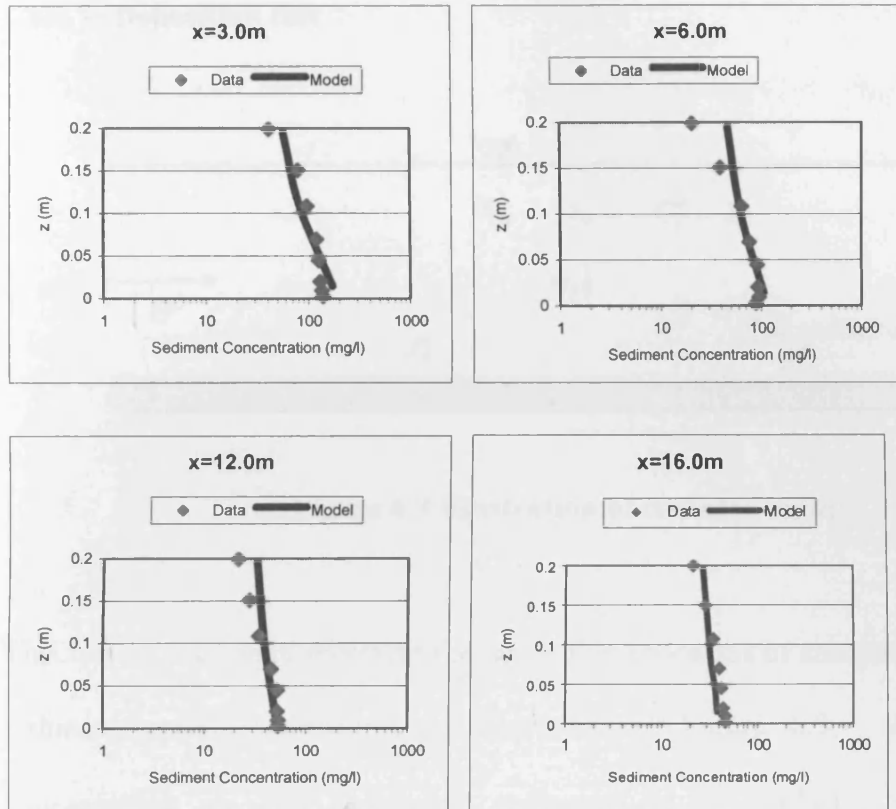


Figure 6.8 Comparison of sediment concentrations for zero entrainment test.

6.4 Sediment-bacteria Interaction Model Test

In this section three analytical solutions for sediment-bacteria interaction case studies have been investigated, namely for a deposition, re-suspension and a vertical distribution test. These solutions were first derived and the numerical model was then set up for validation cases. The numerically predicted results were compared with the analytical results in order to validate the sediment-bacteria interaction properties of the numerical model. After validating the numerical model against these analytical solutions, the numerical model was then validated against a published artificial flooding case.

6.4.1 Derivation of Analytical Solutions

Case 1: Deposition test

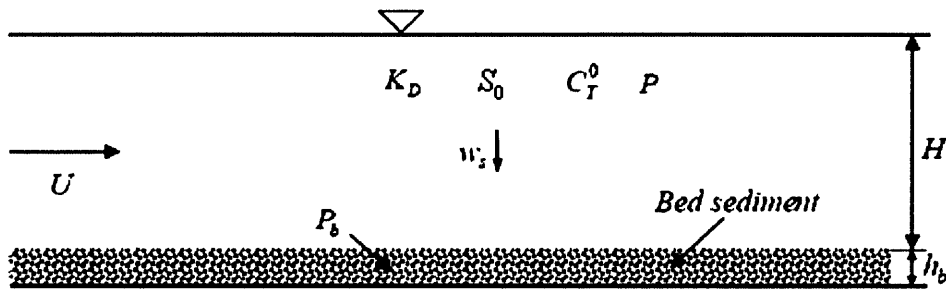


Figure 6.9 Illustration of test case set up

This test was set up to represent the deposition processes of attached bacteria due to a sediment-bacteria interaction, as illustrated in Figure 6.9. P is the bacteria concentration on the suspended sediments in $cfu/(10^{-1}g)$, and the bacteria concentration on the bed sediments is P_b in $cfu/(10^{-1}g)$, H is the water depth and h_b is the bed sediment thickness. S_0 is the initial sediment concentration in the water column in kg/m^3 , which is set to be a constant. C_T is the total bacteria concentration in the water column in $cfu/100ml$.

To simplify this problem, some basic assumptions have been made including:

1. The sediment particle size was assumed to be uniform across the domain, so that the settling velocity w_s was set to be a constant.
2. The initial sediment concentration S_0 was assumed to be greater than the equilibrium concentration S_e , which meant that the sediment and attached bacteria settle down onto the bed and the concentration of the sediment and bacteria in water column would keep decreasing until equilibrium had been reached.

3. The bacteria decay rate was assumed to be a constant in the water column and the decay process in bed sediments was neglected (or treated as conservative).

And then the bacteria and sediment concentrations in the water column and bed can be obtained analytically. Details of the solutions are given in the following.

Under steady and uniform flow conditions the governing equation for total bacteria can be simplified to the following form:

$$\frac{dC_T}{dt} = \frac{1}{H} C_b^p - kC_T \quad (6.2)$$

where C_b^p represents the reduction of bacteria due to the deposition of sediment which is given as:

$$C_b^p = q_{dep}P = \gamma w_s P (S_e - \alpha S) \quad (6.3)$$

and

$$P = \frac{K_D C_T}{1 + K_D S} \quad (6.4)$$

where k is the decay rate.

So in equation (6.2) can be expressed in the following form:

$$\frac{dC_T}{dt} = \frac{\gamma w_s}{H} \frac{K_D C_T}{1 + K_D S} (S_e - \alpha S) - kC_T \quad (6.5)$$

The sediment concentration in this equation can be obtained by solving the sediment transport equation. Under steady and uniform flow conditions the governing equation for suspended sediment transport can be simplified as follow:

$$\frac{dS}{dt} = \frac{\gamma w_s}{H} (S_e - \alpha S) \quad (6.6)$$

Yuan (2007) derived an analytical solution for this sediment transport equation (6.6) and is given as:

$$S = \frac{1}{\alpha} S_e + \left(S_0 - \frac{1}{\alpha} S_e \right) e^{-\lambda t} \quad (6.7)$$

where

$$\lambda = \frac{\alpha \gamma w_s}{H} \quad (6.8)$$

By using this analytical solution for sediment transport equation, the analytical solution of equation (6.5) can similarly be derived.

For the derivation of the analytical solution for equation (6.5), an operator splitting scheme is used. This equation can be treated as the combination of the following two equations:

$$\frac{dC_T}{dt} = \frac{\gamma w_s}{H} \frac{K_D C_T}{1 + K_D S} (S_e - \alpha S) \quad (6.9)$$

$$\frac{dC_T}{dt} = -k C_T \quad (6.10)$$

Yuan (2007) derived the analytical solution of equation (6.9) to validate his heavy metal model, together with the analytical solution for $\frac{dC_T}{dt} = -k C_T$ given as $C_T = C_T^0 e^{-kt}$. Hence the analytical solution of equation (6.5) can be obtained by combining these two analytical solutions to give:

$$C_T = \frac{\alpha + K_D [S_e + (\alpha S_0 - S_e) e^{-\lambda t}]}{\alpha (1 + K_D S_0)} C_T^0 e^{-kt} \quad (6.11)$$

Case 2: Re-suspension test

This case is based on the deposition test, except that the initial conditions are now changed so that the initial sediment concentration S_0 is set lower than the

equilibrium value S_e and the initial bacteria concentration in bed sediment P_b is set to be a constant other than zero.

In this case the fate and transport of the total bacteria can also be expressed using equation (6.5), but here C_b^p represents the source of bacteria due to sediment erosion, giving:

$$C_b^p = q_{ero} P_b = \gamma w_s P_b (S_e - \alpha S) \quad (6.12)$$

Assuming a first order decay for the bacteria concentration in the bed sediments, then:

$$P_b = P_b^0 e^{-k_b t} \quad (6.13)$$

$$\frac{dC_T}{dt} = \frac{\gamma w_s}{H} P_b^0 e^{-k_b t} (S_e - \alpha S) - k C_T \quad (6.14)$$

which gives the analytical solution as:

$$C_T = [C_T^0 + \frac{P_b^0 e^{-k_b t}}{\alpha} (S_e - \alpha S_0)(1 - e^{-\lambda t})] e^{-k t} \quad (6.15)$$

Case 3: Equilibrium Vertical Concentration Distribution

For equilibrium conditions, occurring for steady and uniform flow, and with the only source of bacteria being assumed to occur from the bed sediments, then the total bacteria transport equation can be simplified to give:

$$w_s c_p + D_{tz} \frac{\partial c_T}{\partial z} = 0 \quad (6.16)$$

where c_p = attached bacteria concentration;

c_T = total bacteria concentration

Referring to equations (4.25) and (4.26), then the attached bacteria concentration can be

represented as:

$$c_p = \frac{K_D S}{1 + K_D S} c_T \quad (6.17)$$

For equilibrium conditions, the sediment transport equation can be simplified to give:

$$w_s S + D_{tz} \frac{\partial S}{\partial z} = 0 \quad (6.18)$$

For an assumed constant mixing coefficient, if the reference sediment concentration S_a is known, then the sediment concentration profile can be obtained by solving equation (6.18), which gives:

$$S = S_a e^{-\frac{w_s(a-z)}{D_{tz}}} \quad (6.19)$$

Substituting equation (6.17) and (6.19) into equation (6.16) gives:

$$w_s \frac{K_D S_a e^{-\frac{w_s(a-z)}{D_{tz}}}}{1 + K_D S_a e^{-\frac{w_s(a-z)}{D_{tz}}}} c_T + D_{tz} \frac{\partial c_T}{\partial z} = 0 \quad (6.20)$$

By solving this equation, the vertical bacteria concentration profile can be obtained under equilibrium conditions, giving:

$$\frac{c_T}{c_a} = \frac{1 + K_D S_a e^{-\frac{w_s(a-z)}{D_{tz}}}}{1 + K_D S_a} \quad (6.21)$$

where $c_a = S_a P_b$, which is the reference level bacteria concentration.

6.4.2 Validation of Numerical Model against Analytical Solutions:

In this section details are given of the testing of the sediment-bacteria interaction model against the three analytical solutions derived in the previous section.

Case1: Deposition

The computational parameters were set as follows:

1. Water depth = 1 m, grid step size = 1 m and time step = 10 s.
2. Parameters for sediment transport: $\alpha = 1$, $\gamma = 1$ and the fall velocity $w_s = 0.001m/s$. The equilibrium sediment concentration S_e was set to $1kg/m^3$.
3. Partition coefficient K_D set to $10l/g$. Initial sediment concentration was set to be $2kg/m^3$ and the initial bacterial concentration in the water column was set to $100cfu/100ml$. These parameter values gave an initial ratio of attached bacteria to total bacteria of about 0.952. The decay rate in the water column was set to 1 day^{-1} , and the decay in the bed sediments was assumed to be zero.
4. Initial bacteria bed concentration was assumed to be zero.

The comparisons between the model calculated and analytical solutions are shown in Figure 6.10a, 6.10b, 6.10c, 6.10d. From these plots it can be seen that the model predicted results are nearly identical to the analytical solution for the bacteria and suspended sediment concentrations. The good agreement demonstrates that the numerical solution of deposition is correct. Figure 6.10b shows that the sediment deposition processes reach the equilibrium condition after about 3600 seconds, or 1 hour. After reaching equilibrium conditions the sediment concentrations were kept at a constant level. The decay process meant that the total bacteria concentration kept reducing after equilibrium conditions had been achieved for the sediment transport. It can be seen that the bacteria loss due to the sediment deposition occurred in a fairly short time compared to the loss due to decay.

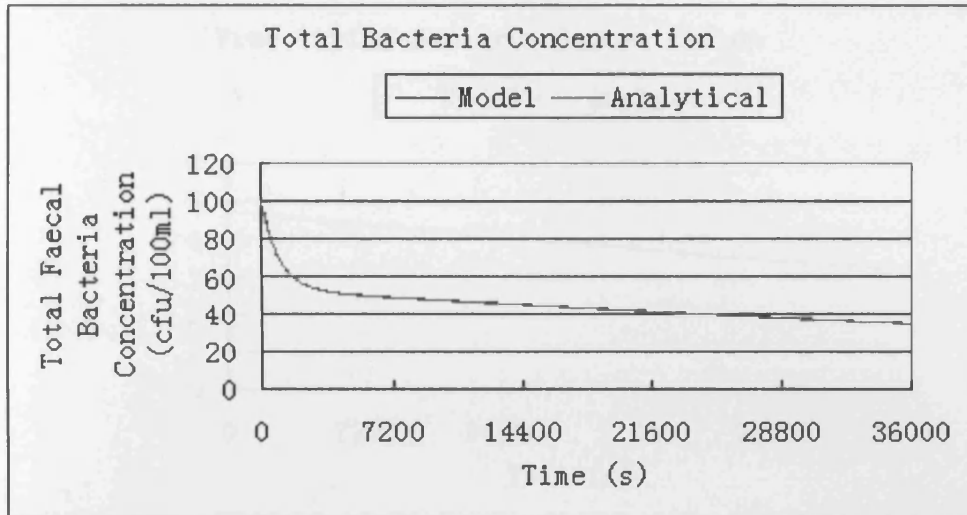


Figure 6.10a Comparison of total bacteria concentration for deposition test

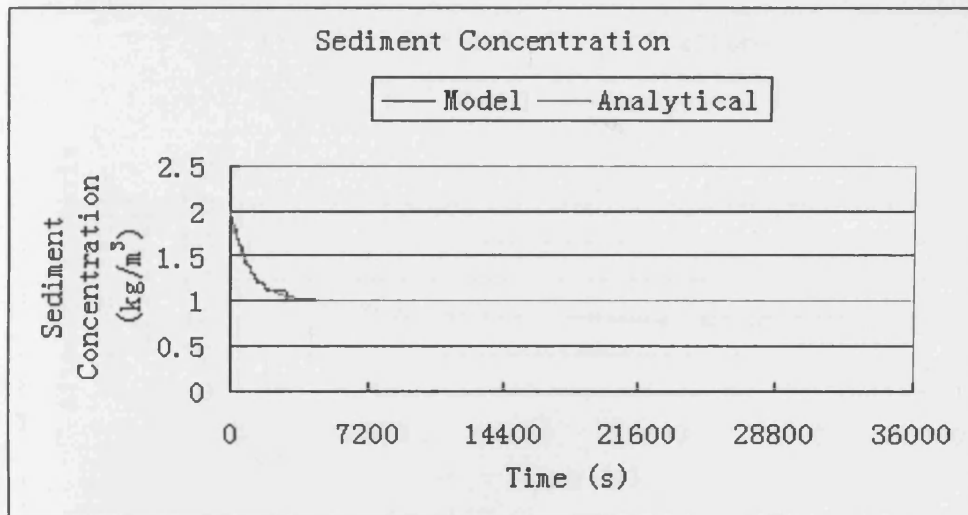


Figure 6.10b Comparison of sediment concentration for deposition test

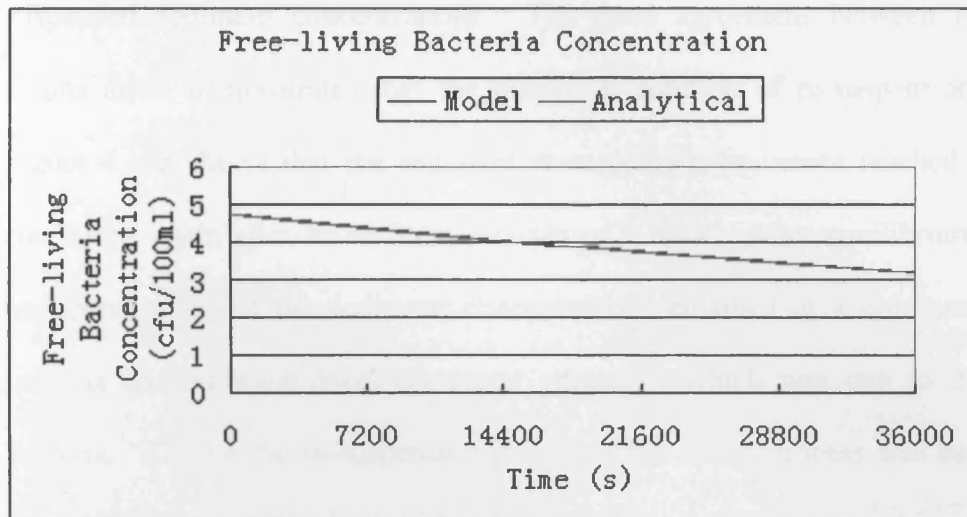


Figure 6.10c Comparison of free-living bacteria concentration for deposition test

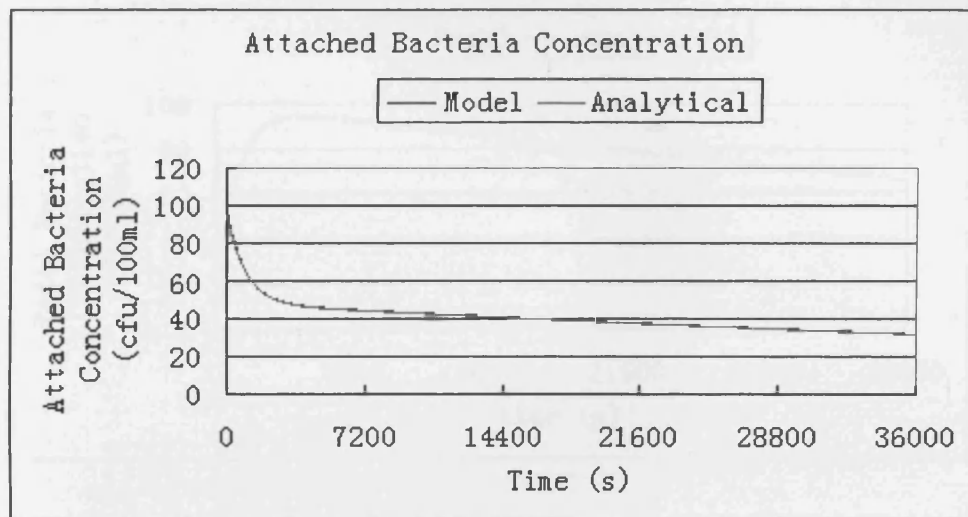


Figure 6.10d Comparison of attached bacteria concentration for deposition test

Case 2: Re-suspension

The set up of the numerical model for this case was the same as that for case 1, except for changes in some initial conditions. For this case $S_0 = 0$, $C_T = 0$ and $P_b^0 = 100cfu / 0.1g$.

The comparison between the model predicted and analytical solutions are shown in Figures 6.11a, 6.11b, 6.11c, 6.11d. From these results it can be seen that the model results are again nearly identical to the analytical results for both the bacteria and

suspended sediment concentrations. The good agreement between both sets of results again demonstrates that the numerical solution of re-suspension is correct. Figure 6.11b shows that the sediment re-suspension processes reached equilibrium conditions again after about 3600 seconds or 1 hour. After equilibrium conditions had been achieved the sediment concentration remained at a constant level. The bacteria concentration level decreased gradually, which was due to decay of the bacteria. During the re-suspension processes the decay process was suppressed by the quick increase of the bacteria level due to the re-suspension.

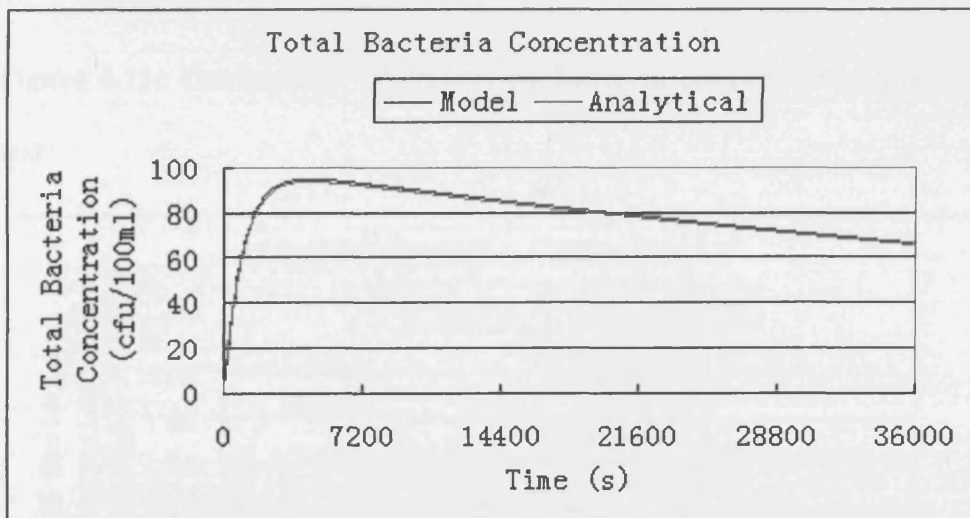


Figure 6.11a Comparison of total bacteria concentration for re-suspension test

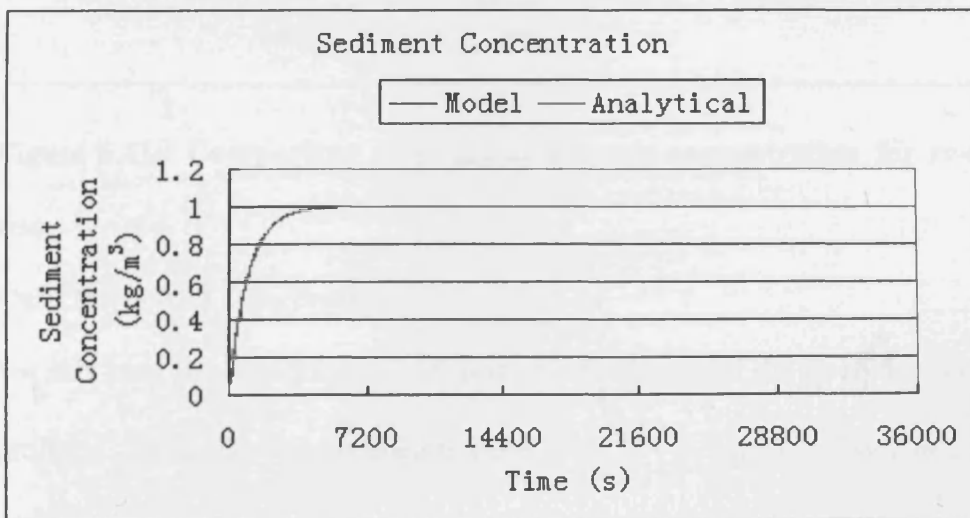


Figure 6.11b Comparison of sediment concentration for re-suspension test

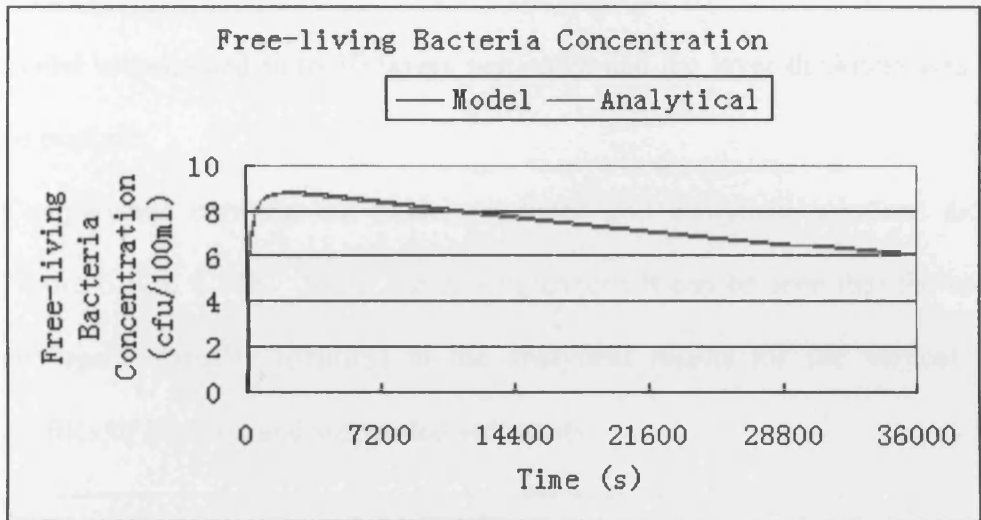


Figure 6.11c Comparison of free-living bacteria concentration for re-suspension test

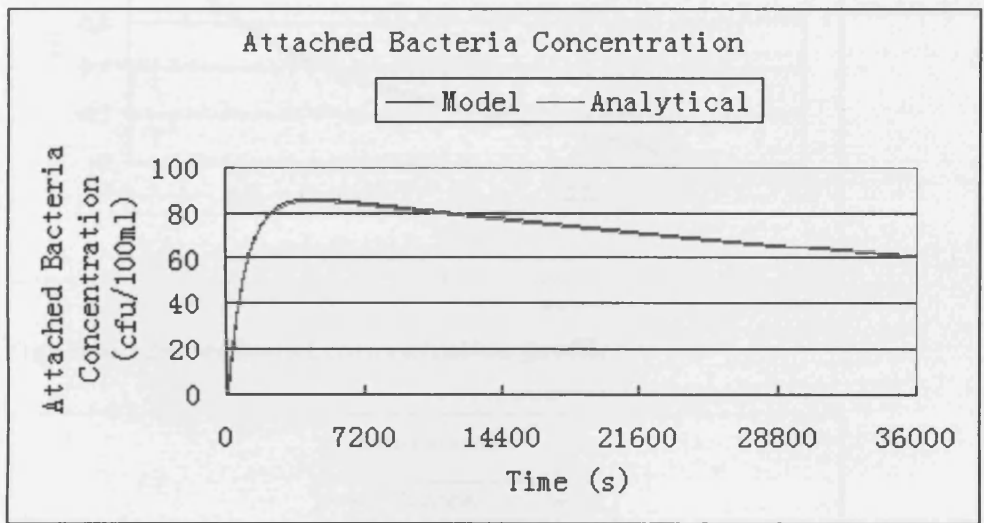


Figure 6.11d Comparison of attached bacteria concentration for re-suspension test

Case 3: Vertical Distribution

For this case the numerical model was validated against the analytical concentration profile. The following parameters were used. $H = 1.0 \text{ m}$, $S_a = 1 \text{ kg} / \text{m}^3$, $a = 0.05 \text{ m}$, $w_s = 0.02 \text{ m} / \text{s}$, $u_c = 0.1 \text{ m} / \text{s}$ and $k_{von} = 0.4$. $P_b = 100 \text{ cfu} / 0.1 \text{ g}$ and $K_D = 10 \text{ l} / \text{g}$.

The mixing coefficient was set to $D_{tz} = \frac{1}{6}ku.H$, as suggested in Van Rijn (1993). The model was divided in to 10 layers vertically, and the layer thickness was assumed to be uniform.

Comparisons between the model predicted and analytical solutions are shown in Figure 6.12a, 6.12b. From these comparisons it can be seen that the model results are again virtually identical to the analytical results for the vertical distribution profiles of bacteria and suspended sediments.

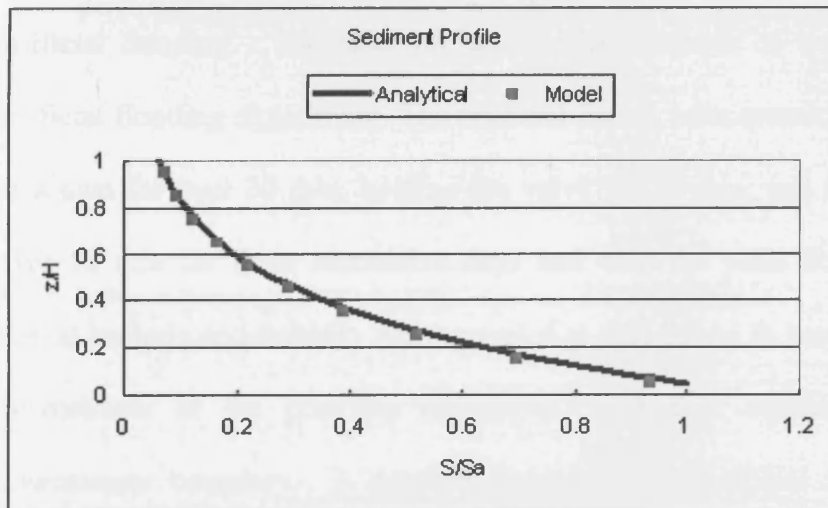


Figure 6.12a Sediment concentration profile

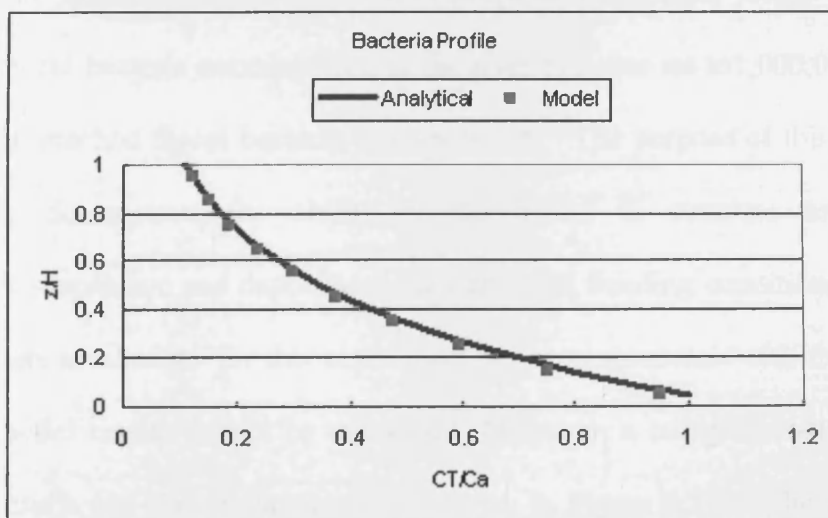


Figure 6.12b Total bacteria concentration profile

Case 4: A Simplified Artificial Flooding Case Study

The numerical model was then tested against the results from a published artificial flooding study. Muirhead et al (2004) conducted a study in Topehaehae Stream in the Waikato Region, New Zealand, to investigate the bacteria transport during floods. This study was reproduced by Bai and Lung (2005). The median flow rate was 260 l/s and the average stream width was 5.8 m. The stream was relatively straight and was therefore simplified to a straight and uniform river. A water supply reservoir, located at the upstream end of the river, was used as the source of water for the artificial flooding. The reservoir was the only source of water supply during the artificial flooding experiment. The artificial floods were created by opening the valve of a dam for over 30 min, holding the valve for 20 min, and then closing the valve over 10 min for three successive days and with the peak flow reaching 4300 l/s. Faecal bacteria and turbidity were sampled at sites A and B, located at 1.3 and 2.5 km downstream of the reservoir respectively. A weir equation was used at the downstream boundary. A detailed account of the artificial flooding procedure is given in Muirhead et al. (2004) and Bai and Lung (2005).

The initial faecal bacteria and sediment concentration levels were set to zero. The faecal bacteria concentration in the river bed was set to 1,000,000 cfu/g and the ratio of attached faecal bacteria was set to 0.8. The purpose of this model test study was to demonstrate the ability of the model to simulate sediment and bacteria re-suspension and deposition under artificial flooding conditions. Due to the limited data availability for this experiment, an accurate match with the predicted numerical model results cannot be expected. However, a comparison of the model predicted results and the measurements is shown in Figure 6.13. The model has reproduced the re-suspension and deposition patterns of the sediment and E coli levels reasonably

well. The differences between the two set of data can explained, not only by the lack of experimental data, but also in that the experimental measurements included turbidity, whereas in the numerical model sediment concentrations were predicted. This was also noted by Bai and Lung (2005).

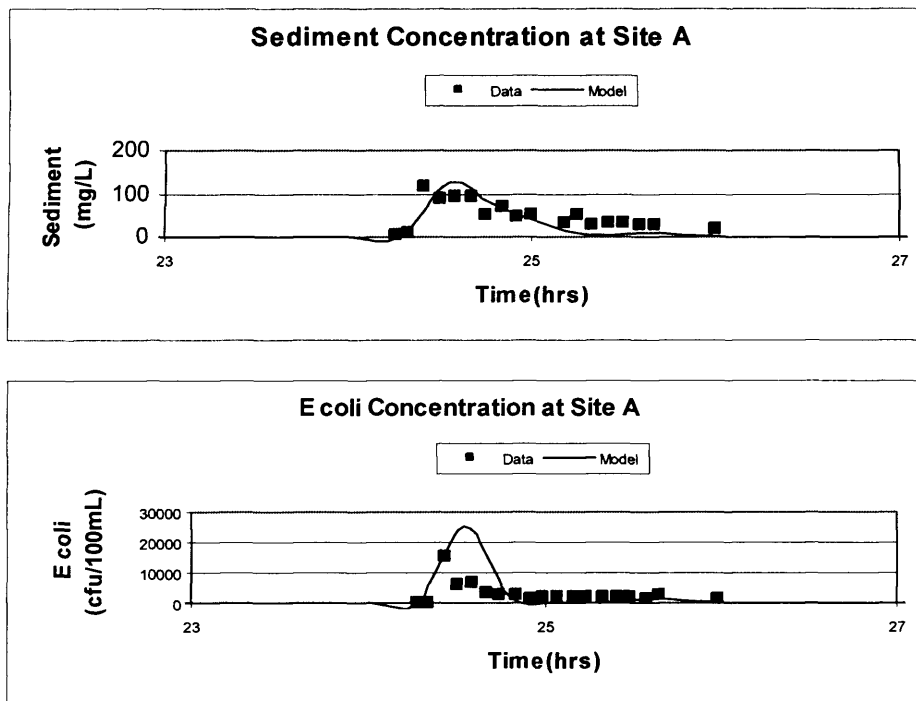


Figure 6.13 Comparison of model results and site data at Site A.

6.5 Idealised Case Application

The sediment-bacteria interaction model has been shown to accurately solve the governing equations and can therefore be used with some confidence to investigate the effects of sediment on the fate and transport of bacteria. In this section idealised test cases were set up to study the effect of removing bacteria from the water column and the subsequent re-suspension of bacteria from the bed.

6.5.1 Removal of Bacteria from the Water Column due to Sediment

6.5.1.1 Effect of the partition coefficient

In order to investigate the effect of the partition coefficient on the removal of bacteria from the water column, partition coefficient K_D values of $10l/g$, $1l/g$, $0.1l/g$ and $0.01l/g$ were used. The initial bacteria bed concentration was assumed to be zero, the initial sediment concentration was set to be $2kg/m^3$ and the initial bacterial concentration in the water column was set to $100cfu/100ml$. The decay rate in water column was set to $1/day$ and the decay rate in the bed sediments was assumed to be zero. The parameters for sediment transport were: $\alpha = 1, \gamma = 1$ and the fall velocity $w_s = 0.001m/s$. The equilibrium sediment concentration S_e was set to be $1kg/m^3$.

The numerical model results are shown in Figure 6.14a, 6.14b, 6.14c. It was observed that with a higher partition coefficient then lower total bacteria concentrations were predicted. The reason for this finding is that the higher partition coefficient gave higher ratios of attached bacteria to total bacteria for the same sediment concentrations, which meant more bacteria being deposited on the bed and thereby giving a lower concentration in the water column.

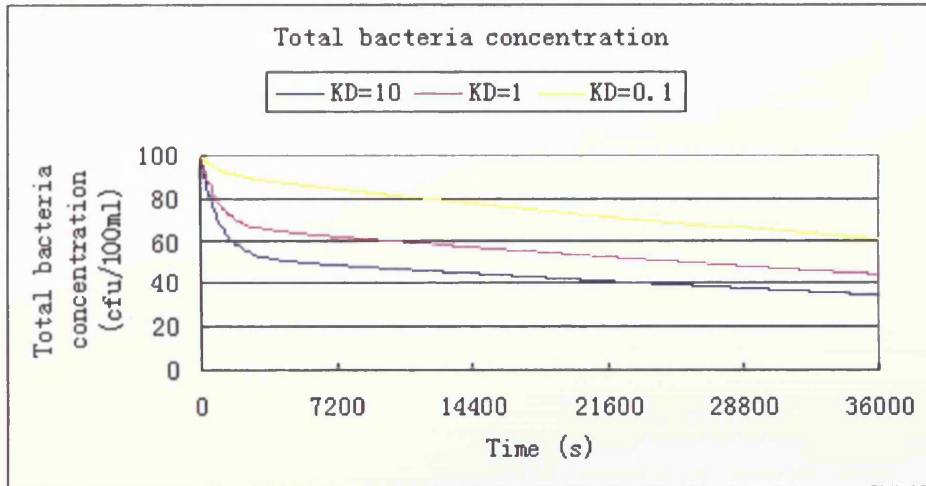


Figure 6.14a Total bacteria concentration for different partition coefficients

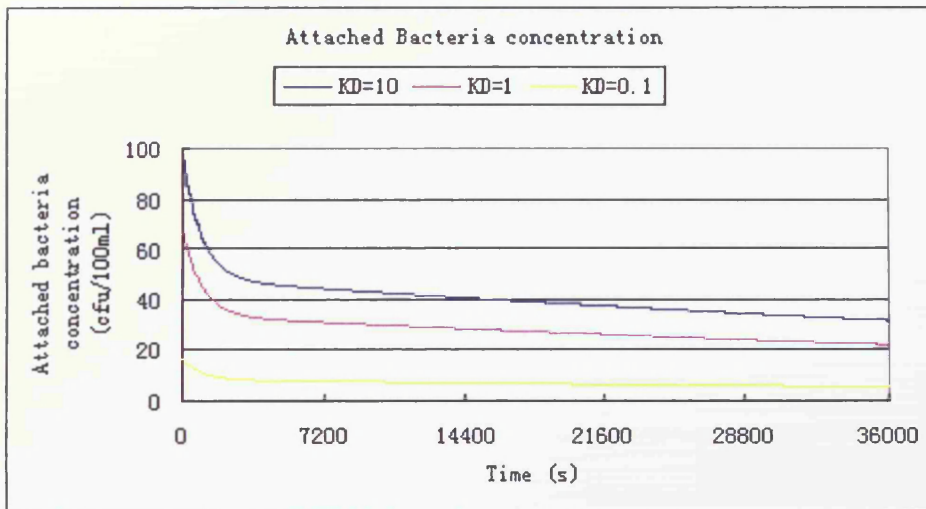


Figure 6.14b Attached bacteria concentration for different partition coefficients

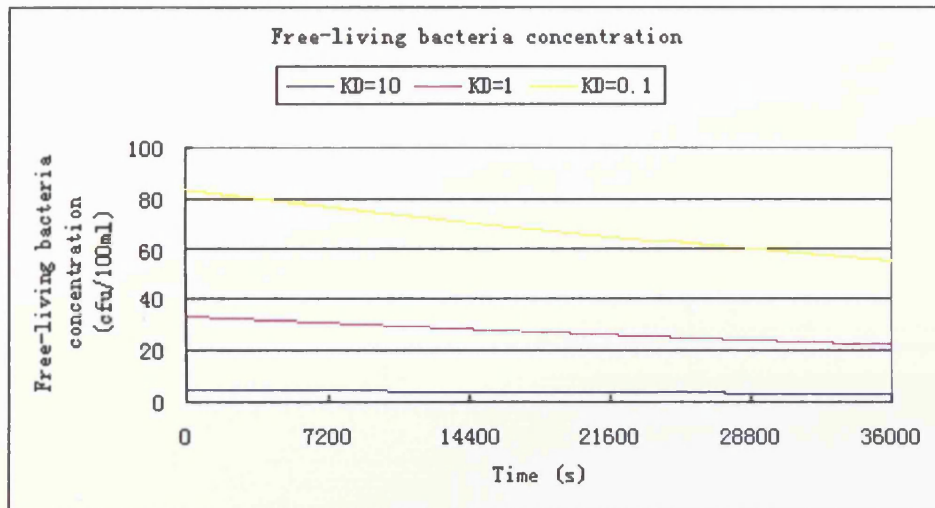


Figure 6.14c Free-living bacteria concentration for different partition coefficients

6.5.1.2 Effect of different sediment sizes giving different settling velocities

Settling velocities of $w_s = 0.001m/s$, $0.0001m/s$, $0.00001m/s$ were used respectively to consider the effects of particle sediment size on the removal of bacteria from the water column. The initial bacteria bed concentration was assumed to be zero, the initial sediment concentration was set to be $2kg/m^3$ and the initial bacterial concentration in the water column was set to be $100cfu/100ml$. The decay rate in water column was set to $1/day$, and the decay rate in the bed sediments was assumed to be zero. The partition coefficient K_D was set to $10l/g$, which gave an initial ratio of attached to total bacteria of 0.952, which would decrease with a corresponding decrease of the sediment concentration in the water column. The equilibrium sediment concentration S_e was set to $1kg/m^3$.

The numerical model results are shown in Figure 6.15a, 6.15b, 6.15c. It can be seen that higher settling velocities reduced the total bacteria concentration level much quicker than the lower settling velocity. The concentration of free-living bacteria was not affected by the settling velocity. The reduction in the free-living bacteria in

the water column was therefore purely due to decay.

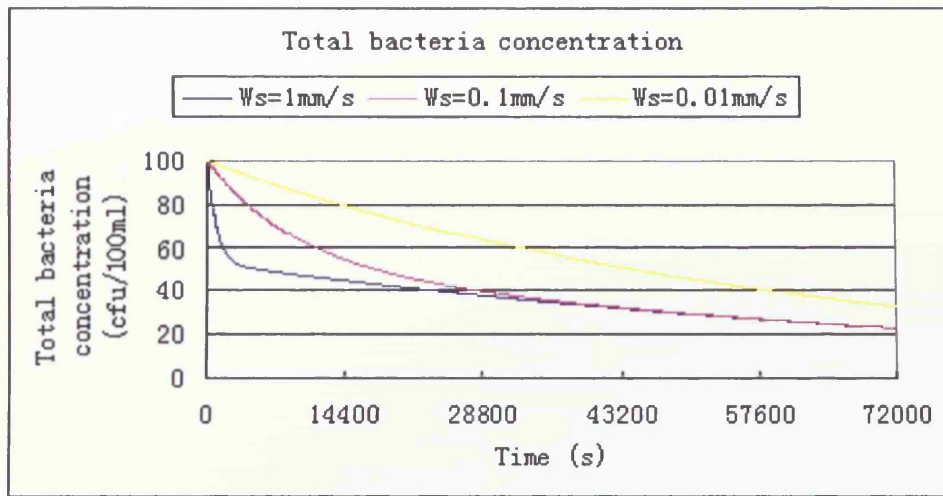


Figure 6.15a Total bacteria concentration for different settling velocities

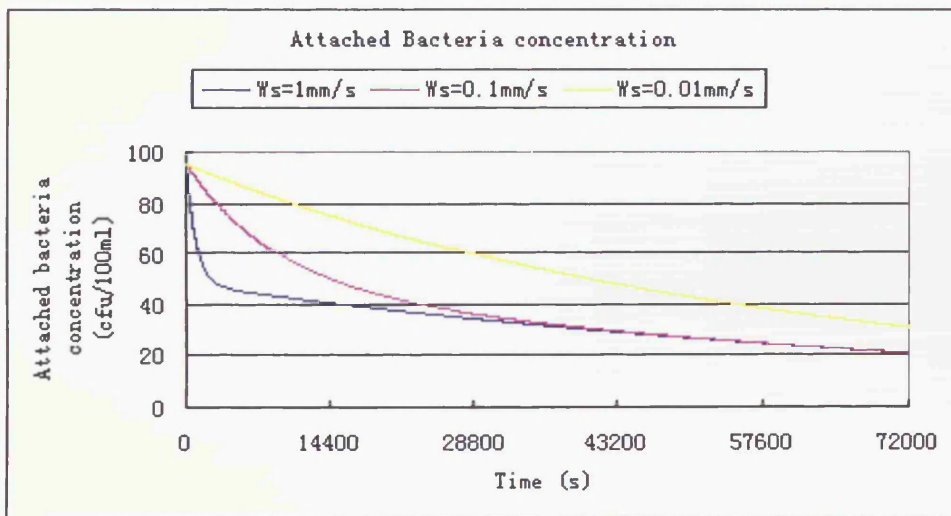


Figure 6.15b Attached bacteria concentration for different settling velocities

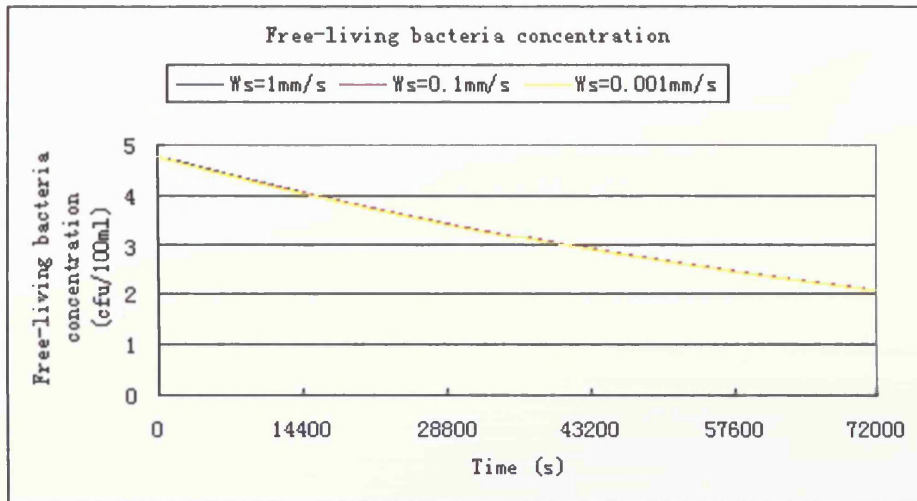


Figure 6.15c Free-living bacteria concentration for different settling velocities

6.5.2 Re-suspension of Attached Bacteria to Water Column

6.5.2.1 Effect of bed bacteria concentration

The initial bed bacteria concentration assumed in the investigations was either $100 \text{ cfu}/0.1 \text{ g}$, or $50 \text{ cfu}/0.1 \text{ g}$, or $10 \text{ cfu}/0.1 \text{ g}$, with this value being used to investigate the effect of the bed concentrations on the re-suspension of the attached bacteria. The initial sediment concentration was assumed to be zero and the initial bacterial concentration in the water column was also set to zero. The decay rate in the water column was set to $1/\text{day}$, and the decay in the bed sediment was assumed to be zero. Parameters for the sediment transport model components included: $\alpha = 1$, $\gamma = 1$, fall velocity $w_s = 0.001 \text{ m/s}$, equilibrium sediment concentration $S_e = 1 \text{ kg}/\text{m}^3$ and the partition coefficient $K_D = 10 \text{ l/g}$.

The numerical model predictions are shown in Figure 6.16a, 6.16b, 6.16c. From these results it can be seen that higher bed bacteria concentrations gave rise to much higher bacteria concentrations in the water column. Higher bed bacteria concentrations mean that more bacteria contribute to the water column under the same conditions as

for re-suspension, i.e. the bacteria re-suspended into the water column with the sediments and then re-partition into the water column.

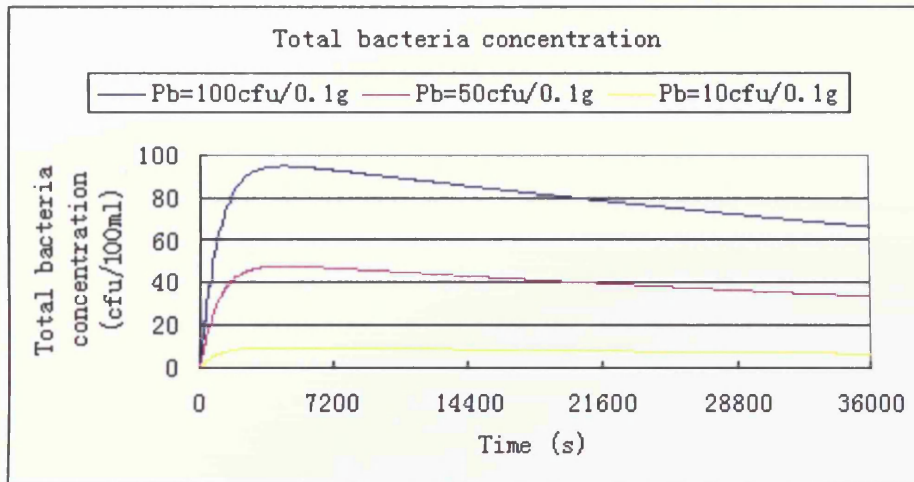


Figure 6.16a Total bacteria concentrations for different bed bacteria concentrations

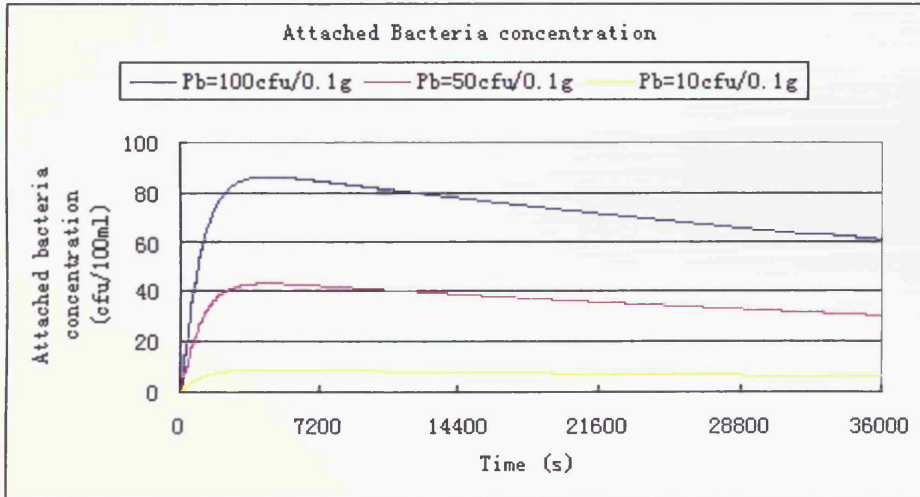


Figure 6.16b Attached bacteria concentrations for different bed bacteria concentrations

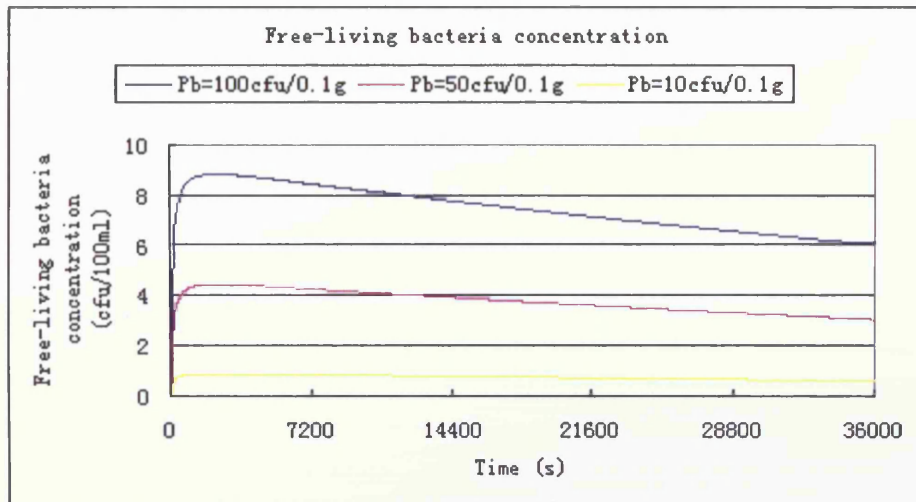


Figure 6.16c Free-living bacteria concentrations for different bed bacteria concentrations

6.5.2.2 Effect of partition coefficient

For this test case different partition coefficients were used to investigate the effect of the partition coefficient on the re-suspension of bacteria and the values considered included: $K_D = 10\text{ l/g}, 1\text{ l/g}, 0.1\text{ l/g}, 0.01\text{ l/g}$ respectively. The initial bed bacteria concentration was assumed to be $100\text{ cfu}/0.1\text{ g}$, the initial sediment concentration was set to zero and the initial bacterial concentration in the water column was set to zero. The decay rate in the water column was set to $1/\text{day}$ and the decay rate in the bed sediments was assumed to be zero. The governing parameters for the sediment transport model were: $\alpha = 1, \gamma = 1$, the fall velocity $w_s = 0.001\text{ m/s}$ and the equilibrium sediment concentration S_e was set to $1\text{ kg}/\text{m}^3$.

The numerical model results are shown in Figure 6.17a, 6.17b, 6.17c, where it can be seen that the partition coefficient does not significantly affect the total bacteria concentration in the water column in the re-suspension mode. It only effects the partitioning between the attached and free-living bacteria, with a higher partition

coefficient giving a higher attached bacteria ratio and a lower free-living bacteria ratio.

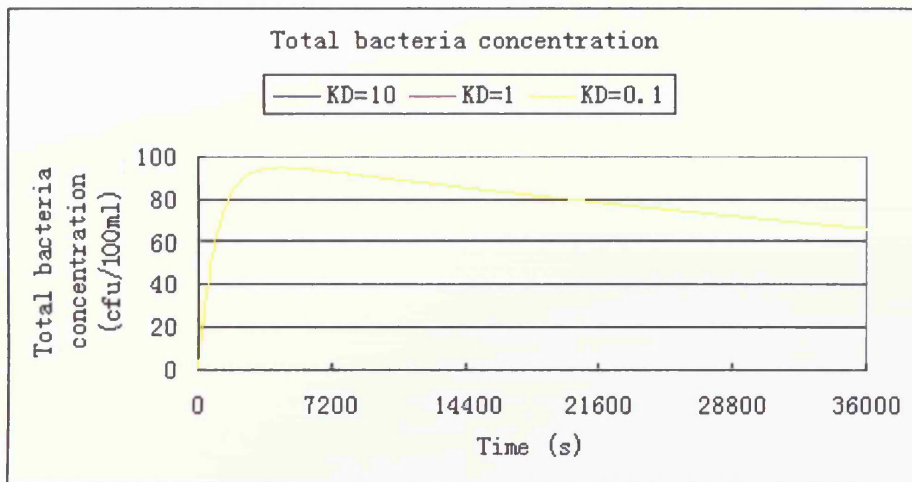


Figure 6.17a Total bacteria concentrations for different partition coefficients

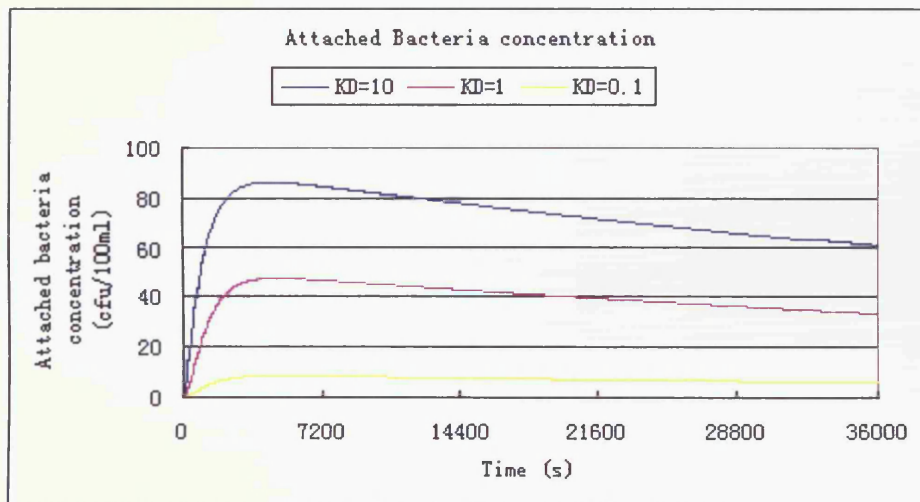


Figure 6.17b Attached bacteria concentrations for different partition coefficients

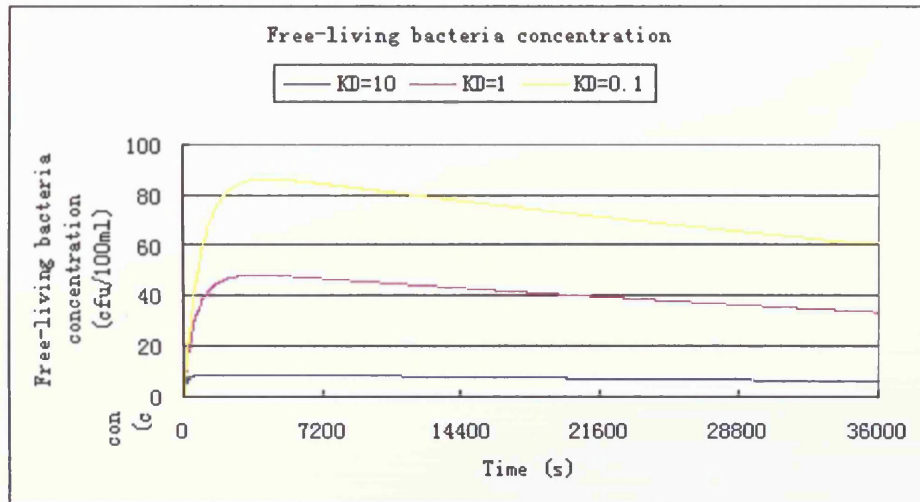


Figure 6.17c Free-living bacteria concentrations for different partition coefficients

6.6 Summary

In this chapter the numerical models have been tested against controlled data, primarily in the form of analytical solutions. Flume experimental data were used to test the hydrodynamic model; published experimental data were used to test the sediment transport model and three sets of analytical solutions were derived and used to test the sediment-bacteria interaction model. The sediment-bacteria model was also tested against data for an artificial flooding scenario. All of these test cases were found to give encouraging results. After validation the models were then set up for an idealised case to investigate the effects of different parameters on the deposition and re-suspension of bacteria.

Chapter 7

Modelling Hydrodynamic, Sediment and Bacterial Processes in the Bristol Channel and Severn Estuary

7.1 Introduction

The Severn Estuary and Bristol Channel is one of the largest estuaries in the UK and is situated on the south west coast between South East Wales and South West England (see Figure 7.1). The estuary has the second highest tidal range in the world, with these tides, particularly during spring conditions, generating large currents (in excess of 3 m/s) and very high suspended concentrations (in excess of 1000 mg/l).



Figure 7.1 Location of the Bristol Channel and Severn Estuary

There are thirty one bathing water compliance locations and twenty nine river input catchment outlets around the Severn Estuary, which are summarised in Stapleton et al (2007) and illustrated in Figure 7.2. There are also thirty four Waste water Treatment Works (WwTW) outfalls located around the Estuary (see Figure 7.3).

Location in the UK:



0 50 km

This map is reproduced from the OS map by the Environment Agency with the permission of the Controller of Her Majesty's Stationery Office. Crown Copyright. Unauthorised reproduction infringes Crown Copyright and may lead to prosecution or civil proceedings. Licence Number GD 08/775

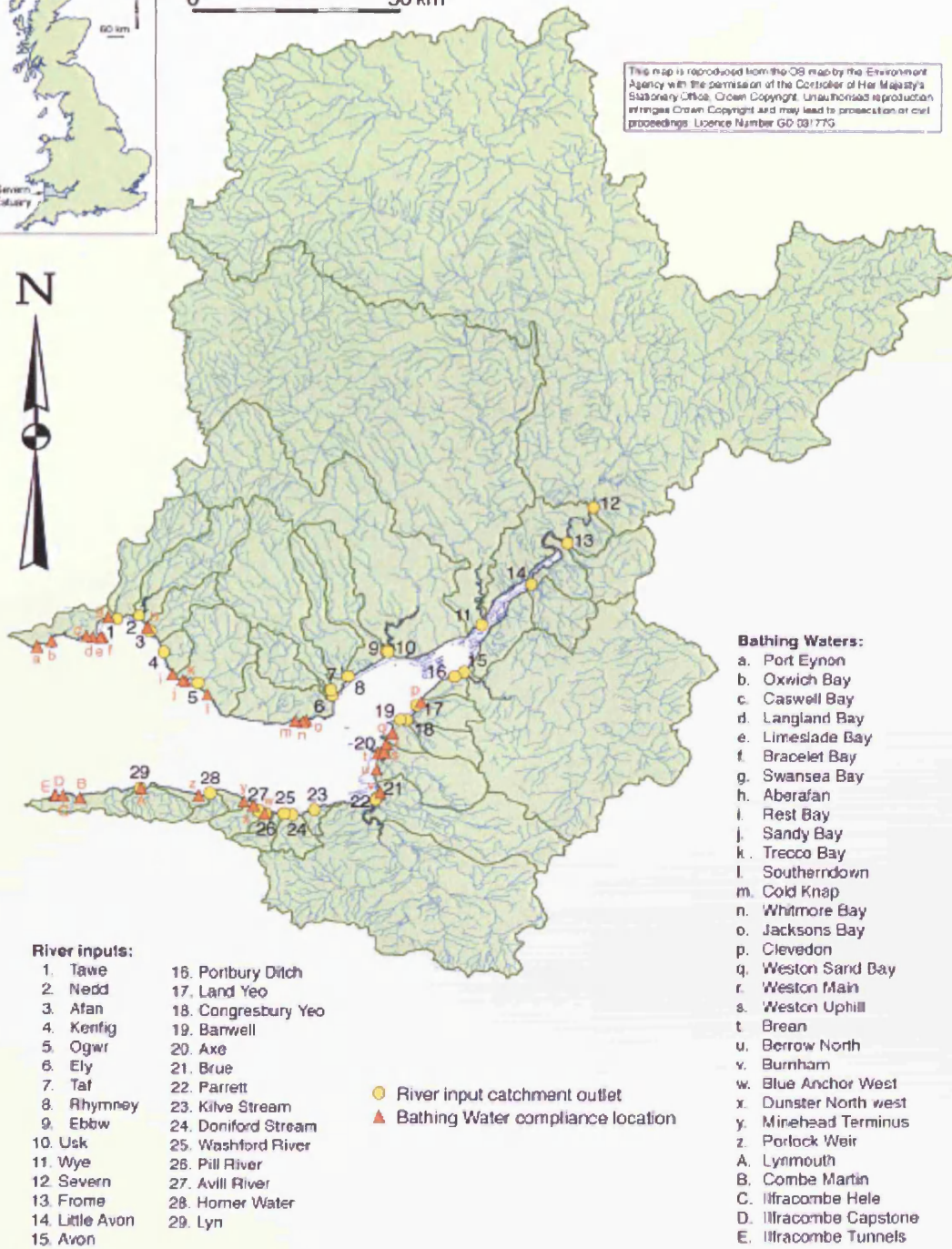


Figure 7.2: Bathing water compliance monitoring sites, main river catchments and locations of outlets to the Severn estuary (Stapleton et al 2007)

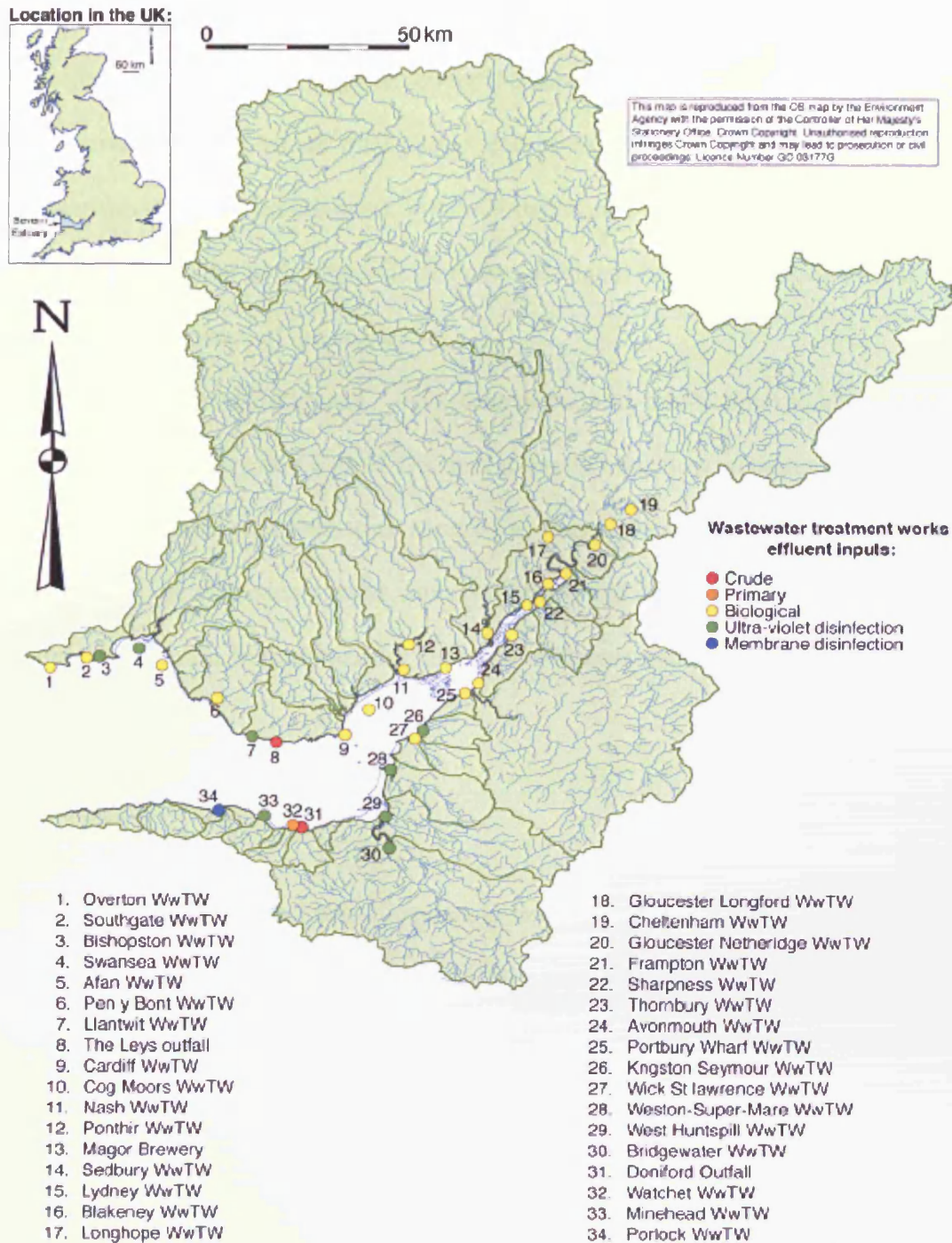


Figure 7.3: Location and treatment type of waste water treatment works effluent inputs, with population equivalents greater than 2000 to the Severn Estuary (Stapleton et al 2007)

With the Severn Estuary having the second highest tidal range in the world, this makes it an ideal basin for extracting tidal energy to supplement the energy demand. There are several means by which tidal energy can be extracted from the basin, including: tidal stream turbines, tidal lagoons and tidal barrages. Such tidal energy devices and structures affect the hydrodynamic features, sediment transport processes and water quality characteristics of the basin.

In this chapter the hydrodynamic and sediment-bacteria interaction model was applied to the Severn Estuary and Bristol Channel to predict the flow, sediment transport and bacterial indicator characteristics across the domain and for a range of different scenarios. The numerical model was also refined and set up to investigate the effects of tidal barrage on hydrodynamic, sediment transport and bacterial processes along the estuary.

7.2 Model Set Up

In this study area one- and two-dimensional flows co-exist along different parts of the estuary, and hence a dynamically linked 1-D (FASTER) and 2-D (DIVAST) model has been set up for this basin. The various methods frequently used for linking the 1-D and 2-D models were reviewed in Lin and Falconer (2005). The method used in this study was originally developed and detailed in Kashefipour (2002) and Kashefipour et al (2002a). The linked numerical model covered the whole of the Bristol Channel and the Severn Estuary up to the tidal limit near Gloucester. Therefore, the model area was divided into two grid systems, namely the 2-D and 1-D regions. The 2-D region covered the Bristol Channel (14,636.2 km²) and outer estuary, which was divided into a mesh of 242×168 grid squares, with a size of 600 m × 600 m. The 1-D part covered the region from the M4 (new) Severn Bridge (i.e. the

downstream boundary of the 1-D model) to Haw Bridge (i.e. the upstream boundary). This model included a total of 351 cross-sections, with an average distance between the cross-sections of 240 m. The downstream (or seaward) boundary was specified as a tidal water elevation boundary, whilst the upstream boundary was specified in the form of an open flow boundary, which was generally set to the average flow rate for the river Severn. For the sediment and bacterial model boundary conditions, it is assumed that there is no input of sediment and bacteria from both the seaward and upstream boundary. The downstream boundary water level was obtained from the Proudman Oceanographic Laboratory (POL) tidal harmonic model for the Bristol Channel.

7.2.1 One-dimensional Model Set Up

The one-dimensional model included a total of 351 cross sections along the reach of the River Severn. The two-dimensional model provided the water elevation data at the downstream boundary of the one-dimensional model. The bed elevation was referenced to Ordnance Datum at Avonmouth. The downstream boundary of this model was set at the M4 (new) Severn Bridge and the upstream boundary extended to the tidal limit of the river at Haw Bridge. The Severn Estuary splits into two channels at Upper Parting, namely the East Channel and West Channel, and at Lower Parting the two channels of the estuary rejoin. This feature was included in the one-dimensional model by using 4 reaches. The first reach was from the M4 (new) Severn Bridge to the Lower Parting; the second reach was the East Channel from Lower Parting to Upper Parting; the third reach was the West Channel from Lower Parting to Upper Parting; and the fourth reach was from Upper Parting to Haw Bridge.

Among the river and WwTW inputs, summarised in Figures 7.2 and 7.3, there are 4 river inputs and 6 WwTW inputs located in the one-dimensional domain; these are listed in Tables 7.1 and 7.2.

Table 7.1: River catchments input in one-dimensional model domain

River inputs	Easting	Northing
Wye	354231	190223
Little Avon	366257	200314
Frome	375173	210497
Severn	381584	219350

Table 7.2: WwTW inputs in one-dimensional model domain

WwTW inputs	Easting	Northing
Thornbury STW	359990	193010
Sedbury	353990	194420
Lydney	363760	200550
Sharpness	367000	201500
Longhopes STW	369060	217880
Blakeney	369110	206040
Frampton	373570	208530
GLocester Netheridge STW	380900	215900
Cheltenham STW	389930	224860
Glocester Longford STW	384730	221180

7.2.2 Two-dimensional Model Set Up

The two-dimensional model was set up for the Bristol Channel and lower Severn Estuary, covering an area of 14,636.2 km², which was divided into a mesh of 242×168 grid squares, with a size of 600 m × 600 m.

The bed elevation data were referenced to Ordnance Datum (OD) across the domain, with the data obtained by digitising the Admiralty Chart and converting the bed data from Chart Datum to Ordnance Datum. The bathymetry of the Bristol Channel and lower Severn Estuary is shown in Figure 7.4.

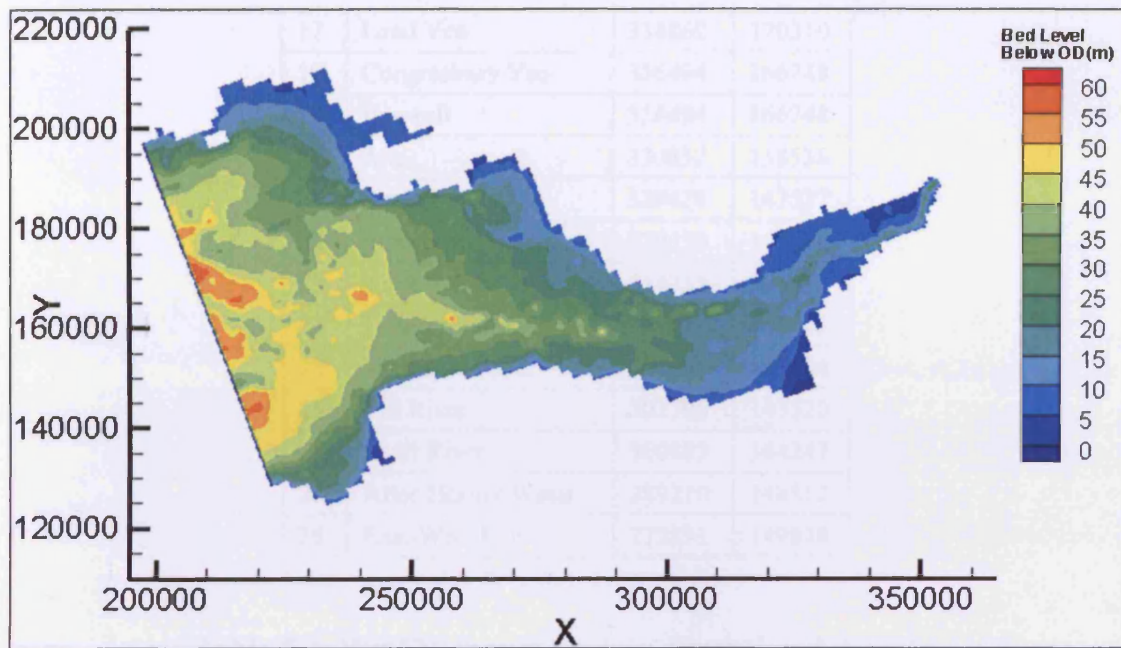


Figure 7.4: Bathymetry of the Bristol Channel and lower Severn Estuary.

Water surface elevations were applied at the seaward boundary. The one-dimensional model provided the velocity or discharge data at the upstream boundary of the two-dimensional model. The river catchment input locations and the WwTW input locations for the two-dimensional domain are summarised in Tables 7.3 and 7.4.

Table 7.3: River catchment inputs for two-dimensional domain

No	River input	Easting	Northin g
1	Tawe	266598	191653
2	Nedd	271881	192432
3	Afan	274556	188667
4	Kenfig	277919	183473
5	Ogwr	286123	175787
6	Ely	318583	172672
5	Taff	318218	172672
8	Rhymney	322282	177474
9	Ebbw	331480	183805
10	Usk	331798	183633
15	Avon	350115	178583
16	Portbury Ditch	347817	177420

17	Land Yeo	338862	170310
18	Congresbury Yeo	336494	166748
19	Banwell	336494	166748
20	Axe	330852	158536
21	Brue	329428	147527
22	Parrett	329130	146844
23	Kilve Stream	314335	144453
24	Doniford Stream	309059	143213
25	Washford River	306997	143524
26	Pill River	302706	143520
27	Avill River	300883	144247
28	Aller-Horner Water	289210	148512
29	East-West Lyn	272291	149678

Table 7.4: WwTW inputs for two-dimensional domain

No.	WwTW inputs	Easting	Northing
1	Overton WwTW	246395	184485
2	Southgate WwTW	255385	187005
3	Bishopston WwTW	258605	187305
4	Swansea WwTW	268370	189437
5	Afan WWTW	274055	185075
6	Pen y Bont WwTW	287845	176845
7	Llantwit Major WWTW	296355	167145
8	The Leys outfall, Aberthaw	302305	165605
9	Cardiff WWTW	325085	173955
10	Cog Moors WwTW	319306	167576
11	Nash WwTW	333455	184115
12	Ponthir WwTW	334665	190435
13	Magor Brewery Effluent	343765	184585
24	Avonmouth WwTW	351900	180700
25	Portbury Wharf WwTW	348550	178150
26	Kingston Seymour WwTW	338400	168660
27	Wick St Lawrence WwTW	336510	166600
28	Weston-Super-Mare WwTW	330580	158690
29	West Huntspill WwTW	329420	146840
30	Bridgewater WwTW	330340	138810
31	Doniford Outfall	308740	144010
32	Watchet WwTW	306520	144550
33	Minehead WwTW	299450	146970
34	Porlock WwTW	288350	148300

7.3. Model Calibration and Validation

Before a numerical model is applied to different scenarios, it first needs to be calibrated to obtain the best possible match between model predictions and measured data. In this study the hydrodynamic model was calibrated against Admiralty Chart data at Sites F, M and V. After calibration the hydrodynamic model was validated against measurement data at Site S Wales and Minehead. The locations of these calibration and validation sites are shown in Figure 7.5. The sediment transport and bacteria transport model were calibrated against measured data, in order to predict the enterococci concentrations at compliance points located along the estuary. The time step was set to 25s. The momentum correction factor was set to 1.016 and wind stress was not considered in this study.

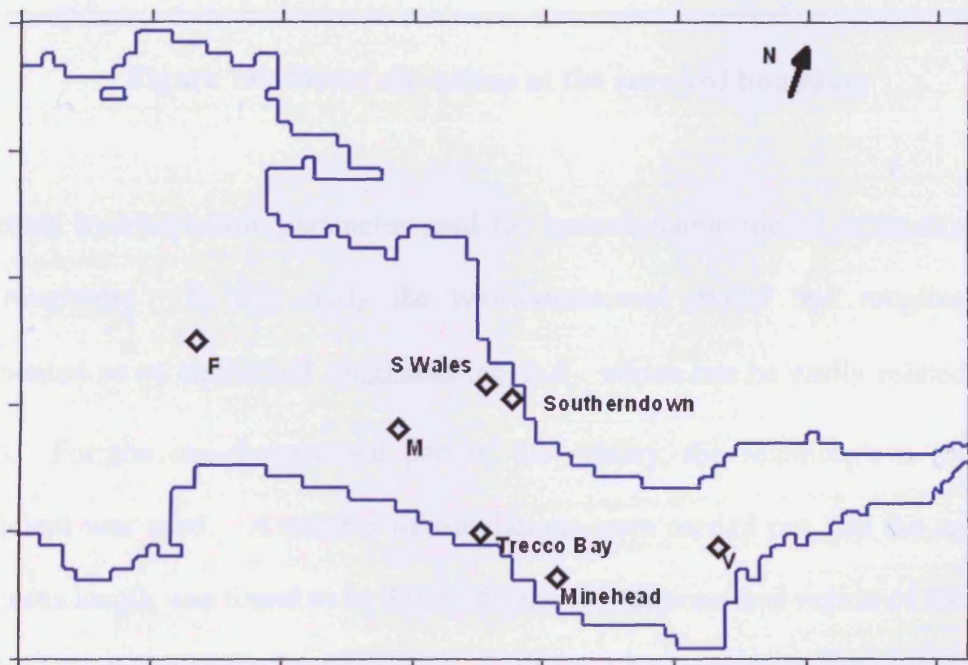


Figure 7.5: Location of calibration sites

7.3.1 Hydrodynamic Model Calibration and Validation

The measured discharges at the tidal limit of the River Sever were not available.

Averaged discharges over the simulation period were used as upstream boundary. The seaward boundary water levels were predicted using the POL Bristol Channel model, which is shown in Figure 7.6. A period of 300 hours was selected for the simulation time and this covered the data measuring period, which included a spring tide, a neap tide and mid-tide cycles.

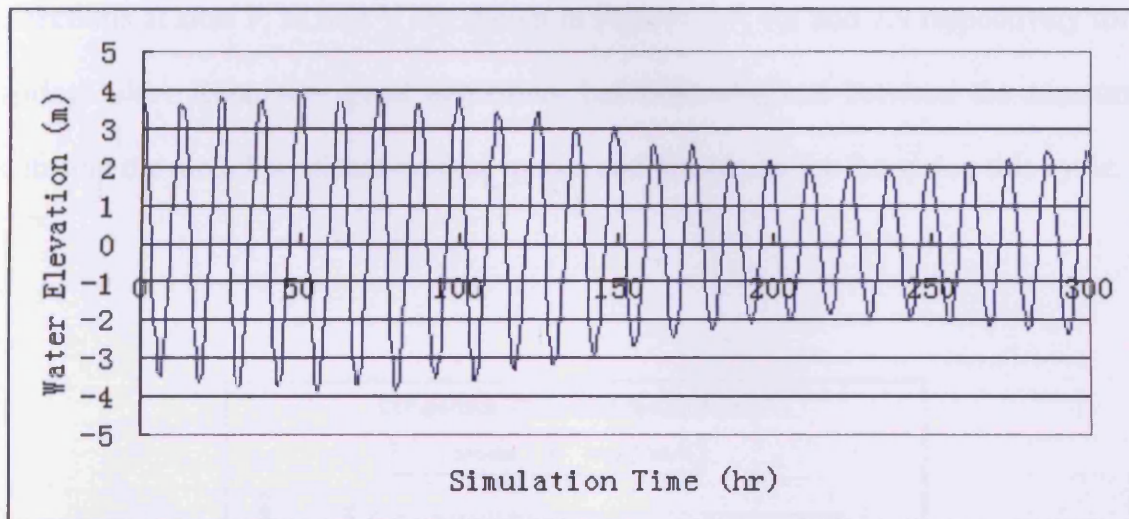


Figure 7.6: Water elevations at the seaward boundary

The main hydrodynamic parameter used for hydrodynamic model calibration is the bed roughness. In this study the two-dimensional model bed roughness was represented as an equivalent roughness length k_s , which can be easily related to bed forms. For the one-dimensional part of the estuary, the Manning's n roughness coefficient was used. A number of simulations were carried out and the calibrated roughness length was found to be 35mm for the two-dimensional region of the model. For the one-dimensional model part, the calibrated Manning's roughness coefficient was optimised at 0.022.

The velocities at the three Admiralty Chart data sites, including Sites F, M and V, were used for the hydrodynamic calibration of the model. The model was then run to

predict the hydrodynamic features and the predictions were compared to the values at these calibration sites, for both spring and neap tides.

Spring tide

Comparisons of the Admiralty Chart data and the predicted current speeds and directions at sites F, M and V are shown in Figures 7.7, 7.8 and 7.9 respectively for a spring tide. Relatively good agreement has been obtained between the measured data and the model predicted current speeds and directions, for the spring tide cycle.

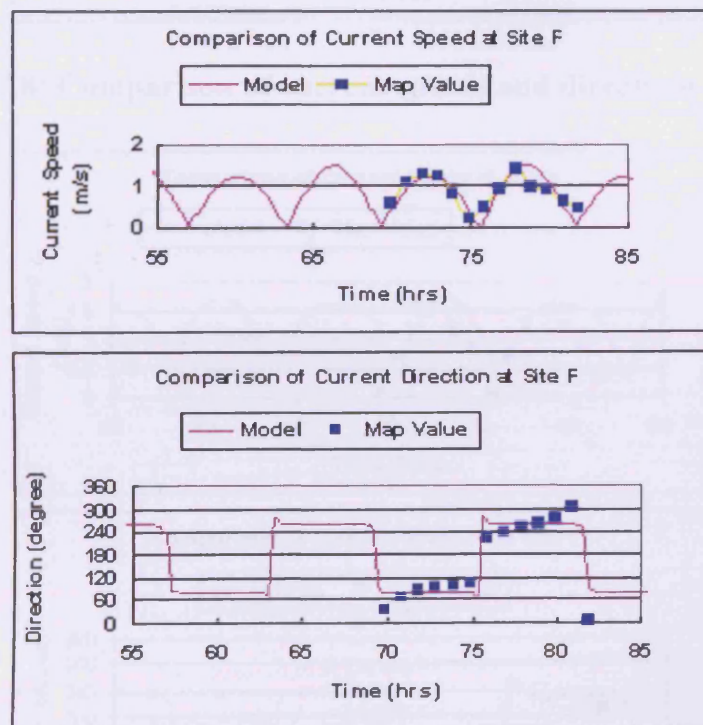


Figure 7.7: Comparison of current speeds and directions at Site F

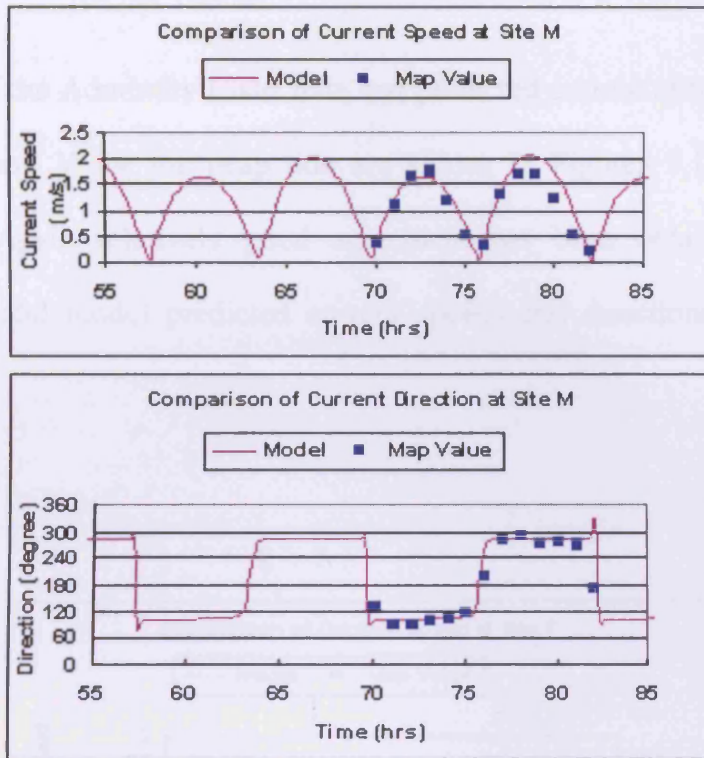


Figure 7.8: Comparison of current speeds and directions at Site M

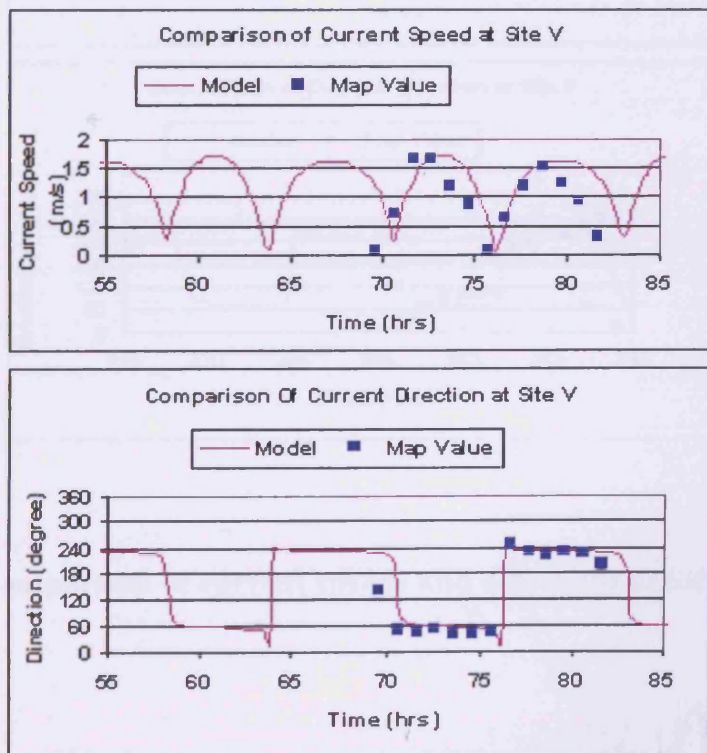


Figure 7.9: Comparison of current speeds and directions at Site V

Neap tide

Comparisons of the Admiralty Chart data and predicted current speeds and directions at Sites F, M and V for the neap tide are shown in Figures 7.10, 7.11 and 7.12 respectively. Again relatively good agreement has been obtained between the measured data and model predicted current speeds and directions for a neap tide cycle.

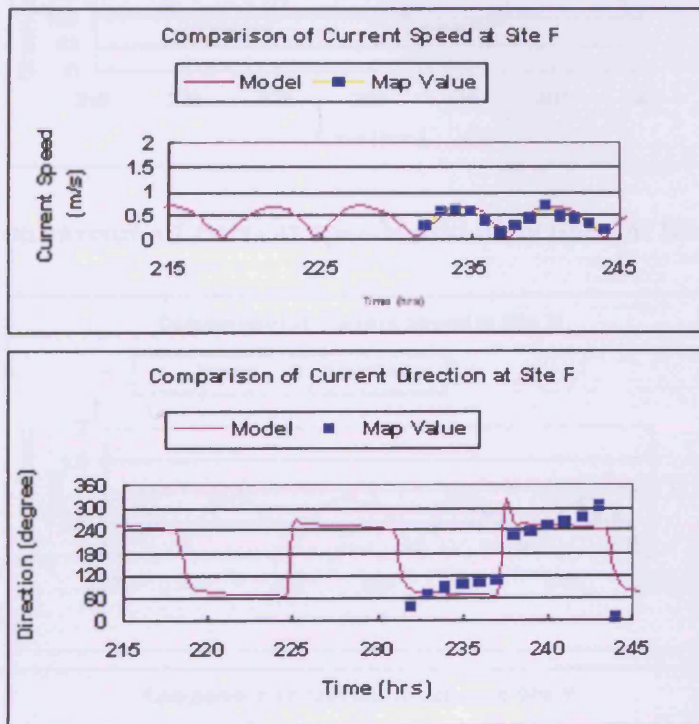


Figure 7.10: Comparison of current speeds and directions at Site F for neap tide

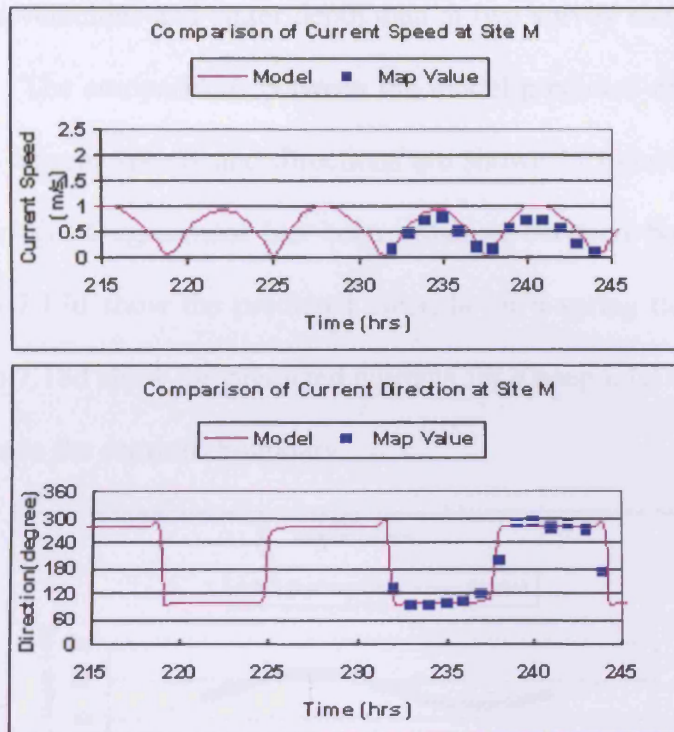


Figure 7.11: Comparison of current speeds and directions at Site M for neap tide

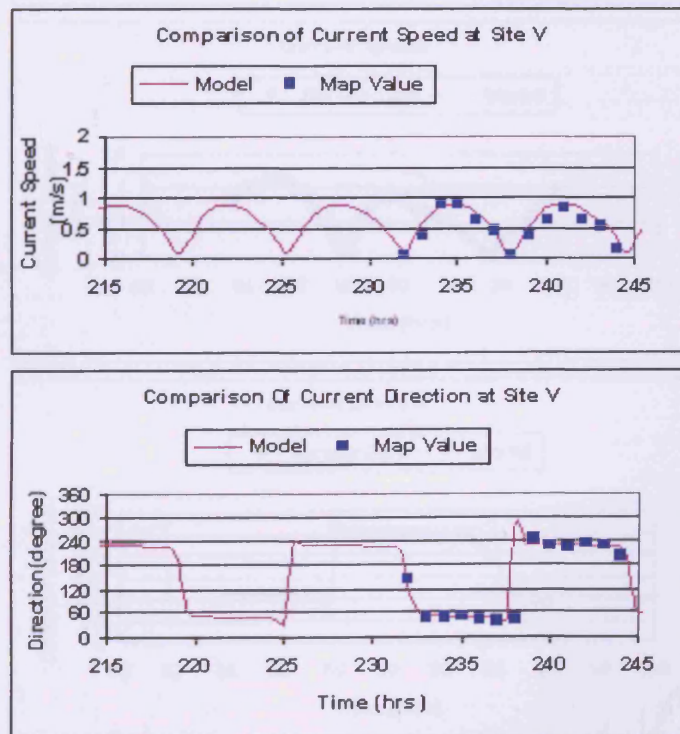


Figure 7.12: Comparison of current speeds and directions at Site V for neap tide

After calibration of the hydrodynamic model, the model was then verified using four

sets of observed velocities and water depth data at two survey sites, namely S Wales and Minehead. The comparisons between the model predicted and measured water depths, and the current speeds and directions are shown in Figures 7.13, 7.14, 7.15 and 7.16. Again good agreement has been obtained between both sets of results. Figure 7.17a to 7.17d show the predicted currents for a spring tidal cycle, whereas Figures 7.18a to 7.18d show the predicted currents for a neap tidal cycle with the tidal phases reference to the seaward boundary.

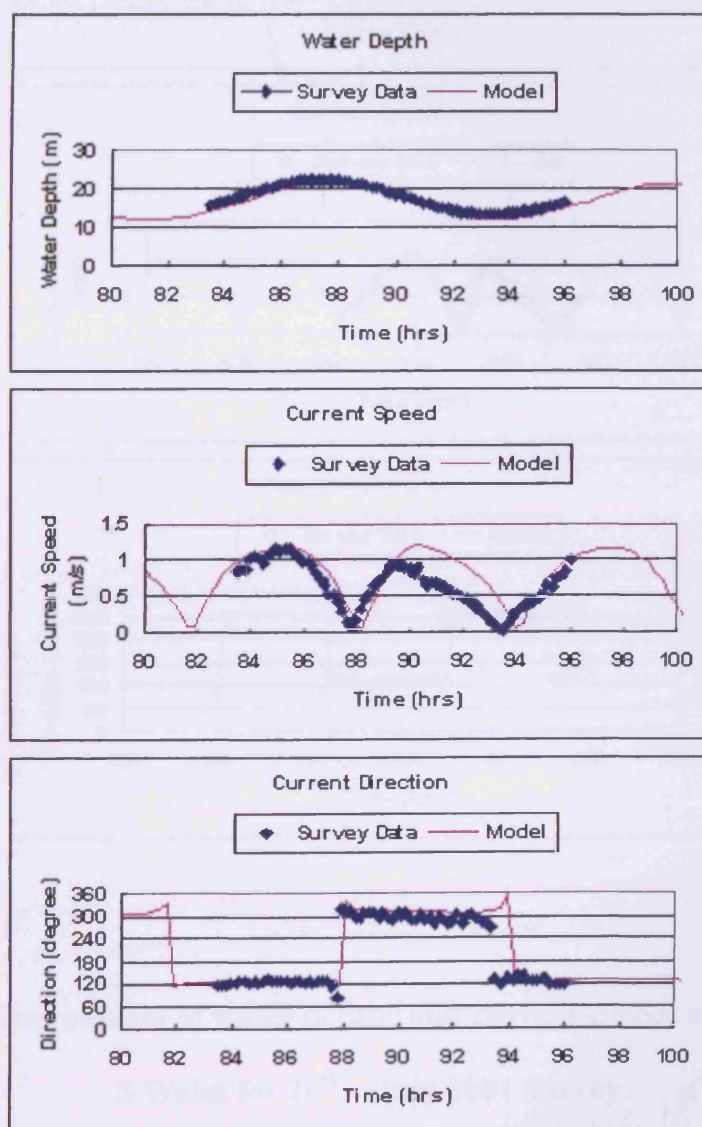


Figure 7.13: Comparison of water depths and current speeds and directions at S Wales for 24th July 2001 Survey

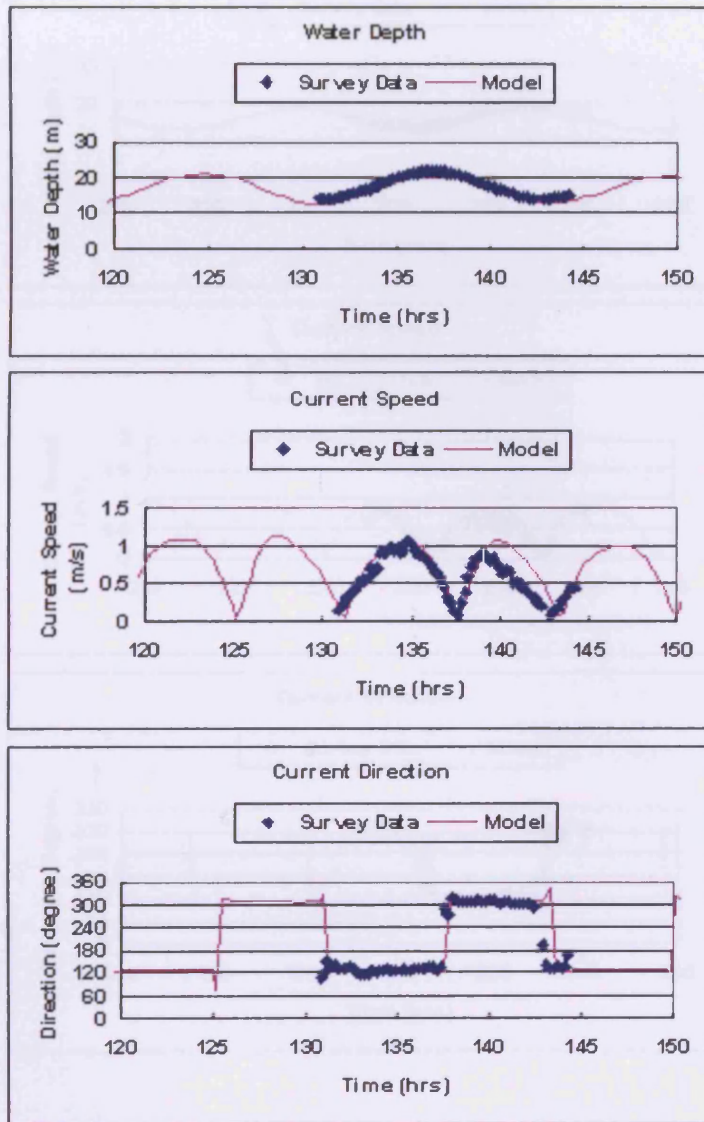


Figure 7.14: Comparison of water depths and current speeds and directions at S Wales for 26th July 2001 Survey

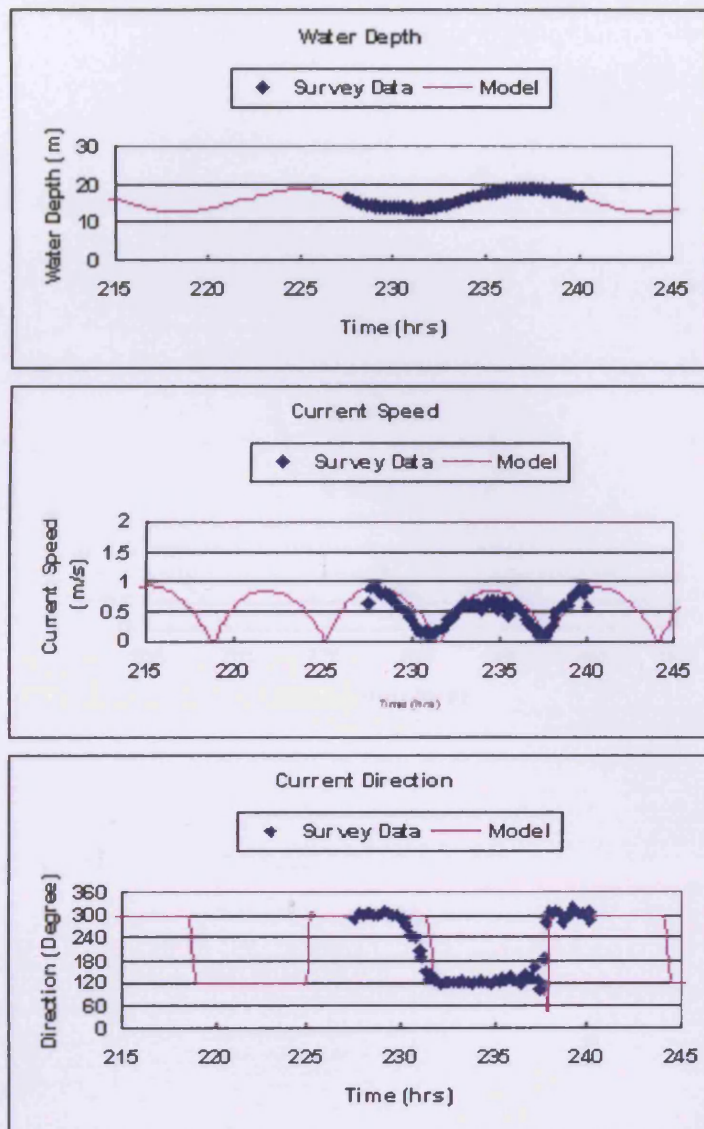


Figure 7.15: Comparison of water depths and current speeds and directions at Minehead for 30th July 2001 Survey

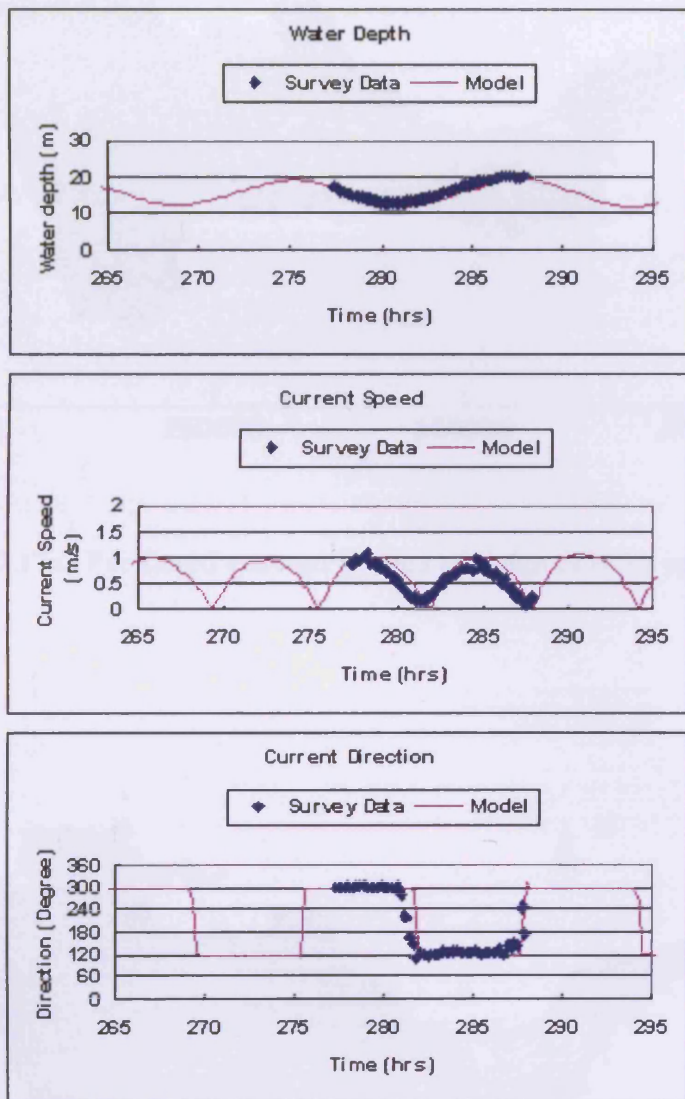


Figure 7.16: Comparison of water depths and current speeds and directions at Minehead for 1st August 2001 Survey

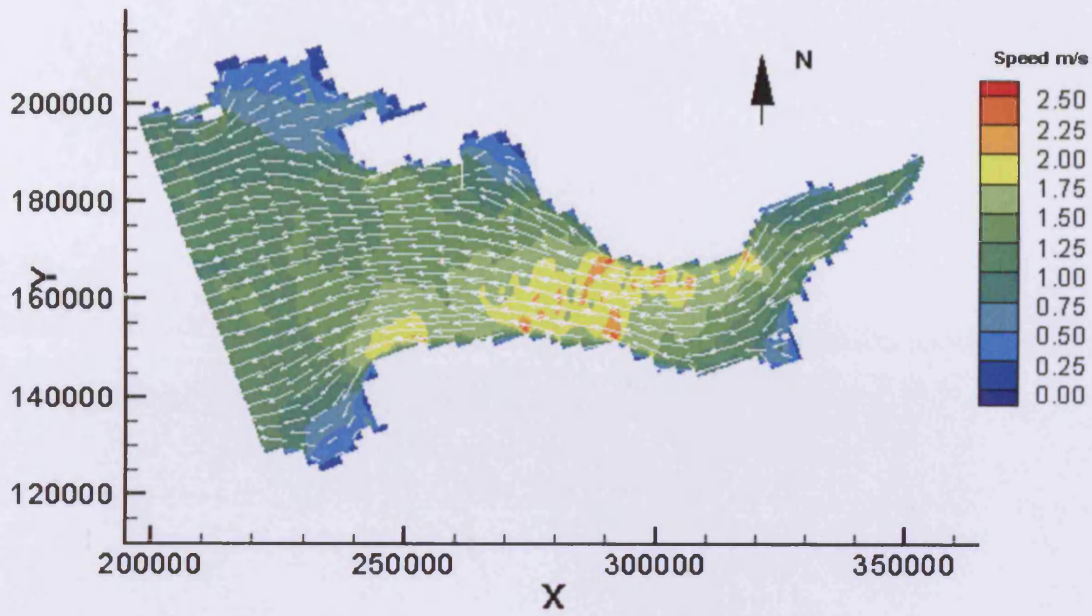


Figure 7.17a: Predicted current speeds at mean ebb for spring tide

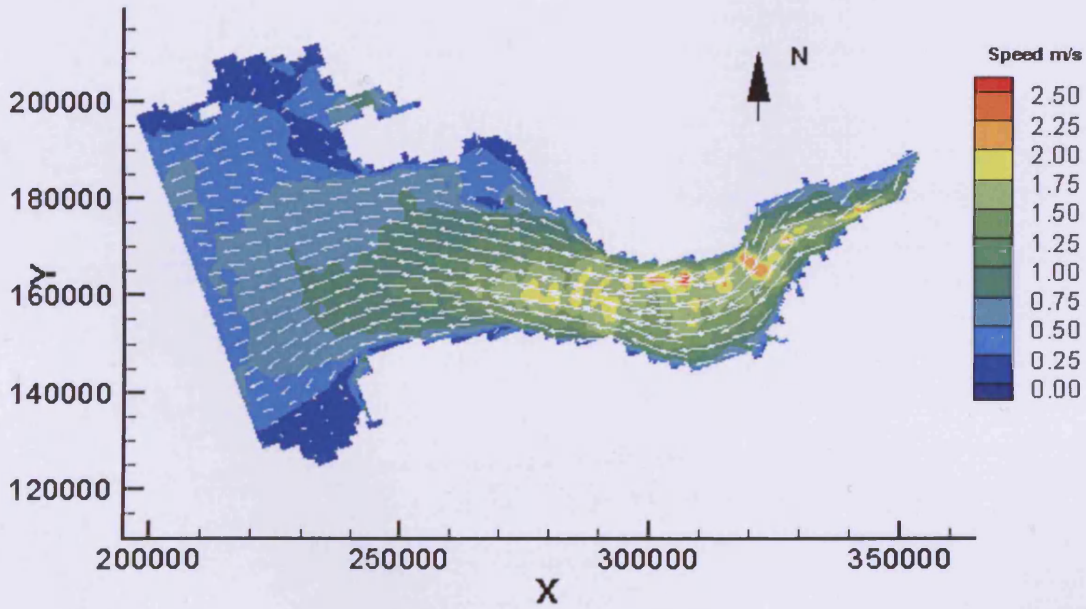


Figure 7.17b: Predicted current speeds at low water level for spring tide

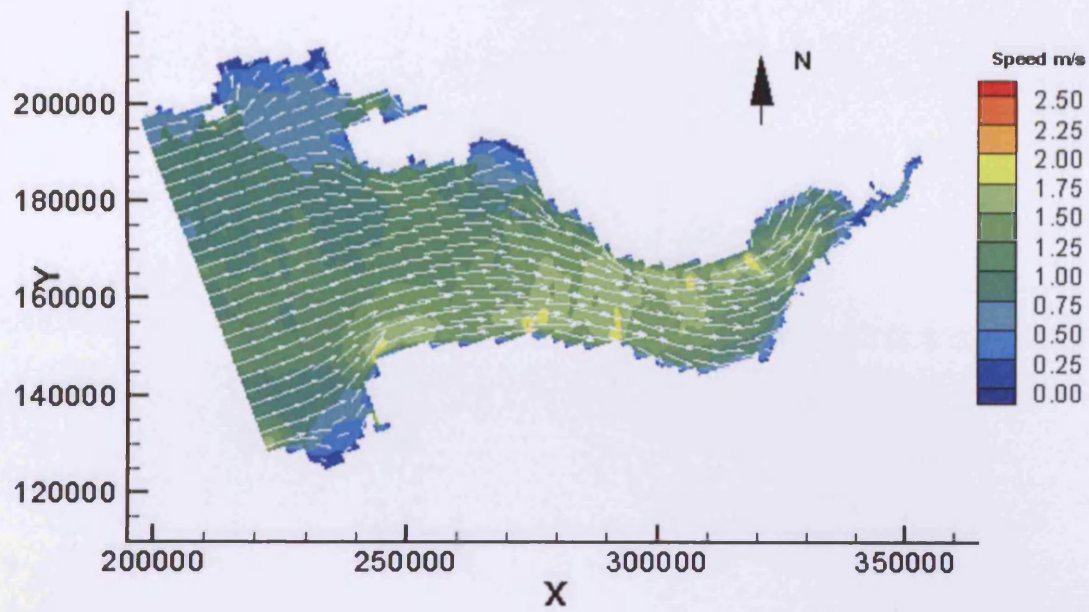


Figure 7.17c: Predicted current speeds at mean flood for spring tide

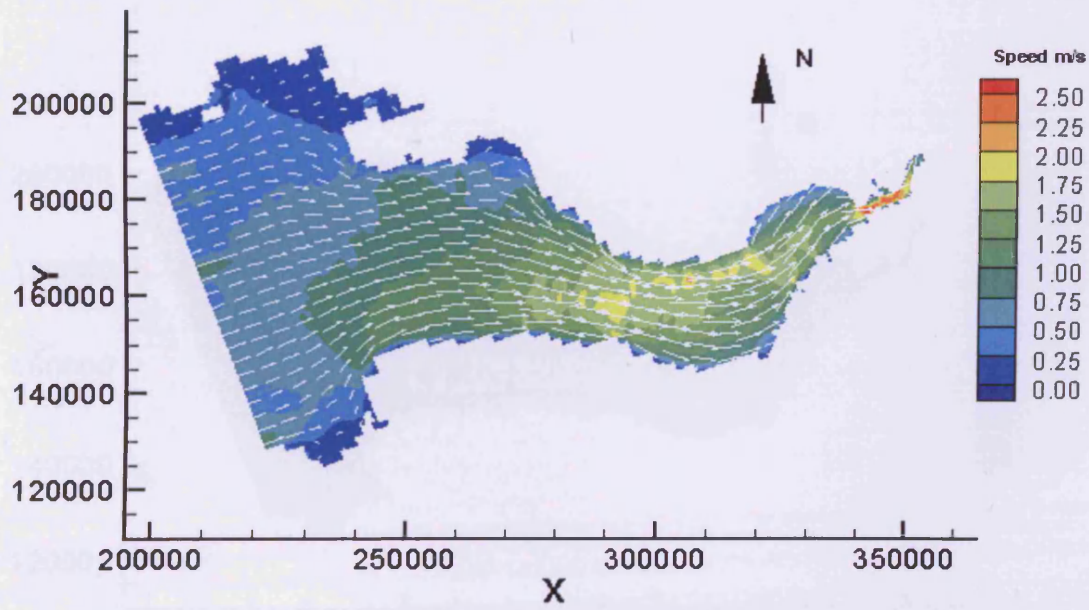


Figure 7.17d: Predicted current speeds at high water level for spring tide

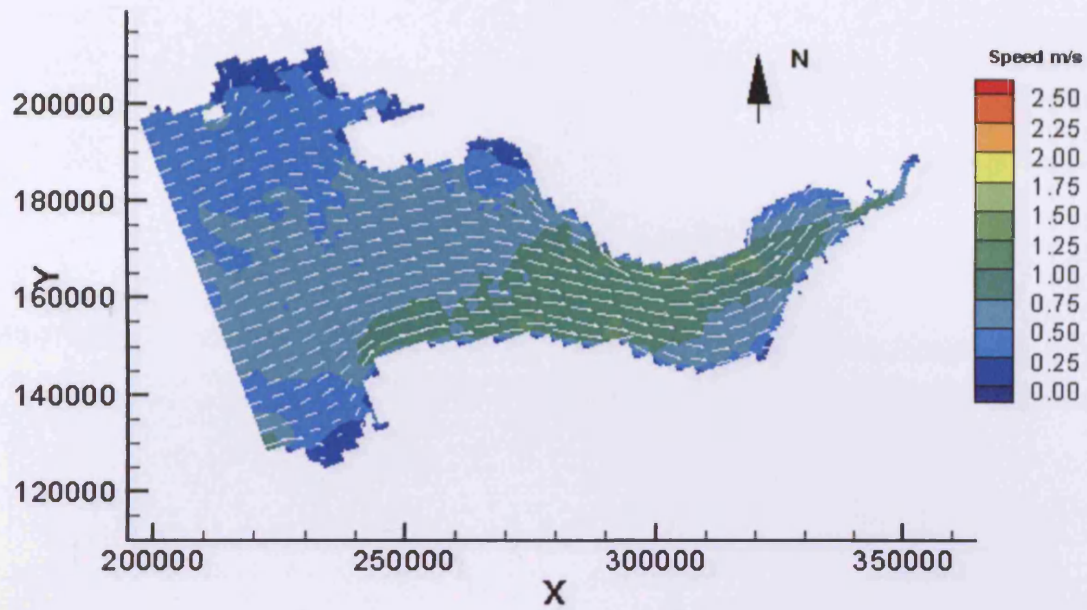


Figure 7.18a: Predicted current speeds at mean flood for neap tide

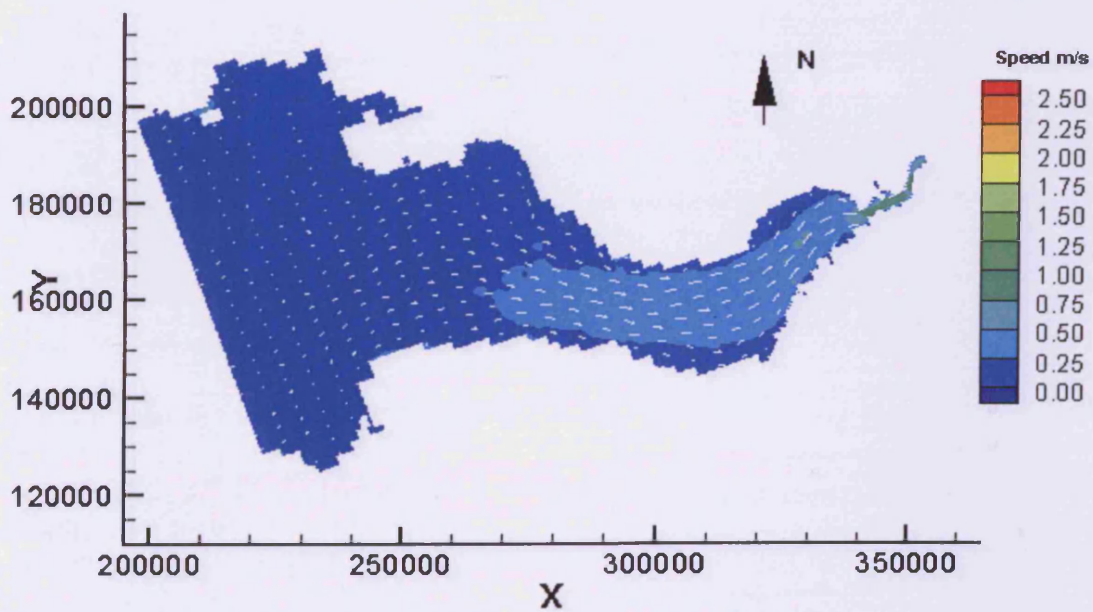


Figure 7.18b: Predicted current speeds at high water level for neap tide

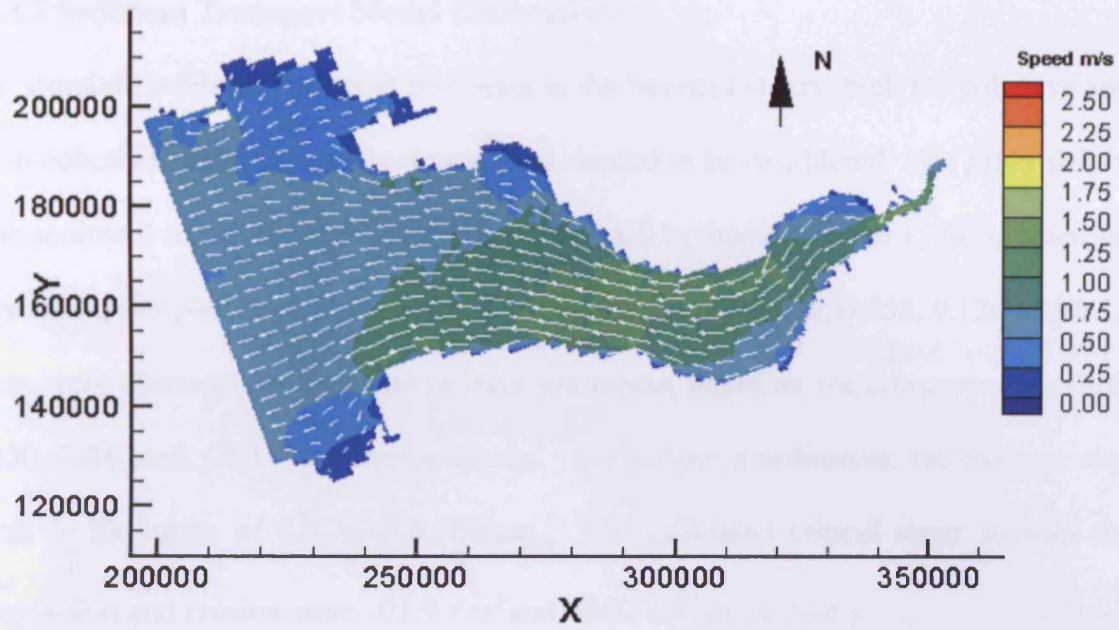


Figure 7.18c: Predicted current speeds at mean ebb for neap tide

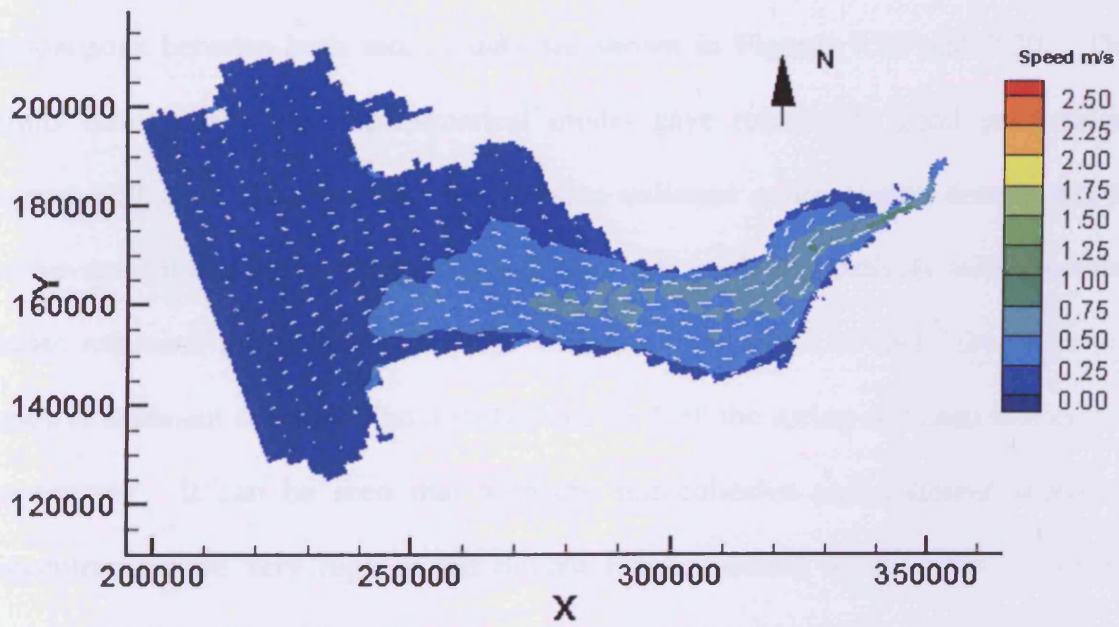


Figure 7.18d: Predicted current speeds at low water level for neap tide

7.3.2 Sediment Transport Model Calibration

To simulate sediment transport processes in the Severn Estuary, both the cohesive and non-cohesive sediment transport processes needed to be considered. The grain size of the sediment in the Severn Estuary was provided in Stapleton et al (2007), based on analysing samples from four sites. The mean values of 0.026, 0.058, 0.126 and 0.15 mm were obtained for the non-cohesive sediments, based on the corresponding D16, D50, D84, and D90 values respectively. For cohesive sediments, the average size was in the range of 0.010 to 0.063mm. The calibrated critical shear stresses for deposition and erosion were $0.1N/m^2$ and $2N/m^2$ respectively.

The numerical model predictions for the suspended sediment concentrations were compared with field measured data, with the predictions being compared at two sites, namely Southerndown and Trecco bay, where field data were available. Typical comparisons between both sets of data are shown in Figures 7.19 and 7.20. The results have shown that the numerical model gave reasonably good predictions. Figures 7.21 and 7.22 show the non-cohesive sediment concentration distribution in the Severn Estuary for a spring tide and neap tide cycle respectively with the tidal phases reference to seaward boundary. Similarly Figures 7.23 and 7.24 show the cohesive sediment concentration distributions for both the spring and neap tide cycles respectively. It can be seen that both the non-cohesive and cohesive sediment concentrations are very high in the Severn Estuary during spring tides, however, during neap tides the predicted sediment concentrations were relatively low.

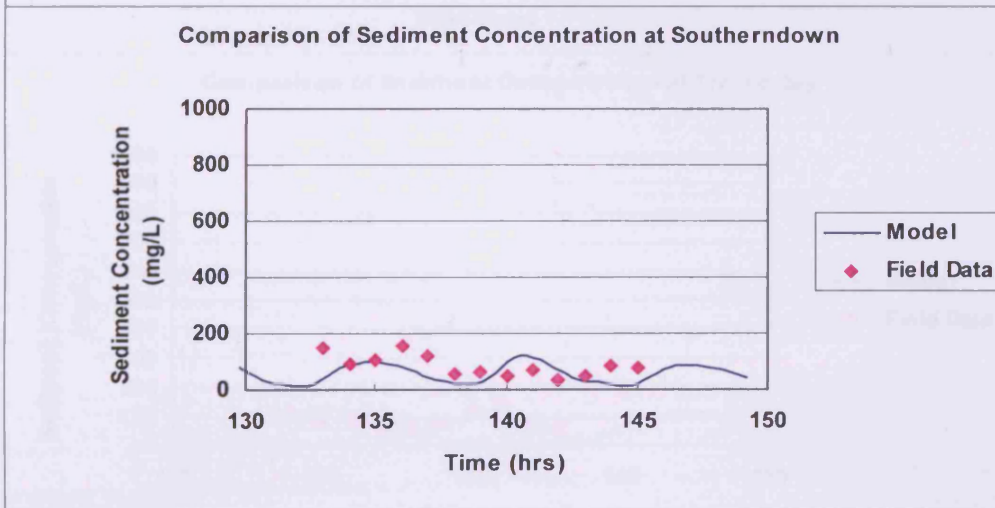
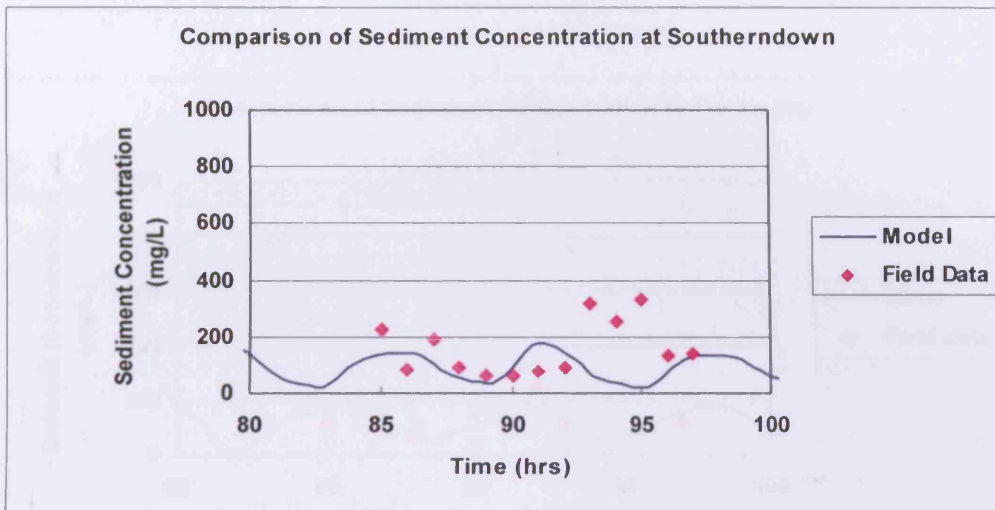


Figure 7.19 Suspended sediment concentrations at Southerndown

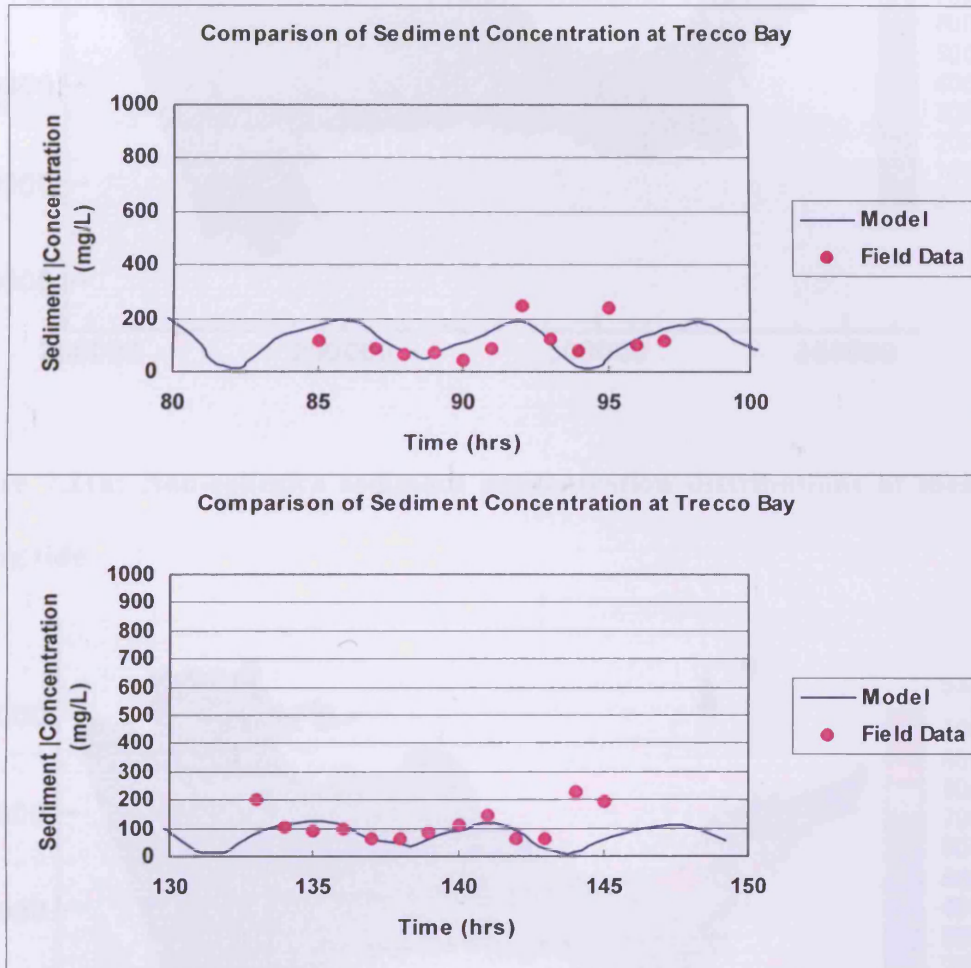


Figure 7.20 Suspended sediment concentrations at Trecco Bay

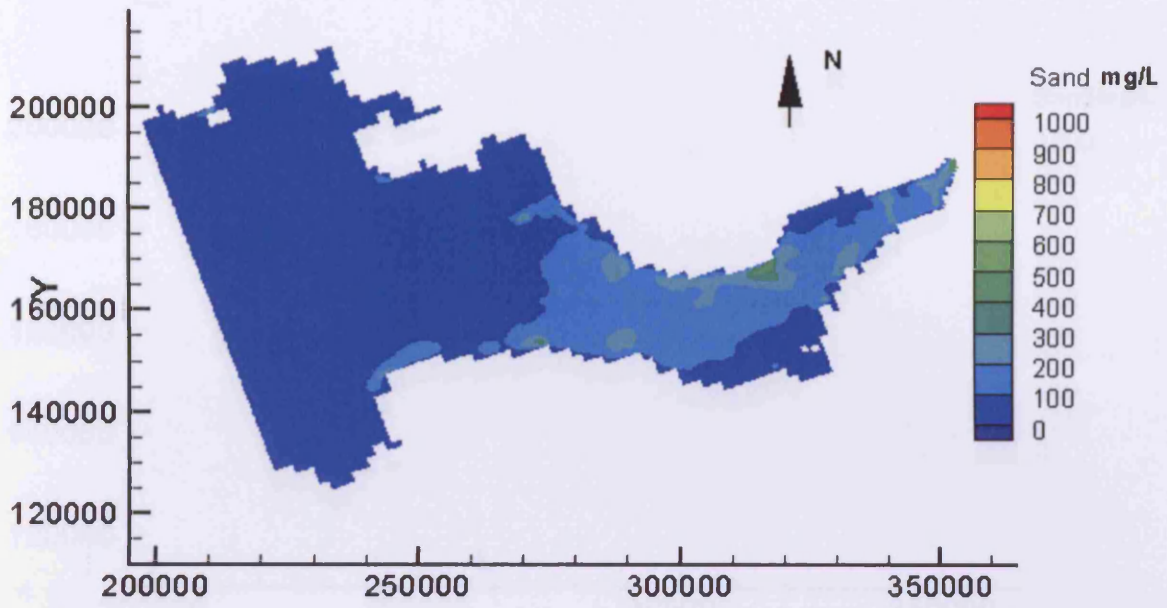


Figure 7.21a: Non-cohesive sediment concentration distributions at mean ebb spring tide

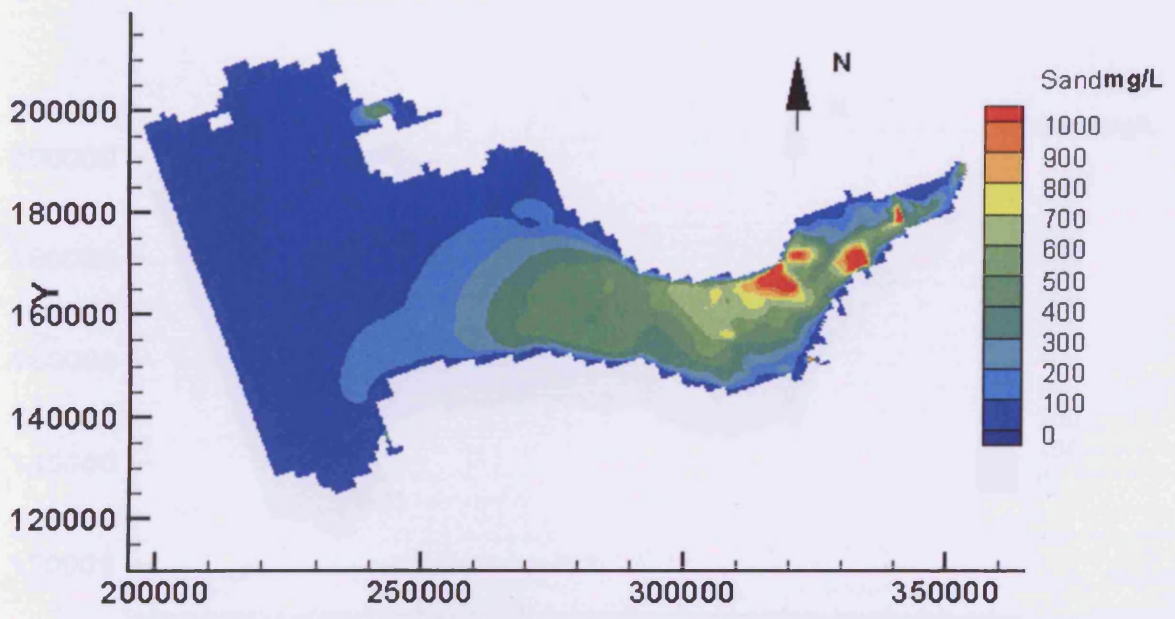


Figure 7.21b: Non-cohesive sediment concentration distributions at low water spring tide

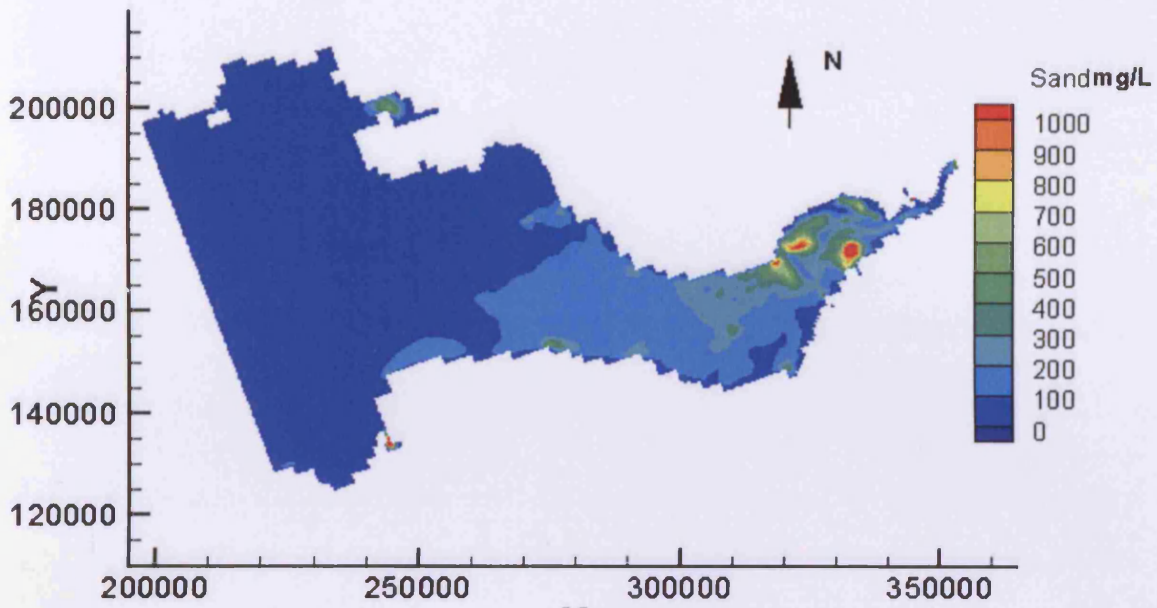


Figure 7.21c: Non-cohesive sediment concentration distributions at mean flood spring tide

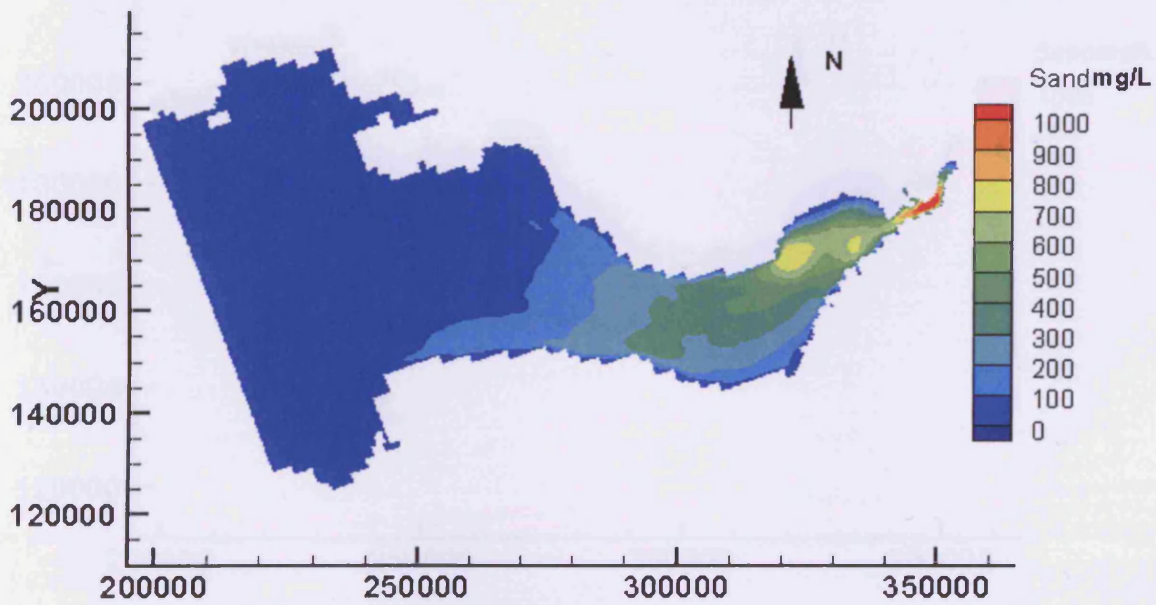


Figure 7.21d: Non-cohesive sediment concentration distributions at high water spring tide

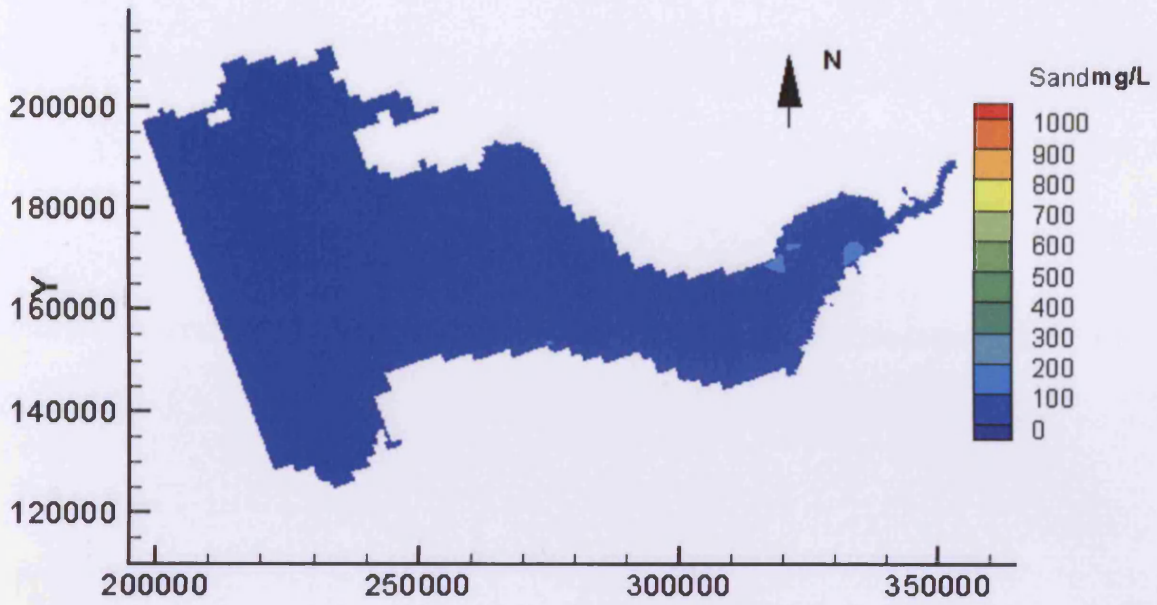


Figure 7.22a: Non-cohesive sediment concentration distributions at mean flood neap tide

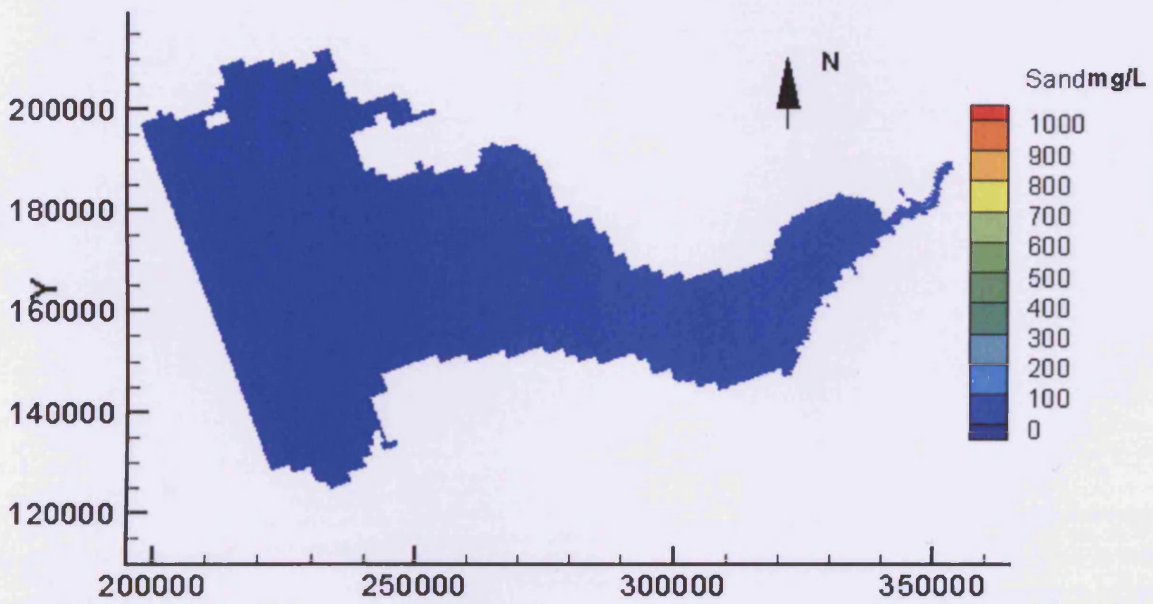


Figure 7.22b: Non-cohesive sediment concentration distributions at high water level neap tide

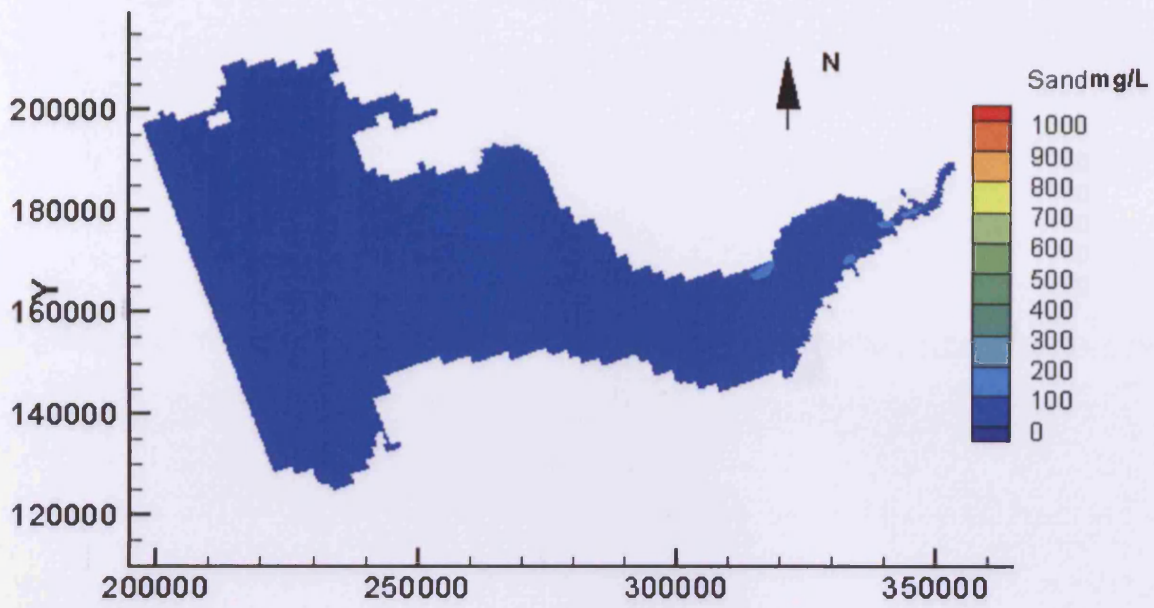


Figure 7.22c: Non-cohesive sediment concentration distributions at mean ebb neap tide

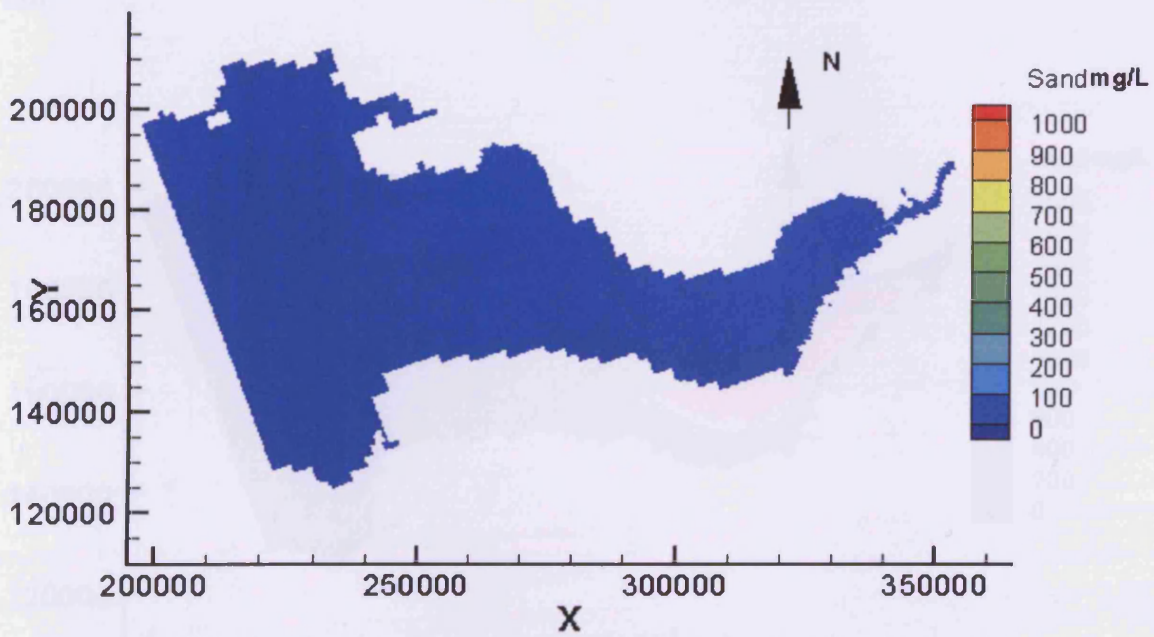


Figure 7.22d: Non-cohesive sediment concentration distributions at low water neap tide

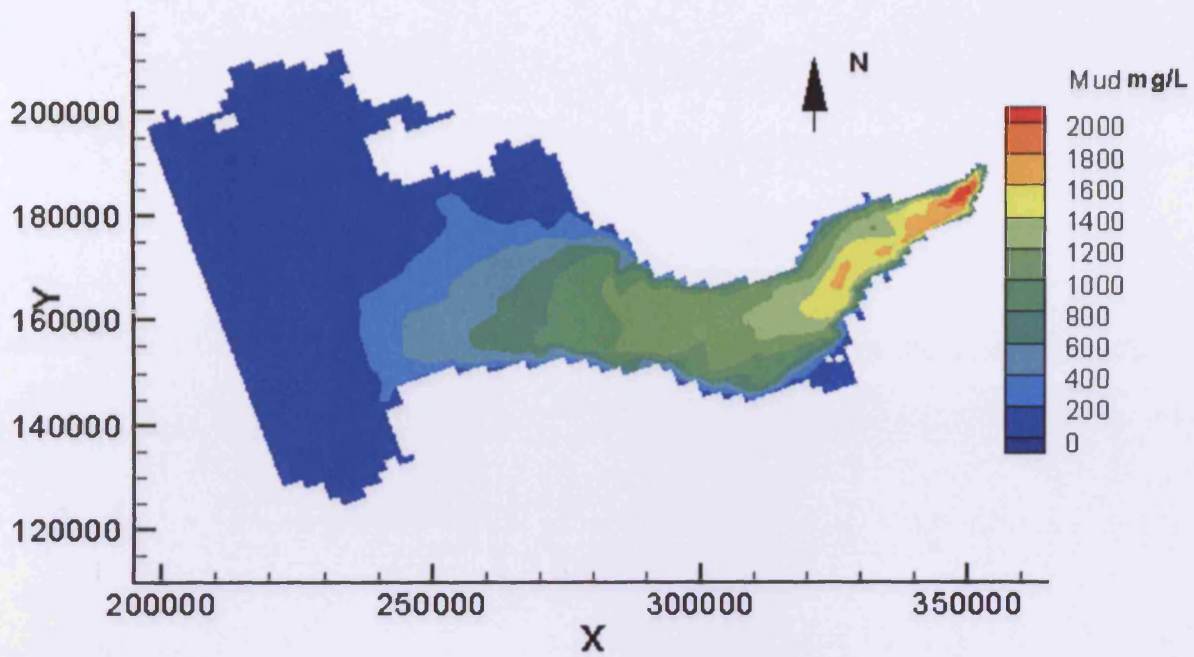


Figure 7.23a: Cohesive sediment concentration distributions at mean ebb spring tide

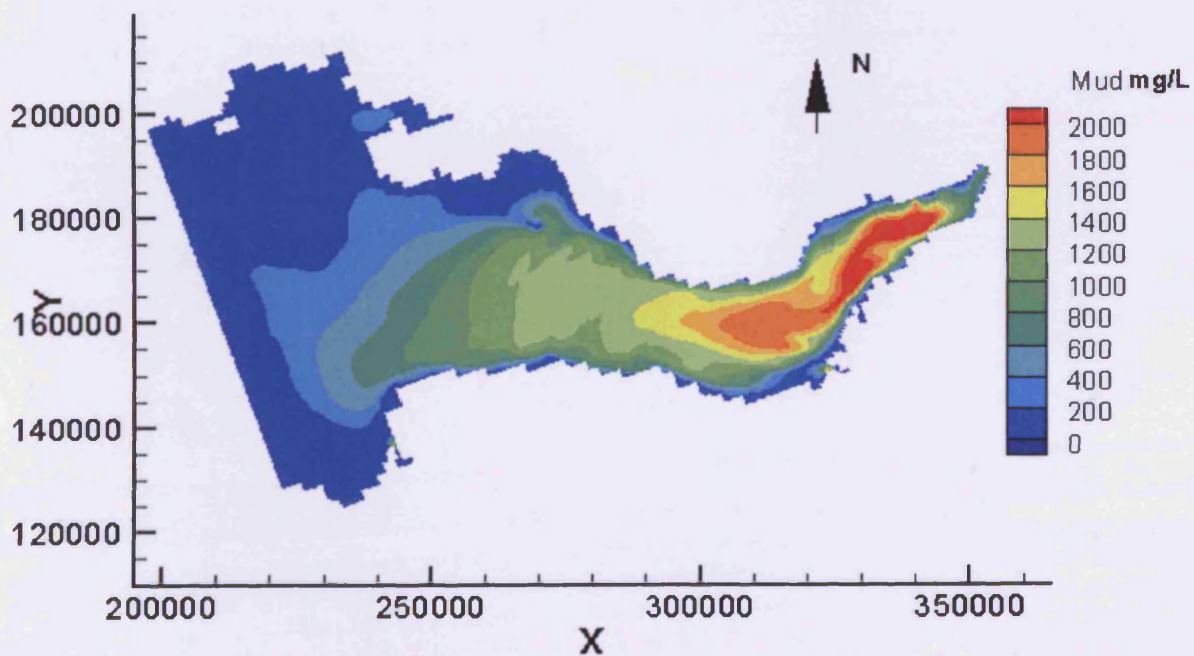


Figure 7.23b: Cohesive sediment concentration distributions at low water spring tide

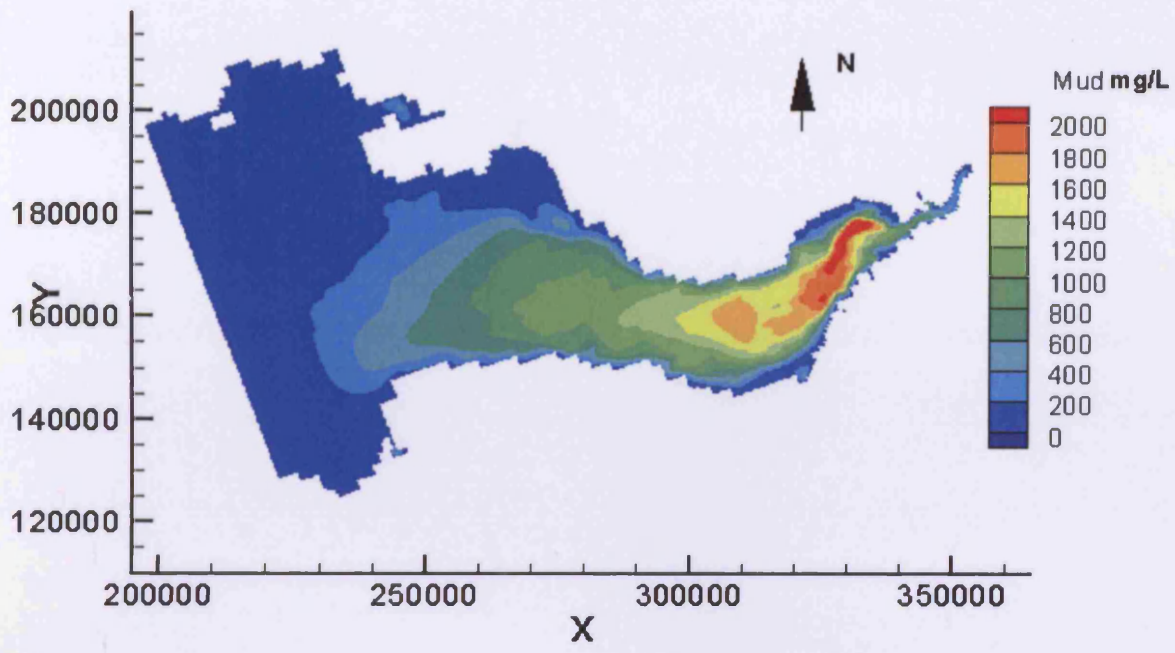


Figure 7.23c: Cohesive sediment concentration distributions at mean flood spring tide

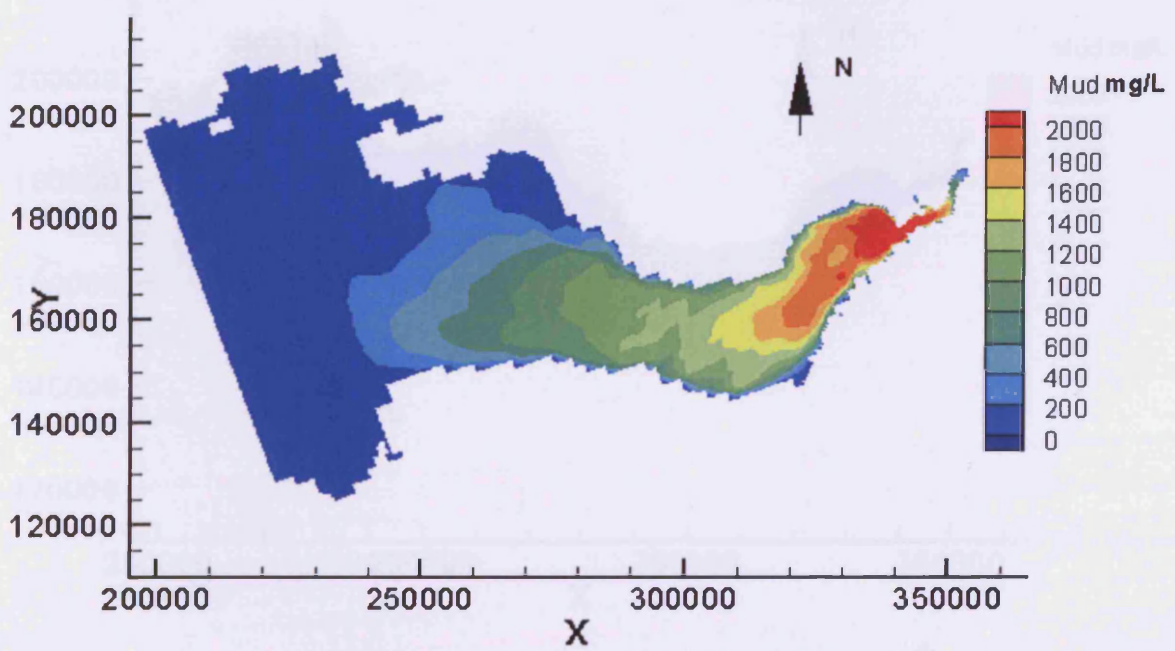


Figure 7.23d: Cohesive sediment concentration distributions at high water spring tide

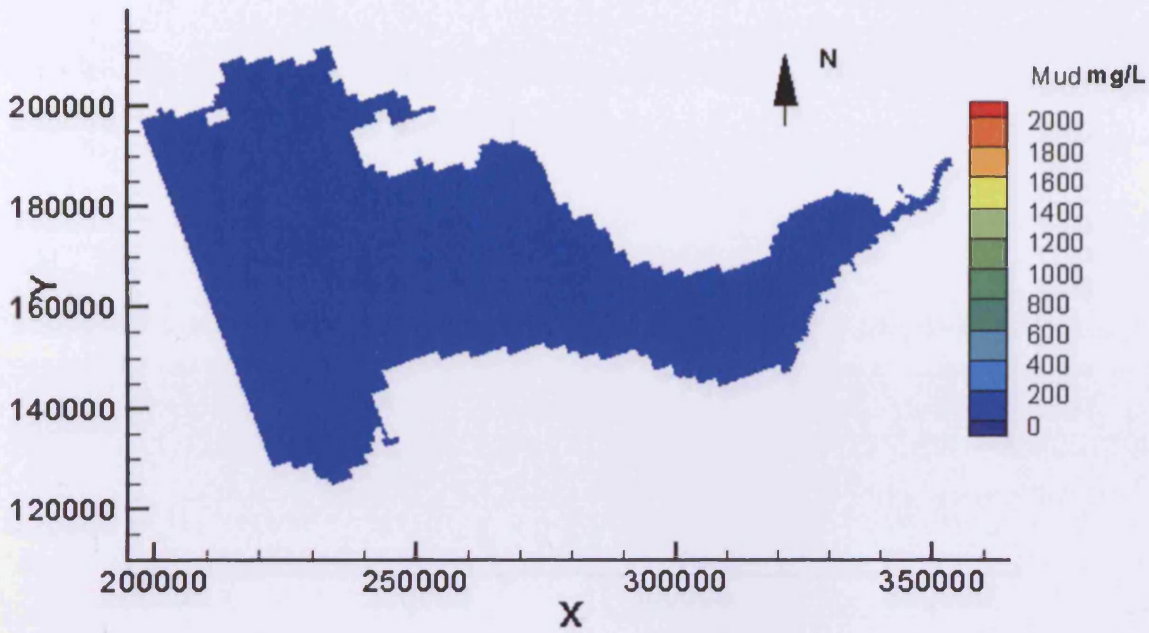


Figure 7.24a: Cohesive sediment concentration distributions at mean flood neap tide

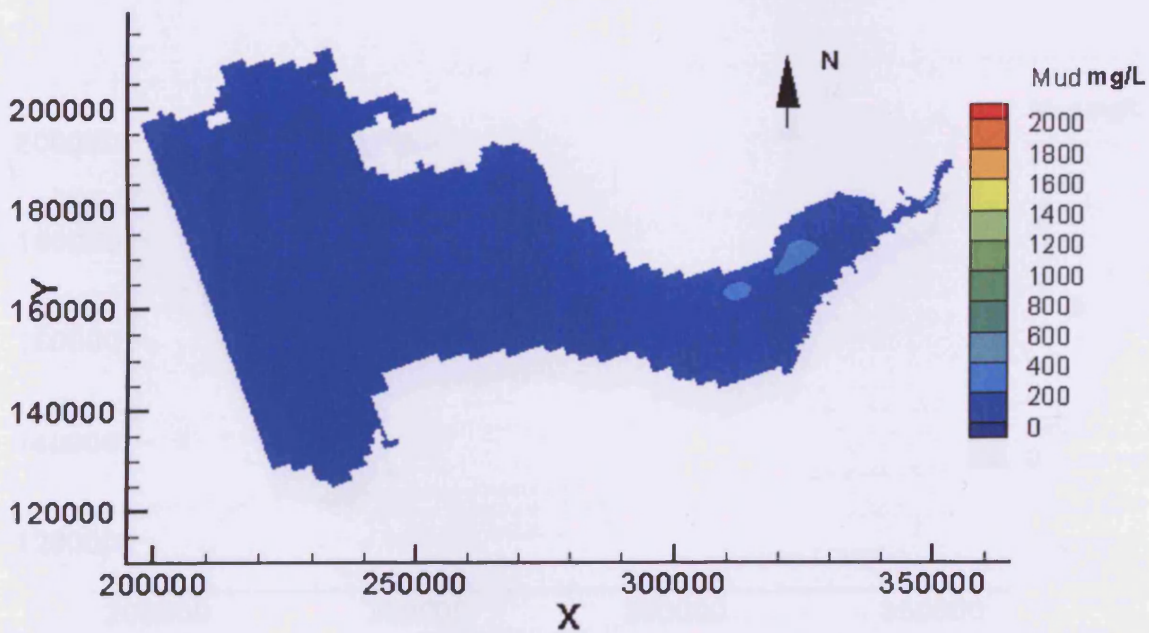


Figure 7.24b: Cohesive sediment concentration distributions at high water neap tide

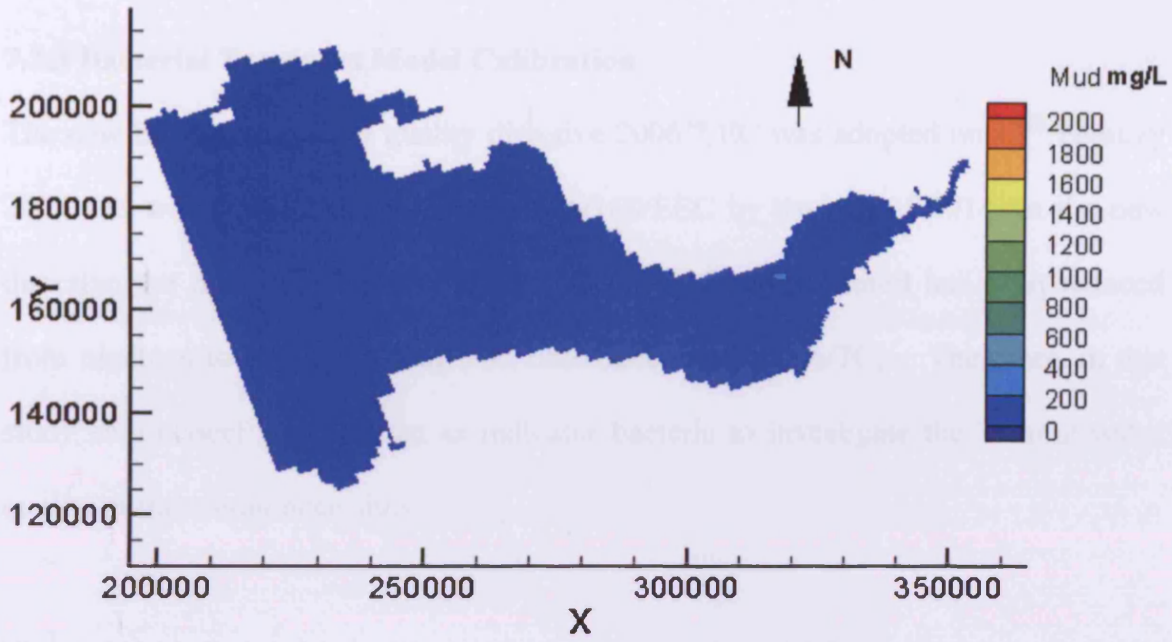


Figure 7.24c: Cohesive sediment concentration distributions at mean ebb neap tide

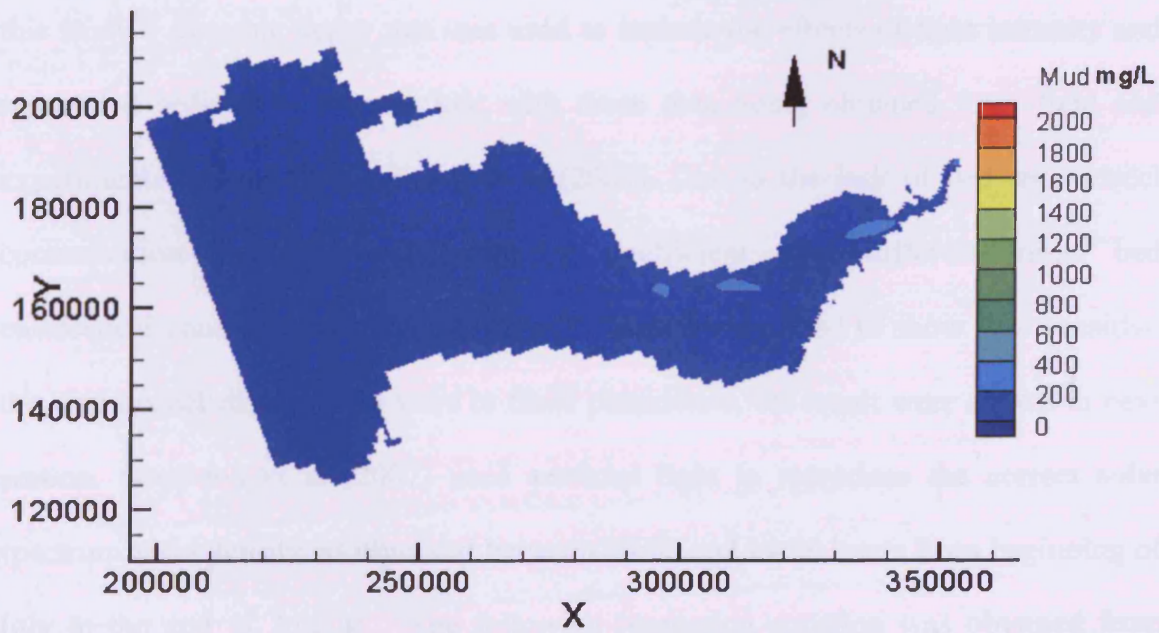


Figure 7.24d: Cohesive sediment concentration distributions at low water neap tide

7.3.3 Bacterial Transport Model Calibration

The new EU bathing water quality directive 2006/7/EC was adopted on 15th February 2006 and will repeal the old Directive 76/160/EEC by the end of 2014. In the new directive the number of water quality indicators to be monitored has been reduced from nineteen to two, i.e. E Coli and Enterococci (EC 2006/7C). Therefore, in this study enterococci were chosen as indicator bacteria to investigate the bathing water quality at the compliance sites.

The main parameter to be calibrated in the numerical model for bacterial prediction is usually the decay rate, which depends on a number of environmental parameters. Therefore, the decay rate can vary for different survey conditions and needs to be estimated for the prevailing weather and water conditions at the time of study. In this study a dynamic decay rate was used to include the effects of light intensity and suspended sediment concentration, with these data being obtained from field and experimental studies by Stapleton et al (2007). Due to the lack of bed enterococci concentration distribution and partition coefficient data, different initial bed enterococci concentrations and partition coefficient were used to show how sensitive the enterococci distributions were to these parameters, the result were shown in next section. Stapleton et al (2007) used artificial light to reproduce the correct solar spectrum and intensity, as observed between 10:00 and 14:00 hours from beginning of July to the end of August. The following regression equation was obtained from these data to give the following relationship for the enterococci decay rate:

$$\begin{aligned} \text{Light excluding outliers: } \log T_{90} &= 0.0047 \text{ Turbidity} + 0.677 \pm 0.2070 \\ \text{Dark excluding outliers: } \log T_{90} &= 0.0019 \text{ Turbidity} + 1.237 \pm 0.199 \end{aligned} \quad (7.1)$$

In the above equation the turbidity is related to the suspended sediment concentrations by the following equation:

$$\text{Turbidity} = 139.479 \text{ Log SS} - 244.736 \pm 32.678 \quad (7.2)$$

The suspended sediment concentrations are given in mg/l, with the values obtained from the sediment transport model.

The above relationships are derived based on assumption of constant light intensity. In order to take account of the effect of time variation of light intensity, Stapleton et al (2007) have used the following equation to represent the T_{90} :

$$T_{90} = T_{90}^2 + (T_{90}^1 - T_{90}^{*1}) \quad (7.3)$$

where: T_{90}^1 is the enterococci mortality rate depending on surface sunlight (I):

$$T_{90}^1 = \ln 10 / (1.1 \times 10^{-5} I) / 60 = 3.5 \times 10^3 I^{-1};$$

$$T_{90}^{*1} = \ln 10 / (1.1 \times 10^{-5} I^*) / 60;$$

In which I^* is the fixed irradiance for the T_{90} vs. turbidity, obtained from experiments (Wm^{-2}); and T_{90}^2 is the enterococci mortality rate obtained from the laboratory experimental equation. The light intensity used in this study has been provided by Environment Agency, which is shown in the Figure 7.25.

The empirical equation (7.1) was obtained using the T_{90} values decided from saline water sample from the estuary. Therefore the T_{90} values have already included the effect of salinity on the decay rate. So the effect of salinity on the decay rate was not considered using separated equation.

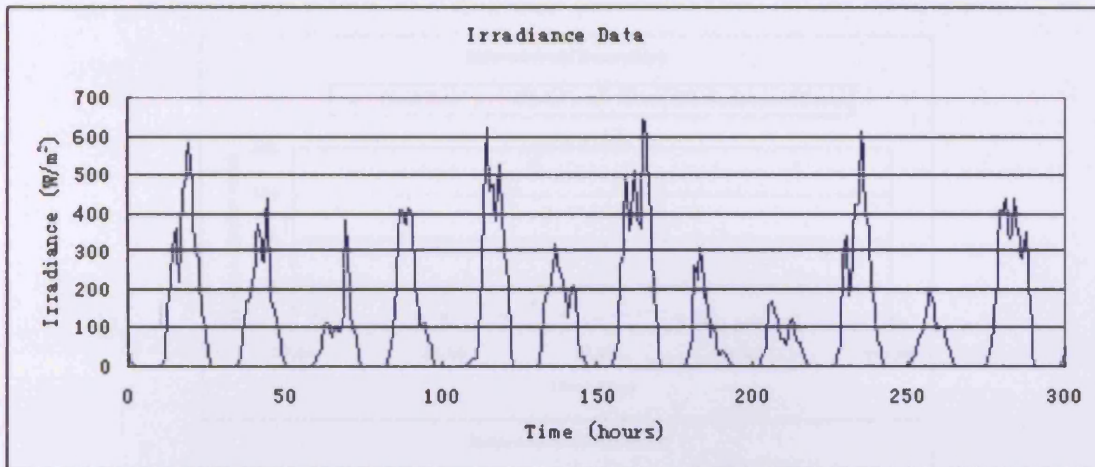


Figure 7.25: Irradiance data at Swansea

The enterococci loads to the Severn Estuary from the catchment rivers and WwTWs in this study have been provided by Stapleton et al (2007). Stapleton et al (2007) applied models developed by CREH (Centre for Research into Environment and Health) to predict the enterococci concentrations at the outlets of river catchments, which discharge to the Severn Estuary. In these models the water quality data are described as land cover data. Enterococci loads from the WwTWs were calculated by Stapleton et al (2007) by using effluent bacterial concentrations obtained through past empirical studies, combined with flow estimated from the Environment Agency and Water Companies data sources.

For the bacteria model calibration, results from the model, including and excluding sediment effects on bacteria, were compared with the field data. The comparisons are shown below in Figures 7.26 and 7.27. It can be seen that the model without the inclusion of the sediment effects on the bacteria transport predicted almost no bacteria concentrations at both sites; however, this result was known to be incorrect. The numerical model predictions with sediment effects on bacteria being included gave reasonable predictions at both sites, although the enterococci concentration levels were relatively low.

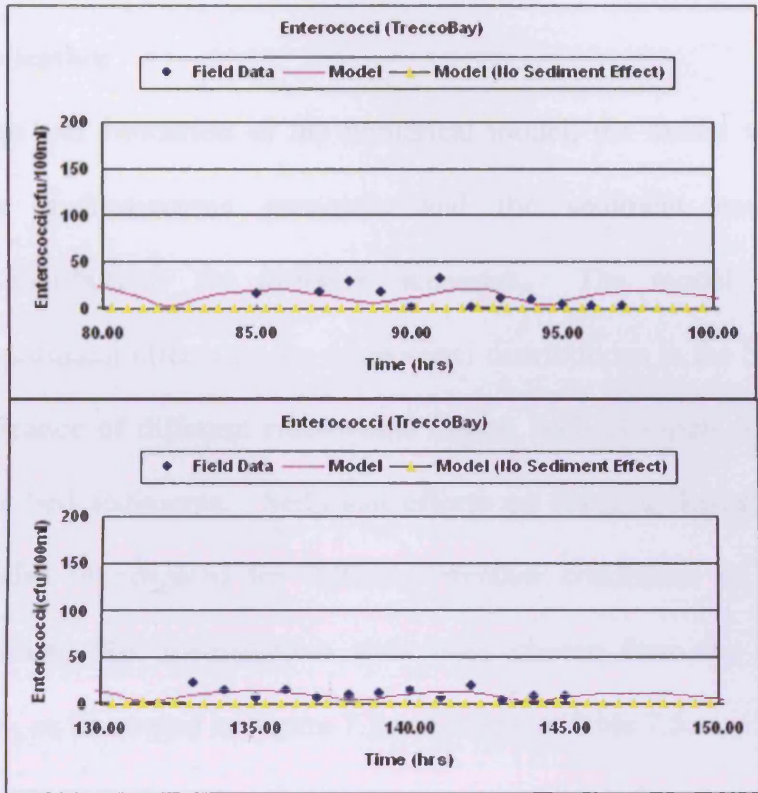


Figure 7.26 Enterococci concentration comparisons at Trecco Bay

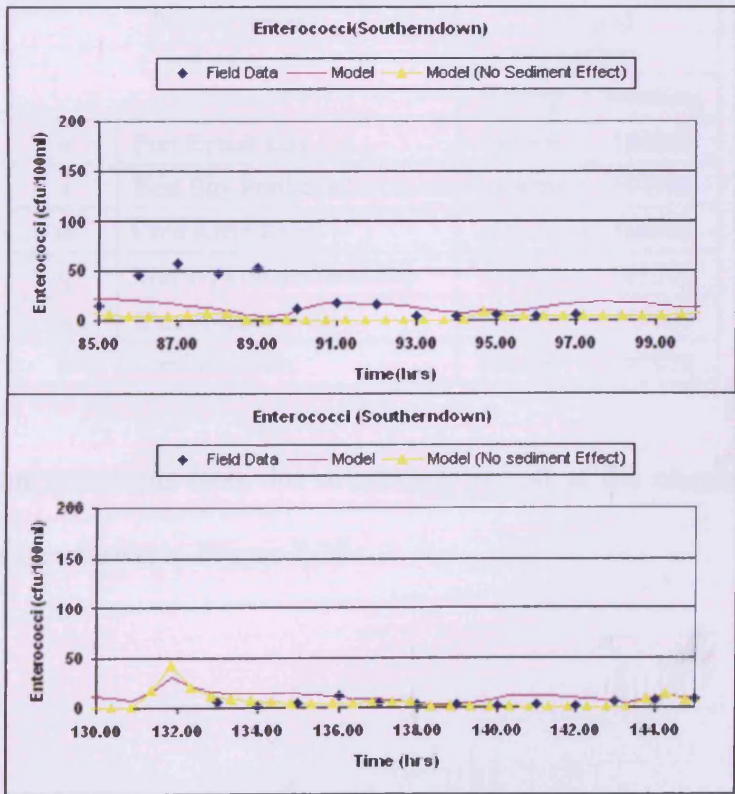


Figure 7.27: Enterococci concentration comparisons at Southerndown

7.4 Model Application

After calibration and validation of the numerical model, the model was applied to investigate the hydrodynamic processes and the sediment and enterococci concentration distributions for different scenarios. The model was used to investigate the sediment effects on the enterococci distributions in the Severn estuary, and also significance of different enterococci inputs, such as inputs from the rivers, outfalls and the bed sediments. Sediment effects on bacteria fluxes in the Severn Estuary were also investigated for differing weather conditions i.e. dry and wet weather conditions. Six investigation sites were chosen from the bathing water compliance sites, as illustrated in Figure 7.2 and listed in Table 7.5.

Table 7.5 Investigation site location

Bathing waters		OS grid (metres)	
		Easting	Northing
a	Port Eynon Bay	247200	184800
i	Rest Bay Porthcawl	280000	177900
m	Cold Knap Barry	309650	166400
q	Weston-s-Mare Sand Bay	333000	163500
w	Blue Anchor West	302300	143500
B	Combe Martin	253550	147920

The sediment concentrations over the simulation period at the chosen bathing water compliance sites are shown in Figure 7.28.

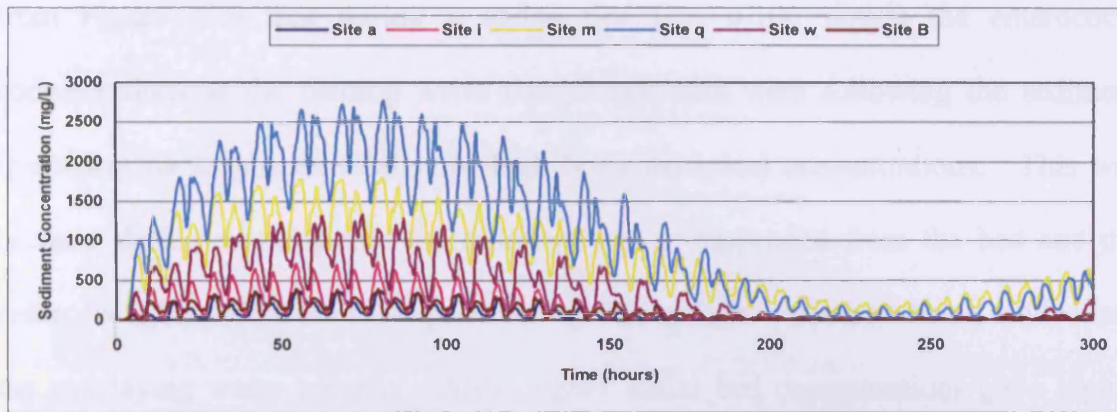


Figure 7.28: Suspended sediment concentrations at the investigation bathing water compliance sites

7.4.1 Sensitivity Test to Bed Bacteria Concentration

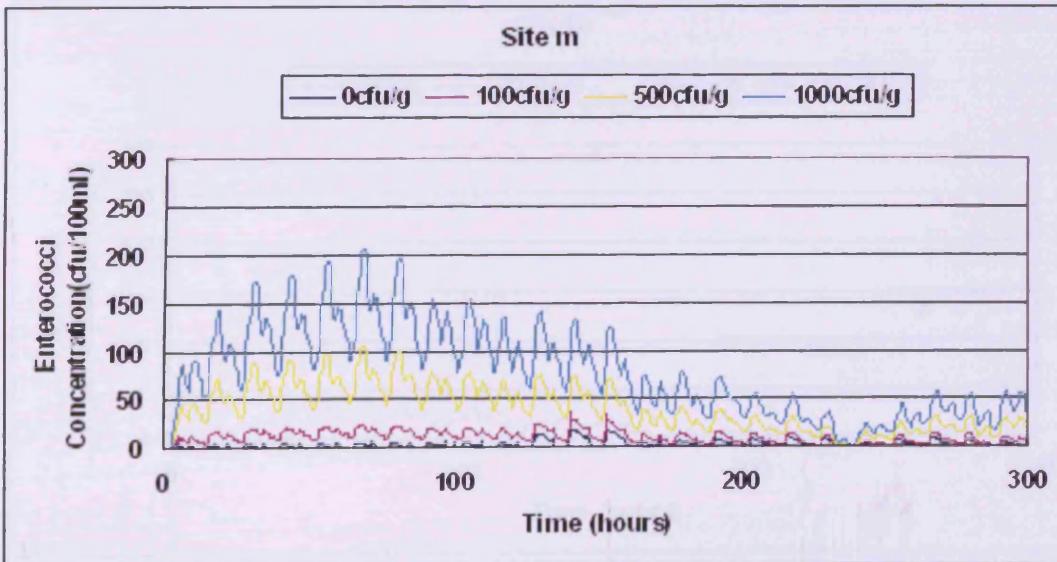
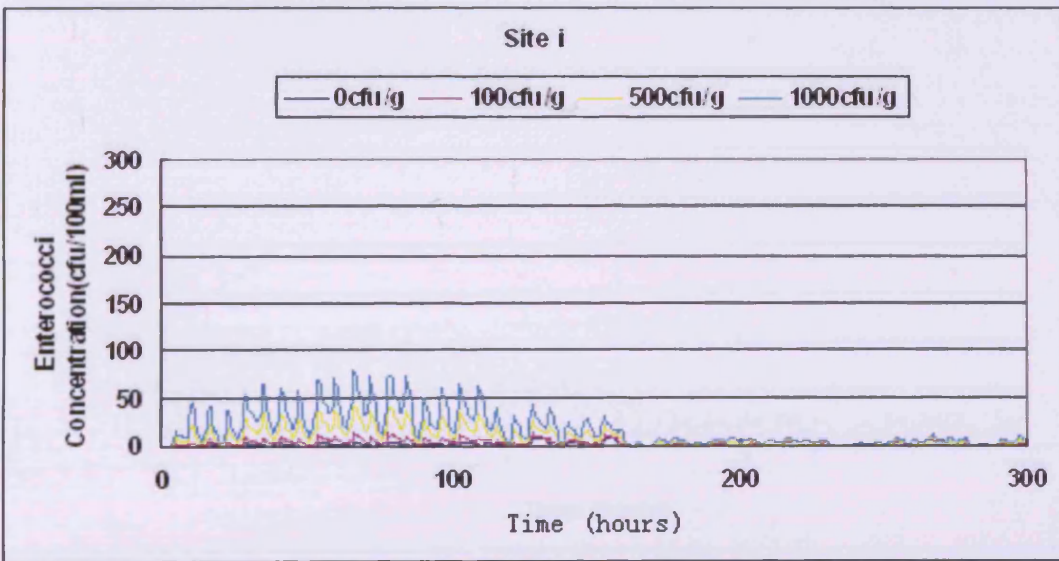
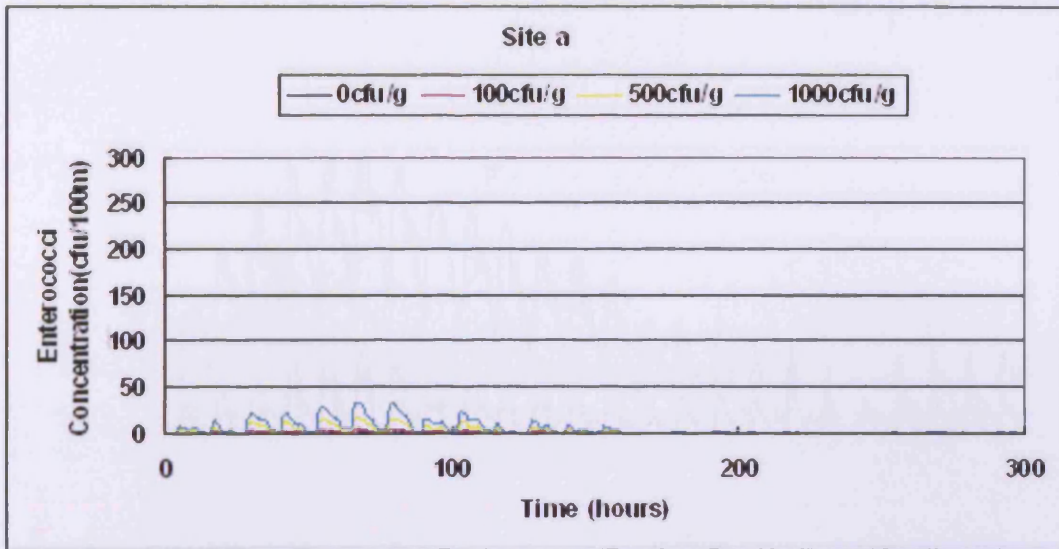
Due to the lack of bed enterococci concentration distribution data, different initial bed enterococci concentrations were used to show how sensitive the enterococci distributions were to the bed concentrations. Enterococci concentrations in the sediment samples from Beachley Slip and Weston-Super-Mare were investigated by Stapleton et al (2007) and it was found that the enterococci concentrations in the bed sediments analyzed were between 3cfu/g and 1088cfu/g. Therefore in this study the bed sediment enterococci concentrations were set to be 0cfu/g, 100cfu/g, 500cfu/g and 1000cfu/g to test the effects of the initial bed bacteria concentrations on the concentrations at the bathing water compliance locations detailed earlier.

During the spring tide cycle, the currents in the domain were very high, leading to very high suspended sediment concentrations. The sediments re-suspended from the bed were the dominant constituents. Therefore, under the condition of high bed enterococci concentrations, the concentration of bacteria was higher than the condition without sediment effects being included with the bacteria. It can be seen

from Figure 7.29 that during a spring tide (i.e. 0-100 hours) the enterococci concentrations at the bathing water compliance sites were following the sediment re-suspension trends, especially for high bed enterococci concentrations. This was because during a spring tide the sediment was re-suspended from the bed and the enterococci bacteria were re-suspended, together with the sediments being eroded into the overlaying water column. Also, higher initial bed concentrations gave higher enterococci concentrations in the water column during spring tides.

During neap tides, the current speed was much smaller than for a spring tide and the shear stress was not large enough to re-suspend bed sediment. Hence, the sediment concentrations were fairly low. Instead of re-suspension of bacteria from the bed, the bacteria were deposited on the bed from the water column. During neap tides (200-300 hours) the enterococci concentrations were not significantly affected by the initial enterococci concentrations assumed on the bed sediments. The reason for this observation is that during neap tides the flow and shear stress are not strong enough to re-suspend sediments from the bed, and with sediment deposition being the dominant process.

The bed bacteria concentration plays an important role in governing the concentration of the overlay water column, especially during conditions of significant sediment transport activity. Figures 30a to 30d and 31a to 31d show the enterococci concentration distributions throughout the domain over a spring and neap tide respectively for different initial bed enterococci concentrations.



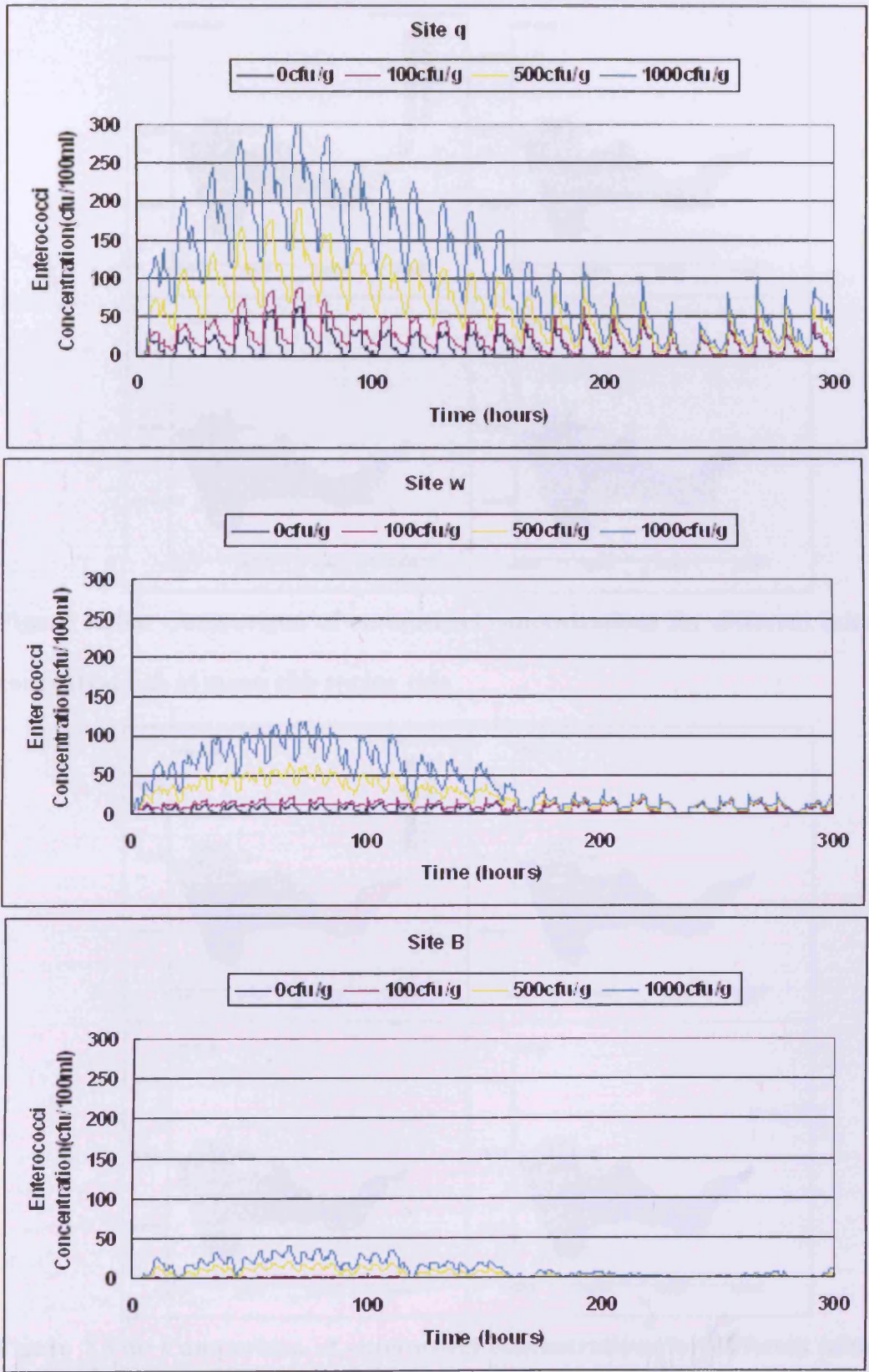


Figure 7.29: Comparison of enterococci concentrations at bathing water compliance sites for different initial bed concentrations

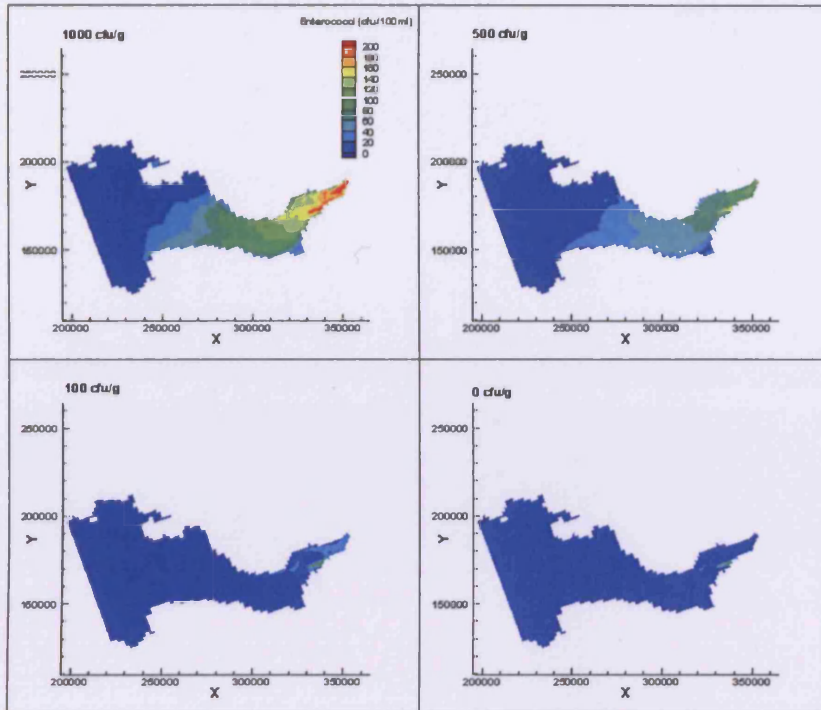


Figure 7.30a: Comparison of enterococci concentrations for different initial bed concentrations at mean ebb spring tide

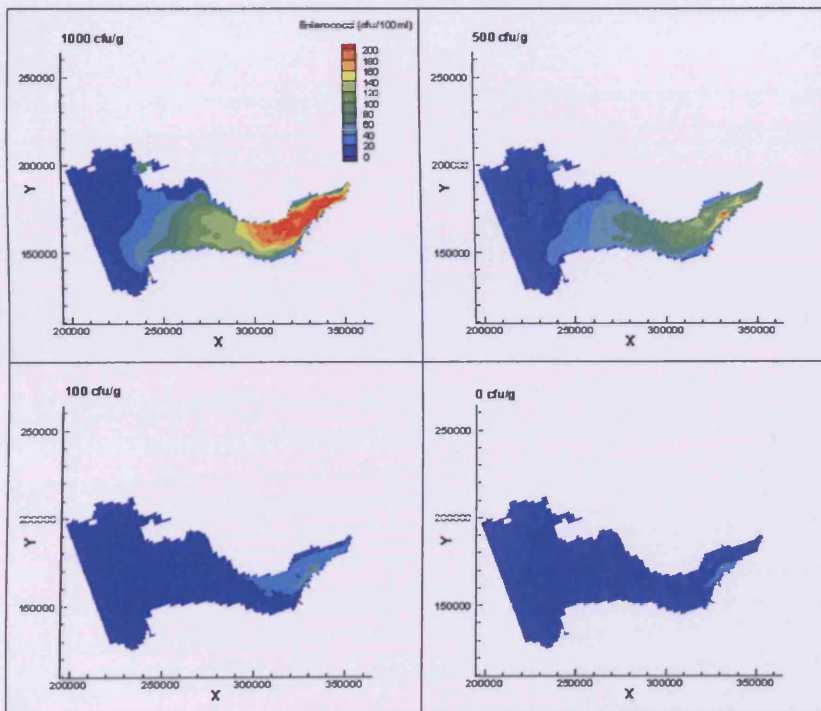


Figure 7.30b: Comparison of enterococci concentrations for different initial bed concentrations at low water spring tide

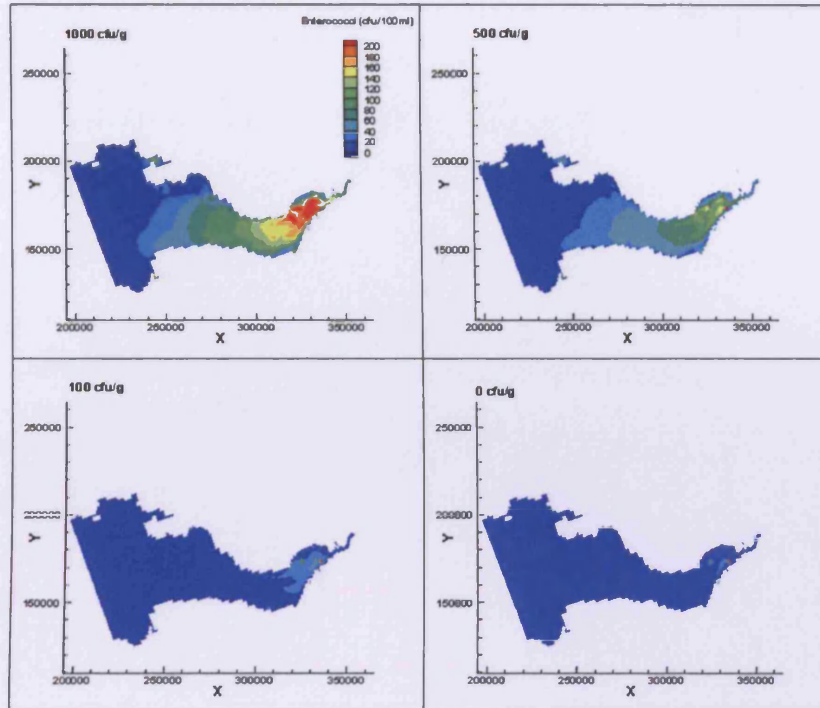


Figure 7.30c: Comparison of enterococci concentrations for different initial bed concentrations at mean flood spring tide

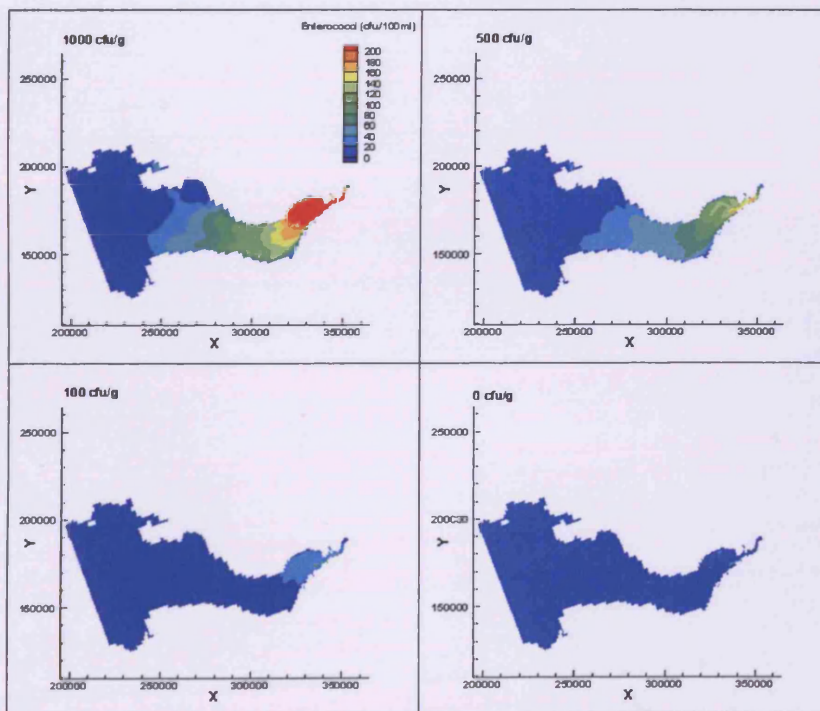


Figure 7.30d: Comparison of enterococci concentrations for different initial bed concentrations at high water spring tide

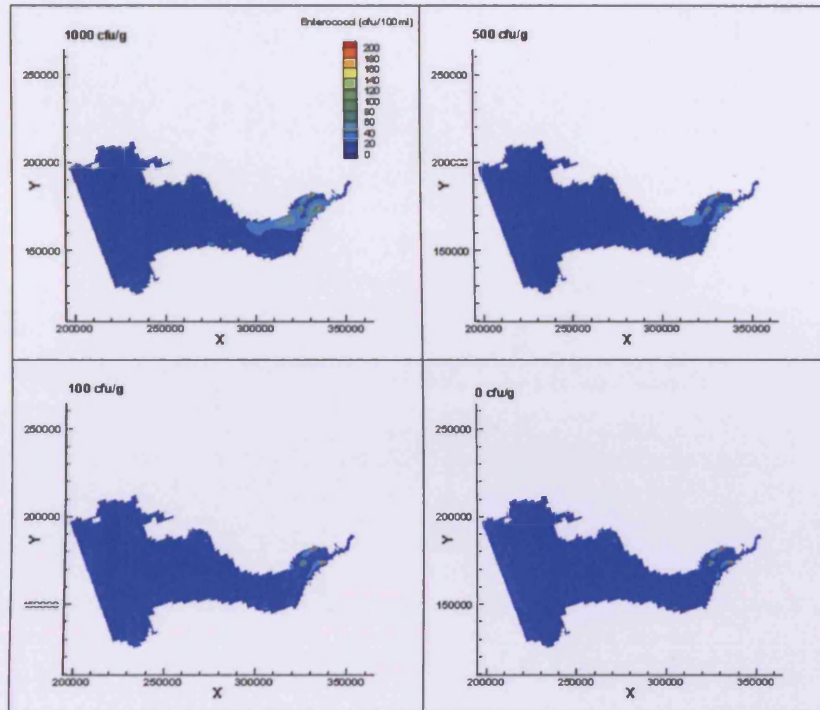


Figure 7.31a: Comparison of enterococci concentrations for different initial bed concentrations at mean flood neap tide

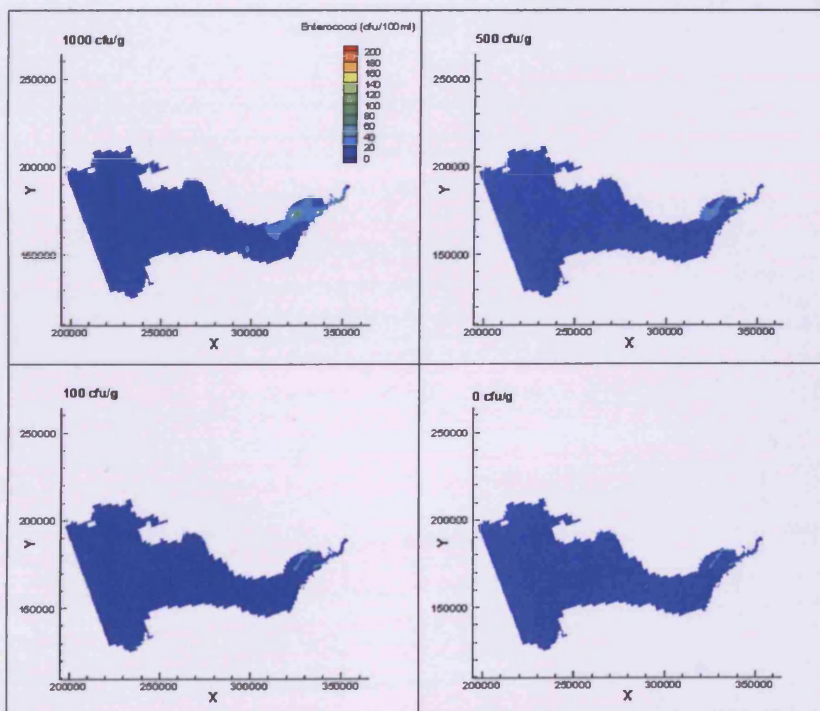


Figure 7.31b: Comparison of enterococci concentrations for different initial bed concentrations at high water neap tide

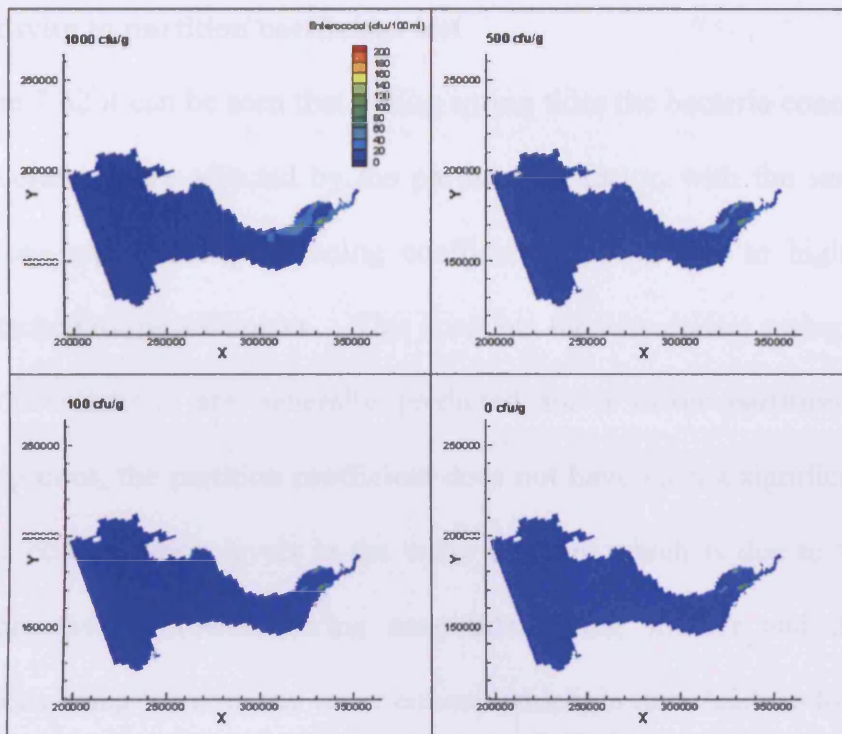


Figure 7.31c: Comparison of enterococci concentrations for different initial bed concentrations at mean ebb neap tide

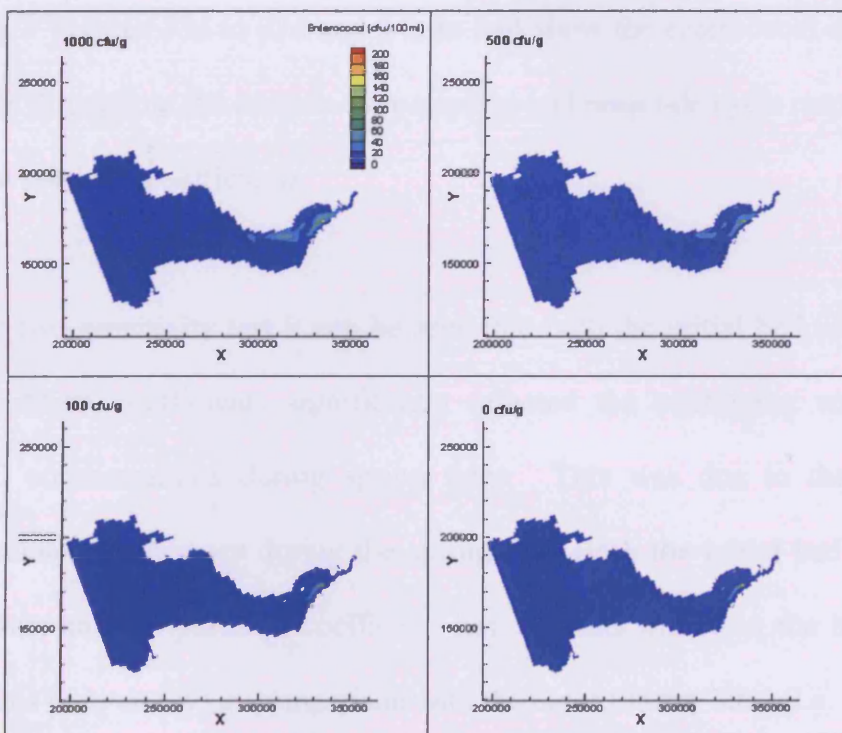


Figure 7.31d: Comparison of enterococci concentrations for different initial bed concentrations at low water neap tide.

7.4.2 Sensitivity to partition coefficient test

From Figure 7.32 it can be seen that during spring tides the bacteria concentrations in the water column were affected by the partitioning factor, with the same sediment concentrations and larger partitioning coefficients giving rise to higher ratios of bacteria attached to the sediments. This accounts for why during spring tides higher bacteria concentrations are generally predicted for a lower partition coefficient. During neap tides, the partition coefficient does not have such a significant effect on the bacteria concentration levels in the water column, which is due to the sediment transport process of erosion during neap tides being smaller and the sediment concentrations being lower in the water column which, in turn, leads to lower ratios of bacteria being attached to the sediments, for both high and low partition coefficients. Therefore, only slightly higher concentrations were predicted for lower partition coefficients. Figures 33a to 33d and 34a to 34d show the enterococci concentration distributions throughout the domain over a spring and neap tide cycle respectively and for different partition coefficients.

From these two sensitivity test it can be seen that both the initial bed concentrations and the partition coefficients significantly affected the overlaying water column enterococci concentrations during spring tides. This was due to the significant sediment transport processes during the spring tide. Both the initial bed enterococci concentrations and the partition coefficient has a greater effect on the inner estuary sites (i.e. sites m, q and w) in comparison with the outer estuary sites (i.e. sites a, i and B). This is because the sediment transport fluxes in the inner estuary are much larger than the corresponding fluxes and concentrations in the outer estuary.

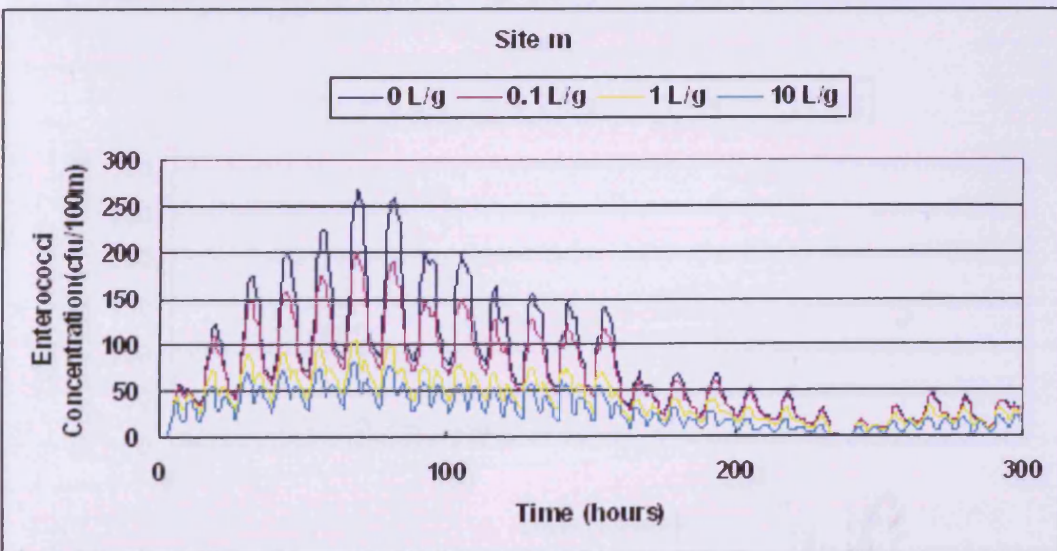
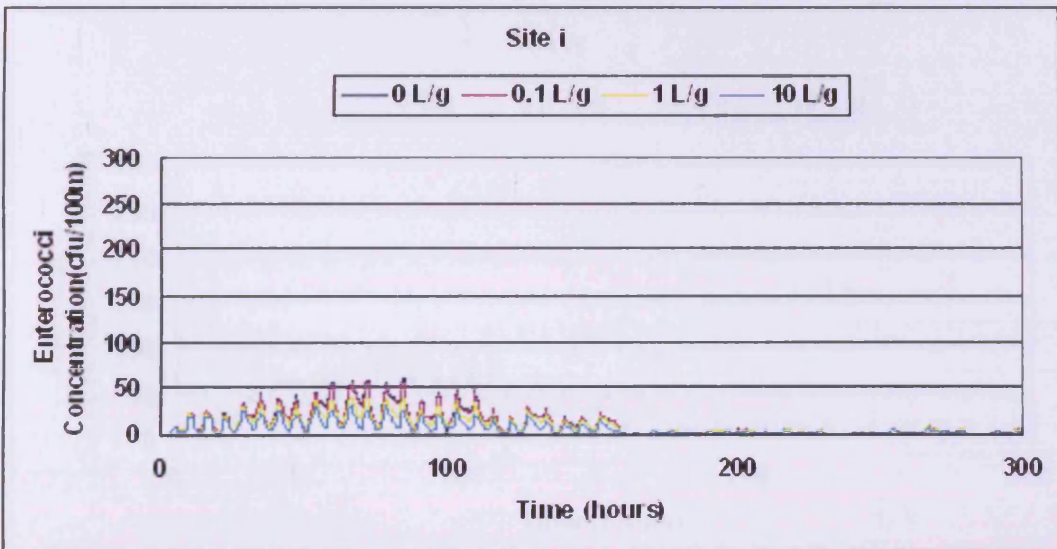
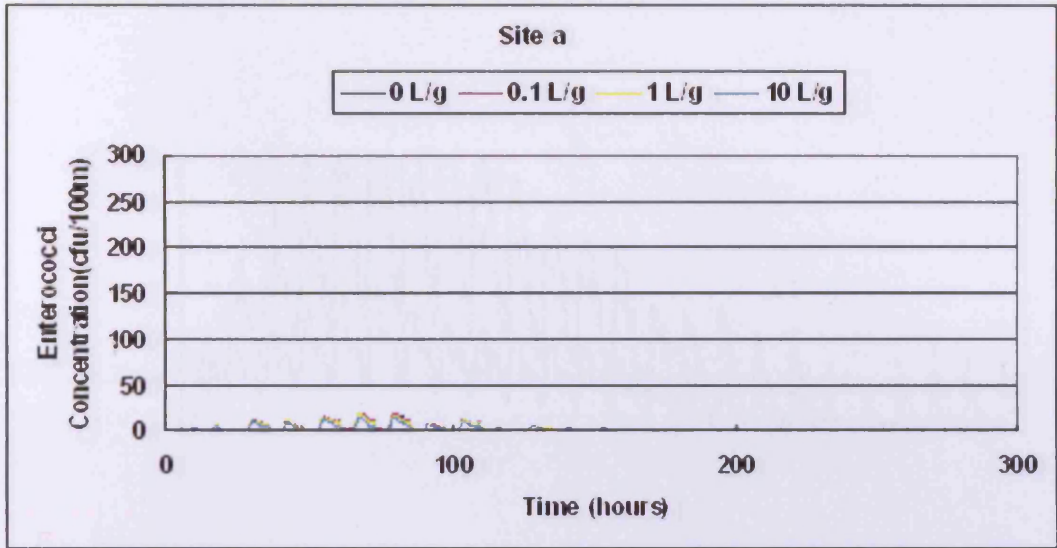


Figure 7.33: Comparison of Enterococci concentration at different sites for different concentrations of disinfectant.

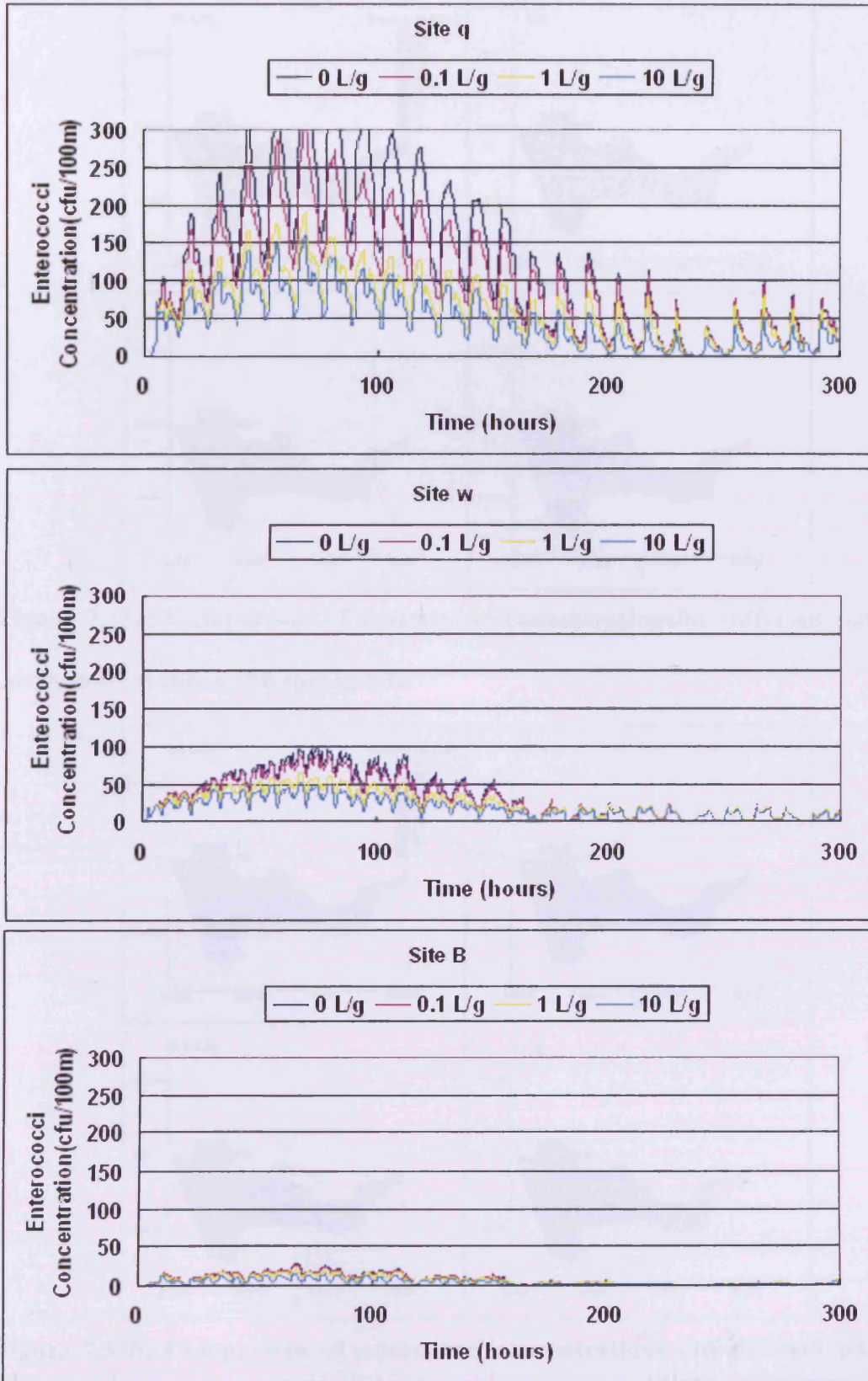


Figure 7.32: Comparison of enterococci concentrations at bathing water compliance sites for different partition coefficients

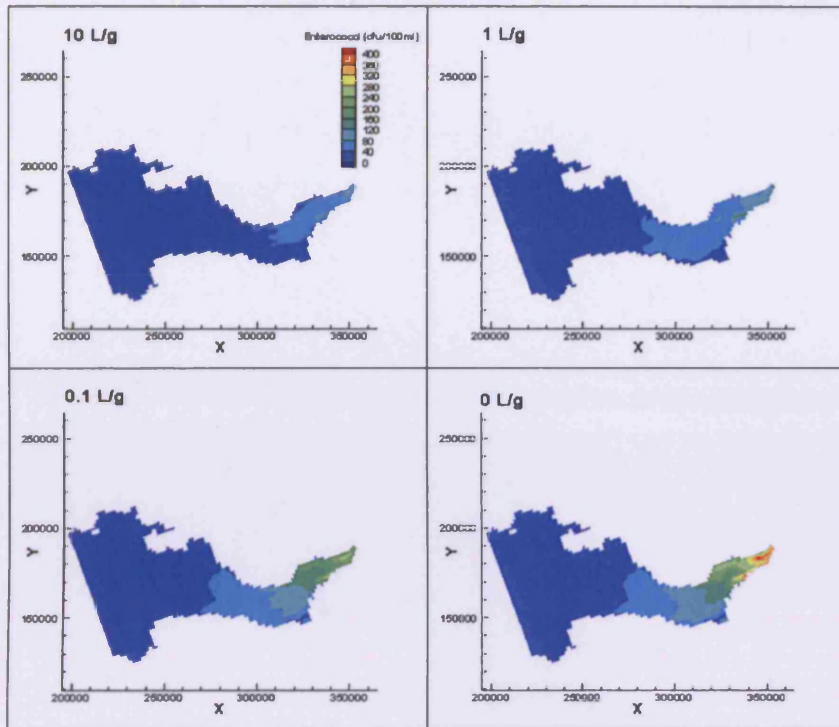


Figure 7.33a: Comparison of enterococci concentrations for different partition coefficients at mean ebb spring tide.

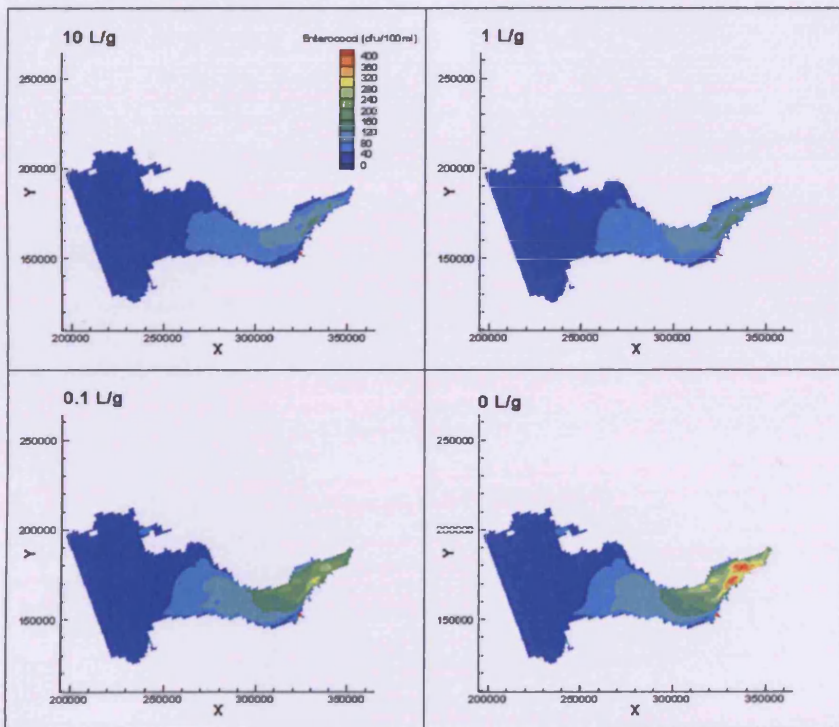


Figure 7.33b: Comparison of enterococci concentrations for different partition coefficients at low water spring tide

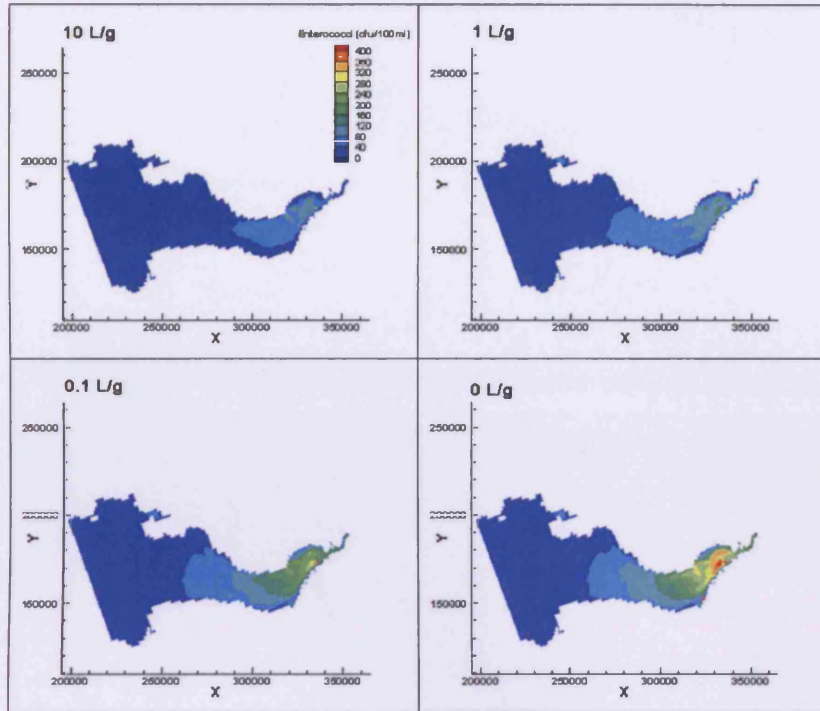


Figure 7.33c: Comparison of enterococci concentrations for different partition coefficients at mean flood spring tide

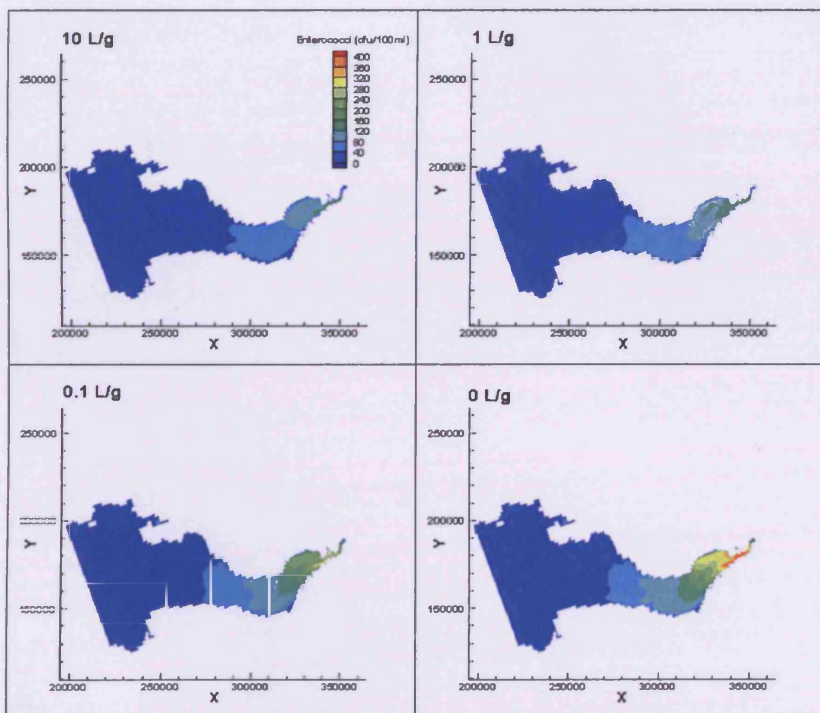


Figure 7.33d: Comparison of enterococci concentrations for different partition coefficients at high water spring tide

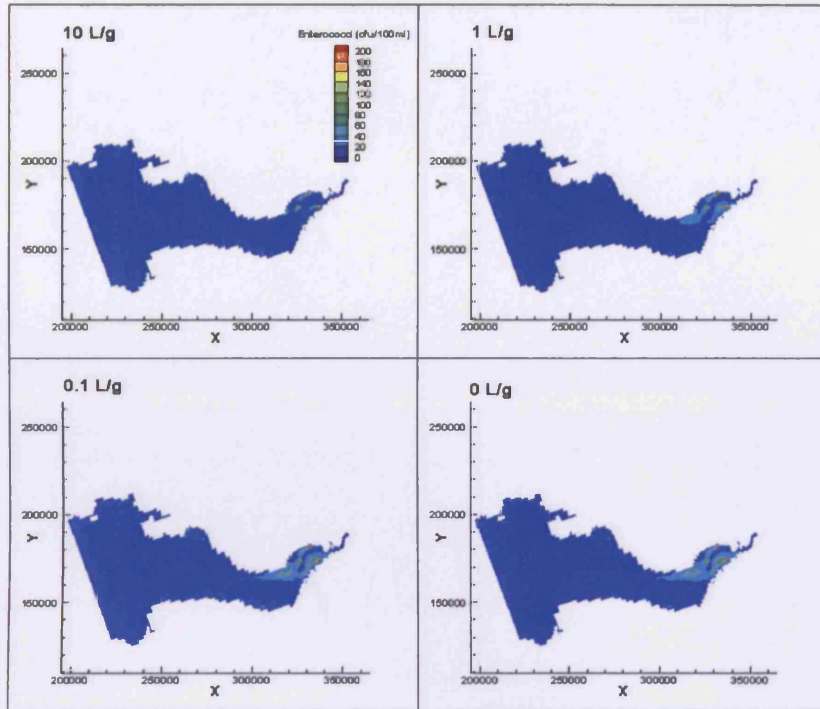


Figure 7.34a: Comparison of enterococci concentrations for different partition coefficients at mean flood neap tide

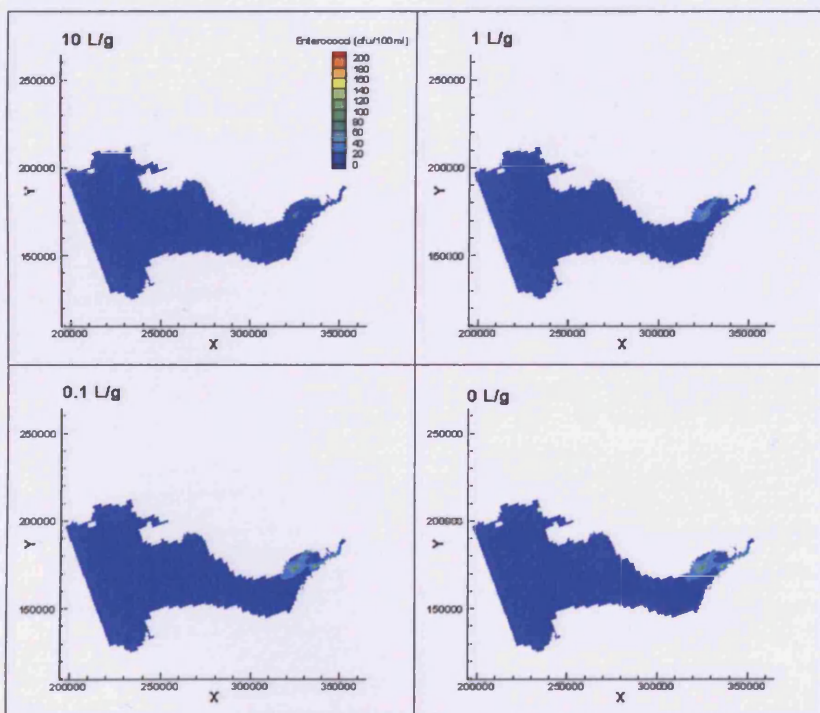


Figure 7.34b: Comparison of enterococci concentrations for different partition coefficients at high water neap tide

Figure 7.34: Comparison of enterococci concentrations for different partition coefficients at mean flood neap tide

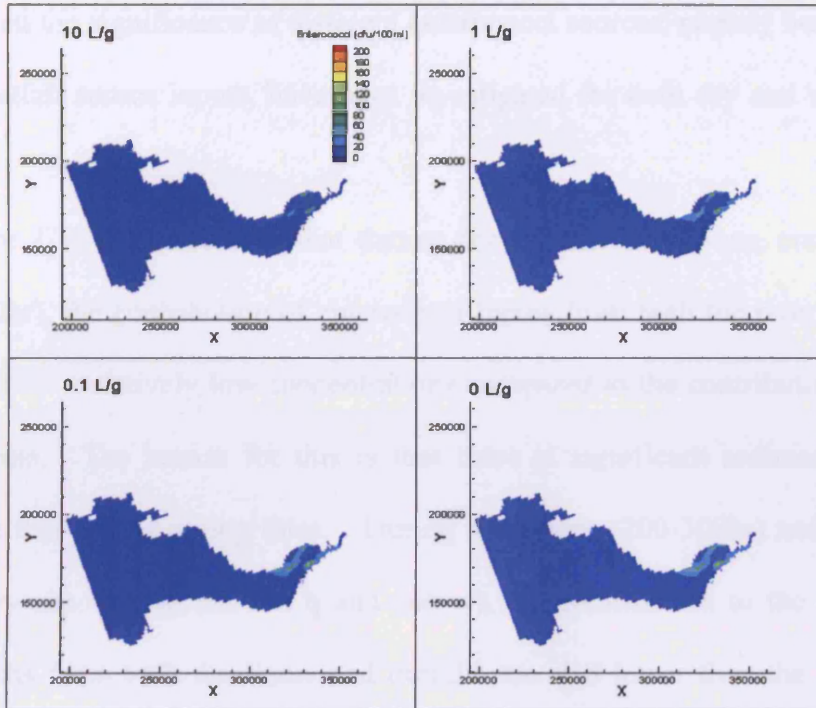


Figure 7.34c: Comparison of enterococci concentrations for different partition coefficients at mean ebb neap tide

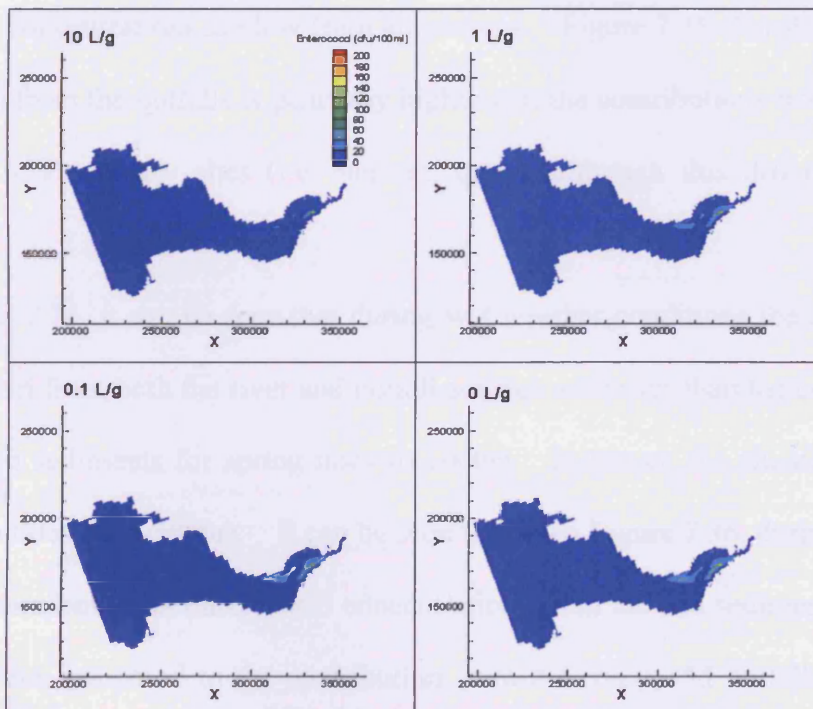


Figure 7.34d: Comparison of enterococci concentrations for different partition coefficients at low water neap tide

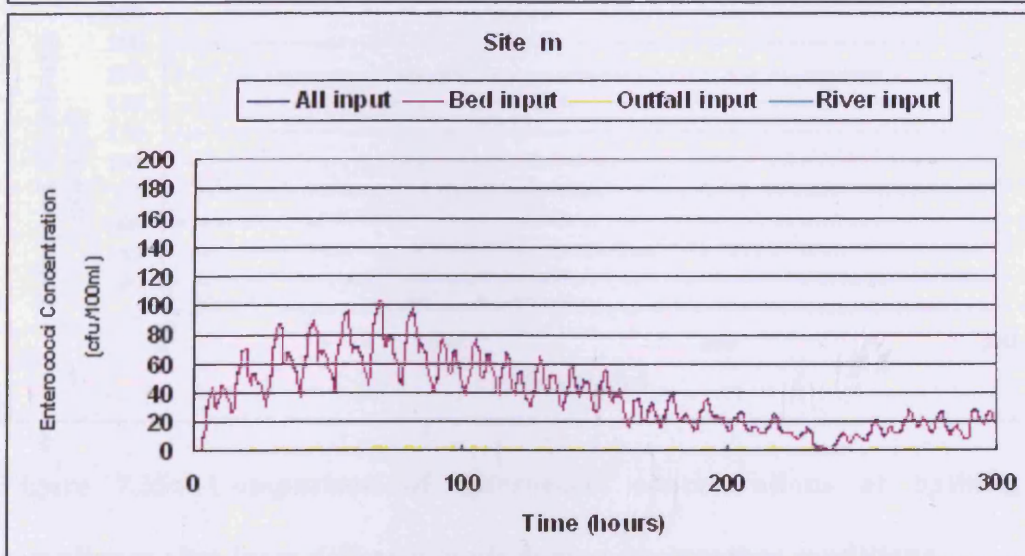
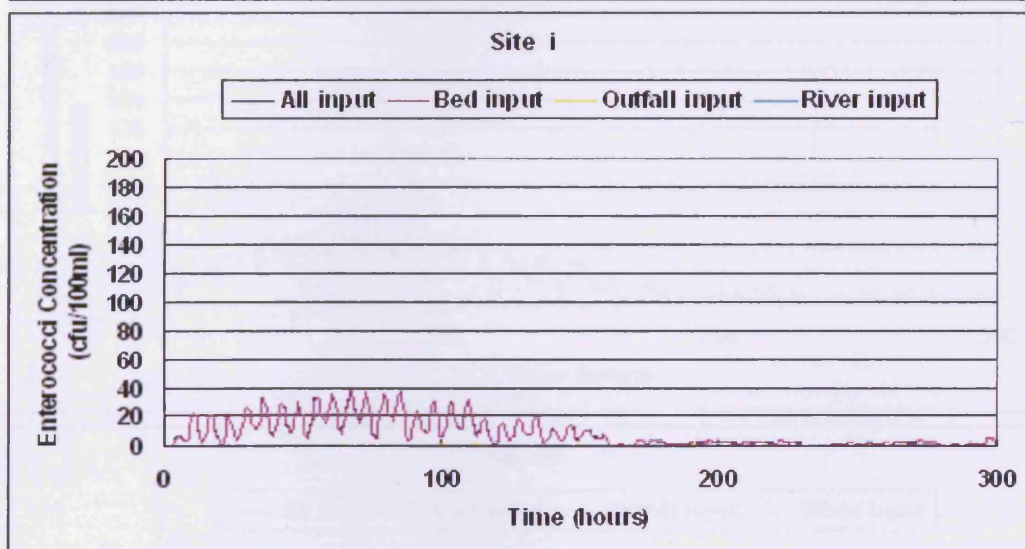
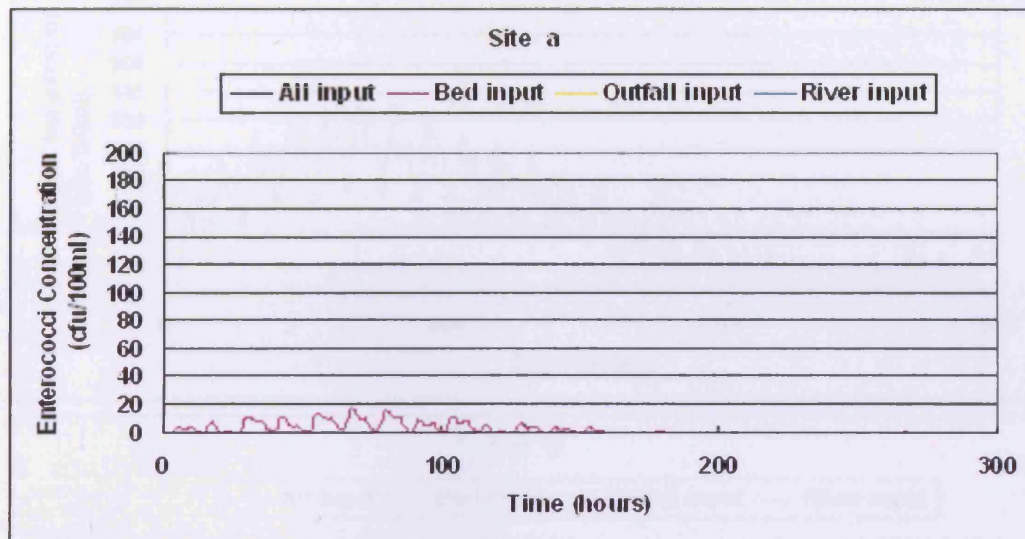
7.4.3 Significance of Different Sources of Bacteria

In this section the significance of different enterococci sources, namely bed sediments, river and outfall source inputs, have been investigated for both dry and wet weather conditions.

From Figure 7.35 it can be seen that during dry weather conditions, and for spring tides (0-100hr), the contribution of enterococci inputs from both the river and outfall sources lead to relatively low concentrations compared to the contribution from the bed sediments. The reason for this is that there is significant sediment transport erosion and flux during spring tides. During neap tides (200-300hr) and within the inner estuary (i.e. at sites m, site q and site w), the contribution to the enterococci concentrations from both the rivers and outfalls are also lower than the enterococci concentrations components from the bed sediments. During neap tides in the outer estuary, where the sediment transport is not significant, then the contribution to the enterococci concentrations are low from all sources. Figure 7.35 also shows that the contribution from the outfalls is generally higher than the contributions from the rivers within the inner estuary sites (i.e. sites m, q, w), although this difference is not significant.

From Figure 7.36, it can be seen that during wet weather conditions the contribution of enterococci from both the river and outfall sources are lower than the contributions from the bed sediments for spring tides (0-100hr). However, the situation changes during neap tides (200-300hr). It can be seen that from Figure 7.36, during neap tide cycle, the contribution of enterococci concentrations from the bed sediments becomes less significant compared to the contribution from the rivers and outfalls for spring tides. The results also show that the contribution from the rivers is generally higher than the contributions from the outfall inputs, except at site w. The expected cause of this anomaly at site w is thought to be due to this site being very close to the

Doniford Outfall (i.e. site 31 in Figure 7.3), which is a crude discharge from a WwTW and has high enterococci levels during wet weather conditions.



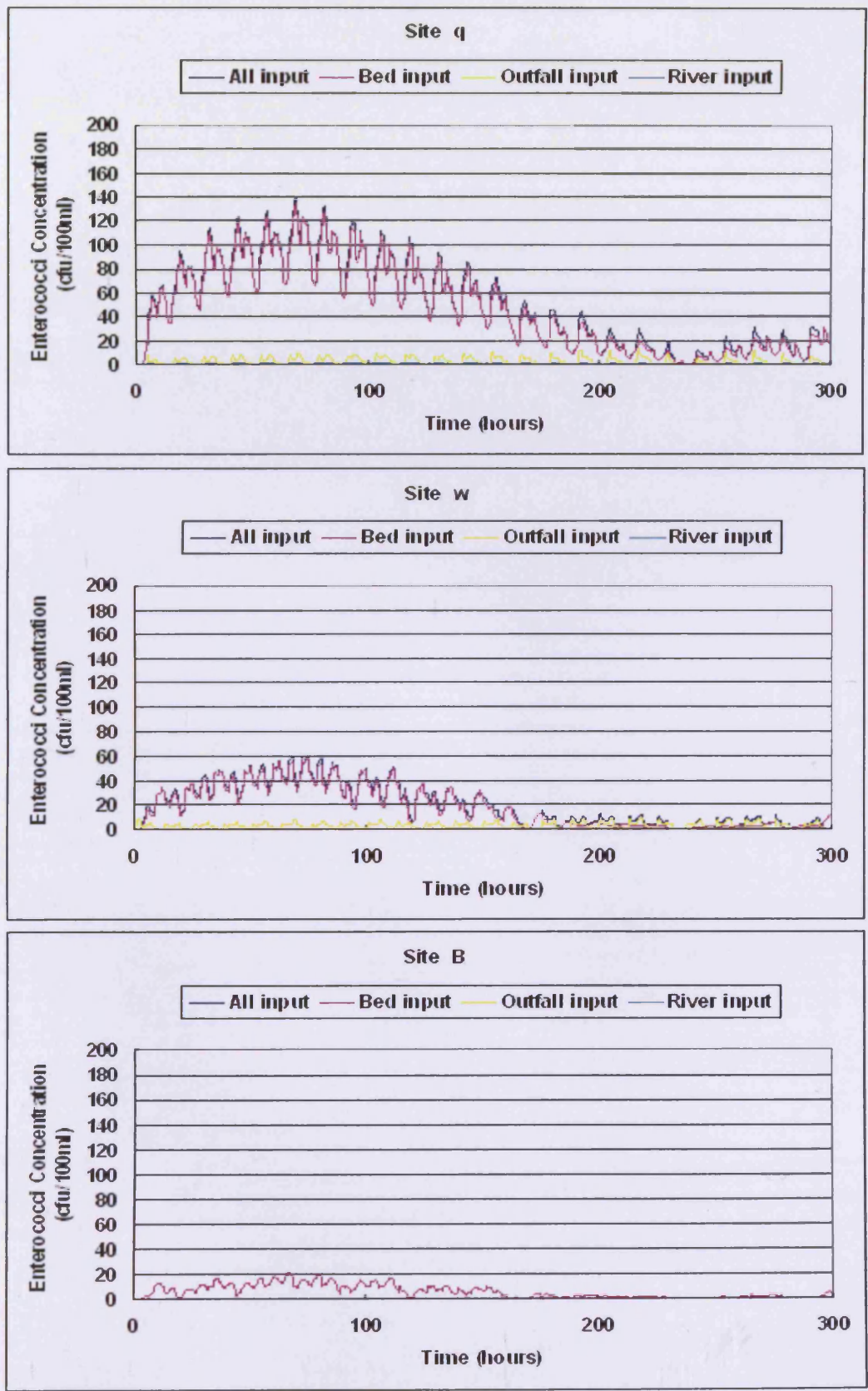


Figure 7.35: Comparison of enterococci concentrations at bathing water compliance sites from different loads during dry weather conditions

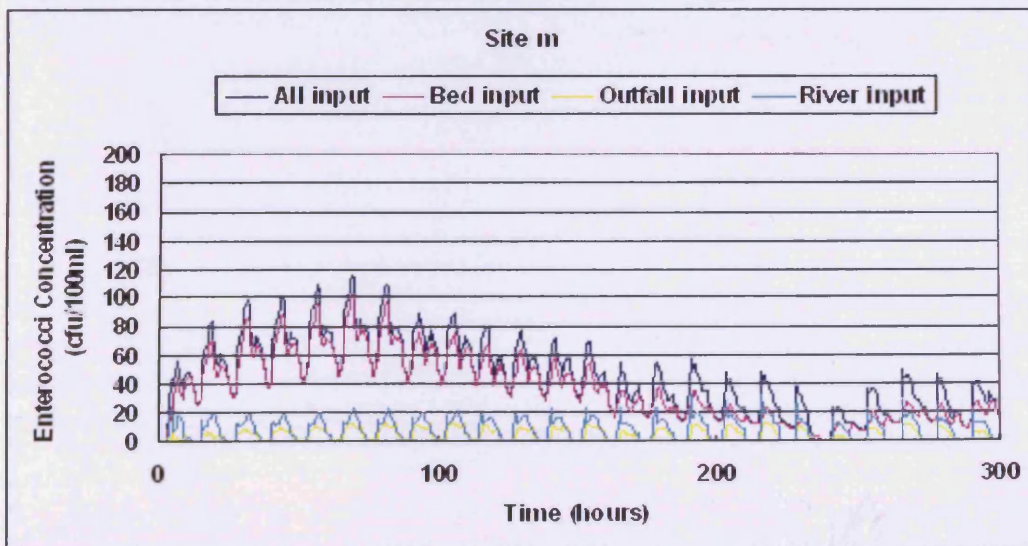
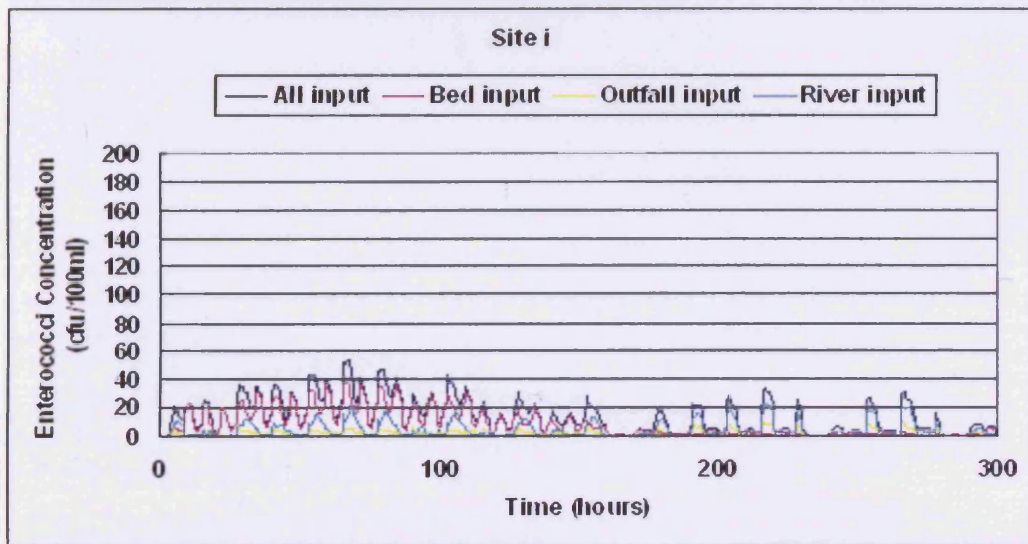
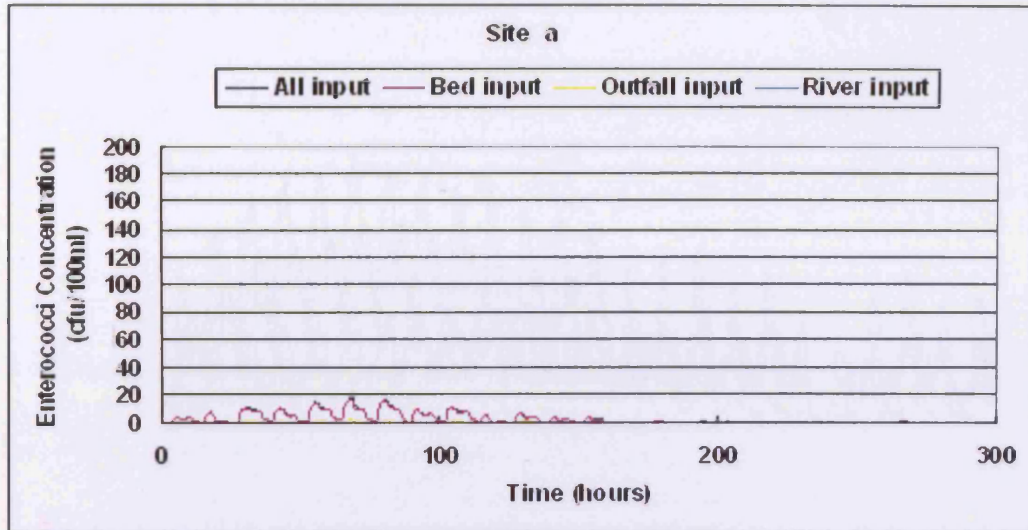


Figure 7.34: Comparison of enterococci concentrations at various sites during wet weather conditions

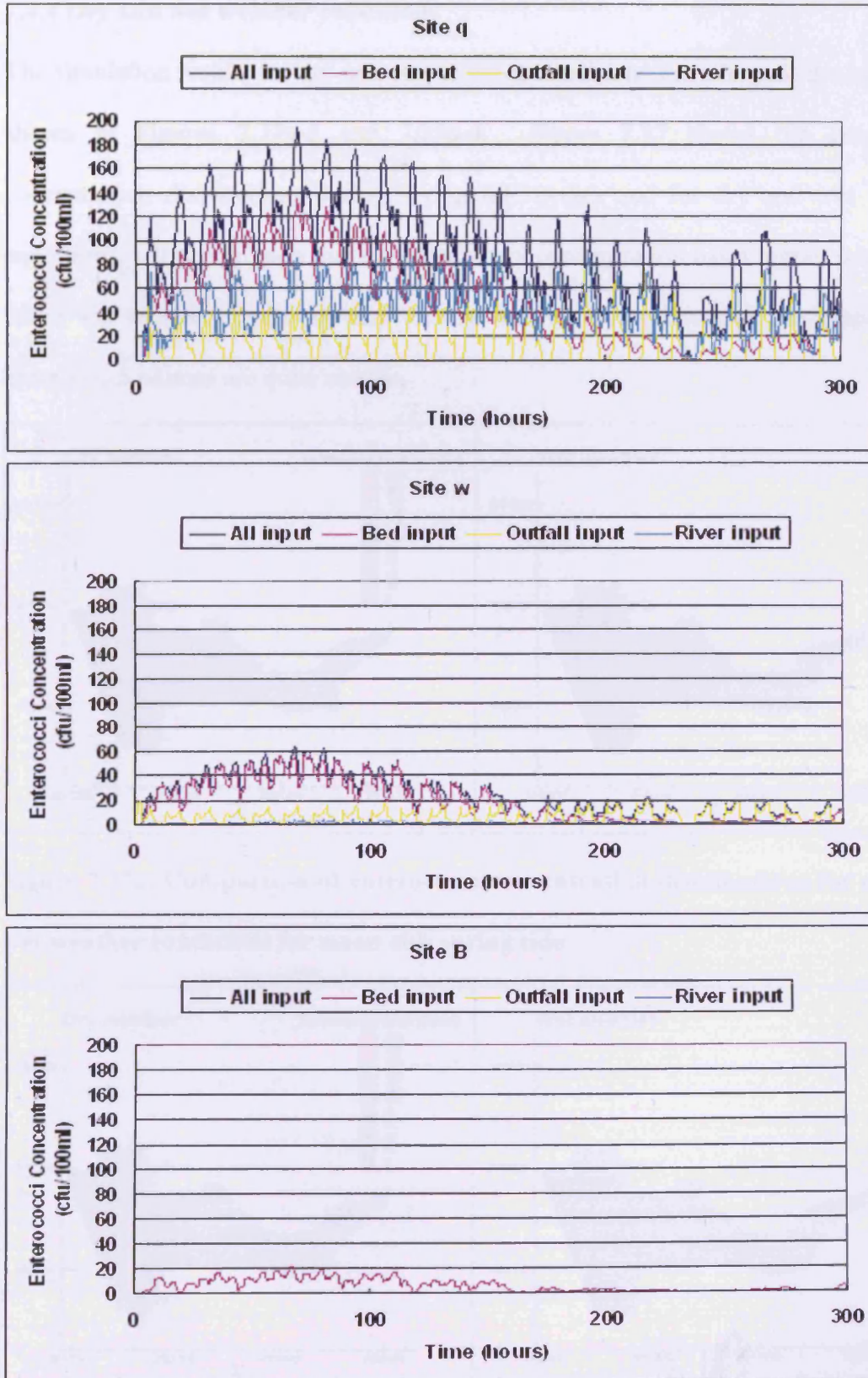


Figure 7.36: Comparison of enterococci concentrations at bathing water compliance sites from different loads during wet weather conditions

7.4.4 Dry and wet weather conditions

The simulation results for dry and wet weather conditions including all the inputs are shown in Figures 7.37a-d and 7.38a-d. Figure 7.37 shows the enterococci concentration distributions during spring tide cycles and for dry and wet weather conditions. It can be seen that the enterococci concentration has a higher peak value under wet weather conditions than for dry weather flows, however, the shape of the enterococci plumes are quite similar.

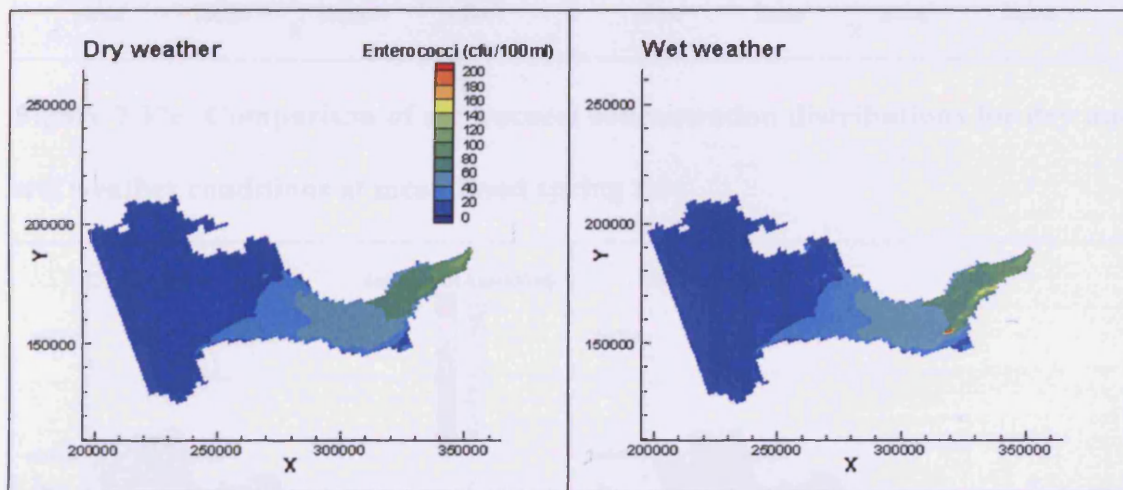


Figure 7.37a: Comparison of enterococci concentration distributions for dry and wet weather conditions for mean ebb spring tide

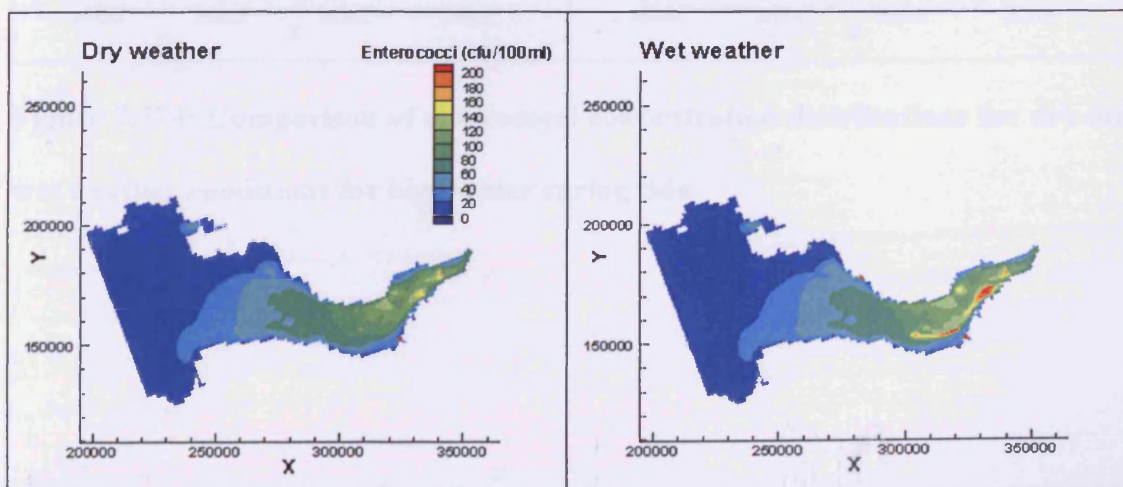


Figure 7.37b: Comparison of enterococci concentration distributions for dry and wet weather conditions for low water spring tide

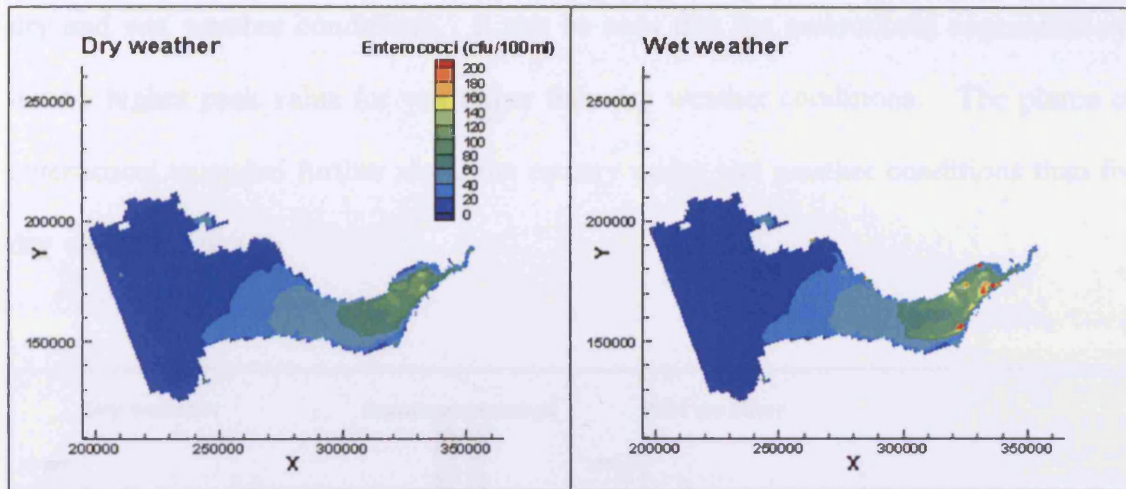


Figure 7.37c: Comparison of enterococci concentration distributions for dry and wet weather conditions at mean flood spring tide

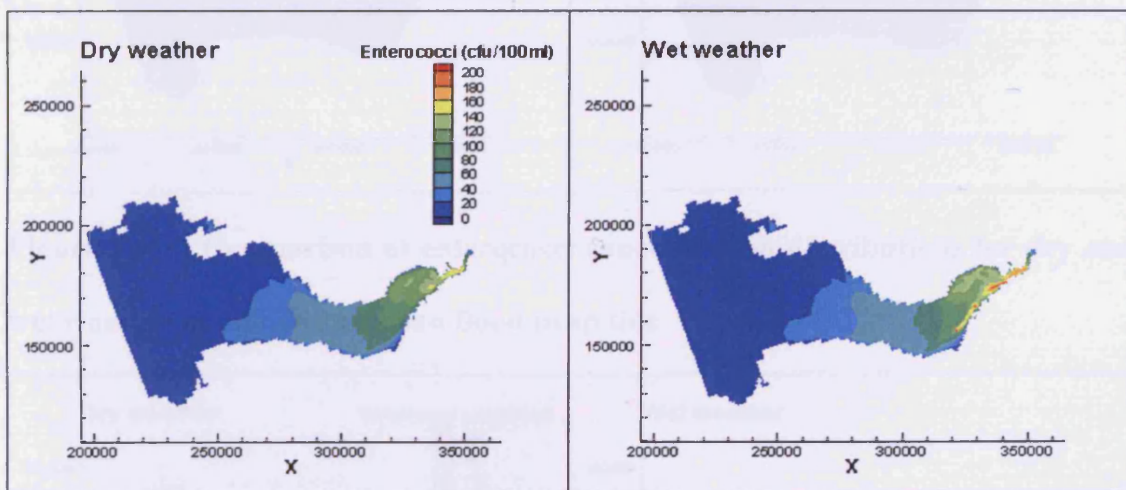


Figure 7.37d: Comparison of enterococci concentration distributions for dry and wet weather conditions for high water spring tide

Figure 7.38a-d shows the enterococci concentration distributions during neap tides for dry and wet weather conditions. It can be seen that the enterococci concentrations have a higher peak value for wet rather than dry weather conditions. The plume of enterococci extended further along the estuary under wet weather conditions than for dry weather flows.

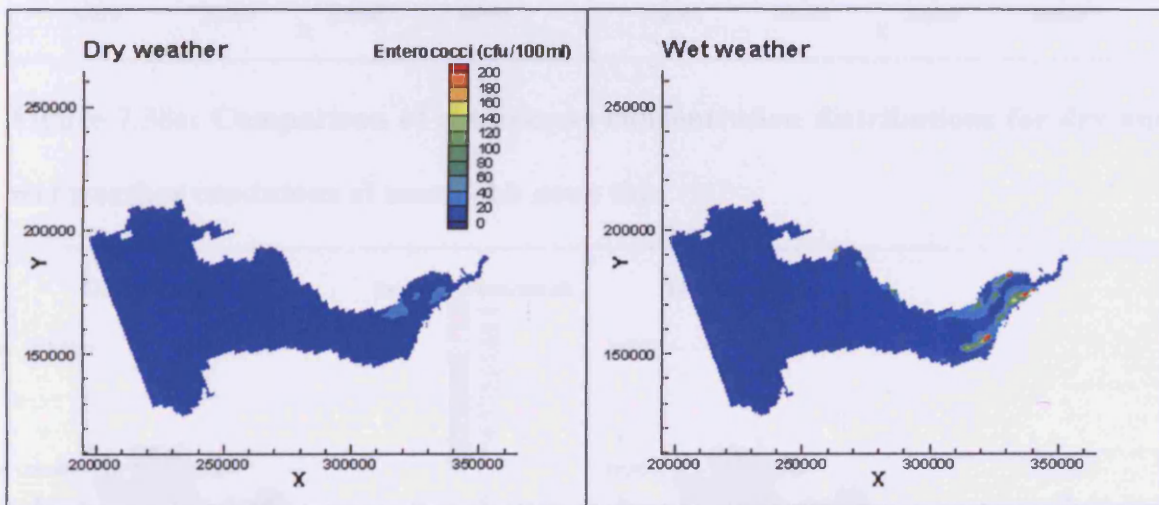


Figure 7.38a: Comparison of enterococci concentration distributions for dry and wet weather conditions at mean flood neap tide

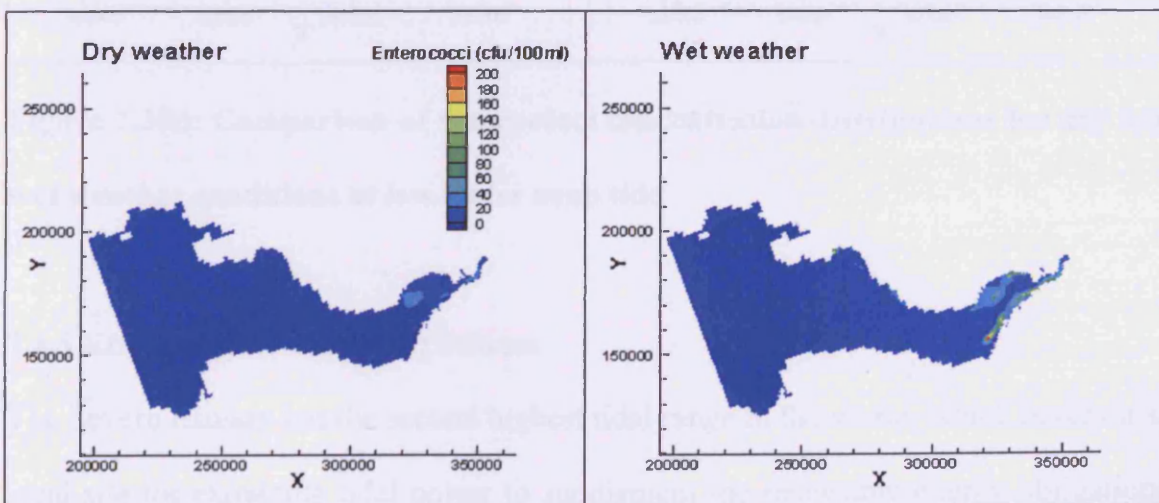


Figure 7.38b: Comparison of enterococci concentration distributions for dry and wet weather conditions at high water neap tide

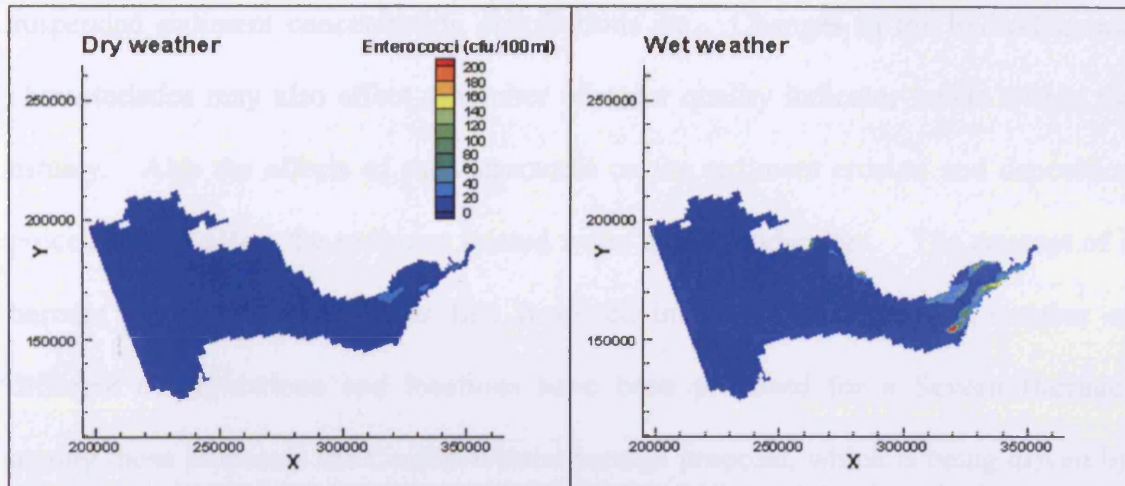


Figure 7.38c: Comparison of enterococci concentration distributions for dry and wet weather conditions at mean ebb neap tide

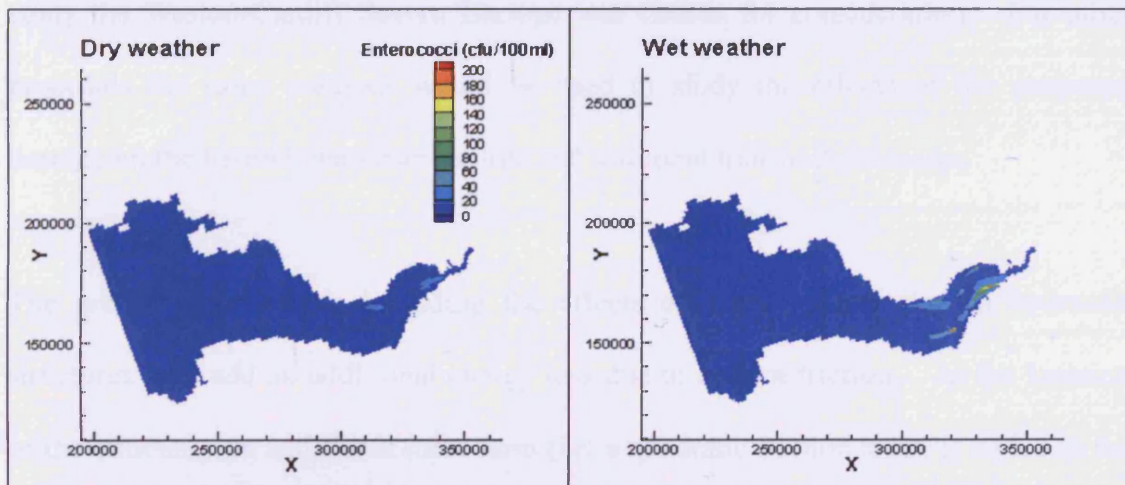


Figure 7.38d: Comparison of enterococci concentration distributions for dry and wet weather conditions at low water neap tide

7.4.5 Effect of tidal energy structures

The Severn Estuary has the second highest tidal range in the world, which makes it an ideal site for extracting tidal power to supplement the renewable energy obligations. The proposed tidal energy structures in the Bristol Channel include a Severn Barrage, tidal lagoons and tidal current turbines. All of these structures will have an impact on the water levels and velocities in the estuary which, in turn, will also affect the

suspended sediment concentration distributions etc. Changes in the hydrodynamic characteristics may also affect a number of water quality indicator levels within the estuary. Also the effects of such structures on the sediment erosion and deposition processes will affect the sediment related water quality indicators. The concept of a barrage across the Severn was first proposed in the 19th century. A number of different configurations and locations have been proposed for a Severn Barrage; among these proposals the Cardiff-Weston barrage proposal, which is being driven by the Severn Tidal Power Group, is one of the most popular and the location and the layout of this proposal is shown in Figures 7.39 and 7.40 respectively. Hence in this study the Weston-Cardiff Severn Barrage was chosen for consideration. For other proposals the same methods would be used to study the effects of the proposed barrage on the hydrodynamic and solute and sediment transport processes.

The present approach to including the effects of energy losses due to hydraulic structures is to add an additional energy loss due to bottom friction. At the location of the structures an additional force term (i.e. a quadratic friction term) is added to the momentum equations, to represent the extra loss of energy (e.g. Delft 3D Flow). In this study the barrage has therefore been modelled as a combination of a movable gate and a quadratic friction term as outlined above. The additional quadratic friction term is of the following form:

$$\text{Momentum loss} = g \frac{\xi_u - \xi_d}{\Delta x} = c_{loss} \frac{U |\bar{U}|}{\Delta x} \quad (7.4)$$

where c_{loss} = the energy loss coefficient. The flows through the barrage can therefore be given as:

$$Q = \mu A \sqrt{2g |\xi_u - \xi_d|} \quad (7.5)$$

where μ = the barrage contraction coefficient, with a value of between 0 and 1.

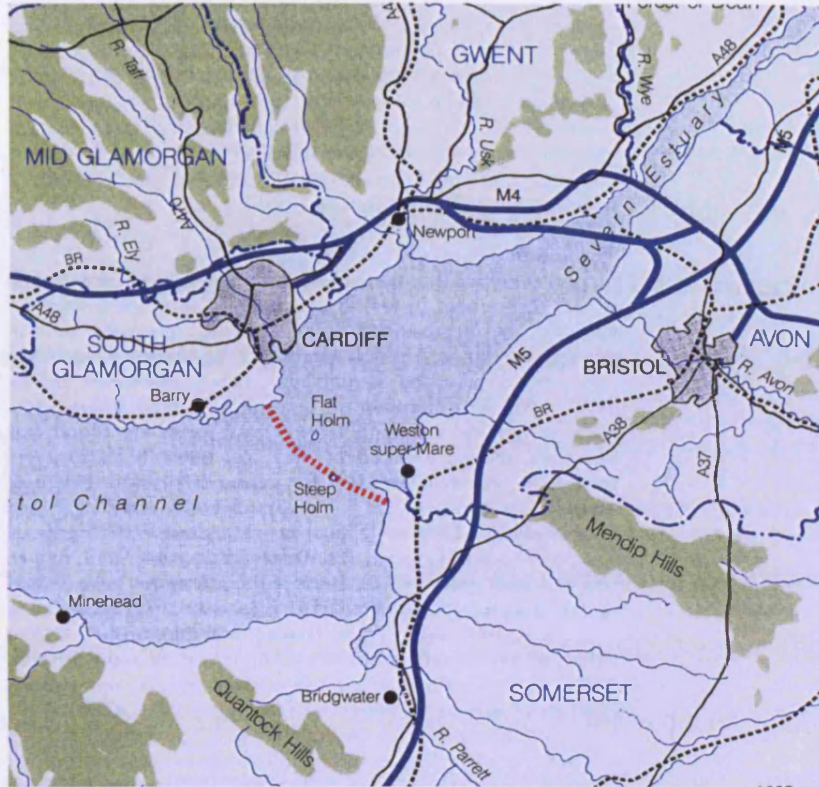


Figure 7.39 Proposed Cardiff-Weston Barrage site (Severn Tidal Power Group)

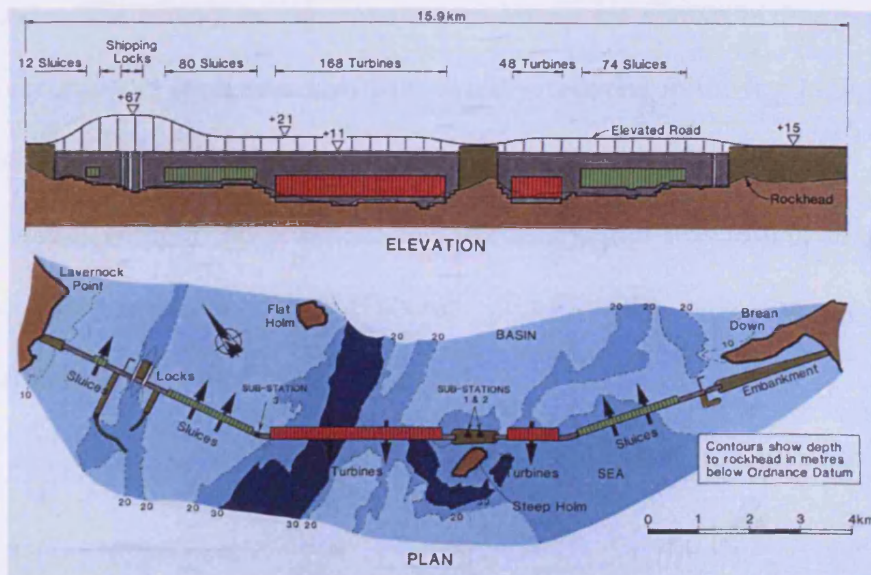


Figure 7.40 Layout of Cardiff-Weston Barrage (Severn Tidal Power Group)

Therefore, the energy loss coefficient is expressed in the following form:

$$c_{loss} = \frac{1}{2\mu^2} \quad (7.6)$$

The simulation results shown in the following graphs highlight the effects of the barrage on the hydrodynamic, sediment concentration and the bacteria levels in the Severn Estuary and Bristol Channel for spring tides and for ebb generation only operation.

It can be seen from Figures 7.41 and 7.42 that the currents in the estuary have been reduced significantly due to the existence of the Cardiff-Weston Barrage. This reduction in the peak currents arises primarily due to the reduced tidal range in the upper part of the estuary. Both the corresponding non-cohesive and cohesive sediment concentrations were also much lower in the estuary, with the construction of the barrage, and with the sediment concentration distributions being shown in Figures 7.43 to 7.46. The effects on the enterococci levels are shown in Figures 7.47 and 7.48. The enterococci level was also significantly reduced following inclusion of the barrage, with the model including sediment-bacteria interaction effects. However, when the model without the sediment-bacteria interaction was tested, then the peak enterococci concentrations did not change significantly, only the shape of the enterococci plume was noted to have changed.

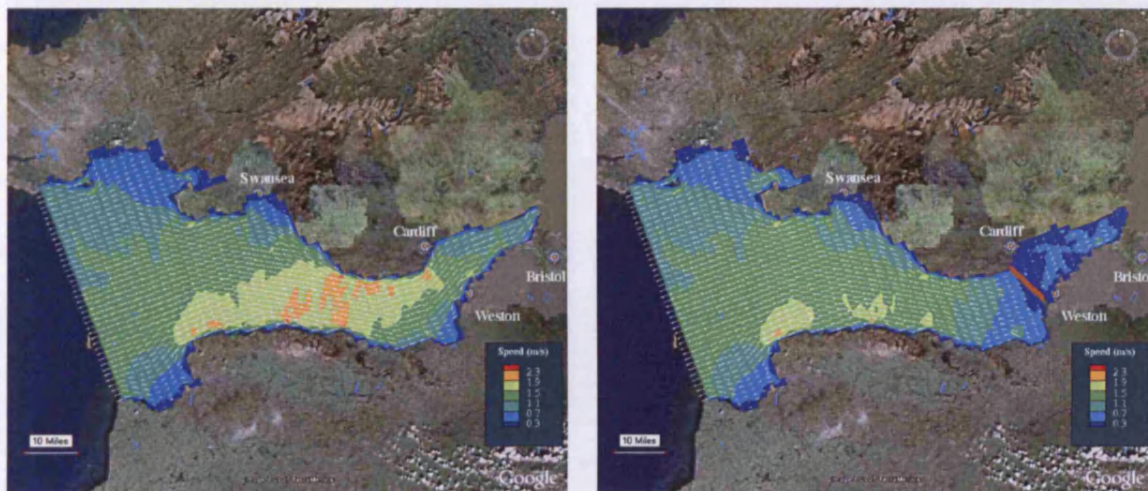


Figure 7.41 Currents at mean ebb tide, both without and with the barrage

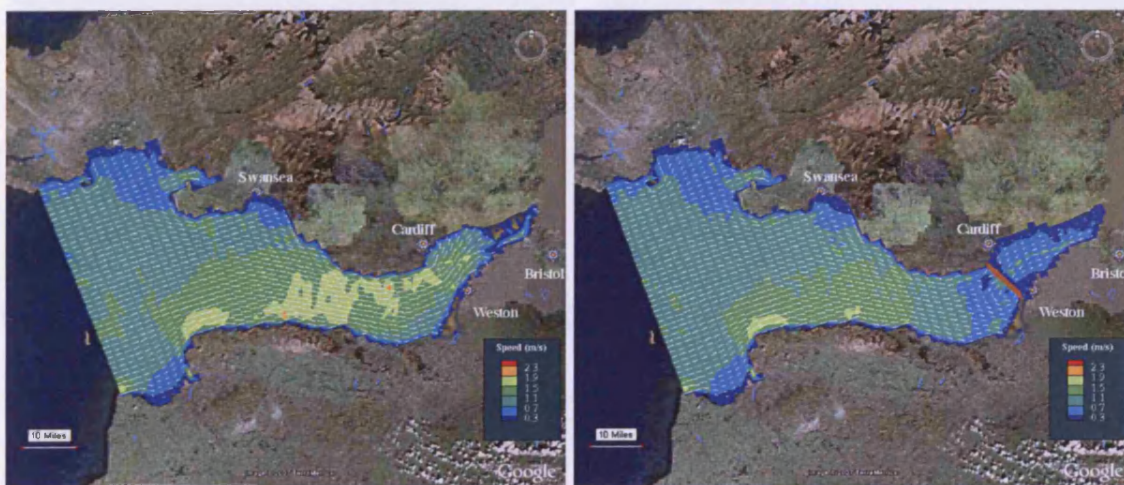


Figure 7.42 Currents at mean flood tide both without and with the barrage

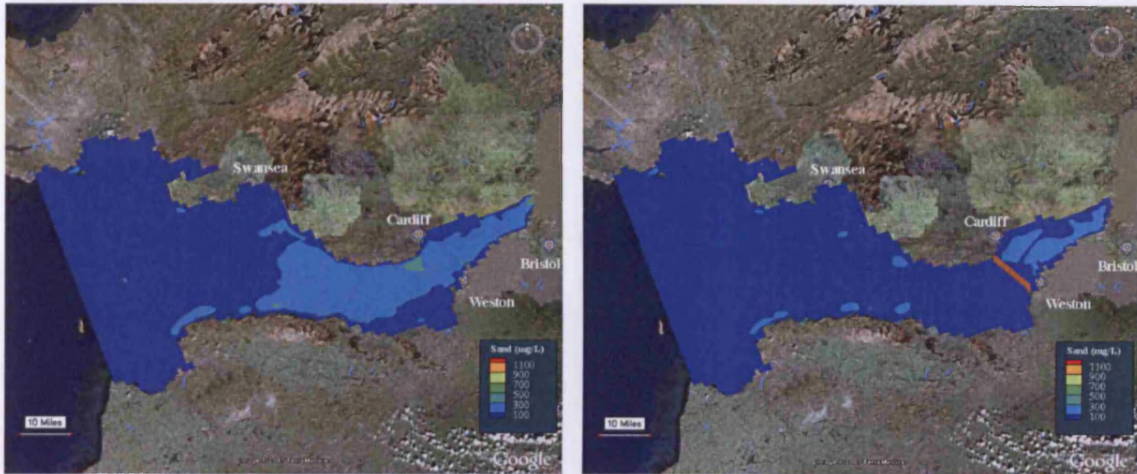


Figure 7.43 Non-cohesive sediment concentrations at mean ebb tide both without and with the barrage



Figure 7.44 Non-cohesive sediment concentrations at mean flood tide both without and with the barrage

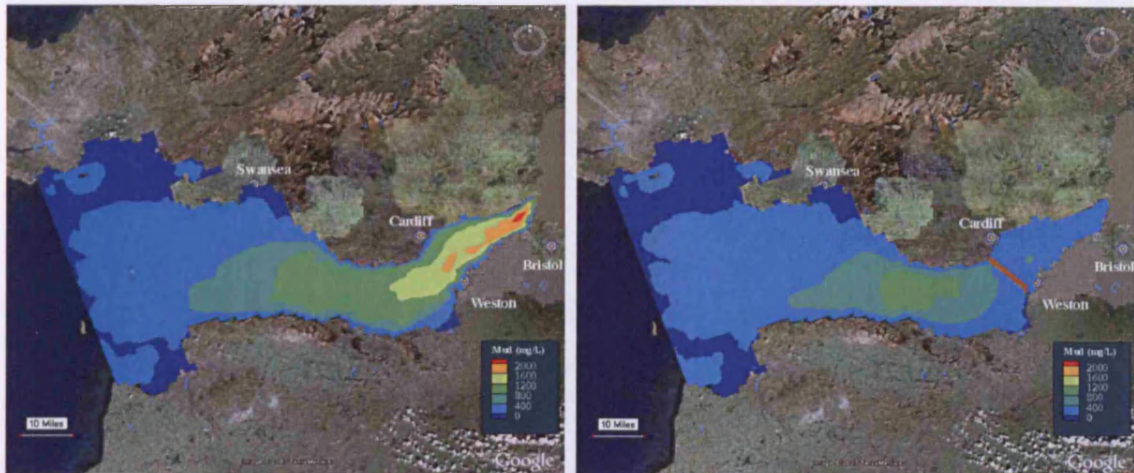


Figure 7.45 Cohesive sediment concentrations at mean ebb tide both without and with the barrage

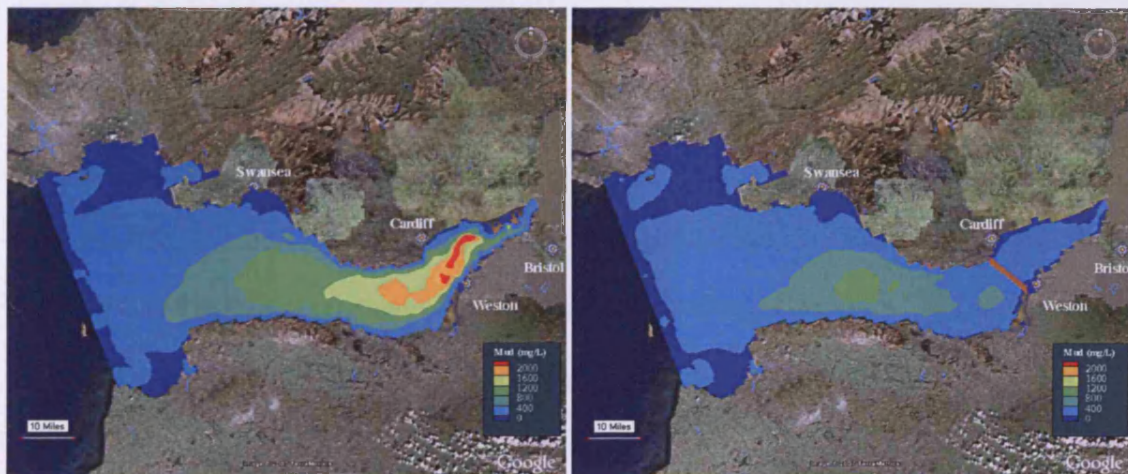


Figure 7.46 Cohesive sediment concentrations at mean flood tide both without and with the barrage



Figure 7.47 Enterococci concentrations at mean flood tide both without and with the barrage and with and without sediment-bacteria interactions

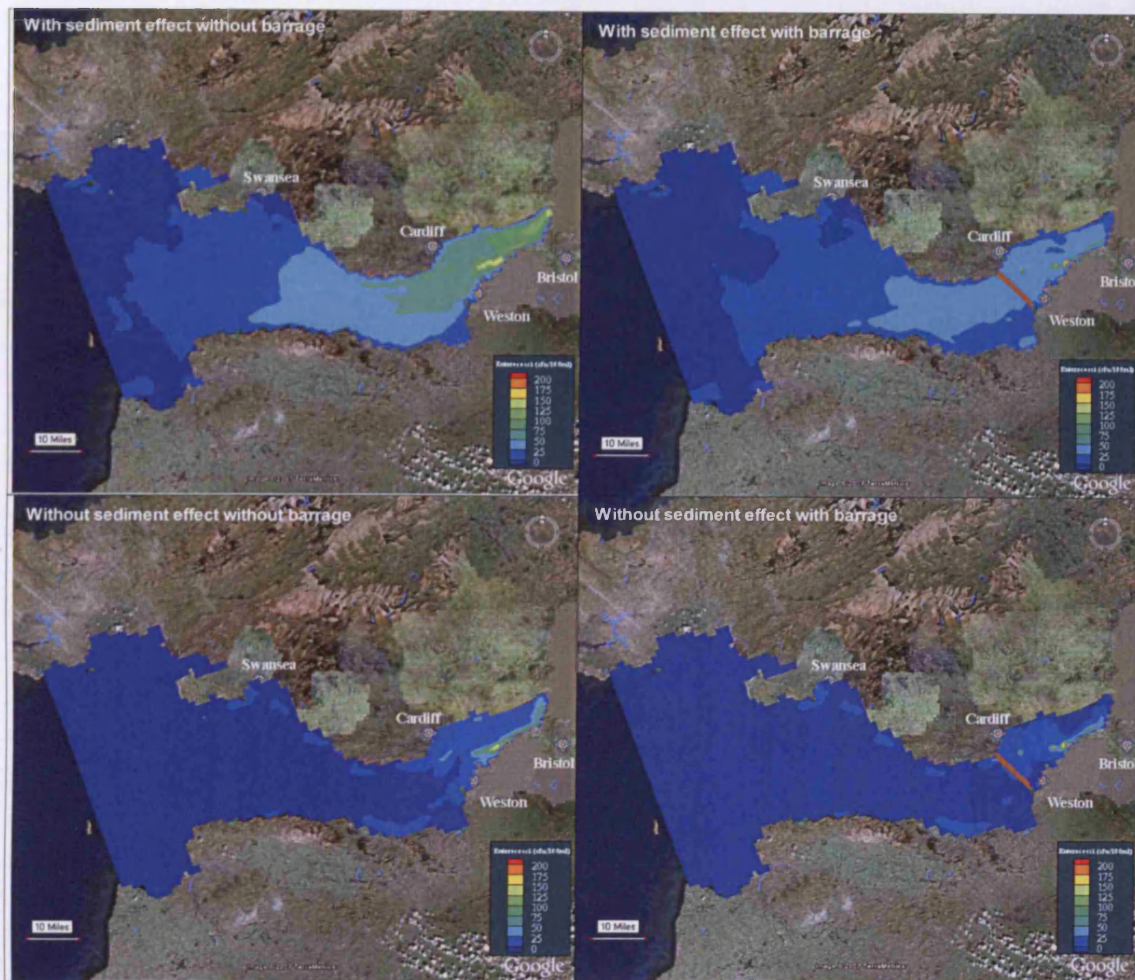


Figure 7.48 Enterococci concentrations at mean ebb tide both without and with the barrage and with and without sediment-bacteria interactions

7.5 Summary

In this chapter the sediment-bacteria interaction model has been developed and set up for the Bristol Channel and Severn Estuary. The hydrodynamic model was first calibrated and validated against various data sets and the sediment transport model was then calibrated against field data. Enterococci was chosen as the bacterial indicator organism and the model was calibrated against measured concentrations and

using empirical decay rate formulae. After calibration the model was applied to predict the enterococci concentrations at selected bathing water compliance sites, located along the Severn Estuary. Different weather and flow conditions were chosen to investigate the bacteria distribution, with sensitivity tests being conducted to investigate the effects of the initial bed bacteria concentrations and the partitioning coefficient values on the receiving water concentration values and distributions. The model was also refined and extended to investigate the effects of a proposed Severn Barrage on the hydrodynamic, sediment transport and bacterial transport processes in the Severn Estuary, with the barrage being shown to have a significant impact on all three parameters.

Chapter 8

Conclusions and Recommendations

8.1 Conclusions

Through this study numerical models, developed within the Hydro-environmental Research Centre at Cardiff University, have been refined for improved predictions of the hydrodynamic, sediment transport and bacterial processes in free surface unsteady flow. The main objective of this study was to improve the accuracy of predictions of the bacteria fluxes in complex estuarine flows and particularly with regard to the sediment-bacteria interactions. The main particular developments in this study include: sediment-bacteria interaction process modelling by using a dynamic partition ratio; and the treatment of the turbulence terms using a simple two layer mixing length model.

The treatment of the turbulence terms was tested against experimental data collected in the laboratory. Analytical solutions for the sediment-bacteria interactions, under steady and uniform flow conditions, and published field experimental data were used to test the sediment-bacteria interaction model. The sediment transport model was also tested against published experimental data. After testing all of these refinements against known data, the models were then applied to a real estuary, namely the Severn Estuary, in the UK.

The main conclusions and findings from this study can be summarised as follows:

- For the main hydrodynamic model refinement, a relatively simple turbulence model was used to predict the complex three-dimensional flow structure in a flume with simulated vegetation. This was thought to be a severe test of the model and the improved accuracy would enable simpler and computationally cheaper three-dimensional flow simulations for real estuaries. In previous studies on vegetated flow modelling, two-equation turbulence models, such as the $k-\varepsilon$ model, were normally used. However, extra computing costs were needed due to two extra partial differential equations needing to be solved and as well as the additional empirical coefficients in these equations included which have not been evaluated for such flow conditions. The main purpose of this part of the study was therefore to try and acquire accurate velocity profiles without the need for more advanced two-equation turbulence models, also requiring values for many unknown coefficients. A simple two layer mixing length model was included in the three-dimensional model. The corresponding predicted results were compared with laboratory data and very good agreements between both sets of results were obtained. The results showed that the simple mixing length model gave accurate complex velocity profile predictions with the advantage of requiring limited coefficient data. This result shows that complex three-dimensional velocity profile can be accurately predicted using simple turbulence model and this turbulence model was then used throughout the remaining studies.
- For the bacterial process modelling study, a traditional constant decay rate is generally assumed in numerical models widely used for hydro-environmental coastal and estuarine studies. Extensive field data taken for this study shows that

the faecal bacteria decay rate is a function of the light intensity and turbidity (Stapleton et al 2007). The current hydro-environmental model was refined to include a dynamic decay for bacteria, with the rate being dependent on variations in light and turbidity. Formulations developed through earlier studies were included in the current numerical model. The model predictions were then tested against field data with good agreement being obtained. The results showed that the predicted concentrations were highly dependent upon these parameters and the model gave excellent comparisons with field data for Severn Estuary.

- Sediment is an important means of transport of bacteria. Bacteria can be absorbed onto bed or suspended sediment and then transported with the sediments via erosion, deposition and partitioning. The bacteria can then be desorbed back from the sediment into the water column. Further refinements to the representation of the transport of bacteria through the flow field have been included in the model by the novel addition of the interaction of bacteria with the sediments. The deposition and re-suspension of sediment absorbed bacteria were taken into account by partitioning the total bacteria into their free-living and attached phases, using a dynamic partitioning ratio, related to the suspended sediment concentrations. The novel method used in this study to involve the re-suspension and deposition of the absorbed bacteria with sediments has been tested against analytical solutions for steady uniform flow conditions, published field experimental data and field data acquired for the Severn Estuary. All of the comparisons have shown very good agreement between the predicted and the data. The models were then applied to an idealised case and to the Severn Estuary. From the model application results it was found that the sediment transport plays

a significant role in controlling the fate and transport of bacteria in surface waters and apparently effects the water column bacteria concentrations. The method used can be extended to modelling other sediment related water quality indicators and such studies are currently on-going.

- The significance of different sources of bacteria for both dry and wet weather was also investigated. It was found that during different weather conditions the significance of the bacteria sources were very different. The significance of the source was also very different during different phases of the tide. During spring tide, the bacteria input from the bed sediments as dominant for both wet and dry weather conditions. However the impact of the input from the rivers and outfalls was much more significant during wet weather conditions. During neap tides and during dry weather conditions the inputs of bacteria from the bed sediment were still dominant, but during wet weather conditions the inputs from river were dominant.
- From the application of the model to the Severn Estuary it was observed that the weather conditions played an important role in the distribution of bacteria along the estuary. It was observed that for spring tides the bacteria concentrations have a higher peak value during wet weather conditions than for dry weather flows. However, the shape of the bacteria distribution plumes was quite similar. It was also observed that during neap tides the bacteria concentrations had a higher peak value for wet weather conditions than dry weather conditions and the bacteria plume extended further along the estuary under wet weather conditions than for dry weather flows. This difference between concentration predictions for spring

and neap tides was generated through the sediment inputs. During spring tides the bacteria input from the bed sediments due to the re-suspension of sediments was dominant for all values of the bacteria distributions, so the distribution of the bacteria are highly related to the sediment distribution. However during neap tides the input of bacteria from river and outfalls are dominant.

- The significance of the sediment effects on bacteria transport were also found to vary for different flow conditions. Both the partitioning coefficient and the initial bed bacteria concentrations contributed significantly during spring tides, having a less but still significant role during neap tide.
- From the model application results for both the idealized cases and the real estuary study, it can be seen that sediment transport plays a very important role in predicting the fate and transport of bacteria in surface waters. Under different flow conditions some parameters had a more significant role than others. During high flow conditions the sediment re-suspensions processes were dominant, therefore the bed bacteria concentrations played a dominant role on the over all bacteria concentration levels in the water column. In contrast, during low flow conditions sediment deposition prevails and bacteria are removed from the water column. The partition coefficient was found to be more important than the bed bacteria concentrations, during low flow conditions.
- The analytical solutions for the sediment-bacteria interaction processes were derived for steady uniform flow conditions and were used to test the sediment-bacteria interaction model. As stated previously the predicted and

analytical concentrations showed very good agreements. These analytical solutions can therefore be used to test other sediment related water quality indicator models directly or with limited modification.

- The numerical model was finally used to investigate the impact of the proposed Cardiff–Weston tidal barrage (or the ‘Severn Barrage’) on the currents, sediment transport and bacterial processes within the Severn Estuary. The results showed that the barrage would reduce the currents, as well as significantly reducing the suspended sediment concentrations and bacteria concentration levels in the estuary. The model results highlighted the importance and necessity in using a sediment-bacteria model to investigate the effects of the barrage on the basin’s hydrodynamic, sediment transport and bacterial levels. The barrage will affect the sediment transport processes dramatically which in turn will affect the sediment related bacteria levels. This latter finding would not be found in using conventional models where the sediment-bacteria interaction are generally not included.

8.2 Recommendations for Further Study

Following on from the studies reported herein a number of future research studies are recommended and particularly in the context of bacteria modeling. These recommendations are summarised below:

- In the studies reported herein the fate and transport of bacteria through bed sediment has only been considered for a well mixed single layer, and the geomechanical processes in the bed sediments have been ignored. This

assumption is thought to be reasonable if the transport of bacteria is only simulated for a short time period. However, if long term fate and transport processes of bacteria are considered, then the geomechanical processes within the bed sediments need to be taken into account. Integrating the fate and transport of bacteria with a morphological model to investigate the long term fate and transport of bacteria in the bed sediment, together with dynamic decay rate would provide a more accurate prediction of the long term behaviour of estuarine system to bacterial inputs.

- The representation of decay rate for bacteria within the bed sediments could be improved through more bio-chemical studies conducted under controlled laboratory conditions. The decay rate in bed sediment has been found to be much smaller than that in the water column, but little is still known about this parameter. Some researchers have even found that growth of faecal bacteria can occur in the bed sediment. Hence, more laboratory and field studies need to be undertaken to determine the decay or growth rate of faecal bacteria in the bed sediments.
- Auer and Niehaus (1993) indicated that from their experiments 90.5% of the faecal coliform bacteria were found to be associated with small particles ($<10\mu m$) and 9.5% were associated with larger particles ($>10\mu m$). Gannon (1983) found a similar trend. This research indicates that bacteria have a preference for attaching to smaller sized particles rather than larger particles. The size of the sediment particles was not considered in the current study during the attachment phase, i.e. it was assumed that the faecal bacteria were adsorbed equally to all size of particles. Therefore ideally the model needs to be refined further to consider the

effect of different sediment sizes on the bacterial levels in the sediments and their corresponding transport through the water column. This requires the sediment transport model to have the capability to predict simultaneously the sediment transport processes for sedimentary beds with a range of particle size.

- In this study, the diffuse sources were first quantified and then used as inputs introduced into the faecal bacteria transport model. This representation can not involve the effect of changes to the diffuse source directly, such as land use changes effects on the surface water quality. Hence an integrated land use model together with a surface water quality model would provide an effective tool for investigating the diffuse effects of diffuse sources on surface water quality.

References:

- Allen, G. et al 1987. Survival of pathogenic bacteria in various freshwater sediments. *Applied and Environmental Microbiology*. vol 53. no.4. pp633-638.
- Anderson I.C., Rhodes M. and Kator H. 1979. Sublethal Stress in *Escherichia Coli*: A Function of Salinity, *Applied and Environmental Microbiology*, vol.38, pp1147-1152.
- APHA—American Public Health Association, 1995. *Standard Methods for the Examination of Water and Wastewater*, 19th ed. American Public Health Association, Washington, DC.
- Auer, M.T. and Niehaus, S.L. 1993. Modeling faecal coliform bacteria-I. Field and laboratory determination of loss kinetics. *Water Research*. v 27 n 4, pp693-701.
- Bai, S. 2004. Developing a Fate and Transport Model of Fecal Coliform Bacteria for Surface Waters. PhD Thesis. University of Virginia.
- Bai, S and Lung, W 2005. Modeling sediment impact on the transport of fecal bacteria. *Water Research*. V39, pp5232-5240.
- Bellair, J.T., Parr-Smith, G.A. and Wallis, I.J. 1977. Significance of Diurnal Variation in Faecal Coliform Die-off Rates in the Design of Ocean Outfalls. *Journal of WPCF*, vol 77(9), pp2022-2030.
- Blumberg, A. F., and G. L. Mellor, 1987: A description of a three-dimensional coastal ocean circulation model. *Three-dimensional coastal ocean models*, Editor: N. S. Heaps, American Geophysical Union, 1-16.
- Chang, Y.C. 1971. PhD Thesis, Uni Iowa, Iowa City.
- Chamberlin, C.E. and Mitchell, R. 1978. A Decay Model for Enteric Bacteria in Natural Waters. In *Water pollution Microbiology Volume 2*. Eds by Mitchell R, Wiley-Interscience, USA .
- Chapra S.C. 1997. *Surface Water-Quality Modelling*, McGraw Hill, New York, pp844
- Chien, N. and Wan, Z-H. 1999. *Mechanics of Sediment Transport*. ASCE Press.
- Council of European Communities 1976 Council directive of 8th December 1975 concerning the quality of bathing water(76/160/EEC). *Official Journal of European Communities*, L31:1-7.
- Council of European Union. 2006 DIRECTIVE 2006/7/EC OF THE EUROPEAN PARLIAMENT AND OF THE COUNCIL. *Official Journal of European Communities*, L64:37-51.
- Dorcheh, S.A.M. 2007. Effect of Rigid Vegetation on the Velocity, Turbulence and

- Wave Structure in Open Channel Flows. PhD Thesis. Cardiff University.
- Dronkers, J.J. 1964 Tidal Computations Rivers and coastal waters. Amsterdam: North Holland Publishing Co.
- Einstein, H.A., 1942. Formula for the transportation of bed load. Trans., Amer. Soc. Civil Engrs, 107: 561-597.
- Elder, J.W. 1959. The Dispersion of Marked fluid in turbulent shear flow. Journal of Fluid Mechanics, 5(4), pp544-560.
- Engelund, F. and Fredsoe, J., 1976. A sediment transport model for straight alluvial channels. Nordic Hydrology, 7:283-306.
- Falconer, R.A. 1993. An introduction to nearly horizontal flows. In: Coastal Estuarial and Harbour Engineers, Reference Book. M.B. Abbott and W.A. Price (eds). London: E and F.N. Spon Ltd. chapter 2. pp 27-36.
- Falconer, R.A. and Chen, Y. 1991. An improved representation of flooding and drying and wind stress effects in a two-dimensional tidal numerical model. Proc. Instn Civ Engrs, part 2, 91, 659-678.
- Falconer, R.A and Chen, Y. 1996. Modeling sediment transport and water quality processes on tidal floodplains. In: Anderson MG, Walling DE, Bates PD, editors. Floodplain processes, Chichester: Wiley.
- Falconer, R.A., B. Lin, E. Harris, and S.M. Kashefipour, (2001), "DIVAST Model: Reference Manual, Cardiff University, Environmental Management Research Centre.
- Falconer, R.A., Lin, B and Kashefipour, S.M. 2005. Modelling Water Quality Processes in Estuaries. In Computational Fluid Dynamics: Applications in Environmental Hydraulics Edited by P.D. Bates, S.N. Lane and R.I. Ferguson. John Wiley & Sons Ltd.
- Falconer, R. A. and Owens, P.H. 1987. Numerical Simulation of Flooding and Drying in a Depth Averaged Tidal Flow Model. Proceedings of the Institution of Civil Engineers. V83, part 2, pp161-180.
- Fischer, H.B. 1973. Longitudinal dispersion and turbulent mixing in open channel flow. Annual Review of Fluid Mechanics, 5, pp59-78.
- Fischer, H.B. et al 1979 Mixing in Inland and Coastal Waters. San Diego:Academic Press Inc. 483pp.
- French, R. 1986. Open-Channel Hydraulics. McGraw-Hill Book Company.
- Fries, J.S. Characklis, G.W. and Noble R.T.2006. Attachment of Fecal Indicator Bacteria to Particles in the Neuse River Estuary, N.C. Journal of Environmental

Engineering, Vol. 132, No. 10, pp 1338–1345

Gameson A.L.H. and Gould D.J. 1975. Effects of Solar Radiation on the Mortality of Some Terrestrial Bacteria in Sea Water. In : Discharge of sewage from sea outfalls: proceedings of an international Symposium held at Church House, London, 27 August to 2 September, 1974.

Gameson A.L.H. and Saxon J.R. 1967. Field studies on on effect of daylight on mortality of coliform bacteria. *Water Research*. Vol.1, pp279-295.

Gannon, J. et al 1983. Faecal coliform disappearance in a river impoundment. *Wat. Res.* 17, 1595-1601.

Garcia-Armisen, T. and Servais, P. 2007. Respective contributions of point and non-point sources of E coli and enterococci in a large urbanized watershed (the Seine river, France). *Journal of Environment Management*. V82, pp 512-518.

Goldstein, S. (1938) *Modern Development in Fluid Dynamics*, Vol. 1, Oxford University Press, Oxford.

Grimes, D.J. 1980. Bacteriological Water Quality Effects of Hydraulically Dredging Contaminated Upper Mississippi River Bottom Sediment. *APPLIED AND ENVIRONMENTAL MICROBIOLOGY*. V39, n4, pp 782-789

Hakimzadeh, H and Falconer, RA. 2007. Layer Integrated Modeling of Three-Dimensional Recirculating Flows in Model Tidal Basins. *Journal of Waterway, Port, Coastal, and Ocean Engineering*, Vol. 133, No. 5, pp324-333.

Hall, P. 1987. The numerical Modelling of Wind-induced Lake Circulation. PhD Thesis. University of Birmingham.

Henderson F.M. 1966. *Open Channel Flow*. Macmillan Co. Ltd. 522p.

Harleman, D.R.F. 1966 Diffusion process in stratified flow. In: *Estuary and Coastline Hydrodynamics*. A.T. Ippen (ed.) New York : McGraw Hill Book Co. Inc. Chapter 12, 575-597

Howell, J.M. et al 1996. Effect of Sediment Particle Size and Temperature on Faecal Bacteria Mortality Rates and the Fecal Coliform/Fecal Streptococci Ratio. *Journal of Environmental Quality*. V25, pp1216-1220.

HydroQual, Inc. 2002. *A Primer for ECOMSED Version 1.3*. HydroQual, Inc.

Jamieson, R.C. et al 2004. Assessing microbial pollution of rural surface waters A review of current watershed scale modeling approaches. *Agriculture Water Management*. V17, pp1-17

Jamieson, R.C. et al 2005a. Resuspension of sediment-associated Escherichia in a natural stream. *J. Environ. Qual.* 34:581-589.

Kashefipour, S.M. 2002. *Modelling Flow, water Quality and SedimentTransport*

- Processs in Riverine Basins. PhD thesis, Cardiff University.
- Kashefipour, S.M. et al 2002a. Hydro-environmental modeling for bathing water compliance of an estuarine basin. *Water Research*. v 36, pp1854-1868.
- Kashefipour, S.M. et al. 2002b. Dynamic Modelling of Bacterial concentration in coastal water: Effects of Solar Radiation On Decay. *Proceedings of 13th IAHR APD Congress, Singapore, World Scientific, vol 2, 993-998.*
- Kirk J.T.O. 1984 . Depemndence of Relationship between Inherent and Apparent Optical Properties of Water on Solar Altitude. *Lminology and Ocean graphy*. Vol.29 ,pp350-356.
- Kolahdoozan, M. 1999. Numerical Modelling of Geomorphological Processes in Estuarine Waters. PhD Thesis. University of Bradford, UK.
- Koutitas, Christopher and Gousidou-Koutita, Maria 1986. A comparative study of three mathematical models for wind-generated circulation in coastal area. *Coastal Engineering* 10(1986) 127-138
- Krone RB. 1962. Flume studies of the transport of sediment in estuarial processes. Final Report, Hydraulic Engineering Laboratory and Sanitary Engineering Research Laboratory, University of California Berkeley.
- Leonard, B.P., (1991), “The ULTIMATE Conservative Difference Scheme Applied to Unsteady One-dimensional Advection”, *Computer Methods in Applied Mechanics and Engineering*, Vol. 88, 17-74.
- Leonard, B.P., and H.S. NIKNAFS, (1990), “Cost- Effective Accurate Coarse-Grid Method for Highly Convective Multidimensional Unsteady Flow”, In *Proceedings of the CFD Symposium on Aeropropulsion, NASA Lewis Research Centre, Cleveland OH, USA*
- Liang, D. Cheng, L and Li, FG. Numerical modeling of scour below a pipeline in currents. Part II: Scour simulation. *Coastal engineering*, 52 (1): 43-62
- Liang, D. Falconer, RA and Lin, B. 2006. Comparison between TVD-MacCormack and ADI-type solvers of the shallow water equations. *Advances in Water Resources*, 29 (12): 1833-1845
- Liang, D. Lin, B and Falconer, RA. 2007 Simulation of rapidly varying flow using an efficient TVD-MacCormack scheme. *International journal for numerical methods in fluids*, v53, pp811-826.
- Lin, B. and R.A. Falconer, (1996), “Numerical Modelling of Three-Dimensional Suspended Sediment for Estuarine and Coastal Waters”, *Journal of Hydraulic Research*, Vol. 34, No. 4, 435-455.
- Lin, B. and Falconer, R.A. (1997a) Tidal flow and transport modelling using the ULTIMATE QUICKEST scheme. *Journal of Hydraulic Engineering, ASCE*,

Vol.123, No. 4, 303-314.

Lin, B. and Falconer, R.A. (1997b). Three-dimensional Layer-integrated Modelling of Estuarine Flows with Flooding and Drying. *Journal of Estuarine, Coastal and Shelf Science*, v44, pp737-751.

Lin, B and Falconer, R.A. 2005. Integrated 1-D and 2-D Models for Flows and Water Quality Modelling. XXXI IAHR Congress. pp545-552.

Mancini J.L. 1978. Numerical Estimates of Coliform Mortality Under various Conditions. *Journal of Water pollution Control Federation*. vol.38, no. 3, pp2477-2484

Mehta, A.J. et al 1989. Cohesive Sediment Transport. I: Process Description. *Journal of Hydraulic Engineering*. V115, n8, pp1076-1093.

Mehta A.J. 1993. Hydraulic behavior of fine sediment. In: Abbott MB, Price WA, editors. *Coastal, Estuarial and Harbor Engineers' Reference Book*. London: E & FN Spon, pp577-84.

Muirhead R.W. et al. 2004. Faecal bacteria yields in artificial flood events: quantifying in-stream stores. *Water Research*. V38, pp1215-1224.

Owens, P.H., (1987), "Mathematical Modelling of Sediment Transport in Estuaries", PhD Thesis, University of Birmingham, UK, 220pp.

Plummer D.M., Owens N.J.P. and Hebert R.A. 1987. Bacteria-particles Interactions in Turbid Estuarine Environments. *Continental Shelf Research*, vol 7, No. 11/12, pp 1429-1433.

Pommepuy, M. et al 1992. Enteric bacteria survival factors. *Wat.sci. Tech.*, vol 25(12), pp93-103.

Preston, R.W. 1985. The Representation of Dispersion in Two-Dimensional Shallow Water Flow. Central Electricity Research Laboratories. Report No. TPRD/U278333/N84, May, 13pp

Rodi, W. 2000. *Turbulence Models and Their Application in Hydraulics*. Second edition, International Association for Hydraulics Research, Delft, the Netherlands, 104 pp.

Solic M. and Krstulovic N. 1992 Separate and Combined Effects of Solar-Radiation , Temperature, Salinity , and PH on the Survival of Fecal-Coliforms in Seawater. *Marine Pollution Bulletin*. Vol.24, No,8 pp. 411-416

Sotiropoulos, F. 2005. Introduction to statical turbulence modelling for hydraulic engineering flows. In *Computational Fluid Dynamics: Applications in Environmental Hydraulics* Edited by P.D. Bates, S.N. Lane and R.I. Ferguson. John Wiley & Sons Ltd.

- Stapleton, C.M., Wyer, M.D., Kay, D., Bradford, M., Humphrey, N., Wilkinson, J., Lin, B., Yang, Y., Falconer, R.A., Watkins, J., Francis, C.A., Crowther, J., Paul, N.D., Jones, K. and McDonald, A.T., 2007. "Fate and Transport of Particles in Estuaries, Volume I, II, III, IV. Environment Agency Science Report SC000002/SR1-4.
- Tetra Tech, Inc., 2002: Theoretical and computational aspects of sediment and contaminant transport in EFDC. A report to the U. S. Environmental Protection Agency, Fairfax, VA.
- Thomann, R.V. and Mueller, J.A. 1987 Principles of Surface Water Quality Modeling and Control. New York: Harper Collins Publishers Inc.
- Tannehill, J.C. , D.A. Anderson, and R.H. Pletcher, (1997), "Computational Fluid Mechanics and Heat Transfer", 2nd Ed., Taylor & Francis, USA, 792pp.
- Van Rijn, L.C., (1984a), " Sediment Transport, Part I: Bed Load Transport", Journal of Hydraulic Engineering, ASCE, Vol. 110, No. 10, 1431-1457.
- Van Rijn, L.C., (1984b), " Sediment Transport, Part II: Suspended Load Transport", Journal of Hydraulic Engineering, ASCE, Vol. 110, No. 11, 1613-1641.
- Van Rijn, L.C., 1986. Mathematical modelling of suspended sediment in non uniform flows, Journal of Hydraulic Engineering, ASCE, Vol. 112, No. 6, pp433-455.
- Van Rijn, L.C., (1993), "Principles of Sediment Transport in Rivers, Estuaries and Coastal Seas", Aqua Publications, Netherlands.
- Vieira, J.K. (1993) Dispersive processes in two-dimensional models. In: Coastal, Estuarial and Harbour Engineers' Reference Book, M.B. Abbott and W.A. Price (eds), E.&F.N. Spon Ltd., London, Chapter 14, 179-190.
- Vreugdenhil , C.B. 1994. Numerical Methods For Shallow-Water Flow. Kluwer Academic Publications.
- Wang, Z.B. and Ribberink, J.S., 1986. The validation of a depth-integrated model for suspended sediment transport. Journal of Hydraulic Research, 24(1): 53-66.
- World Health Organization, 2001. Water quality: guidelines, standards and health. In: Fewtrell, L., Bartram, J. (Eds.), Assessment of Risk Management for Water-related Infectious Disease. WHO Water Series. IWA Publishing, London, UK.
- Wilkinson, J. Jenkins, A. Wyer, M and Kay, D. 1995. Modelling faecal coliform concentrations in streams. Institute of Hydrology. Report No. 127.
- Winterwerp, J.C. and Van Kesteren, W.G.M. 2004. Introduction to the Physics of Cohesive Sediment in the Marine Environment. ELSEVIER B.V.
- Wu, J.1969 Wind stress and surface roughness at air-sea interface. Journal of

Geophysical Research, 74, pp444-455.

Wu, W. Rodi, W. and Wenka, T .2000. 3D NUMERICAL MODELING OF FLOW AND SEDIMENT TRANSPORT IN OPEN CHANNELS. Journal of Hydraulic Engineering. V126, n1, pp4-15.

Wu, Y and Falconer, RA 1998. Modelling of water flows and cohesive sediment fluxes in the humber estuary, UK. Marine Pollution Bulletin. V37,pp 182-189.

Wu, Y and Falconer, RA 2000. A mass conservative 3-D numerical model for predicting solute fluxes in estuarine waters. Advances in WaterResources. V23, pp531-543.

Wu Y., Falconer R.A., and Lin B. 2001. Hydro-environmental modelling of heavy metal fluxes in an estuary. In: Proceedings of XXIX IAHR Congress, Theme B: Environmental Hydraulics, pp. 732-739.

Wu, Y. Falconer R.A. and Lin B.2005. Modelling trace metal concentration distributions in estuarine waters. Estuarine, Coastal and Shelf Science. V.64,pp.699-709.

Wu, Y. Falconer R.A. and J. Struve.2001. Mathematical modelling of tidal currents in mangrove forests. Environmental Modelling & Software.V16, pp.19-29.

Wyer, M.D. et al. 1997. Non –outfall sources of faecal indicator organisms affecting the compliance of coastal water with directive 76/160/EEC. Wat. Sci Tech. Vol 35, No. 11-12,pp151-156.

Xu, P. Brissaud, F. and Fazio A. 2002. Non-steady-state modelling of faecal coliform removal in deep tertiary lagoons. Water Research. V36, pp 3074–3082

Yalin, M.S., 1972. Mechanics of Sediment Transport. Pergamm Press, N.Y., pp290

Yang, L. 2005. Development of Hydroinformatics Software Tool Enteric BacteriaTransport Modelling Associated With Sediment Transport PhD Thesis Cardiff University.

Yuan, D. 2007. Development of An Integrated Hydro-environmental Model and its Application to a Macro-tidal Estuary. PhD Thesis. Cardiff University.

Yuan, D. Lin, B. Falconer, RA and Tao, J 2007. Development of an integrated model for assessing the impact of diffuse and point source pollution on coastal waters. Environmental Modelling & Software. v22, pp871-879.

